acta physica slovaca vol. 59 No. 4, 305 – 535 **August 2009**

BREAKING OF OCEAN SURFACE WAVES

A.V. Babanin[1]
Swinburne University of Technology, Melbourne, 3122 Australia

Received 2 July 2009, accepted 9 July 2009

Wind-generated waves are the most prominent feature of the ocean surface, and so are breaking waves manifested by the appearance of sporadic whitecaps. Such breaking represents one of the most interesting and most challenging problems for both fluid mechanics and physical oceanography. It is an intermittent random process, very fast by comparison with other processes in the wave system. Distribution of the wave breaking on the water surface is not continuous, but its role in maintaining the energy balance within the continuous wind-wave field is critical. Ocean wave breaking also plays the primary role in the air-sea exchange of momentum, mass and heat, and it is of significant importance for ocean remote sensing, coastal and maritime engineering, navigation and other practical applications.

Understanding the wave breaking, predicting its occurrence, the breaking rates and breaking strength, and even ability to describe its onset has been hindered for decades by the strong non-linearity of the process, together with its irregular and ferocious nature. Recently, this knowledge has significantly advanced, and the review paper is an attempt to summarise the facts into a consistent, albeit still incomplete, picture of the phenomenon.

In the paper, variety of definitions related to the wave breaking are discussed and formulated, and methods for breaking detection and measurements are examined. Most of attention is dedicated to the research of wave-breaking probability and severity. Experimental, observational, numerical, analytical and statistical approaches and their outcomes are reviewed. Present state of the wave-breaking research and knowledge is analysed and main outstanding problems are outlined.

PACS: 92.05.Bc, 92.10.H-, 92.10.hb

KEYWORDS: Wave breaking, Breaking onset, Breaking probability/occurrence, Breaking severity/strength, Wave-breaking phases, Breaking threshold, Limiting breaking steepness, Induced breaking, Cumulative effect, Whitecapping dissipation

[1]E-mail address: ababanin@swin.edu.au

Contents

1 Introduction

Wind-generated waves are the most prominent feature of the ocean surface. As much as the oceans cover a major part of our planet, the waves cover all of the oceans. If there is any object of the oceanography which does not need introduction, this is the surface waves generated by the wind.

Being such a conspicuous entity, these waves, however, represent one of the most complex physical phenomena of nature. Three major processes are responsible for wave evolution in a general case, with many more whose significance varies depending on conditions (like wave-bottom interaction which is only noticeable in shallow areas). The first process is energy and momentum input from the wind. The waves are generated by the turbulent wind, and the turbulence is most important both for their initial creation and for subsequent growth [e.g. Phillips, 1957, Janssen, 1994, Kudryavtsev *et al.*, 2001, among many others]. There is, however, no closed theory of turbulence to begin with! And experimentalists have to deal with tiny turbulent fluctuations of air which are of order $10^{-5} - 10^{-6}$ of the mean atmospheric pressure and have to be measured very close to the water surface, typically below the wave crests [e.g. Donelan *et al.*, 2005]. The wind-input process is very slow and it takes hours of wind forcing (thousands of wave periods) and tens and hundreds kilometres of fetch for waves to grow a considerable height.

The second process is weak resonant non-linear interactions within the wave system which can only be neglected for infinitesimal waves. For most of its existence, the wind wave can be regarded as almost sinusoidal (i.e. linear), but its very weak mean non-linearity (i.e. deviation of its shape from the sinusoid) is generally believed to define the wave evolution. This is due to such waves, unlike the linear sinusoids, exchanging energy when they cross-path. And they do cross-path because waves of different scales (i.e. different frequencies and wavelengths) propagate with different velocities, and because waves also tend to propagate in a range of angles with respect to the mean wind direction. Such weak interactions appear to be of principal importance. The longer (and higher) the waves are, the faster they move, and therefore the visibly dominant waves move with speeds close to the wind speed. This means that they virtually move in the still air and there is almost no wind for them. If they are yet obviously wind-generated, how does the wind produce such waves? The answer, as it is most commonly accepted now, is that the wind pumps energy mostly into shorter (high-frequency) and slowly-moving waves which then transfer this energy across the continuous spectrum of waves of all scales towards longer (lower-frequency) components and thus allow those to grow - by means of non-linear interactions. So, this small non-linearity plays a large role in developing the wind waves as we know them. Analytically, to account for this sort of interactions the theoreticians have to solve relevant equations of hydrodynamics with accuracy down to expansion terms of the third order [e.g. Zakharov, 1968, Hasselmann *et al.*, 1994, Badulin *et al.*, 2005]. Experimentally, such interactions could not have been studied directly because of a great number of technical difficulties, one of which - slowness of the process, thousands of wave periods being its time scale. Here, we would also like to mention that there are alternative approaches to explaining the evolution of long wind-generated waves.

The third most important process which drives wave evolution is the wave energy dissipation. Common experience tells us that wind-generated waves, no matter how strong the wind is and how long are its duration and wave fetch, do not grow beyond some limit. In absence of mainland in the Southern Ocean, high continuous westerly winds are free to run the waves round the globe

and thus provide conditions of unlimited wind-wave forcing and growth. Yet, the significant wave height (height of one third of highest waves) rarely goes beyond 10 m. Individual waves of some 30 m are occasionally reported [e.g. Liu *et al.*, 2007], but those are very seldom and would certainly be the ultimate limit for the wind-generated waves on the planet. Therefore, there is a process which controls the wave growth from above, and that is the wave dissipation.

1.1 Wave breaking: the process which controls the wave energy dissipation

There are a number of physical mechanisms in the oceanic and atmospheric boundary layers which contribute to the wave energy dissipation [e.g. Babanin, 2006, Ardhuin *et al.*, 2009], with the wave breaking being the most significant. In well-developed deep-water wind-forced waves, it is believed that the breaking accounts for more than 80% of the dissipation. Wave energy is proportional to the wave height squared, and therefore a sudden reduction of wave height during breaking by, for example, two times, signifies a four-times reduction of the energy. Obviously, provided there is a sufficient amount of waves breaking, such dissipation mechanism is much more efficient compared to the viscosity, to the interaction of waves with winds, currents, background turbulence and to other ways of gradual decline. The energy lost to breaking is spent on injecting turbulence and bubbles under the ocean interface, and thus the wave breaking, and the wind-generated waves in general, play a very significant role in negotiating the exchange of momentum, heat and gases between the atmosphere and the ocean.

Breaking happens very rapidly, it only lasts a fraction of the wave period [Rapp & Melville, 1990, Babanin *et al.*, 2009a], but the wave may indeed loose more than a half of its height [Liu & Babanin, 2004]. Thus, the wave energy slowly accumulated under the wind action and through the non-linear transfer over thousands of wave periods is suddenly released in the space of less than one period. Obviously, this process, the breaking-in-progress process of wave collapse, is a highly non-linear mechanism of very rapid transfer of wave energy and momentum to other motions. So far, there are no adequate mathematical and physical descriptions of such process.

Conceptually, however, physics of the wave collapse is completely different from the physics leading to the breaking onset. While the collapse is driven, to a greater extent, by gravity and inertia of the moving water mass and, to a lesser extent, by hydrodynamic forces, the breaking onset occurs mostly due to dynamics of the wave motion in the water. Approaching the breaking onset by a background wave is also very rapid, and also happens in the space of one wave period [e.g. Babanin *et al.*, 2007a, 2009a,b], but it should be considered separately from the following wave collapse. Essentially, the breaking process consists of two different physics - one leading to the breaking and another driving the wave breaking once it started. These are not entirely disconnected, however, and the outcome of the breaking collapse appears to 'remember' the 'input' which made a wave to break. This will be discussed in more detail below.

Distinct difference between the whitecapping dissipation and other processes involved in wave evolution is also determined by the fact that not every wave breaks whereas every wave experiences continuous energy input from the wind and continuous non-linear energy exchange with other components of continuous wave spectrum. A typical picture of wavy surface under moderately strong wind conditions is shown in Figure 1.1. Waves of all scales, forming a continuous spectrum in terms of wave periods and lengths, exist simultaneously and run concurrently with different phase speeds, riding on the top of each other or intercepting momentarily at different directions. All these waves are subject to wind input and non-linear exchange, but as it is

Fig. 1.1. Wind-wave pattern at a moderate wind. Waves of all scales are present simultaneously, representing continuous wave spectrum. Only a small fraction of them are breaking at each scale.

seen in Figure 1.1 just a small fraction of them breaks. It is only under very strong winds, rate of breaking crests can reach 50% or more, but normally it is well below 10% [Babanin *et al.*, 2001]. This means that on average it is every 20th or even every 50th wave that breaks, and that is sufficient to hold the energy balance in the wave system where every single wave gains the energy one way or another. In the continuous time-space environment of continuous wave spectrum and continuous physical processes, the random breaking which is intermittent in time and does not cover the surface uniformly appears to control the equilibrium and ultimately the wave growth. There are evidences that coverage of the ocean surface with the breaking has a fractal dimension rather than being a two-dimensional surface [Zaslavskii & Sharkov, 1987], and this fact provides further mathematical complications if description of this phenomenon is attempted by means of hydrodynamics or statistics.

It is important to mention at this stage that the three major processes, wind energy input, energy redistribution due to non-linear interactions and energy dissipation, are closely coupled, affect each other and are equally important in wave evolution. Obviously, there would be no waves if they were not generated by the wind, but the wind-input mechanism alone cannot explain the evolution at any extent. As soon as the waves grow beyond the infinitesimal stage, non-linear interactions begin to play their important role, and soon after that, once individual steeper waves start to break, the whitecapping dissipation assumes its responsibility as the balance holder.

The so-called whitecapping dissipation is the dissipation due to wave breaking, but it is not always that the waves form whitecaps when they break (i.e. so-called micro-breaking discussed in Section 2.8 below). Since such a notion contradicts to a general intuitive perception of the wave breaking, we have to first answer a question: what do we call the wave breaking?

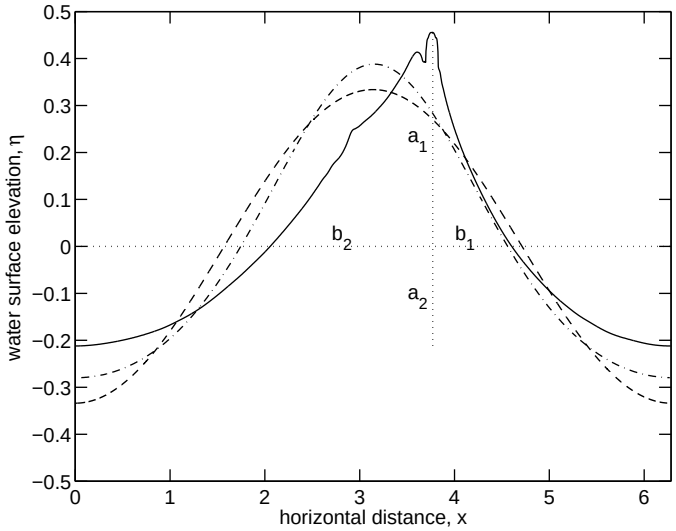

Fig. 1.2. Geometric definition of wave skewness and asymmetry. The wave propagates from left to right. b_1 and b_2 are horizontal distances from the breaker crests to the zero-upcrossing and -downcrossing respectively. a_1 and a_2 are the breaker crest height and trough depth respectively. Solid line – numerically simulated incipient breaker (skewness is $S_k = 1.15$, asymmetry is $A_s = -0.51$). Dashed line – harmonic wave of the same wavelength and wave height ($S_k = A_s = 0$). Dash-dotted line – non-linear wave of the same length and height obtained by means of perturbation theory ($S_k = 0.39$, $A_s = 0$). Dotted lines – mean (zero) water level (horizontal) and line drawn from the breaker crest down to the level of its trough (vertical).

1.2 Concept of the wave breaking

Definitions pertaining to different physical and mathematical aspects of the wave breaking process will be formulated in Section 2 below. Here, we would like to discuss a common concept of the breaking - that is what and how is generally perceived as a wave breaking event.

In Figure 1.2, a linear harmonic sinusoidal wave (sometimes called Airy wave, dashed line), a Stokes wave, and an incipient breaker of the same height and length, i.e. all being waves of the same average steepness, are compared graphically. This Figure tests our ability to describe non-linear behaviour of waves theoretically. Stokes wave is a perturbation solution of hydrodynamic equations, assuming that steepness of the waves is small (dash-dotted line). Obviously, although this traditional approach does produce a non-linear wave shape, it does not look like anything close to a breaking wave as we perceive it. Needless to say that steepness of a breaking wave can hardly be expected to be small.

An incipient breaker shown in Figure 1.2 (solid line) is produced numerically by means of the Chalikov-Sheinin model (hereinafter CS model [Chalikov & Sheinin, 1998, 2005]) which can simulate propagation of two-dimensional waves by means of solving non-linear equations of hydrodynamics explicitly. Shape of such a wave is very asymmetric, with respect to both vertical

and horizontal axes, and even visually the wave looks unstable.

Instability is a key word in the breaking process. The wave which we interpret as the incipient breaker in Figure 1.2 cannot keep propagating as it is: it will either relax back to a less steep, skewed and asymmetric shape or collapse. We will define the steepness, skewness and asymmetry (with respect to the vertical axis) as

$$\epsilon = ak = \pi \frac{H}{\lambda}, \tag{1.1}$$

$$S_k = \frac{a_1}{a_2} - 1, \tag{1.2}$$

$$A_s = \frac{b_1}{b_2} - 1 \tag{1.3}$$

respectively (see Figure 1.2). Here, a is wave amplitude, H is wave height ($a = H/2$ in the linear case), $k = 2\pi/\lambda$ is wavenumber and λ is wavelength, a_1 and a_2 are the wave crest height and trough depth, and b_1 and b_2 are horizontal distances from the breaker crests to the zero-upcrossing and -downcrossing respectively. Thus, the steepness ϵ is an average steepness over the wave length, and obviously, local steepness is much higher near the crest and is lesser than average at the trough. Positive skewness $S_k > 0$ represents a wave with a crest height greater than the trough depth (a typical surface wave outside the capillary range), and negative asymmetry $A_s < 0$ corresponds to a wave tilted forward in the direction of propagation. Importantly here, experimentally observed negative asymmetry A_s has been broadly associated with the wave breaking [e.g. Caulliez, 2002, Young & Babanin, 2006a].

Intrinsically, both the asymmetry and the skewness are natural features of steep deep-water waves regardless of their size, crest length, forcing or generation source. In Figure 1.3, examples of real waves are demonstrated which exhibit both these properties. The left panel shows a wind-generated and wind-forced wave of height $1.6m$ measured in a natural directional wave field in the Black Sea. The right panel shows a very small two-dimensional wave of height $4cm$ freely propagating without wind forcing. This wave was mechanically generated in the Air Sea Interaction Salt water Tank (ASIST) of the University of Miami.

Once the skewness is non-zero and the amplitude a is not clearly defined, a definition of the wave steepness in terms of ak becomes ambiguous. Therefore, unless otherwise specified, the steepness will be expressed in terms of wave height $H = a_1 + a_2$ rather than wave amplitude a, as $\epsilon = Hk/2$. In these terms, a steepness $\epsilon = 0.335$ of the wave shown in the Figure far exceeds the limits of a perturbation analysis.

The dashed line in Figure 1.2 represents a steep sinusoidal wave ($S_k = A_s = 0$). Such a wave will immediately transform itself into a Stokes wave [e.g. Chalikov & Sheinin, 2005] (dash-dotted line). This steep Stokes wave is highly skewed ($S_k = 0.39$), but remains symmetric (i.e. $A_s = 0$). The incipient breaker in Figure 1.2 ($S_k = 1.15, A_s = -0.51$) was produced by the CS model, in a simulation which commenced with a monochromatic wave of $\epsilon = 0.25$. Such a wave profile visually looks realistic for a breaker and corresponds to, or even exceeds, experimental values of skewness and asymmetry for breaking waves previously observed (e.g. up to $A_s = -0.5$ instantaneously in Caulliez [2002] or $A_s = -0.2$ on average in Young & Babanin [2006a]). It is worth noting that the steepness of the individual wave has grown very significantly at the point of the breaking: from $\epsilon = 0.25$ to $\epsilon = 0.335$.

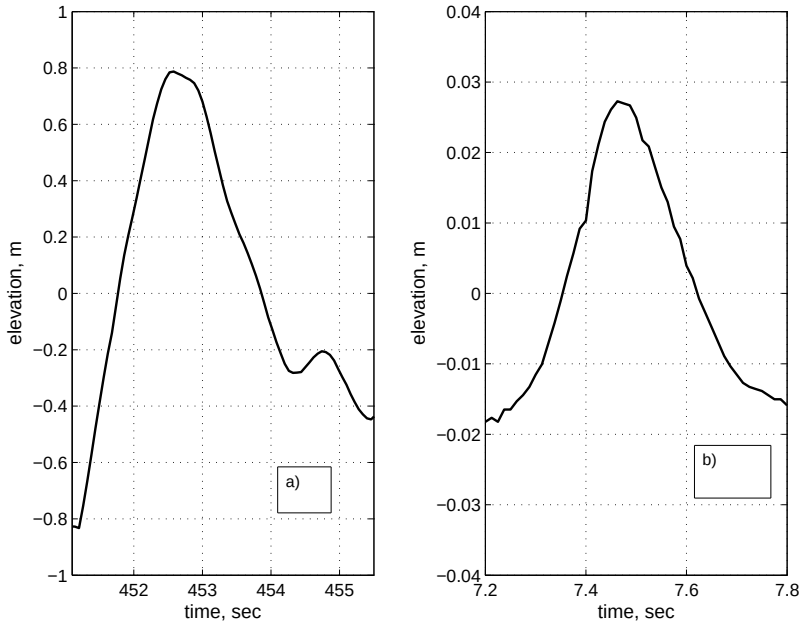

Fig. 1.3. Real waves exhibiting both skewness and asymmetry. The waves propagate from right to left. a) Field wave measured in the Black Sea; b) laboratory (two-dimensional) wave measured in ASIST.

When collapsing, the wave shape becomes singular at least at some points along the wave profile (i.e. space derivatives of the surface profile have discontinuities). This stage of wave subsistence is called breaking. Breaking of large waves produce a substantial amount of white-capping, but smaller waves, the micro-breakers, do not generate whitecaps or bubbles and loose their energy directly to the turbulence.

Examples of various breaking and non-breaking waves are shown in Figures 1.4-1.8. Figures 1.4-1.5 picture deep-water waves. Swell in Figure 1.4 are former wind waves which left the storm region where they were generated. They most closely conform to our intuitive concept of what the ideal waves should look like: uniform and long-crested, with crests marching parallel to each other. Their steepness is low and they do not break until reach a shore.

Wind-forced waves hardly resemble this ideal picture. They look random and chaotic, they are multi-scale and directional, and they break. In Figure 1.5 a deep-water breaker is shown whose height is in excess of 20 m.

In Figure 1.6, waves breaking in finite depths and, ultimately, in the surf zone are pictured. In finite depths, waves break more frequently. Possible reasons are two. Mainly, the waves break due to the same inherent reason as in the deep water, but they do that more often because the bottom-limited waves are steeper on average. Another fraction of waves break due to direct interaction with the bottom, this fraction is growing as the waters are becoming shallower [see Babanin *et al.*, 2001, for more details].

Fig. 1.4. Ocean swell are former wind waves propagated outside the storm area. They have low steepness and do not break. The photo is courtesy of Sonia Ponce de Leon.

Fig. 1.5. Large wave breaking in deep water. Distance from the mean water level to the lowest deck of the Fulmar Platform in the North Sea is 21 m. The photo is courtesy of George Forristal.

If deep-water waves enter very shallow environments, as shown in Figure 1.7, all of them will break and ultimately loose their entire energy to interaction with the bottom, to sediment transport, to production of turbulence, bubbles and droplets, to mean currents and to generation of small amount of waves reflected back into the ocean.

In the close-up picture of Figure 1.8, the waves can still be breaking even though it is now not possible to spot visually. Short (in terms of wave length) and small (in terms of wave height) ripples can nevertheless be quite steep. Such micro-breakers do not generate whitecapping, but demonstrate all the other singular surface features and irreversibly loose a significant part of their

Fig. 1.6. Deep-water waves approach finite depths, grow steep and break.

Fig. 1.7. Shallow water breaking. 100% of waves coming into the shallows break and loose all their energy.

height and dissipate their energy [see, e.g. Jessup *et al.*, 1997a].

At very strong wind-forcing conditions, the wave breaking behaviour is different yet again, and even the definition of the breaking needs to be adjusted. As seen in Figure 1.9, the air-water interface is now smeared, atmospheric boundary layer being full of droplets (spray) and water-side boundary layer is filled with bubbles. The distinct interface is effectively replaced by a two-phase medium and the notions of wave shape and its singularity become vague.

While the breaking due to inherent hydrodynamic reasons still takes place, the wind is now capable of instigating the process. Additionally, the wind blows off the steep wave crests. The

Fig. 1.8. Wave ripples. Such waves are steep and break frequently, but do not form whitecapping.

Fig. 1.9. Ocean surface at extreme wind forcing.

latter event does break the surface, creates surface singularities and reduces the wave energy, but cannot be treated as the conventional breaking. Wave breaking and wave energy dissipation in such extreme conditions are poorly understood even in phenomenological sense.

Thus, in order to avoid ambiguity, the wave breaking process requires more specific definitions before further discussions are conducted. Therefore, the notion of the breaking onset, a classification of the wave-breaking phases, definitions of the breaking probability and breaking severity, and the concept of micro-breaking will be discussed next in Section 2.

2 Definitions for the wave breaking

Following the intuitively familiar concept of the wave breaking discussed in Section 1.2, a variety of phenomenological definitions can be formulated. Wikipedia suggests such a definition, applicable across the range of wave processes, including water waves as well as electromagnetic waves, waves in plasmas and in other physical media: "In physics, a breaking wave is a wave whose amplitude reaches a critical level at which some process can suddenly start to occur that causes large amounts of wave energy to be dissipated. At this point, simple physical models describing the dynamics of the wave will often become invalid, particularly those which assume linear behavior" (`http://en.wikipedia.org/wiki/Wave_breaking`). Glossary of Meteorology of the American Meteorological Society defines more specifically the breaking of ocean surface waves: "A complex phenomenon in which the surface of the wave folds or rolls over and intersects itself. In the process it may mix (entrain) air into the water and generate turbulence. The causes of wave breaking are various, for example, through the wave steepening as it approaches a beach, through an interaction with other waves in deep water, or through the input of energy from the wind causing the wave to steepen and become unstable" (`http://amsglossary.allenpress.com/glossary/browse?s=w&p=11`).

As discussed above, a more explicit physical, and yet alone mathematical definition of the wave-breaking phenomenon is hardly possible. The wave breaking can occur due to a number of different causes which will result in different appearances of the wave breaker, different physics of the wave energy dissipation in the course of the breaking and different outcomes in terms of impact on the wave field, on subsurface water layer and even on the solid bottom in finite-depth environments. While being breaking, a wave and associated underwater motion goes through a number of different stages, with different dynamics, different surface, acoustic, void-fraction, optical and other signatures. It is these stages that we will classify in this Section which will help us to avoid ambiguity through the rest of the paper. We will also define here the main quantitative characteristics used to describe the frequency of occurrence of the wave breaking and the strength of the breaking, and will describe the notion of micro-breaking.

2.1 Breaking onset

Figure 1.2 above demonstrates an incipient wave breaker modelled by means of CS model (solid line). Visually and intuitively, shape of the breaker appears quite realistic, and therefore it is instructive to review the model's definition of the breaking onset. A numerical model cannot operate by means of phenomenological definitions, and obviously the inception of the breaking had to be explicitly defined in mathematical terms.

In the numerical simulations, a wave is regarded as breaking if the water surface becomes vertical at any point [Babanin *et al.*, 2007a, 2009a,b]. Criterion for terminating the model run was defined by the first appearance of a non-single value of surface in the interval $x = (0, \lambda)$:

$$x(i+1) < x(i), i = 1, 2, 3..., N-1, \tag{2.1}$$

where N is the number of points on the wave profile over its length λ.

This definition is further illustrated in Figure 2.1, also simulated by means of the CS model. Here, development of a very steep harmonic wave with initial steepness $\epsilon = ak = 0.32$, is shown in terms of dimensionless time (in the horizontal scale, 2π corresponds to the wave period). This

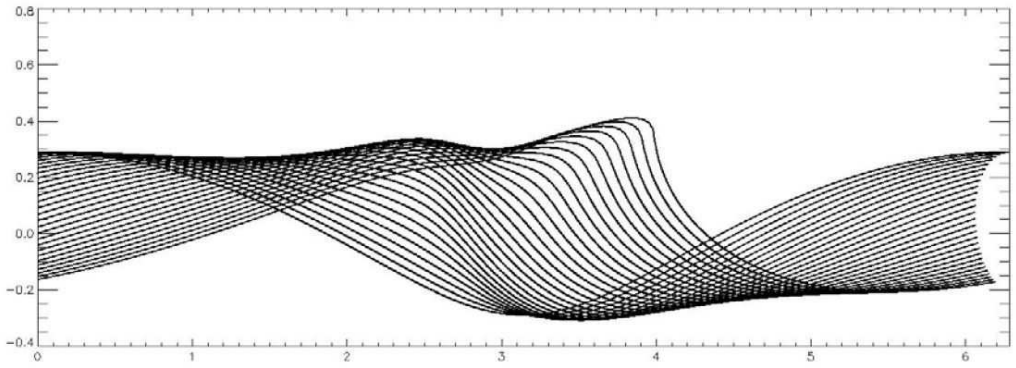

Fig. 2.1. Numerical simulation of a steep wave evolving towards breaking, as predicted by the CS model. The wave propagates from left to right.

is effectively a rapidly developing breaker, as in the two-dimensional CS model such waves break within one period.

The model has obvious limitations in simulating the final stages of incipient breaking and was stopped when the water surface became vertical at any point. Strictly speaking, this geometrical property of the surface can be used as a physical definition of the breaking onset. In the numerical simulations it was noticed that the local steepness can be very large, but the carrier wave can still recover to a non-breaking state. If, however, a negative slope appears locally, the wave never returns to a non-breaking scenario because the water volume intersecting the vertical line tends to collapse. That is, after the moment when the criterion (2.1) has been reached, the solution never returns to stability: the volume of fluid crossing the vertical $x(i)$ rapidly increases. Apparently, the same considerations are applicable to the physical waves too.

At present, the concepts of incipient breaking and breaking onset are poorly defined and even ambiguous. Traditionally, the initial phases of a breaker-in-progress are treated as incipient breaking. As an example, let us consider how 'near-breaking' was defined by Caulliez [2002]. In this paper, surface elevations were recorded, differentiated, and the wave was regarded as a 'near-breaker' if its slope exceeded 0.586 anytime between two subsequent zero-downcrossings. This criterion is an estimate of the highest slope which a Stokes wave can reach [Longuet-Higgins & Fox, 1977]. But if this slope is exceeded, then the wave is not about to break – it is already breaking. This is not an incipient breaker, but represents breaking in progress. Features and physics of breaking-in-progress, however, may be very different to that of incipient breaking (Section 2.2). Thus, investigation of geometric, kinematic, dynamic and other properties of breaking-in-progress, such as whitecapping, void fraction, acoustic noise emitted by bubbles etc., will be of little assistance if we are seeking to understand the causes of breaking and the breaking onset.

In the present paper, as in Babanin *et al.* [2007a, 2009a,b], we suggest that the breaking onset is defined as a such instantaneous state of wave dynamics where a wave has already reached its limiting-stability state, but has not yet started the irreversible breaking process. That is, the breaking onset is the ultimate point at which the wave dynamics caused by initial instabilities is

still valid. This definition allows identification of the onset and, once the location of the breaking onset can be predicted, allows measurement of the physical properties of such waves. The state of breaking onset is instantaneous unlike the stages of incipient breaking and the breaking-in-progress (see Sections 2.2 and 2.4 below). The latter can be further subdivided into stages with different properties and different dynamics [Rapp & Melville, 1990, Liu & Babanin, 2004].

2.2 Breaking in progress

Beyond the point of onset, breaking occurs very rapidly, lasting only a fraction of the wave period [Rapp & Melville, 1990, Babanin *et al.*, 2009a], but the wave may lose more than a half of its height [Liu & Babanin, 2004]. Thus, the wave energy that slowly accumulated under the wind action and through the weak non-linear transfer over hundreds of wave periods is suddenly released in the space of less than one period. Obviously, this process, the breaking-in-progress process of wave collapse, is also a highly non-linear mechanism. Conceptually, however, it is different from the processes leading to breaking onset and should be considered separately. As mentioned is Section 1, while the collapse is driven, to a greater extent, by gravity and inertia of the moving water mass and, to a lesser extent, by hydrodynamic forces, the breaking onset occurs mostly due to dynamics of the wave motion in the water. Waves are known to break even in the total absence of wind forcing, provided hydrodynamic conditions are appropriate [e.g. Melville, 1982, Rapp & Melville, 1990, Brown & Jensen, 2001, Manasseh *et al.*, 2006, Babanin *et al.*, 2007a, 2009a,b]. Therefore, processes leading to the wave breaking, i.e. the stage of incipient breaking, can be simplified by studying only the water side of the surface behaviour, whereas for the breaking in progress, the air-sea interaction part, such as whitecapping [e.g. Guan *et al.*, 2007], void fraction [e.g. Gemmrich & Farmer, 2004], work against the buoyancy forces [e.g. Melville *et al.*, 1992], wind-wave momentum/energy exchange [e.g. Babanin *et al.*, 2007b] are of very essential importance.

The pre- and post-breaking physics are not entirely disconnected, and the outcome of the breaking collapse appears to 'remember' the 'input' which made a wave to break. This will be discussed in more detail below. Here, we would like to emphasise that among the wave-breaking definitions, the breaking in progress has to be considered separately and can be further subdivided in distinctly different phases.

There is at the present no prevalently established classification of wave-breaking phases, and here we will follow the logic suggested by Liu & Babanin [2004]. They envisaged and quantified in terms of relative duration a single breaking event as passing through several distinctive stages, from both the external appearances of the breaking and the underlying physics involved. These stages are incipient breaking, developing breaking, subsiding breaking and residual breaking. The first stage leads to the breaking onset as described in Section 2.1 above. The developing breaking and subsiding breaking are different phases of the breaking in progress. The residual breaking is a follow-up dynamic impact of the breaking event, rather than wave breaking as such, it will be discussed in Section 2.3 below.

Liu & Babanin [2004] aimed at testing the Liu [1993] breaking-detection approach based on wavelet technique, by means of field data (see Section 3.7 below). The wavelet analysis indicated a wave breaking if the downward acceleration, obtained from surface-elevation series, exceeded a predetermined threshold value. The data were obtained under a variety of wind-wave conditions in the deep water in the Black Sea and in the finite-depth environment in Lake George, Australia.

Both data sets included synchronised time series of surface elevations and wave breaking marks. Both had been extensively used to study the breaking statistics for different wave spectra and in different environmental conditions, and therefore detailed results of the analyses were available for comparisons [Babanin, 1995, Babanin & Soloviev, 1998a,b, Banner *et al.*, 2000, Babanin *et al.*, 2001].

In the Black Sea, the wave breaking were detected and marked visually [Babanin, 1995], and in Lake George the detection was conducted by acoustic means [Babanin *et al.*, 2001]. Overall statistics of the number of breaking events and their frequency of occurrence matched the outcomes of the wavelet technique very well. Detailed examination of the results, however, indicated essential differences. The wavelet approach, along with the measurements was generally successful in capturing breaking wave events at many occasions, although at some other occasions one of them failed to detect a breaker while the other indicated that the breaking occurred. This is not unexpected as both the measurements, i.e. detection of the breaking by visual or acoustic means, and the theoretical wavelet approach should be anticipated as relevant to different phases of wave breaking.

At the incipient stage, the wave starts to find its continuous surface become strenuous to sustain so it is about to break, but is not breaking yet. An incipient breaker does not have whitecapping coverage as the breaking crest does not happen to overturn. This is how Phillips *et al.* [2001] described development of the crest breaking: "A single breaking event is generally initiated at some point on the wave crest and spreads laterally so that its average length is of order half its ultimate length, the width of the broken patch". Before this broken patch starts developing, the wavelet method will already be detecting the breaking because the downward acceleration will exceed the threshold value while closing the breaking onset. The visual technique implemented at the Black Sea and the acoustic technique implemented at Lake George, however, will not detect a breaking. The two experimental techniques effectively make use of whitecapping occurrence at the basic measurement spot and, since there is no whitecapping, i.e. no 'broken patch', they will fail to detect the wave crest as a breaking crest.

The developing stage, is characterised by the lateral spread of breaking with a whitecapping appearance for the crest to pass over the measurement spot, so a developing breaker should be readily detected by the whitecap-oriented measurements. But the developing breaker also exhibits an increase of wave front steepness until it leads to subsiding. Rapp & Melville [1990] in their subsection 3.4 defined the front steepness as ratio of crest-to-front-zerocrossing height to crest-to-front-zerocrossing length and showed that it is larger, compared to the incipient breaking front steepness, for both spilling and plunging breakers. As shown by Liu & Babanin [2004], even though the front steepness is not unambiguously linked to the maximal instantaneous downward acceleration, this is an indication that the over-limiting acceleration values may persist through the developing stage, and thus the developing breaker will be detected by the wavelet method as well.

The relaxing or subsiding stage of breaking has not received as much attention in the literature as the developing breaking. Therefore it is not quite clear, for example, what will happen to the breaking crest once it has reached its maximal length according to Phillips *et al.* [2001] or when the front steepness of breakers, described by Rapp & Melville [1990], will start to decrease. But at some stage it will start to decrease. In Figure 2.2, a segment of a Black Sea record is plotted which shows surface elevations with wave breaking marked by visual observations of whitecaps (dots) and by means of the wavelet analysis (vertical bars). For the Black Sea waves shown,

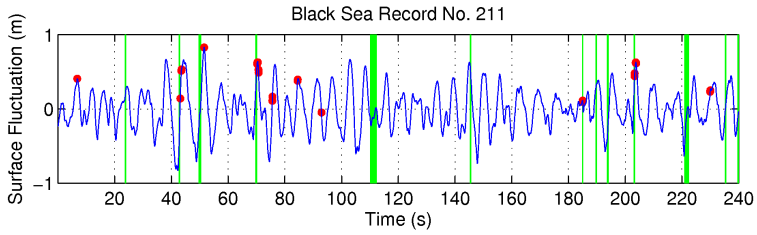

Fig. 2.2. Segment of a Black Sea record. Surface elevations with wave breaking marked by visual observations of whitecaps (dots) and by means of the wavelet analysis (vertical bars).

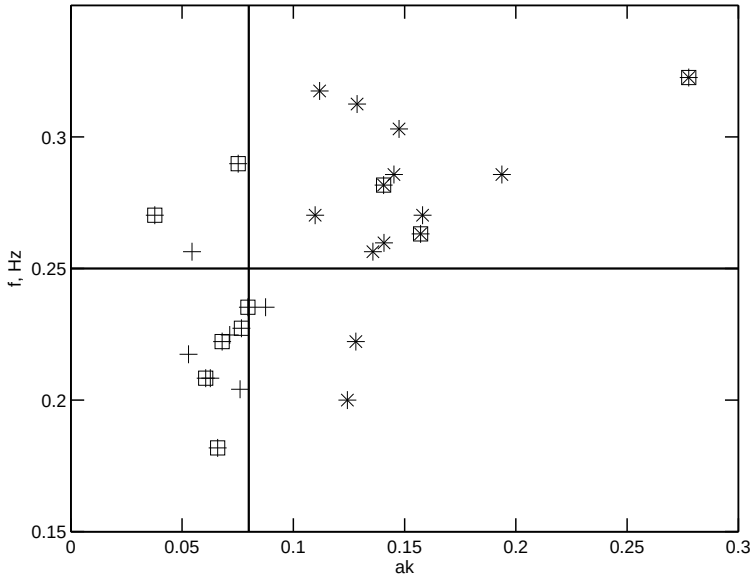

Fig. 2.3. Properties of individual waves in the range of frequencies $f = f_p \pm 0.3 f_p$ of a Black Sea record with $f_p = 0.25$ Hz (Rec. 244, Table 5.1). Frequency (inverse period) f versus steepness ϵ. + - all waves, * - those waves with $\epsilon > 0.08$, squared - those waves exhibiting whitecapping. Solid lines show peak frequency $f_p = 0.25$ Hz (horizontal) and the breaking threshold $\epsilon = 0.08$ (vertical.

mean front steepness was 0.045. The second and the third breakers picked up by the visual method have the front steepness of 0.052 and 0.075 which is greater than the mean steepness as one can intuitively expect for a breaking wave. The first breaker, however, which was detected visually because a whitecapping crest propagated past the measuring wave probe, has a front steepness of 0.011 well below the mean wave steepness. Clearly, this broken wave which still carries along a whitecapping patch is not expected to be detected by the wavelet method based on the acceleration criterion.

Figure 2.3 further illustrates the necessity of subdivision of the breaking process into the

three phases. It shows properties of individual waves in the range of frequencies $f = f_p \pm 0.3 f_p$ of a Black Sea record with peak frequency $f_p = 0.25$ Hz. Frequency f (inverse period $f = 1/T$) of each wave in the record is plotted versus steepness ϵ of this wave. $+$ indicates all waves, $*$ are those waves with $\epsilon > 0.08$, squared boxes correspond to waves exhibiting whitecapping. Solid lines indicate the peak frequency (horizontal line) and the breaking threshold $\epsilon = 0.08$ (vertical) below which even two-dimensional waves are not expected to break [Babanin *et al.*, 2007a, 2009a,b, see also Section 5].

A significant number of waves, however, detected as those breaking visually, are below the threshold. Some of them have steepness as low as $\epsilon = 0.03$ and still exhibit whitecapping. This is the subsiding (not breaking) phase, still detected as breaking if relied on whitecap observations. On the other end, out of two waves with $\epsilon \approx 0.27$ which is very high for field waves by any standards, one wave does not exhibit whitecaps and another does, that is the first one is on its way up to the limiting steepness (incipient breaker) and another is on its way down while collapsing (developing breaker). These observations highlight uncertainties and ambiguity of existing definitions of breaking rates and the need for classifying the wave-breaking phases.

2.3 Residual breaking

The last, residual stage is introduced here formally following Rapp & Melville [1990] as such phase of breaking process when the whitecap is already left behind, but the underwater turbulent front is still moving downstream. During this fourth stage of breaking, whitecaps are decreasing in size as entrained bubbles rise to the surface but spatial evolution of mixing continues [Rapp & Melville, 1990, Melville & Matusov, 2002].

This stage will not be detectable by either wavelet or similar analytical methods based on interpretation of surface elevation, or by means of whitecapping-oriented measurement approaches. Rapp & Melville [1990] used dye to investigate propagation of the injected turbulence following a breaking event. They found that the propagation of turbulent front continues for many wave periods, although at a much slower speed once the breaking wave has passed by. Horizontal extent L of the turbulent mixing reaches $kL \approx 5$ and the vertical extent D reaches $kD \approx -1$ where k is the wavenumber of breaking wave and positive values of the turbulent plume mean propagation forward and upward.

Rapp & Melville [1990] experiments were conducted with wave breaking caused by superposition of linear waves. Post-breaking dynamic effects and outputs of such breaking can be very different to those due to other breaking mechanisms, for example, due to breaking brought about as a result of non-linear modulation in the wave train or even due to superposition of non-linear waves. Therefore, it is actually not clear whether the residual stage is a general feature of wave breaking and will persist in case of breaking other than that caused by the linear superposition.

The residual-breaking process should be important for the upper-ocean mixing. As far as the wave field and air-sea boundary-layer interactions are concerned, however, the dynamic impact of the breaking event by this stage is already spent: the wave has already lost the associated momentum and energy to the turbulence and mean currents, the air bubbles have been injected under the surface and the droplets suspended into the air, flow-separation and other impacts on the atmospheric boundary layer are exhausted. The wave as such has already left the spot of the underwater turbulent front and even if there is interaction of surface waves with this enhanced sub-surface turbulence, it is subsequent waves in the wave train which are now involved.

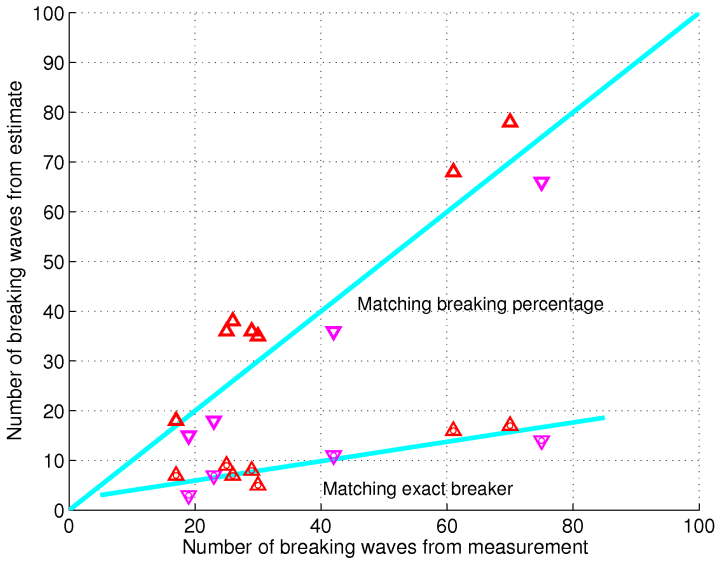

Fig. 2.4. Comparison of breaking-detection quantities obtained by means of the wavelet analysis (vertical scale) and observations of whitecaps (horizontal scale). The total breaking counts (by either of the methods) are designated with the open triangles and counts of perfect matchings are designated by the triangles with a circle inscribed inside. The Lake George finite-depth cases are shown by triangles with vertex points up, and the Black Sea deep-water cases are shown with triangular vertex points down. The two lines are the one-to-one correlation line (upper line) and the best linear fit to the exact-match data points (lower line).

2.4 Classification of the wave-breaking phases

Thus, following Liu & Babanin [2004] we classify the wave breaking process into four stages: incipient breaking, developing breaking, subsiding breaking and residual breaking. As discussed in Section 2.2 above, we expect both whitecapping-based breaking measurements and analytical approaches based on limiting breaking-onset criteria to detect the same breaking events only at the developing stage of the breaking phases. The incipient breakers, for example, will be detected by the wavelet method and will not be detected by the measurements, and the subsiding breakers, on the other hand, will be detected by the measurements whereas the wavelet method will fail to pick them up [Liu & Babanin, 2004].

Relative duration of the different breaking phases is not immediately clear, especially those of incipient and the subsiding phases as the least investigated. If the latter two phases are comparable in terms of duration, then the breaking count, i.e. total number of breakers detected on the basis of measurements and those obtained by the wavelet approach will be the same even though there will be no 100% match of waves indicated as breakers. This is checked in Figure 2.4.

Two kinds of counts are shown here: the total breaking counts are designated with the open triangles and counts of perfect matchings are designated by the triangles with a circle inscribed inside. The Lake George finite-depth cases are shown by triangles with vertex points up, and the Black Sea deep-water cases are shown with triangular vertex points down.

The straight line through the points of total breaking counts in the Figure is the one-to-one correlation line. The points follow the line with a 0.94 correlation coefficient and a 0.19 deviation index (DI) defined as

$$DI = \frac{1}{M} \sum \frac{|N_{wavelet} - N_{measured}|}{N_{measured}} \tag{2.2}$$

where M is the total number of records available and $N_{measured}$ and $N_{wavelet}$ are the breaking cases detected by the measurements and by the wavelet method respectively.

Thus, the wavelet method effectively predicts the same breaking statistics as the measurements, based on single-point observations of whitecaps or related acoustic noise. This implies that the incipient and the subsiding phases of the wave breaking have approximately the same relative duration.

The straight line through the triangles with circles is the best linear fit to the data. The data points are the number of perfect matchings we can really amass. In terms of percentages, the results range from a low of 16.7% to the high of 41.2% with an average of 28.4% of perfect matching cases. This outcome reveals the relative duration of the developing breaking phase where both analytical and observational methods are expected to detect the same events.

Slope of the lower line is nearly 1/3 of the total-count curve. The total count in fact only includes two phases (i.e. incipient breaking plus developing breaking in case of the wavelet method and developing breaking plus subsiding breaking in case of the whitecapping observations). This means that the second breaking stage lasts for approximately one half compared to either incipient or subsiding phases. Thus, the developing phase is the shortest (fastest) stage and only accounts for some 20% of the wave breaking (and even less if the residual stage is included). Note that our present interpretation of Figure 2.4 is somewhat different to the conclusions made by Liu & Babanin [2004].

As seen in Figure 2.4, there are small differences between wave-breaking detection, and therefore the breaking phases in deep water (Black Sea) and finite depth (Lake George). Wave breaking in finite depths does exhibit some peculiarities which will be discussed in Section 5 below. These peculiarities, however, are not of principal nature and here, quite likely, the minute differences observed are technical rather than physical.

Indeed, the wavelet analysis somewhat overestimates the total breaking percentage measured at Lake George and slightly underestimates that measured in the Black Sea compared to the one-to-one line. At Lake George, the acoustic method used only allowed to detect the dominant breakers in $\pm 30\%$ vicinity of the spectral peak [Babanin *et al.*, 2001], and therefore the wavelet method, whose performance is not limited by the spectral peak band, may have an extra number of breakers contributing into the total statistics. In the Black Sea, on the contrary, the breakers were detected visually and did not have an upper-frequency bound except that of physical capability of the observer to actually see small whitecaps. Therefore, the wavelet detection method may have failed for small breakers whose profile was not sampled well enough but whose whitecapping was detected by the observer, and this would lead to underestimation of the deep-sea breaking rates. Details of the experimental techniques are described in Section 3.

Another possible contributor into the observed deep-water – finite-depth variation can be actual physical dissimilarity in relative durations of the breaking phases in the two environments. Such dissimilarity, if exists, should be further investigated and cannot be addressed with certainty here. With some certainty, however, we can say that there appears no difference in duration of

the developing-breaking phase between the deep water and finite depths. At the lower line, the Black Sea and Lake George points are scattered evenly around which means that the second-phase duration does not depend on whether the breaking occurs in deep or in finite-depth water.

Relative duration of the fourth, residual breaking phase, with respect to the other three phases, is much longer. While the total duration of the first three breaking stages only accounts for a fraction of the wave period, the residual phase lasts for a number of wave periods (see Section 2.3 above). It is essentially a different, post-breaking process of dissipation of turbulence generated by the wave-breaking impact which occurred during the active phase of a breaking event.

2.5 Breaking probability (frequency of occurrence)

Breaking probability, or as it is often called breaking rates or frequency of breaking occurrence is one of the most important statistical characteristics of wave fields which contain the breaking events. Since the wave breaking is the main sink of energy in such fields, but not every wave is breaking, the breaking probability, together with the breaking severity (Section 2.7), provide the means of statistical description of the wave energy dissipation and other dynamic impacts caused by the breaking.

In order to achieve this description, understanding of distribution of the breaking probability, as well as the breaking severity, across the spectrum is needed. In other words, we need to be able to predict how frequently waves of different scales will break and how much energy they will loose in a breaking event. It is also most important to understand physics which controls the breaking rates and severity, and quantify and parameterise dependences of the breaking occurrence and severity on the wave-development and other environmental characteristics. These will be the main topics of Sections 5 and 6 below, and here we will suggest the main definitions.

Previous authors used various characteristics and parameters to describe breaking statistics or probabilities. Wu [1979] provided a summary of whitecap coverage statistics based on field observations by Monahan [1971] and Toba & Chaen [1973] who analysed photographs of the water surface. Longuet-Higgins & Smith [1983] detected 'jumps' in the rate of change of the elevation signal related to the passage of breaking crests. Weissman *et al.* [1984] analysed changes of spectral energy in the $18 - 32$ Hz frequency band to detect breaking events. Ding & Farmer [1994] used an array of four hydrophones to identify and track breaking waves and thus determine their duration, velocity, and spacing in terms of 'active acoustic coverage.' In his Loch Ness measurements, Thorpe [1992] associated large time derivatives of the signal strength in sonograph records with the occurrence of breaking wave crests. Gemmrich & Farmer [1999] detected breaking waves from a buoy on the basis of air entrainment within breaking waves measured by changes in the electrical conductivity of the water at fixed depths just below the water surface.

More details on the measurements of breaking probability and statistics will be provided in Section 3 below. It is evident that there are empirical thresholds underlying most of these methods and there is no standardisation amongst them. Besides, in terms of breaking rates some of the statistics appear ambiguous. The same whitecap coverage, for example, can be achieved at different frequencies of occurrence of breaking events, depending on whether the events (waves) are large or small and whether the severity is strong or weak.

Here, following Babanin [1995], Banner *et al.* [2000], Babanin *et al.* [2001] we define the breaking probability b_T for the dominant waves as the mean passage rate past a fixed point of

dominant wave breaking events per dominant wave period T_d or, in other words, the percentage of number of breaking crests n within the sequence of N wave crests:

$$b_T = \frac{nT_d}{t} = \frac{n}{N} \tag{2.3}$$

where $t = NT_d$ is duration of wave record. Another definition of the breaking probability for dominant waves is also possible (2.35), and is in fact of a greater practical significance, but it will be introduced and justified in Section 2.7 because its meaning cannot be fully appreciated before the issues of breaking strength are discussed.

The nondimensional quantity b_T is expressed in terms of the main temporal scale of the wave field, making it convenient for comparisons and analysis. The definition, however, is not as simple as it first seems. Due to the continuous-spectrum nature of the wind-generated waves, even the notion of dominant waves needs a clarification. Yet alone, ambiguous will be any spectral distribution of breaking rates defined this way, i.e. $b_T(f)$ dependence on frequency f:

$$b_T(f) = \frac{n(f)T}{t} = \frac{n(f)}{N(f)}. \tag{2.4}$$

Indeed, count of crests of waves of exact specific period $T = 1/f$ makes no physical sense as such count will return zero value.

Therefore, any spectral characteristic of the breaking probability $b_T(f)$, including breaking of dominant waves with peak frequency f_p, from the very beginning implies use of a spectral band $f \pm \Delta f$ such that wave crests with frequencies (periods) within this band, i.e. individual waves with frequencies of

$$f - \Delta f \le f \le f + \Delta f \tag{2.5}$$

can be counted. In Banner *et al.* [2000], Babanin *et al.* [2001], the dominant waves were assumed to have frequencies within $\pm 30\%$ vicinity of the spectral peak, i.e.

$$f = f_p \pm \Delta f_p = f_p \pm 0.3 f_p, \tag{2.6}$$

following the width of the peak enhancement region of the JONSWAP formulation for the frequency spectrum $F(f)$ [Hasselmann *et al.*, 1973]:

$$F(f) = \alpha g^2 (2\pi)^{-4} f^{-5} \exp\left[-\frac{5}{4}\left(\frac{f}{f_p}\right)^{-4}\right] \cdot \gamma^{\exp\left[-\frac{(f-f_p)^2}{2\sigma^2 f_p^2}\right]}. \tag{2.7}$$

Here, α is the level of equilibrium interval (tail) of the spectrum, g is gravitational constant, γ is the peak enhancement factor, and σ is the width of spectral peak. In the original JONSWAP formulation, γ, the right width σ_{right} and left width σ_{left} were chosen constant, but in reality α, σ and γ depend on wave development stage and in general vary very significantly [e.g. Donelan *et al.*, 1985, Babanin & Soloviev, 1998a].

Based on comparisons of the count for dominant breaking conducted by two independent acoustic techniques, the dominant frequency band was later reassigned as

$$\Delta f_p = \pm 0.35 f_p \tag{2.8}$$

[Manasseh *et al.*, 2006]. Other frequency bands, such as $\Delta f = \pm 10\%$ are also often employed [e.g. Banner *et al.*, 2002, Babanin & Young, 2005, Manasseh *et al.*, 2006, Babanin *et al.*, 2007c]. This narrower band is usually needed when breaking probabilities are defined for frequencies other than the spectral peak. Away from the peak, the spectral density decays very rapidly which would make count of the crests and relative importance of the breaking waves very uncertain if the spectral band was too broad.

Is there a physical meaning for the spectral band implied in the breaking-probability definition (2.3)-(2.5)? For the dominant waves, such physical meaning can be certainly pointed out. That is, the width of the spectral peak defines characteristics of the groups of dominant waves, and the wave-breaking frequency of occurrence depends on this groupiness.

Indeed, for a narrow-banded spectrum, which the spectral peak of wind-generated waves is, the width of the peak is related to modulational properties in the train of dominant waves. This relation was investigated by Longuet-Higgins [1984] by statistical means. He suggested nondimensional bandwidth parameter ν to describe such modulational properties:

$$\nu^2 = \frac{m_2 m_0}{m_1^2} - 1 \tag{2.9}$$

where m_i is the spectral moment of order i and in general case is defined as

$$m_i = \int_0^\infty f^i F(f) df. \tag{2.10}$$

Longuet-Higgins [1984] found that integral limits in (2.10) have to be set to

$$\Delta f_p = \pm 0.5 f_p \tag{2.11}$$

in order to explain experimentally observed properties of wave groups. This limit is somewhat larger than the width of the JONSWAP peak enhancement or the $\Delta f = \pm 30 - 35\%$ in the breaking statistics of dominant waves, but it is a reasonably close value.

Once they exist, the groups of dominant waves have a verified association with the breaking probability. Donelan *et al.* [1972] reported observing up to several consecutive waves breaking at the peak of the group envelope before sufficient energy was lost from the group. In another open-ocean study, Holthuijsen & Herbers [1986] found a significant influence of wave groups on the wave breaking. When breaking occurred, the position of the first breaker in a group was slightly ahead of the centre of the group. They concluded that the overall fraction of breaking occurring within wave groups was close to 70%.

Support to the connection between frequency bandwidth, wave groups and breaking occurrence also comes from hydrodynamic, rather than just statistical studies of modulational instabilities of wave trains. Theoretical approaches, started by Zakharov [1966, 1967], Benjamin & Feir [1967], Longuet-Higgins & Cokelet [1978] (see Yuen & Lake [1982] for an essential review, but the progress on this topic is continuing), numerical models [e.g. Dold & Peregrine, 1986, Chalikov & Sheinin, 1998, 2005] and laboratory experiments [e.g. Babanin *et al.*, 2007b, 2009a,b, Shemer *et al.*, 2007] all point out that conditions for the onset of breaking, i.e. a very steep individual wave can result from evolution of non-linear wave groups. Initial conditions for such evolution consist of steep monochromatic waves with sidebands, i.e. also involve some characteristic bandwidth defined by the sidebands.

Interpretation of applicability of this kind of modulational instabilities to field waves, however, is at present an essentially blur area and has to be done with caution. First of all, the field waves have a continuous spectrum and therefore the notion of primary waves and sidebands is uncertain: waves at every frequency can be treated as both primary waves and sideband disturbances. There have been attempts to draw analogies between the monochromatic wave trains with sidebands and spectral waves. It has been shown [Onorato *et al.*, 2001, Janssen, 2003] that the modulational properties in a spectral system of non-linear waves depend on the ratio of wave steepness $\epsilon = ak_0$ to spectral bandwidth $\Delta\omega/\omega_0$, where k_0 and ω_0 are some characteristic wavenumber and radian frequency respectively ($\omega = 2\pi f$), a is the mean amplitude at this wavenumber and $\Delta\omega$ is a characteristic width of the spectral peak:

$$M_I = \frac{\epsilon}{\Delta\omega/\omega_0}. \tag{2.12}$$

This same ratio, if properties of primary wave and sidebands are used, was shown important in the original studies of instabilities of weakly modulated trains of monochromatic carrier waves of small amplitudes. Here, we will denote this ratio as M_I (Modulational Index). Physical applicability and interpretation of the analogy, however, is still a subject of debate. Note that even if applicable in case of continuous spectrum, definition (2.12) has physical meaning for the modulational properties of dominant waves only, as there are no characteristic k_0, ω_0 and $\Delta\omega$ away from the spectral peak.

The second major uncertainty is the essentially two-dimensional nature of the hyrdrodynamic modulational instabilities discussed. The theories, numerical simulations and laboratory experiments mentioned above are two-dimensional or quasi-two-dimensional. And what is certainly against direct extrapolation of outcomes of these studies into field conditions is the known experimental and theoretical results on limitations which the non-linear modulational mechanism has in broad-band, and particularly in three-dimensional fields [e.g. Brown & Jensen, 2001, Onorato *et al.*, 2002, 2009a,b, Waseda *et al.*, 2009a]. In particular, Waseda *et al.* [2009a] demonstrated that for a typical directional spread of wind waves the modulational mechanism is ineffective. This will be further discussed in Section 5.4.

Thus, a concrete physical mechanism (or a number of mechanisms) which connect the breaking probability of dominant waves with the bandwidth in the definition (2.3), (2.8) is not fully certain, but links between the breaking rates and the wave groups, and therefore the breaking rates and the spectral-peak bandwidth, are apparent. This is not the case, however, with the bandwidths of spectral bins other than the spectral peak in (2.4), (2.5). Wave process at those scales is not narrow-banded, and therefore the artificially imposed bandwidths have no meaning in terms of wave groups and modulation of wave trains of respective scales. While the choice of the bandwidths for higher-frequency parts of the spectrum $F(f)$ is usually done by analogy with the spectral-peak region, the physical analogy is not applicable in this case, and therefore defining the breaking probabilities in the same terms appears to be a matter of convenience rather than physics [see Babanin & Young, 2005, Babanin *et al.*, 2007c, for a discussion of differences of physics of breaking at the spectral peak and in the higher-frequency region]. These issues will be discussed in more detail in Sections 5.3.1 and 5.3.2.

Another potential complication of the definitions (2.3)-(2.5) has to also be clearly stated. When breaking probabilities according to these definitions are estimated experimentally, the numbers of wave crests are counted. For each determined breaker, the frequency f (period

T) of the wave is also extracted, by zero-crossing analysis [e.g. Manasseh *et al.*, 2006], riding wave removal method [Schulz, 2009] or by some other means. Thus the total number of breaking waves $n(f)$ is found for each frequency. The total number of expected waves at a frequency is

$$N(f) = t/T = t \cdot f \tag{2.13}$$

and expressions (2.3)-(2.4) can then be used. As discussed in this Section above, in practice, in order to obtain $n(f)$ and $b_T(f)$, the wave frequencies are effectively discretised into bands $f \pm \Delta f$ (2.5) because $n(f)$ and $b_T(f)$ are not spectral densities but statistical quantities, and there are no exact matches between measured wave periods and a given $T = 1/f$.

It is clear, however, that if the waves of any given period $T = 1/f$ are counted by the zero-crossings or other means in a wave record of duration t, the resulting count $N_c(f)$ will be less than the nominal reference count $N(f)$ given by (2.13), because in real seas, waves of periods different to $1/f$ will occupy some part of the duration t. In terms of the breaking-probability definition, it would not matter if the ratio $N_c(f)/N(f)$ were constant across the frequency and therefore the crest count were simply proportional to the reference count. This is, however, not the case.

Banner *et al.* [2002] demonstrated that if the bandwidth $\Delta f = \pm 0.3 f_c$ were chosen for a central frequency f_c in their experiment, $N_c(f)/N(f)$ was about 0.65 at the spectral peak ($f_c = f_p$) and gradually decreased for higher frequencies ($f_c > f_p$), asymptoting to 0.2 at $f_c/f_p > 2$. The ratio also depended on the choice of bandwidth, i.e. it would be different, for example, for $\Delta f = \pm 0.1 f_c$. Therefore, to avoid this additional ambiguity, the breaking probability b_T used in the present paper will be based on the reference count (2.13) rather than on actual count of total number of wave crests in each frequency bin, unless stated otherwise.

2.6 Dispersion relationship

Dispersion relationship, that is the relationship between the temporal (wave period/frequency) and spatial (wavelength/wavenumber) scales is a general property of surface water waves rather than a wave-breaking characteristic. It has to be introduced among definitions here, however, because it will be frequently mentioned and used throughout this paper in the wave-breaking context.

In a general case of a weakly non-linear deep-water unidirectional modulated wave train, it can be written as

$$\omega^2 = gk\left(1 + \frac{1}{2}a^2k^2 + \frac{a_{xx}}{8k^2a}\right)^2 \tag{2.14}$$

[e.g. Yuen & Lake, 1982]. In deriving (2.14), the steepness $\epsilon = ak$ (1.1) was assumed a small parameter, and therefore subsequent perturbation terms of higher orders of ϵ are not shown. The last term in (2.14), where a_{xx} is the second derivative of wave amplitude a with respect to spatial coordinate x, comes from assuming wave frequency, wavenumber and amplitude being slowly varying functions in space and time. It is only relevant for non-linearly modulated wave trains and is usually omitted. The first term on the right characterises linear frequency dispersion of surface waves, and the second term describes non-linear correction to the dispersion due to finite amplitude.

For wave trains with constant frequency, wavenumber and amplitude, the phase speed c is

$$c = \frac{\lambda}{T} = \frac{\omega}{k} = \sqrt{\frac{g}{k}(1 + \frac{1}{2}a^2k^2)}. \tag{2.15}$$

When waves can be treated linear, that is their steepness (1.1) is small

$$\epsilon = ak \to 0, \tag{2.16}$$

then linear dispersion relationship is simply

$$\omega^2 = gk \tag{2.17}$$

and linear phase speed is

$$c = \sqrt{\frac{g}{k}} = \frac{g}{\omega}. \tag{2.18}$$

As seen in (2.18), even linear waves with different frequencies/wavenumbers propagate with different phase speeds. For the non-linear waves, their phase speed (2.15) additionally depends on wave amplitude/steepness. These properties of surface waves are broadly used in wave-breaking experimental techniques to achieve frequency or amplitude focusing of waves of different scales at a particular point in space/time in order to make such wave break.

Phase speed $c(\omega)$ of waves is different to the group velocity $c_g(\omega)$ which characterises the speed of propagation of wave energy. The difference is significant, and for linear waves in the deep water the ratio is

$$c_g = \frac{d\omega}{dk} = \frac{1}{2}\sqrt{\frac{g}{k}} = \frac{1}{2}c = \frac{1}{2}\frac{g}{\omega}. \tag{2.19}$$

Group velocity is another most important characteristic to be employed in the wave-breaking studies as it describes speed of wave envelopes (groups). The dominant waves exist as wave groups whose elevation envelope decays away from the peak magnitude close to the centre of the group. Thus, the individual waves propagate through the group at the relative speed $\frac{1}{2}c$ and correspondingly change their height as they propagate. Close to the centre of the group their height/steepness is largest, and that is where they most frequently break.

2.7 Breaking severity

Breaking severity is another most important characteristic of the wave breaking. As the breaking severity, or the breaking strength, we mean amount of energy lost in an individual breaking event. Here, we will be interested in defining this property in such a way that, together with the breaking probability from Section 2.5, they will determine the wave energy dissipation rate. This way, if both the breaking probability and breaking severity can me measured experimentally, whitecapping dissipation can be estimated experimentally including spectral distribution of the dissipation. So far, the spectral dissipation functions employed in wave models remain, to a large extent, are speculative formulations.

Note that in the case of breaking severity a breaking event does not comprise a breaking wave only, but rather the wave group which the breaking waves are propagating through. Such details

will be discussed in the current Section below. Like with the breaking probabilities in Section 2.5, however, there are further uncertainties even within such a simple and general definition. In case of the breaking severity, these uncertainties are even deeper due to the fact that this property has received far less attention, and the energy loss in the course of breaking is a much less studied process compared to the phenomena leading to the breaking occurrence.

Difficulties in studying the breaking severity are indeed serious. While hydrodynamic theories, even such simplified versions of them as those based on irrotational wave motion and assumptions of small initial amplitudes and disturbances, can be employed to investigate the probability of a breaking onset to some extent, those are clearly not applicable once the onset happens. Yet alone no such theories can describe in detail the process of the wave collapse and associated energy loss to generation of turbulence, entraining the air bubbles and pockets into the water and emitting spray into the air. In absence of the theory, the numerical modelling of the breaking strength suffers obvious limitations too. With no explicit theory to model, it can only resort to indirect parameterisations.

Thus, applications which involve the breaking severity have to rely on experimental data. These are quite sparse and difficult to obtain too, and the difficulties are many. Most importantly, in order to estimate the loss of energy, contact measurements are usually needed. That is, at the very least, the wave energy loss has to be estimated by a direct measurement immediately before and immediately after a breaking event. This is a complicated exercise even in laboratory because involves a controlled breaking at a particular location, between the wave probes.

While possible in principle [e.g. Pierson *et al.*, 1992, Rapp & Melville, 1990, Meza *et al.*, 2000, Manasseh *et al.*, 2006, Babanin *et al.*, 2007a, 2009a,b], the controlled-breaking approach has many limitations. First of all, the controlled breaking is often achieved by artificial means, for instance through focusing many linear waves of different scales by using their different phase speeds. It is quite likely that this is not the way, or at least not the only way which controls the breaking in general and the breaking severity in particular in natural environments [Babanin *et al.*, 2009a,b]. Second, keeping the controlled breaking between two particular probes significantly limits variety of wave properties and environmental dependences which can be investigated. And finally, some processes leading to the wave breaking, and in particular the most important mechanism of modulational instability of non-linear waves trains, are impaired in three-dimensional natural field circumstances, which fact further depletes the generality of conclusions achieved in two-dimensional wave tanks. See Section 6 below for more details.

In the field, estimating the breaking strength by means of measuring wave breaking events before and after a breaking is a challenge. The breaking is random, sporadic and infrequent, and probability of it to start and end between two deployed wave gauges is very low. To achieve this, long measurement series would have to be taken by an extensive spatial array of wave probes, concurrent with detailed monitoring and recording of information on wave breaking, i.e. the start, the end and the direction of propagation of the breaking waves through the array. Depending on the instrumentation employed, a significant complication of contact in situ measurements is the destructive power of wave breaking which can damage the equipment, particularly as the most interesting are the most severe breaking events.

While many remote-sensing techniques have been developed to investigate the wave breaking, these are mostly intended on detecting the breaking events and measuring the breaking probabilities rather than the energy losses (see Section 3.6 below). In this regard, the bubble-detection method of Manasseh *et al.* [2006] is a significant promise. Size of the bubbles formed

in the course of breaking can be determined by passive acoustic means, i.e. virtually by listening to the noise produced by a breaking wave and quantifying characteristics of this noise. Essentially, the bubble size appears to be connected to the strength of the breaking. Thus, the new acoustic technique, once it is fully validated and calibrated, has a potential to allow the measurements of the breaking severity by means of underwater hydrophones. The hydrophones are very small and easy to deploy devices, they are cheap and therefore cost-effective even in case of their loss in a field experiment. Their power consumption is low which would allow long-term deployments and observations with power supply based on batteries. Also importantly, because the sound attenuation in the water is relatively low, the hydrophones can be deployed well below the surface, even at the bottom in case of finite-depth field sites, and thus avoid the destructive impact of wave-breaking events [see Babanin *et al.*, 2001, Young *et al.*, 2005, Manasseh *et al.*, 2006].

In the meantime, reliable and comprehensive understanding of the breaking severity is the principal issue for all applications which involve dissipation of wave energy, and thus range from engineering problems to the general topics of air-sea interaction, extending as far as climate modelling. Indeed, in order to estimate the rate of energy loss from the wave field, whether it is then converted into energy of impact on engineering structures or into mixing of the upper ocean, it is necessary to know how frequently the waves break and how much energy they loose in a breaking event. If we denote the breaking severity, i.e. the mean energy loss due to breaking of waves of particular scale f as $E_s(f)$, then the amount of energy dissipated per wave crest at this scale $D(f)$ is:

$$D(f) = b_T(f)E_s(f). \tag{2.20}$$

In terms of the spectral dissipation function S_{ds} employed in the wave forecast models, the dissipation rates per unit of time are:

$$S_{ds}(f) = \frac{n(f)E_s(f)}{t} = \frac{D(f)}{T}. \tag{2.21}$$

This practical definition can be used to estimate the spectral distribution of dissipation by experimental means [Manasseh *et al.*, 2006, Babanin *et al.*, 2007c]. It has, however, the same obvious issues with the spectral band (2.5), as does the practical definition of the breaking probability in Section 2.5 above, because, again, $n(f)$ and $E_s(f)$ in the right-hand side are not spectral densities but are statistical quantities.

Since the normalised (by $\rho_w g/8$, ρ_w - density of water) potential wave energy per unit of area can be expressed in terms of the wave height $H(f)$ as

$$E(f) = H(f)^2, \tag{2.22}$$

then, for generality and for parameterisation purposes, it is convenient to represent the severity in nondimensional terms as a fraction s of this energy which is lost to the breaking:

$$E_s(f) = s(f)E(f) = s(f)H(f)^2, \tag{2.23}$$

that is

$$S_{ds}(f) = \frac{s(f)n(f)H(f)^2}{t}. \tag{2.24}$$

In linear waves, kinetic energy $Q(f)$

$$Q(f) = u(f)^2 + w(f)^2 \tag{2.25}$$

equals potential energy (2.22) (here, u and w are horizontal and vertical components of the surface orbital velocity respectively), and the total energy can be easily estimated. In strongly non-linear waves, this is not true and therefore (2.22)-(2.24) and further expressions in terms of wave height H should be applied to wave trains measured before and after the rapid transient processes of the breaking as such occur. This is how experiments intended for measuring the breaking severity are usually designed [e.g. Rapp & Melville, 1990, Manasseh *et al.*, 2006, Babanin *et al.*, 2009a,b], but to avoid ambiguity this should be mentioned explicitly.

The severity coefficient s, or simply breaking severity or breaking strength hereinafter, is often treated as a fixed fraction, for instance

$$s = 50\% \tag{2.26}$$

of the energy which a wave had before the breaking (this is approximately the estimate which was obtained, for example, in laboratory experiments by Xu *et al.* [1986]). Such estimate, however, is not general due to four main reasons, and resulting deviations from this mean estimate can be enormous.

The first reason is the cause of the wave breaking, or in other words the means by which the wave breaking was achieved in the laboratory. These means are quite many. For example, the waves can be made breaking by an artificial obstacle or a submerged shoal, and this is a robust practical way to investigate relevant wave-breaking properties and phenomena [e.g. Manasseh *et al.*, 2006, Calabresea *et al.*, 2008]. If natural deep-water processes leading to the breaking are simulated, there is still a variety of possibilities: superposition of linear waves achieved through use of frequency dispersion [e.g. Longuet-Higgins, 1974, Rapp & Melville, 1990, Meza *et al.*, 2000, see (2.17)], superposition of non-linear waves through amplitude dispersion [e.g. Donelan, 1978, Pierson *et al.*, 1992, (see 2.14)], evolution of non-linear wave groups [e.g. Melville, 1982, Babanin *et al.*, 2007a, 2009a,b]. The latter evolution to the breaking will exhibit essentially different characteristics in directional wave fields [Onorato *et al.*, 2009a,b, Waseda *et al.*, 2009a]. In case of the wind forcing, wave breaking may be affected, and this effect is of principal significance as far as the breaking strength is concerned [Babanin *et al.*, 2009a]. Wave breaking and severity of short spectral waves to a large extent is caused or at least is impacted by the effects brought about by longer waves [e.g. Donelan, 2001, Babanin & Young, 2005, Babanin *et al.*, 2007c]. Breaking of the laboratory waves can as well be made random if the waves are, for example, wind-generated [e.g. Xu *et al.*, 1986, Hwang *et al.*, 1989], in which case physical mechanism leading to the breaking is one of the above or a combination of them.

Whatever laboratory practice is chosen, the breaking severity can now be estimated. Relevant differences between the estimates due to the different breaking mechanisms, however, appear to be of a very essential nature [Babanin *et al.*, 2009a,b] which places the notion of roughly constant breaking strength in serious doubt. How applicable this notion in the field is another very important question. The field breaking is a combination of the various mechanisms, although some may prove less frequent and less significant, and the linear superposition is likely to be among the latter [Babanin *et al.*, 2009a,b]. In any case, breaking severity seen in Figure 2.3, based on the Black Sea measurements, is very different from the 50%. In this Figure, waves

displaying whitecapping, i.e. breaking waves are shown squared for the spectral-peak frequency band. Their steepness ranges from $\epsilon = ak = 0.27$ down to $ak = 0.03$. If the ratio signifies the loss of wave height in the course of breaking, then it amounts to 9 times and translates into energy loss

$$\frac{E_{after}}{E_{before}} = \frac{\epsilon^2_{after}}{\epsilon^2_{before}} = 0.012 \tag{2.27}$$

or, according to (2.22),

$$E_s = H^2_{before} - H^2_{after} = \frac{4}{k^2}(\epsilon^2_{before} - \epsilon^2_{after}) = 0.988 H^2_{before}. \tag{2.28}$$

If, however, at the breaking onset the steepness was even higher (i.e. $ak = \frac{H}{2}k = 0.44$ as it was measured by Brown & Jensen [2001] for the linear-superposition breaking and by Babanin *et al.* [2007a] for the modulational-instability breaking), then the energy loss is even greater:

$$E_s = H^2_{before} - H^2_{after} = 0.995 H^2_{before}. \tag{2.29}$$

Above, E_{before}, ϵ_{before}, H_{before} are respectively the wave energy, wave steepness and wave height immediately before the breaking, and E_{after}, ϵ_{after}, H_{after} immediately after breaking correspondingly.

Estimates (2.27)-(2.29) should be treated with some caution because the wavelength somewhat changes in the course of breaking [e.g. Babanin *et al.*, 2007a, 2009a,b] and therefore the change of steepness ϵ in (2.27)-(2.29) depends on the change of wavenumber k too, not only on the reduction of the wave amplitude a. Besides, as mentioned above, expression for the total wave energy in terms of wave height (2.22) is strictly valid for linear waves and can be biased in case of strongly non-linear waves which the breakers are. In any case, however, the breaking strength exhibited by an individual wave in the Black Sea is more like

$$s = 99\% \tag{2.30}$$

rather than 50% in the laboratory experiment (2.26).

This brings us to the second reason of why the (2.26)-like constant-fraction estimate of the severity coefficient s for a single breaking event should not be general. While in laboratory, wave-energy (2.23) can be treated in terms of a single wave which was breaking, in the field the change of wave height of an individual wave is an ambiguous property. As was mentioned in Section 2.6, the dominant waves exist as wave groups, and the individual waves propagate through the group at the relative speed $\frac{1}{2}c$ and correspondingly change their height as they propagate.

Dominant waves usually break close to the peak of the group envelope [e.g. Donelan *et al.*, 1972, Holthuijsen & Herbers, 1986]. This means that once a wave started breaking at the top of a group, its height is decreasing due to both the breaking and its moving towards the front face of the group. The latter reduction would occur regardless the fact whether the wave was breaking or not.

Since the active phase of wave breaking lasts a fraction of wave period [e.g. Rapp & Melville, 1990, Babanin *et al.*, 2009a], and the wave group typically consists of 7-10 waves [e.g. Longuet-Higgins, 1984], then a wave propagating at the relative speed $\frac{1}{2}c$ will start and finish the breaking

within the group. It is logical and more accurate, therefore, to estimate the breaking strength in terms of the group breaking severity s_g, by integrating the wave energy loss over the group:

$$E_{sg} = s_g \frac{8}{\lambda_g} \int_0^{\lambda_g} \eta(x)^2 dx. \tag{2.31}$$

Here, E_{sg} is the energy loss from the entire group, λ_g is length of the group, and the surface elevations $\eta(x)$ are integrated along the distance x within the group before the breaking started. The factor of 8 is included in order to have the wave energy expressed in terms of wave height H, rather than amplitude a, for consistency with definitions (2.22)-(2.29). Note that there is no frequency scale f explicitly mentioned here, because the wave grouping is a property of dominant waves only. Therefore, in the spectral sense definition (2.31) is applicable to the frequency band of the spectral peak which is according to (2.5)-(2.8), (2.11) is in the range $\Delta f_p = \pm(0.3 - 0.5)$.

With such definition, the whitecapping dissipation function should be estimated as

$$S_{ds} = \frac{n_{group} E_{sg}}{t}, \tag{2.32}$$

where n_{group} means count of wave groups where a breaking occurred. Values of severity s_g estimated this way will be essentially lower than the severity measured for individual waves because the energy loss effect is smeared over all waves in the group. They can approximately be related to the severity s through the number n_g of waves in the group:

$$s = n_g s_g. \tag{2.33}$$

Count n_{group} is different to the count n of breaking waves in (2.4) and (2.21) because typically more than one individual wave break within a wave group in close proximity in time and space [e.g. Donelan *et al.*, 1972, Babanin *et al.*, 2009a,b, among many others]. As have already been mentioned, field observations of Donelan *et al.* [1972] revealed up to several consecutive waves breaking at the peak of the group envelope. This was interpreted in a quasi-linear sense: that is, subsequent waves propagate with their phase speeds within the group according to (2.19), exceed a limiting height/steepness as they approach the peak of the group, and keep breaking until sufficient energy is lost from the group. Babanin *et al.* [2009a,b], in a laboratory experiment with two-dimensional wave breaking due to modulational instability, found that number of one-after-another breaking waves in wave group can be one or more, depending also on the wind forcing and breaking severity. They showed that subsequently-breaking waves are strongly coupled if the breaking strength is large enough.

Therefore, subsequent breaking of a number of waves on the top of the wave group is effectively a single breaking event in the dynamics of groups. Although different individual waves are breaking, they cannot be separated in order to measure the wave-group energy loss (2.31) for each of the breakers. Thus, the typical scenario for a breaking event is

$$\begin{aligned} n_{group} &= 1, \\ n &\geq 1. \end{aligned} \tag{2.34}$$

In this regard, it is helpful to introduce a group breaking probability b_{Tg} in terms of a relative number of wave groups containing one or more breaking waves coupled in such a way that they can be treated as a single breaking event:

$$b_{Tg} = \frac{n_{group} T_g}{t} = \frac{n_{group}}{N_{group}} \tag{2.35}$$

where T_g is period of the wave group, N_{group} is the total number of wave groups in wave record.

These issues of individual waves breaking within the group can be illustrated by means of Figures 6.2 and 6.3 of Section 6. Starting from Figure 6.3, we can see what happens with waves propagating through the group without breaking or with a gentle breaking. The time series are compared immediately before (solid line) and immediately after the breaking (dashed line). Breaking of the four incipient breakers (highest waves in each solid-lined wave group) started and ended between the two probes. The breaking was very gentle when visually observed and the wave following this gentle incipient breaker did not break. The time necessary to travel the distance between the two probes was estimates as 1.04 s and therefore the dash-lined record was shifted back by 1.04 s in order to superpose the two wave trains.

As mentioned above, the individual waves and the group propagate with different speeds. In case of deep-water waves of 1.5 Hz frequency shown in Figure 6.3, and in a close-to-linear scenario, according to (2.19) the relative speed of wave propagation within the group is $c_{relative} = 0.52$ m/s and relative position of a wave over 1.04 s will be shifted by 0.5 m. This is comparable with one wave length of such waves $\lambda = 0.69$ m. That is, in absence of breaking, each wave would approximately move one position ahead, and the highest wave in the solid-lined group would become the second highest (in front of it) in the dash-lined group. Because of this, height of the highest wave would be significantly reduced without any breaking.

Since a breaking occurred, the pattern is more complicated. The breaking was quite gentle visually, and indeed its impact on the individual wave which broke (now the second wave in each dash-lined group) is not that large. It is quite significant, however, over the entire group due to, obviously, non-linear coupling between different waves in the course of the breaking event. Other details of such breaking impact will be discussed in Section 6, and here we would like to highlight the fact discussed above: that is, in case of wave breaking within a wave-group structure, estimating the breaking strength in terms of measurements of the breaking wave only is ambiguous and even misleading.

Even more so, this is valid for a strong breaking, when two or more subsequent waves break one after another. This is demonstrated in Figure 6.2. Again, wave series immediately before and after the breaking are compared. Breaking of the three incipient breakers seen in the solid-lined wave train happened (started and finished) between the two probes. The wave which is seen following the incipient breaker at the second probe also broke between the two probes. These breakings happened in a period of 1.2 s, the time required by the waves to travel the distance between the probes. Therefore, the dash-lined record is time-shifted by 1.2 s in an attempt to superimpose the two wave trains.

Now that a strong breaking has occurred, the correlation between the two time series is quite poor. The incipient breaker and wave following it practically disappeared, as well as the entire modulation. The number of waves in the segment has also changed. This is a collapse of the wave group which from this point in time and space should restart its evolution in hydrodynamic terms, from the new initial conditions. Again, further details will be examined in Section 6, but it is apparent that the severity can only be estimated in terms of the wave group (2.31) rather than in terms of individual waves.

The third reason for the (2.26)-like constant-fraction estimates of the severity coefficient s being not general is influences of various environmental conditions in real wave fields. Ocean waves are directional (i.e. three-dimensional), wind-forced and experience many sorts of interactions with background currents, turbulence and other phenomena which may affect the breaking

strength, with or without alterations of the breaking probability. For example, Babanin *et al.* [2009a,b] demonstrated that presence of the wind increases the breaking probability due to modulational instability of non-linear wave groups, but decreases the breaking severity. The reduction extends to the severity becoming virtually zero at reasonably strong wind forcing, which effectively means that the wind may essentially impair or even erase the breaking caused by the evolution of wave groups. Thus, both breaking probability and breaking severity become functions of the wind forcing, with opposite trends, and such fact will affect the breaking dissipation (2.24) and (2.32) in a way which is hard to predict at this stage:

$$\begin{aligned} b_T &= b_T(U/c), \\ s &= s(U/c). \end{aligned} \tag{2.36}$$

Here, U is some characteristic wind speed, and therefore ratio U/c describes the wind forcing, that is how fast is the wind with respect to the phase speed of waves c. In any case, the notion of roughly constant breaking severity is absolutely inapplicable is such scenario.

And the fourth reason to be highlighted is the spectral nature of breaking severity in real wave fields. Except for the case of pure swell which do not break anyway, the ocean waves have a continuous spectrum extending to higher and lower frequencies, and often having multiple peaks. And in the realistic spectral environment, it is quite rare that a physical process is limited to a particular frequency or wavelength scale and does not have an impact across the spectrum. This is certainly true with respect to such strongly non-linear processes which determine the breaking severity.

An example of spectral distribution of the breaking severity is demonstrated in Figure 6.1. In Figure 6.1a, spectra of the time series of Figure 6.2 are plotted: solid line is the pre-breaking spectrum and dashed line is the after-breaking spectrum. Figure 6.1b is the ratio of the two spectra.

Even though the laboratory waves were generated monochromatic, they are now strongly non-linear and the 1st, 2nd and 3rd harmonics are clearly visible in their spectra, indicated by the vertical solid lines (again, solid lines correspond to the pre-breaking state and the dashed lines are close to the after-breaking state). The breaking severity effect (the ratio in Figure 6.1b) is distinctly spectral. While it is the main wave which is breaking (around frequency of 2 Hz at the pre-breaking), the energy is lost from all the harmonics as well. In both absolute and relative terms, most of the loss came from the peak which was reduced by a factor of 5. With the exception of the second harmonic (reduced and shifted to 3.6 Hz), the other harmonics have almost completely disappeared. For frequencies above the spectral peak, the average ratio is approximately 1.7. Across the entire range of relevant frequencies, from the peak up to 11 Hz, the average ratio is 1.8 which translates into a total spectral loss of $s_{spectral} = 45\%$. Here, spectral severity is defined as

$$\begin{aligned} 16E_{s_{spectral}} &= 16\int_0^\infty F_{before}(f)df - 16\int_0^\infty F_{after}(f)df \\ &= s_{spectral}16\int_0^\infty F_{before}(f)df \end{aligned} \tag{2.37}$$

where $E_{s_{spectral}}$ is the energy loss across the entire spectrum, $F_{before}(f)$ and $F_{after}(f)$ are wave frequency spectra before and after the breaking event. The factor of 16 is introduced for

consistency, as by definition the significant wave height H_s is

$$H_s = 4\sqrt{m_0} = 4\sqrt{\int_0^\infty F(f)df}. \tag{2.38}$$

This way, the energy in (2.37) is expressed in terms of wave height, like in (2.22)-(2.31).

In case of spectrum being estimated over a single wave group, or in circumstances when breaking occurs in every wave group like in dedicated laboratory experiments [e.g. Babanin *et al.*, 2009a,b],

$$s_{spectral} = s_{group}. \tag{2.39}$$

Otherwise,

$$s_{spectral} = \frac{n_{group}}{N_{group}} s_{group}. \tag{2.40}$$

In case of field waves, because wave groups at scales other than the spectral peak cannot be identified, definitions (2.39)-(2.40) are only relevant for the breaking of dominant waves.

Apart from the mere energy loss, downshift of the spectral energy also occurred in Figure 6.1, and the peak frequency moved from 2 Hz to less than 1.8 Hz. Both the spectral downshift in the course of breaking [e.g. Tulin & Waseda, 1999] and the spectral distribution of the energy loss due to a breaking [e.g. Pierson *et al.*, 1992, Meza *et al.*, 2000] have been reported in a number of other studies. The latter two papers, however, provide an account for the spectral pattern of the breaking severity quite different both to Figure 6.1 [i.e. Babanin *et al.*, 2009a,b] and to each other.

Meza *et al.* [2000], who studied the dissipation of energy of laboratory two-dimensional waves by means of frequency dispersion, found that the energy is lost almost entirely from the higher frequencies whereas the spectral peak remained unchanged after breaking. Pierson *et al.* [1992], who stimulated the laboratory breaking through the amplitude dispersion, reached an opposite result: that is, most of the energy is lost from the primary wave. This main conclusion is similar to that of Babanin *et al.* [2009a,b], but the spectral breaking impact in their experiment is yet different. In the experiments by Pierson *et al.* [1992], while the dominant wave looses energy, some components of the spectrum actually gain it. This outcome is quite physical because the breaking is known to be associated with generation of short waves, whether it is by means of production of the parasitic capillary waves on the front face of the breaker [e.g. Ebuchi *et al.*, 1987] or because of plunging jet impacting the surface [e.g. Hwang, 2007].

This brings us to another issue relevant to the breaking severity in a spectral environment. It is well-known that the field waves do not necessarily break at the spectral peak (dominant breaking), but in fact the breaking occurs more frequently at smaller scales [e.g. Melville & Matusov, 2002, Banner *et al.*, 2002, Babanin & Young, 2005, Babanin *et al.*, 2007c, Hwang, 2007, Mironov & Dulov, 2008]. Here, as the smaller scales we mean frequencies/wavenumbers of the spectrum tail, away from the spectral peak, that is waves relatively shorter than the dominant waves rather than just short waves in terms of some dimensional limit of length. As discussed above, such waves do not form groups, at least not in the narrow-banded wave-group sense. Therefore, the problem of the breaking severity distributed across the group is not relevant for them. Instead, other issues which are non-existent in case of the dominant breaking come into importance.

These waves can potentially be breaking because of two reasons. First of all, one would expect them to break due to inherent physical processes which lead surface waves to the breaking in any scenario. Secondly, their breaking is induced by the longer waves. This is either forced breaking [Babanin & Young, 2005, Young & Babanin, 2006a] or the straining action of longer waves [Donelan, 2001]. The forced breaking is the breaking of short waves triggered by the large breaker. The straining action takes place because of modulation of short wave trains by the underlying large waves and causes the short-wave steepness to increase at the forward faces of longer waves, which result in their frequent breaking. One way or another, but similarly to the subsequent breaking of dominant waves on the top of their groups described above, sequential or simultaneous breaking of short waves is expected in this case. This sequence is linked to the phase of longer waves (i.e. happens on the front face, at the top or in the wake of the long wave). If these short breakers (wavelengths λ_{short}, frequencies f_{short}) are also coupled in non-linear sense, then, similarly to the definition (2.31) for groups of dominant waves, the short-breaker severity s_{short} needs to be defined in terms of value averaged over the period of dominant wave:

$$E_{s_{short}} = s_{short}\frac{8}{\lambda_{long}}\int_0^{\lambda_{long}} \eta_{short}(x)^2 dx. \tag{2.41}$$

Here, $E_{s_{short}}(f)$ is the energy lost due to breaking of short waves, λ_{long} is the length of modulating underlying wave, and $\eta_{short}(x)$ are surface elevations just before the breaking started, but with the low-frequency/wavenumber oscillations of the mean surface ($\lambda > \lambda_{short}, f < f_{short}$) been filtered out. Wavelength λ_{long} is also not a constant value of, for example, dominant waves with frequency f_p. There has to be

$$\begin{gathered}\lambda_{long}(f_{long}) \gg \lambda_{short}(f_{short}),\\ f_{long} \ll f_{short},\end{gathered} \tag{2.42}$$

but other than that λ_{long} and f_{long} can take on any scale.

We should note that the severity of breaking of short waves may depend on their scale f_{short} and therefore $E_{s_{short}}$ can be treated as a spectral function $E_{s_{short}}(f)$. Like the the breaking probability of Section 2.5, in practical terms frequency f implies some spectral band $f \pm \Delta f$ (2.5) such that surface elevations $\eta_{short}(x)$ in (2.42) are bandpassed into this band.

Outcome of the induced breaking is so the called cumulative effect [Babanin & Young, 2005, Young & Babanin, 2006a, Babanin *et al.*, 2007c], accumulation of the breaking energy losses at smaller scales which are coupled with behaviour of longer waves. Further from the spectral peak, the cumulative energy loss grows and tends to dominate over the inherent breaking severity. This is a purely spectral effect which is always present regardless the fact whether the dominant waves break or not.

Therefore, as far as the spectral impact of the breaking severity is concerned (i.e. spectral distribution of the energy loss in a single breaking event), there appears to be a broad range of possibilities, uncertainties and ambiguities. Depending on the physics leading up the to the wave breaking, energy may or may not be lost from the primary breaking wave. In all scenarios, energy loss is endured across the entire spectrum, certainly at the scales smaller than that of the primary breaker. These smaller scales may be harmonics of the primary wave or free waves [e.g. Meza *et al.*, 2000, Young & Babanin, 2006a], but in any case their breaking occurrence and breaking strength are strongly coupled with the breaking and severity of the primary waves.

Additionally, the wave energy is downshifted as a result of the breaking, at least if the breaking is strong enough [Babanin *et al.*, 2009a,b]. This means that part of the energy, which is lost from the primary breaking scale, is not in fact removed from the wave system. Finally, some scales in the wave spectrum, distant from the scale of the primary breaker, may actually acquire energy as a result of the breaking. These scales are both below and above the scale of the breaker [Pierson *et al.*, 1992]. Overall, the (2.26)-like notion of a fixed or even a reasonably approximated average value for the severity s is a gross simplification or is simply inapplicable in a spectral environment.

In summary, we have provided four definitions for the breaking severity (2.23), (2.31), (2.37) and (2.41). While it may seem confusing and even discouraging, there appears an apparent order which should allow for measurements and quantifying the breaking strength. The basic definition of the energy lost by a single isolated breaker (2.23), although most obvious, has perhaps the least practical significance and can only be employed in refined conditions when the breaking is due to superposition of linear or non-linear modes, or due to a subsurface obstacle, mostly in laboratory.

Eq.(2.37) is the most general definition in spectral terms. It accounts for spectral impact of a breaking, which can include energy losses, energy gains and energy exchange (shifting) between different wave scales in the spectrum. Since the spectrum, however, is a resolution of waves, often non-linear, into linear modes, the spectral distribution of breaking strength can signify both the actual energy lost by free shorter waves and a reduction of non-linearity of the primary waves (bound harmonics). Also, attenuation of the short waves in the wake of large breaking can occur without breaking, for example, because of interactions of the short waves with intensive turbulence in the trace of the large breaker [e.g. Banner *et al.*, 1989]. In physical space, this loss will be attributed to the large breaker, or to the group where this breaker occurred, and in the spectral sense it will be placed at high frequencies/wavenumbers even though the waves at those scales may not break. Obviously, the spectral definition of breaking severity (2.37) can be rewritten for any spectral band $f_1 < f < f_2$ if there are reasons to believe that the loss of energy is restricted to this band, or if such band is of a dedicated interest:

$$\begin{aligned} E_{s_{spectral}}(f_1, f_2) &= \int_{f_1}^{f_2} F_{before}(f)df - \int_{f_1}^{f_2} F_{after}(f)df \\ &= s_{spectral} \int_{f_1}^{f_2} F_{before}(f)df. \end{aligned} \tag{2.43}$$

Note that in the formally introduced definition (2.43) the primary breaker, which originally caused the energy loss, does not have to necessarily belong to the frequency range of $f_1 < f < f_2$.

Definitions (2.31) and (2.41) describe the breaking severity measured in the physical space. The first one accounts for all energy losses which take place due to a breaking within a wave group. As discussed above, these are breakings of dominant waves, although the spectral impact may be distributed across all wave scales. The second definition relates specifically to the energy losses of waves short compared to the spectral peak f_p according to (2.42). Most important significance of these definitions is that, together with measurements of the breaking probability (2.35) and (2.4), they allow to experimentally estimate the spectral dissipation function (2.21). As already mentioned, this function has so far been the most elusive and speculative property of wave modelling and forecasting [see e.g. Young & Babanin, 2006a, Babanin *et al.*, 2007c,

Babanin & van der Westhuysen, 2008].

2.8 Types of breaking waves: plunging, spilling and micro-breaking

Breaking waves are usually subdivided into three types: plunging, spilling and micro-breaking [e.g. Weissman *et al.*, 1984]. Plunging breaker is the most commonly perceived picture of a breaking wave: at the breaking onset, the crest curves forward and forms a plunging jet, which impacts and penetrates the water surface in front of the wave, entrains air and turbulence deep under the surface, and potentially can trap an air pocket between the jet and the former front face of the wave, which pocket will then disintegrate into large bubbles with corresponding consequences in terms of gas exchange across the interface and particularly in terms of acoustic noise produced by the event. The spilling type is a less dramatic, but somewhat more frequent [e.g. Katsaros & Atakturk, 1992] kind of breaking when the crest destabilises and collapses, spilling the water over the front slope of the wave. In many regards, this is analogous to having multiple smaller jets impacting the water surface, and these jets also lead to formation of the bubbles and generation of turbulence. Plunging breaking is more energetic in terms of energy/momentum loss from the waves and correspondingly the energy/momentum transferred to the ocean, as well as in terms of turbulence generation, bubble penetration depth, gas exchange across the surface, but other than that physics of the plunging and spilling breaking is essentially the same [e.g. Rapp & Melville, 1990].

Micro-breaking phenomenon deserves to be mentioned separately among other wave-breaking definitions not so much because it is a different kind of the breaking, but rather in order to avoid confusions and to state that dynamics of the micro-breaking is basically the same as that of the regular breaking. Different is an external signature of such breaking, that is the micro-breaking does not exhibit whitecapping.

Term 'whitecapping' is often used inter-changeably with the term wave breaking, and even the dissipation function employed in the spectral wave modelling is routinely called the whitecapping dissipation. Significant part of the spectral distribution of such dissipation, however, corresponds to the scales where waves break without producing whitecaps. These are short gravity waves, short in absolute rather than relative terms, whose breaking intensity is too week to warrant air entrainment visible as whitecapping (or too week to overcome the surface tension at wave crest and form a jet [Tulin & Landrini, 2001]). Investigators of such micro-scale breaking point out that this phenomenon is in fact much more widespread than the whitecaps [e.g. Jessup *et al.*, 1997a]. According to Tulin & Landrini [2001], these are waves of

$$\begin{array}{rcl} \lambda & \leq & 25\ \mathrm{cm}, \\ f & \geq & 1.44\ \mathrm{Hz}, \end{array} \tag{2.44}$$

i.e. in most of the cases this is a major part of the wave spectrum.

Since the micro-breaking is not visible, new means had to be developed in order to detect and yet alone to quantify its breaking rates and severity. Katsaros & Atakturk [1992] used high-resolution video recording for this purpose, which involved a significant manual effort to process the data and obtain the statistics. Jessup *et al.* [1997a] employed infrared imagery what allowed automatic data processing. The idea is based on the fact of existence of the 'skin' thermal layer at the ocean surface. Depth of this layer is of the order of 0.1 mm, and the top of the layer is a few tenths of a degree Celsius cooler than the bottom. Micro-breaking disrupts the skin layer and

exposes the water with bulk upper-ocean temperature to the very surface where the temperature differences between the micro-breaking wake and the background surface can be observed in the infrared-light range.

Jessup *et al.* [1997a] write: "The conceptual model we present, which explains our infrared observations, suggests that thermal detection of microscale wave breaking may serve as a de facto definition of the phenomenon itself". In other words, as much as the visually observed whitecapping can be treated as a de facto definition of the breaking in the common sense, regardless the physics behind the phenomenon, the infrared signature defines the micro-breaking. We agree this is true, with a small addition: the disruption of the thermal skin layer identifies the micro-breaking provided the breaking does not generate whitecaps. Obviously, the large breakers, which do produce whitecapping, also break the skin layer [Jessup *et al.*, 1997b].

Lowen & Siddiqui [2006] compared three methods of detecting the micro-breaking: the wave slope, the areal extent of the thermal wake and the variance of the vorticity in the micro-wave crest region, based on empirical threshold values. The comparisons showed that the vorticity method is the most accurate, although it is obviously a difficult method to apply in field conditions. Infrared remote-sensing techniques intended to deal with the micro-breaking will be discussed in more detail in Section 3.6.

Tulin & Landrini [2001] investigated the micro-breaking by means of numerical simulations of the breaking onset with account for capillary effects, and by means of radar observations of micro-breakers in laboratory. They provide interesting insights in hydrodynamics of formation and propagation of micro-breaking waves. According to them, surface tension has a significant impact on the breaking of waves shorter than 2 m, to such an extent that for waves characterised by (2.44) no jet is produced at the crest. Instead, "forward facing bulge growing out of the wave crest is formed... Unlike energetic breakers where the shape continually evolves in transient fashion,... the microbreaker can propagate for a considerable distance without significant change of shape". Tulin & Landrini [2001] also pointed out that for very short waves (sub-micro-breakers) the bulge separates from the main flow "forming a cup on top of the wave as noted by Ebuchi *et al.* [1987]".

2.9 Criteria for the breaking onset

The wave breaking, obviously, happens when the water surface looses stability and collapses. What is the physics leading to this collapse is basically the main question of the wave-breaking studies, and is the main topic of the present paper. Understanding this physics has been elusive, but dealing with the breaking is necessary across a very broad range of oceanographic applications as described throughout this paper. Therefore, in the course of wave-breaking investigations various criteria, which supposedly indicate a breaking onset and therefore may help to detect it, have been employed. They may or may not assist in understanding the physics, and may not even rely on the physics as such, but they need to be at least outlined at this stage in order to explain experimental, analytical, statistical, probabilistic and numerical methods described in this paper.

The wave-breaking criteria are typically broadly classified into three categories: geometric, kinematic and dynamic criteria [e.g. Wu & Nepf, 2002]. Most commonly employed are those which follow from the Stokes limiting steepness [Stokes, 1880]:

$$\frac{H}{\lambda} = \frac{1}{7} = 0.142. \tag{2.45}$$

If converted into typically used these days steepness parameter ϵ (1.1), this criterion reads:

$$\epsilon_{limiting} = (ak)_{limiting} = 0.443. \tag{2.46}$$

In a wave of such limiting steepness, the crest takes the angle of a

$$\theta_{limiting} = 120^{\circ} \tag{2.47}$$

corner flow.

The Stokes limit can be also translated into kinematic limit, i.e. surface wave orbital velocity becomes greater than the wave's phase speed:

$$u_{orbital} = a\omega = c, \tag{2.48}$$

or downward surface acceleration, i.e. a dynamic limit of

$$a_{downward} = \frac{1}{2}g. \tag{2.49}$$

Because of their significance for the wave-breaking studies, these criteria have been extensively revisited in the modern literature, both in theoretical and experimental studies, and we refer the reader to Longuet-Higgins *et al.* [1963], Longuet-Higgins [1969, 1974], Stansell & MacFarlane [2002], Wu & Nepf [2002], among many others.

In particular, Stansell & MacFarlane [2002] specifically investigated the kinematic criterion (2.48) in a dedicated laboratory experiment. Since three different interpretations of what is the wave's phase velocity is possible, they verified the criterion with respect to all the three definitions: "The first definition, based on the equivalent linear waves, is constant over the wavelength of the wave. The second, based on partial Hilbert transforms of the surface elevation data, is local in space and time giving instantaneous values at all space and time measurements. The third, based on the speed of the position of the crest maximum, is local in time but not in space". The orbital velocity at the crest of breaking and non-breaking waves was measured by means of particle image velocimetry (PIV), and the breaking in an intended location was achieved through the linear focusing.

The conclusions were not overly supportive for the classical criterion. The ratio of orbital velocity to phase velocity was found, at most, to be 0.81 in the plunging breakers and 0.95 in a spilling breaker. In this regard, we would like to make two comments. First of all, this finding means that when the criterion (2.48) is satisfied, the waves are definitely breaking, and therefore experimental-detection techniques, statistical and theoretical approaches based on this criterion will underestimate rather than overestimate the breaking probabilities. Secondly, the linear focusing is quite likely a mechanism of a secondary importance when it comes to the natural field wave breaking (see Sections 4 – 6). The breaking caused by the instabilities of non-linear wave trains appears to be a feasible common mechanism for the field breaking, and its physics is quite different to that of the breaking because of the linear superposition. For such breaking onset, brought about by the modulational instability, experiments and findings of Stansell & MacFarlane [2002] have to be revisited.

For this type of breaking, an unconventional interpretation of the kinematic criterion was given by Tulin & Landrini [2001]. In a comprehensive overview of wave-breaking investigations conducted by their research group during a period over more than 15 years, the authors, in particular, provided analytical derivation and experimental validation of their version of this criterion:

"... upon passing through the peak of a modulation group, when the orbital velocity at the wave crest, u_c, exceeds the wave group velocity $d\omega/dk = c_g$, then the wave crest and trough both rise, the front face steepens, the wave crest sharpens, and eventually a jet forms at the crest, leading finally to splashing and a breakdown of the wave".

Thus, the criterion is stated for the wave breaking due to modulational instability (see Sections 4 and 5 about evolution of non-linear wave groups to the breaking). It does not signify the ratio of orbital and phase velocities at the point of breaking onset, like (2.48), but rather a point of no-return: i.e. if the orbital velocity at the crest exceeded group velocity, it may still be increasing (and perhaps even reach values comparable with those given by (2.48)), but the wave will inevitably eventually break:

$$u_{orbital} = \frac{d\omega}{dk} = c_g. \tag{2.50}$$

If the crest-particle velocity is below (2.50)-value, the wave will not proceed to the breaking. According to Tulin & Landrini [2001], the criterion is true not only for the deep-water waves, for which ratio of phase and group velocities are determined by (2.19), but also for modulating trains in finite depths where this ratio is smaller.

Analytically, the criterion is justified by considering propagation of Stokes waves through a wave group. In case of a uniform wave train, the trajectory of the crest is a horizontal line. In the case of the crest passing through the peak of concave envelope, it must decelerate which, for gravity waves, is impossible unless values of the crest orbital velocities are below those defined by (2.50). This convincing derivation is supported by substantial experimental observations further outlined by Tulin & Landrini [2001]. Potentially, this criterion can serve to separate observed wave breakings occurred due to different physical causes, for example, the modulational-instability breaking from the directional-focusing breaking which does not bring about modulation of wave trains [Fochesato *et al.*, 2007].

Since most of wave measurements are conducted as time series of the surface elevation, where wave period (frequency) rather than wavelength (wavenumber) is known, the Stokes steepness (2.46) can be further converted into its height/period version. This is usually done by means of linear dispersion relationship (see 2.17). Then, the criterion suggests that the waves will break if

$$H \geq 0.027 g T^2. \tag{2.51}$$

A variety of other criteria, both related and unrelated to the Stokes limit have also been proposed. Among the geometric limiters, Longuet-Higgins & Fox [1977]'s maximal inclination of the surface, which the Stokes wave can reach before breaking, should be mentioned:

$$\theta_{critical} = 30.37^\circ, \tag{2.52}$$

as it has been broadly employed in experimental studies (see Section 3.3).

Other widely used geometric properties of the pre-breaking wave shape are skewness S_k (1.2) and asymmetry A_s (1.3) (statistically, they are the third moment of the surface elevation and the third moment of the Hilbert Transform of the surface elevation respectively). These are empirical, rather than theoretically-justified criteria based on the common perception of the breaking wave as one with a sharp crest and the front face leaning forward (see Section 1.2

and Figure 1.2). One of quantitative criteria for the asymmetry, for example, was suggested by Kjeldsen & Myrhaug [1980] based on field observations and Tulin & Landrini [2001] through numerical simulations. In addition, Kjeldsen & Myrhaug [1980] found that the front trough of the incipient breaker is shallower compared to the rear trough, which is a persistent feature of wave breaking due to modulational instability, observed in the laboratory [Babanin *et al.*, 2009a] and produced by means of fully non-linear numerical simulations [Dyachenko & Zakharov , 2005, see also Section 4].

Tulin & Landrini [2001], however, point out that deformations of the wave shape prior to breaking "has to be viewed as a consequence of the breaking process and not the cause of it", and we fully agree with this. In particular, recent investigations of the breaking onset brought about by the modulational instability of wave trains showed that the asymmetry at the breaking point is a rapidly changing characteristic, with a value close to zero and increasingly becoming negative. Thus, it would be difficult to employ the asymmetry as a certain geometric breaking criterion. The skewness, on the contrary, indeed tends to asymptote a limiting value of

$$S_{k_{limiting}} = 1 \tag{2.53}$$

Babanin *et al.* [2007a, 2009a,b].

Returning to the dynamic criteria, the most significant difficulty of applying the limiting downward-acceleration (2.49) to the real sea waves is the fact that the natural wave fields are multi-scaled and therefore the surface elevation at any point and any instance of time is a superposition of an unlimited number of wave components. Therefore, among other dynamic criteria, we should mention the downward acceleration derived by Longuet-Higgins [1985] for a complicated sea, rather than for a monochromatic Stokes wave:

$$a_{downward} = g. \tag{2.54}$$

As a general approach, the acceleration criterion is treated in a sense that the wave surface will break when its downward acceleration exceeds a limiting fraction γ, which is a tuning parameter, i.e.

$$a_{downward} = a\omega^2 > \gamma g. \tag{2.55}$$

When it is applied to a monochromatic wave, this approach is straightforward even though there are uncertainties about the value of γ. In theoretical/statistical studies of the limiting-steepness Stokes wave, it has generally been assumed that $\gamma = 0.5$ [(2.49), Longuet-Higgins *et al.*, 1963, Snyder *et al.*, 1983]. Laboratory studies of Hwang *et al.* [1989] showed that γ is closer to 0.4, and some field measurements [e.g. Holthuijsen & Herbers, 1986, Liu & Babanin, 2004] further indicated that the value of γ could be even lower.

For more breaking-onset properties and criteria, we can refer the reader to a near-comprehensive Table of the possible wave-breaking threshold variables in Snyder & Kennedy [1983]. In this paper, in addition to those already mentioned here, such characteristics as vertical velocity gradient, horizontal velocity divergence, surface curvature and vertical acceleration gradient are included.

This brief summary of the breaking onset indicators would be incomplete without mentioning a family of criteria which came from numerical simulations of the evolution of non-linear wave groups with imposed modulation [Banner & Tian, 1998, Song & Banner, 2002, Banner

& Peirson, 2007]. In the general terms, these criteria can be regarded dynamic, i.e. the rate of change of the local mean wave energy density/ the rate of change of the momentum flux averaged over half a wavelength/ the local average mean energy flux to the energy maximum in the wave group. These thresholds have caused a considerable discussion in the literature recently, but such criteria can hardly be employed in any practical sense and even their verification in refined laboratory conditions proved intangible and inconclusive. Since the issue of modulational instability is important for the topic of the present paper, these dynamic criteria will be specially discussed in Section 4.2.

Overall, we would like to say that the indicative breaking-onset criteria proved very useful and successful in wave-breaking studies of all kinds, but once the physics of the breaking is understood better, their significance will diminish or even become eventually redundant, with the definite exception for the Stokes steepness limit (2.46). As we will try to show below (Sections 4, 5), it appears that the waves break not because of some particular physical mechanism, but rather because in the course of their evolution they reach this limiting steepness and the water surface becomes unstable, regardless the processes behind the steepness growth. The same growth mechanism, if it does not bring the wave height up to the Stokes limit (or its modification in case of directional waves), will not make the wave break. Therefore, probably, no single criterion, except the limiting steepness, can be a robust breaking predictor in all circumstances. Mechanisms which can lead to such a steep wave occurrence can be a few, with the modulational instability likely to be largely responsible for the breaking of dominant waves.

2.10 Radiative Transfer Equation

Radiative Transfer Equation (RTE) plays an important role in the context of wave-breaking and breaking-dissipation studies, their intentions and motivations. It will not be explicitly used in the present paper for derivations or modelling, but it will be referred to, and therefore needs to be mentioned and described among the other relevant definitions related to the wave-breaking process.

Since it was first proposed by Hasselmann [1960], RTE has been widely used in scientific studies and practical applications related to the evolution of wind-generated waves. In water of finite depth, this equation takes the general form [Komen *et al.*, 1994]

$$\left[\frac{\partial}{\partial t} + (\mathbf{c}_g + \mathbf{U_c}) \cdot \frac{\partial}{\partial \mathbf{x}} - \nabla\Omega \cdot \frac{\partial}{\partial \mathbf{k}}\right] \frac{\Phi}{\omega} = S_{in} + S_{nl} + S_{ds} + S_{bf} \tag{2.56}$$

where the left-hand side represents the evolution of the wave action density Φ/ω as a result of the physical processes of atmospheric input from the wind (S_{in} term), non-linear interactions of various orders within the spectrum (S_{nl} term), dissipation due to 'whitecapping'/breaking (S_{ds} term 2.24), and decay due to bottom friction (S_{bf} term). $\Phi(f, k, \theta)$ is the directional wave spectrum, i.e. θ is direction of wave propagation. All the source terms on the right are spectra along wavenumber-frequency-direction, as well as functions of other parameters. $\mathbf{U_c}$ is the surface current and $\Omega(\mathbf{k})$ is the Doppler-shifted frequency $\Omega(\mathbf{k}) = \omega(k) + \mathbf{k} \cdot \mathbf{U_c}$.

The dissipation-due-to-breaking source (sink) term S_{ds} (2.24) was introduced and defined above (Section 2.7) and will be mentioned a number of times throughout this paper. While the waves would not be generated without the wind input S_{in} in the first place, the other terms in (2.56) are not of secondary importance as it may seem. Without S_{ds}, the wind-generated waves

would grow unlimited which case obviously does not happen. Immediately as the waves pass the infinitesimally-small stage, the dissipation switches on. The dissipation due to breaking does not turn on until the spectral threshold value is overcome (see Sections 5.2, 5.3.2), but once it is active it becomes as significant as the wind input and the other two general terms mentioned in (2.56), as far as the wave evolution is concerned. Many more less general source/sink terms in RTE are possible, but the four introduced in (2.56) are invariably important in the finite-depth wave environment, and the first three in deep water.

Knowledge of the terms other than dissipation, based on either experimental or analytical (or both) approaches, is incomplete but still rational [see Komen *et al.*, 1994, The WISE Group, 2007, in general and Donelan *et al.* [2006], Babanin *et al.* [2007b] on recent developments on the wind input S_{in}]. In contrast, understanding of the dissipation term remains poor. A number of theoretical and conjectural approaches have been attempted to predict the spectral dissipation function, but none of these have been experimentally validated. It is generally assumed that S_{ds} is a function of the wave spectrum Φ:

$$S_{ds}(f,k,\theta) \sim \Phi(f,k,\theta)^n, \tag{2.57}$$

but there is no agreement even on such basic ground as whether the spectral dissipation $S_{ds}(f,k,\theta)$ is linear in terms of the spectrum $\Phi(f,k,\theta)$ or not, i.e whether $n = 1$ or $n > 1$. On the other hand, such experimentally known features of the wave-breaking dissipation as threshold behaviour, cumulation of dissipation at smaller scales, dependence of dissipation on the wind at extreme-forcing conditions have not been accounted for in present-day dissipation terms in any way. See Sections 5 and 6 on more detailed discussions of these issues and The WISE Group [2007] for an up-to-date discussion of the entire topic of the state-of-art wave modelling.

3 Detection and measurements of the wave breaking

Measurements and even detection of the wave breaking is a challenging task, particularly if carried out by unattended devices in the open ocean. As a result, there are vast amounts of wave records accumulated, and most of them contain breaking waves, but information about the breaking cannot be extracted. There is an obvious need for methods and instrumentation to directly detect the breaking events and measure their properties, and for the analytical means and criteria to identify the breaking waves in existing time series of surface elevations.

Until recently, visual observations were arguably the only reliable means of breaking detection. These are based on viewing and quantifying information on whitecaps produced by breaking waves and are obviously biased towards large breakers (see Section 2.8). During the last two decades, more technological methods became available, both by contact means and by remote sensing of the ocean surface or subsurface. These utilise acoustic (passive and active), optical (both visible and infrared range), reflective and other properties of breakers which distinguish them from the more homogeneous background wave field. Without giving a comprehensive review, we will mention here passive acoustic techniques based on air bubbles ringing while being created during the air entrainment [e.g. Lowen & Melville, 1991a, Ding & Farmer, 1994, Babanin *et al.*, 2001, Manasseh *et al.*, 2006], sonar observations of bubble clouds produced by breaking wind waves [e.g. Thorpe, 1992], aerial imaging [e.g Melville & Matusov, 2002], infrared remote sensing of breaking waves [e.g. Jessup *et al.*, 1997a], radar observations of the microwave backscatter from breakers [e.g Jessup *et al.*, 1990, Lowen & Melville, 1991a, Smith *et al.*, 1996, Phillips *et al.*, 2001], conductivity measurements of void fraction produced by breakers [e.g Lammarre & Melville, 1992, Gemmrich & Farmer, 1999], among others. New analytical methods of detecting the breaking in wave records have also become available, for example, by means of Hilbert Transform [e.g. Huang *et al.*, 1998] or wavelet analysis [e.g. Liu & Babanin, 2004] applied to the wave series.

This Section gives a brief review of wave-breaking detection and estimation techniques. We start from visual observations of whitecapping which have been a traditional way of investigation of the phenomenon and remain a valid and highly effecient method today. Contact measurements of the breaking properties provide means of direct estimates, which, unlike the visual observations, are not subject to human error. These are subdivided into two Sections dedicated to the laboratory techniques and to their counterparts applicable in field experiments where, as far as the wave breaking is concerned, requirements for in situ devices are very different to the laboratory. Remote sensing approaches are outlined next. Of these, the acoustic methods are singled out into a separate subsection because, in our view, they are the most advanced and most promising with regard to the breaking studies. Finally, analytical techniques are briefly reviewed. These include a Section on detecting the breaking events in existing surface-elevation time series and a Section on analyses of the wave-breaking statistics based on some initial assumptions. Both the approaches appeal to outliers, either in wave records or in probability distributions, which should not have taken place if the waves were not breaking.

It should be mentioned that majority of the wave-breaking measurement and analysis methods are intended for studies of the breaking rates or probability, whereas the breaking severity measurement means are underdeveloped if not marginal. In this regard, almost all experimental techniques mentioned above and described in more detail below give a promise, but have never been sufficiently elaborated for the purpose of estimating the severity. The most direct way to

estimate the breaking energy loss is of course measuring the wave train immediately before and immediately after a breaking event (see Section 2.7), but even in laboratory this is problematic. Among the other methods, acoustic (Section 3.5) and infrared (Section 3.6) techniques have a proven record of being able to qualitatively distinguish breaking events of different strengths, but even them are still to be advanced into a quantitative calibration stage. In the meantime, as mentioned in Section 2.7, knowledge and understanding of the breaking severity remain quite poor, but are as important as those of the breaking probability. Therefore, it is worth emphasising at this stage that the lack of progress in the breaking-strength topic is not only due to the need for relevant dedicated studies, but to a great extent is hampered by the absence of robust and reliable experimental techniques.

3.1 Early observations of wave breaking, and measurements of whitecap coverage of ocean surface

Early documented scientific observations of the wave breaking date back to the late 40s [Munk, 1947] and were followed by a number of research attempts which intensified in the 60s [i.e. Blanchard, 1963, Gathman & Trent, 1968, Cardone, 1969, Monahan, 1969, 1971, Monahan & Zietlow, 1969]. They all dealt with some identification of the whitecap coverage of the ocean surface, usually by means of photography and without actual collocated measurements of the waves. Wave-measurement techniques were still under development in those days, and data logging and computer facilities for recording, storage and processing long time series of surface elevations were not available. Therefore, the whitecap measurements were interpreted and parameterised in terms of wave-generating winds. Some observations [i.e. Munk, 1947] were quantified as the number of foam patches per unit area and thus allow to relate them to the breaking probability (see Section 2.5). Majority of the results were expressed as percentage of the whitecap coverage of the surface which property depends on a combination of the breaking probability, the breaking strength and lifetime of the whitecap foam. The first two properties combined relate to the overall dissipation due to wave breaking (2.20), where contributions of the breaking rates (Section 2.5) and breaking strength (Section 2.7), however, cannot be separated. The whitecapping lifetime depends on environmental conditions, such as water temperature and salinity, and technically speaking is not a characteristic of wave breaking. Therefore, the whitecap coverage bears essential uncertainties if treated as a property of wave breaking or a quantitative feature of wave energy dissipation.

Parameterisation of the breaking dependences, including the whitecap surface coverage, in terms of the surface-wind speed is of course a reasonable approach as the waves are generated by the wind and many characteristic properties of the wave field ultimately correlate with the wind. Because of the very large density difference between the air and the water, however, the wind impact on the breaking is mostly indirect. That is, the wind slowly pumps energy into the waves, which gradually grow under the wind action, and as their steepness increases, the hydrodynamic mechanisms (rather than wind forcing) lead some waves to the breaking. This will be discussed in detail in Sections 4 – 6. Here, we will mention that capacity of the wind to stimulate or even affect the breaking onset as such is marginal, unless the wind forcing is very strong [i.e. $U/c > 10$, see Babanin *et al.*, 2009a,b], and the physics of the wave-breaking parameterisations should be expressed in terms of the wave, rather than the wind properties [e.g. Banner *et al.*, 2000, Babanin *et al.*, 2001].

The last two studies combined data from four diverse water bodies, ranging from a small shallow lake to the Southern Ocean, and argued that the relating the breaking probability to the wind speed provided a reasonable correlation within each individual data set, but when the diverse data were combined, these correlations essentially degraded (Section 5.3.1 and Figure 5.19). In the combined data set, with a broad range of dominant wave lengths ($10 - 300$ m) and wind speeds ($5 - 20$ m/s), there was no correlation between the breaking rates and the wind speed, whereas dependence of the breaking probability on properties of the wave field remained.

Having this understanding in mind, it is interesting to revisit the early results. They clearly exhibited many features of the wave-breaking behaviour which are being 'rediscovered' years later, and they set many standards to follow. For example, Munk [1947] concluded that there were no breaking at wind speeds $U < 6$ m/s and Gathman & Trent [1968] found no whitecaps at $U < 3.1$ m/s. Similarly, Blanchard [1963] demonstrated a significant increase in whitecap coverage at $U > 3$ m/s and Monahan [1969] observed that the fractional coverage was very small, less than 0.1% for light winds and only started to grow and depend on the surface wind at $U > 4$ m/s. Such results are consistent with later observations [e.g. Donelan & Pierson, 1987, Babanin *et al.*, 2005], but most importantly agree with the recently found threshold behaviour of the breaking. These days, the threshold is expressed in terms of the characteristic steepness of the wave field rather than in terms of the wind speed, which makes difference in cases of complicated wave fields or wave fields non-unambiguosuly coupled with the local wind [Banner *et al.*, 2000, Babanin *et al.*, 2001, 2007a].

Furthermore, we can mention that Cardone [1969] suggested an analytical model of the whitecap-coverage dependence on the wind by assuming that the whitecaps are a manifistation of the wave energy dissipation which balances the energy input to the waves from the wind. This idea was to be followed by great many studies in the subsequent decades [e.g. Wu, 1979, Zhao & Toba, 2001, Guan *et al.*, 2007].

The apparent quantitative differences between the early observations were not unexpected due to both technical and physical reasons. On the technical side, variations in accuracy and methodology of the wind measurements were pointed out by the authors of the early studies themselves [Monahan, 1971]. Shortcomings of the manual techniques of processing the photographic images became clearer once digital methods were developed [see, e.g. Stramska & Petelski, 2003]. For example, the manual methods did not take into account the geometry difference of the near-field and far-field in the oblique photography, and as a result the whitecapping coverage of the former was overestimated and of the latter underestimated. This would bring about discrepancies between observations taken at different angles of incidence and introduce scatter and bias, particularly significant at low wind speeds where presence or absence of a breaking event in the near-field could essentially distort the overall statistics.

Physical processes which can affect size and the duration of persistence of whitecaps in different environmental circumstances are very many, and they could certainly contribute to the quantitative disagreements too. The early researchers were aware of some of them and not aware of the others, and here we refer to a recent update by Stramska & Petelski [2003]: "For example, wind history, local hydrodynamic conditions such as currents and swell, directionality of the wave field, presence of biological surfactants, and variations of the water temperature and atmospheric stability all can contribute to variability in the W versus U_{10} relationship".

Envelope of dependence of the fractional whitecap coverage W on wind speed U_{10} at 10 m height above the mean sea level (i.e. experimental fit through the highest-coverage values at

various wind speeds) was suggested by Monahan [1971] for the ocean whitecapping as following:

$$W = 0.00135 U_{10}^{3.4}. \tag{3.1}$$

Monahan [1971] reviewed the earlier observations and found, as we have just discussed, that available parameterisations were similar qualitatively, but quantitative deviations were essential.

The earlier observations concentrated on the whitecap coverage, rather than on more detailed and coupled-with-waves characteristics of the wave breaking, out of necessity, because of the lack of experimental techniques and data handling capacities. Later, studies of such coverage acquired importance in its own right due to development of methods of remote sensing of the ocean surface (see Section 3.6). Such methods either rely directly on measurements of whitecap coverage in order to estimate the surface winds by means of (3.1)-like dependences [e.g. Wu, 1969, 1979, Monahan *et al.*, 1981], or have to take such coverage into account as the whitecaps are up to 10 times brighter than the water surface [e.g. Moore *et al.*, 1997] and therefore alter the observed ocean colour and other remote-sensing properties of the ocean [e.g. Monahan & O'Muircheartaigh, 1986, Ester & Arnone, 1994, Gordon, 1997, Sharkov, 2007].

In the view of such importance, experimental dependences of W versus U_{10} continue to be revisited, and a larger number of new dependences, or modifications to existing dependences have been proposed. In a recent paper, based on a combined empirical-statistical-analytical approach, Yuan *et al.* [2009] suggested an upper envelope for such dependences. For any given wind speed, such envelope would describe whitecap coverage at infinite wave fetch under infinite wind duration. Vast literature on this topic cannot be reviewed in the current Section and we refer the reader to the books by Monahan [1986], Sharkov [2007] and most recent updates by Zhao & Toba [2001], Stramska & Petelski [2003], Guan *et al.* [2007], Yuan *et al.* [2009] and respective references in these publications. Here, we would like to highlight the studies most relevant for the discussions of the present paper.

Wu [1979] further reviewed available observations of whitecap coverage (3.1) almost 10 years after the first such review by Monahan [1971] and at that stage suggested, based on some semi-theoretical/semi-empirical argument, that the data are not inconsistent with such dependence:

$$W = \alpha U_{10}^{3.75}, \tag{3.2}$$

where coefficient $\alpha = 1.30 - 2.90$ varies mainly as a function of stability conditions of the atmospheric boundary layer. Stramska & Petelski [2003] introduced a wind-speed threshold into this kind of dependences:

$$W = \begin{cases} 4.18 \cdot 10^{-5}(U_{10} - 4.93)^3 & \text{if } U_{10} \geq 4.93, \\ 0 & \text{if } U_{10} < 4.93. \end{cases} \tag{3.3}$$

If the wind is below the threshold, no breaking/whitecapping is observed, otherwise the whitecap coverage W depends on the excess of the wind speed above its threshold value, rather than on the wind speed itself. The threshold was determined as

$$U_{10_{threshold}} = 4.93 m/s. \tag{3.4}$$

Such threshold-like dependences are consistent with parameterisations of the breaking probability (see Section 5), at least for straightforward wave-development conditions when the threshold wind speed can be related to the threshold characteristic steepness in the wave field.

When using the power of 3 in (3.3), Stramska & Petelski [2003] followed approach prevailed in the 90s [e.g. Monahan & Lu, 1990, Monahan, 1993]. While in the earlier parameterisations of

$$W \sim U_{10}^{p}, \tag{3.5}$$

the power p was obtained by means of fitting the experimental data points, the latter approach assumes and enforces $p = 3$. The semi-theoretical reasoning behind such assumption is the same as that of Wu [1979] whose conclusion, however, was $p = 3.75$. Therefore, it is worth to briefly outline the argument, and somewhat review it in the light of more recent knowledge.

The physical argument states, by definition, that the total energy flux from the wind to the waves, and therefore the total wave energy dissipation rate in a quasi-stationary case approximately are:

$$S_{ds} = \tau U, \tag{3.6}$$

where

$$\tau = \rho_a u_*^2 = \rho_a C_D U_{10}^2 \tag{3.7}$$

is the wind stress or the momentum flux from the air to the water, U is some characteristic velocity of energy propagation in the low atmospheric boundary layer, u_* is so-called friction velocity, ρ_a is air density, and

$$C_D = \frac{u_*^2}{U_{10}^2}, \tag{3.8}$$

is the drag coefficient, a parameter introduced for convenience of converting the U_{10} wind into u_*. Thus, according to (3.6)-(3.7), the dissipation is proportional to some wind speed cubed, but precise nature of this proportion depends on what is the characteristic speed U.

If $U = u_*$ [e.g. Wu, 1979, Soloviev *et al.*, 1988, Agrawal *et al.*, 1992, Melville, 1994], then

$$S_{ds} = \rho_a u_*^3 = \rho_a C_D^{3/2} U_{10}^3. \tag{3.9}$$

If $U = U_{10}$ [e.g. Demchenko, 1993, Bister & Emanuel, 1999], we obtain

$$S_{ds} = \rho_a u_*^2 U_{10} = \rho_a C_D U_{10}^3. \tag{3.10}$$

Obviously, a conclusion on the speed U depends on a model of the boundary layer employed, and other options are possible between the two extremes mentioned, including more complicated characteristic speeds defined by integral properties of the sheared boundary-layer air flow [e.g. Kudryavtsev *et al.*, 2001].

Treating the whitecap coverage W (3.5) as a direct indicator, or even as a property directly proportional to the dissipation S_{ds} (3.10) is a significant over-simplification which is quite poorly justified. While the $S_{ds} \sim U^3$ relationship for steady wind-wave fields is true, it does not necessarily imply that $W \sim U^3$, even if dependence of the bubble lifetime on environmental conditions does not play its role. Dominant waves, if they break, provide a major contribution to the whitecapping. For mature seas, however, they do not break [e.g. Banner *et al.*, 2000, Dulov et al., 2002], and for developing seas a combined effect of frequency of their occurrence and severity of their breaking is not necessarily proportional to U^3 [e.g. Babanin *et al.*, 2009a,b]. And there

are multiple evidences that bulk of energy flux to the waves is supported by short waves [e.g. Terray *et al.*, 1996] which bulk is also lost through the dissipation at high frequencies [e.g. Babanin *et al.*, 2007c]. Such short-wave breaking has strong connection with the dominant waves, rather than the wind directly, and the energy-containing waves appear to strongly modulate the respective whitecapping which is located near the dominant crests. At the spectral end of very short waves, furthermore, their breaking produces little or no whitecapping (see Section 2.8).

Having that in mind, let us review the theoretical argument based on the assumption that coverage W is proportional to the wind energy flux (3.6). If the drag coefficient

$$C_D = constant, \tag{3.11}$$

we arrive on $p = 3$ assumed in (3.3) and similar dependences. It is, however, not constant. There is a great variety of experimental parameterisations of C_D versus U, and none of them suggests the drag coefficient being independent of wind speed. Wu [1979], based on Wu [1969], Garratt [1977], used

$$C_D \sim U_{10}^{1/2} \tag{3.12}$$

and obtained $p = 3.75$ in (3.2). Most of experimental dependences are much steeper than (3.12). We refer to Babanin & Makin [2008] for a recent review and to their 'ideal-condition' parameterisation of

$$C_D = 1.92 \cdot 10^{-7} U_{10}^3 + 0.000953. \tag{3.13}$$

In any case, (3.3) and similar approximations, where $p = 3$ was assumed, cannot be expected to remain general. Whatever power p is chosen or fitted, however, deviations from the fit are still observed at high wind speeds [e.g. Monahan, 1971, Wu, 1979, Stramska & Petelski, 2003, and others]. Explanation of such effect seems apparent. At the high wind speeds, whitecap coverage can no longer characterise the balance (3.6) between the wind input and wave dissipation. As Munk [1947] puts it, for 'fresh breeze' "spume tends to be blown from the breaking wave crests". According to Munk [1947], the fresh breeze are winds in excess of 8.7 m/s. The blown spume should create an enhanced foam coverage, in addition to the coverage due to strength of wave breaking, and the respective bias for the W versus U dependences. Therefore, any of such paremeterisations should be treated with caution for applications in extreme weather conditions and even at reasonably strong winds.

This brings us to further caution considerations regarding validity of interpretations of the whitecap coverage as a characteristic for the wave energy dissipation. Bondur & Sharkov [1982] introduced a classification of the whitecap systems which we will describe by using a direct quote from a later book of one the authors [Sharkov, 2007]: "... specific form of foam systems in optical images allows us to confidently identify at least two classes (types) of foam formations: (1) 'wave crest foam' (i.e. 'whitecaps'), the so-called 'short-living form' (i.e. 'dynamic foam') of foam activity with a lifetime of units of seconds; and (2) spotty structures (or 'foam streaks'), 'static foam' (or 'residual foam') with a lifetime of about 10 seconds to several minutes... At wind velocities higher than $15ms^{-1}$ there arises a special class of stable foam systems: the thread-like systems caused by capture of air bubbles by Langmuir vortices (i.e., Langmuir circulation)" [e.g. Langmuir, 1938, Craik & Leibovich, 1976, Stolte, 1992, Smith, 1998, Melville *et al.*, 1998, Phillips, 2003, 2005, Thorpe, 2004].

The classification is generally accepted now as it was re-introduced later by Monahan [1993] named Stage A and Stage B whitecaps respectively. It is apparent that, even if the both Stages are connected with the breaking probability and breaking strength, the diffusive Stage B depends to a great extent on lifetime of the residual bubble clouds. This lifetime, as it was already known from the early observations, is an environmental characteristic rather than a property of wave breaking or dissipation. Monahan [1971] compared diffusion rates of oceanic whitecaps with those in the fresh water [Monahan, 1969] and found that the fresh-water whitecap area decays approximately 1.5 times faster. Thus, an essential variation of the whitecap coverage, in similar meteorological conditions and similar wave fields, is expected for the water bodies with different salinity.

It is interesting to notice that there is a considerable controversy in the literature regarding further roles played by the salinity in this regard. While some researchers find that the bubbles are smaller in the salt water [e.g. Haines & Johnson, 1995], the others claim they are not [e.g. Cartmill & Su, 1993, Wu, 2000]. Wu [2000] found that, rather, "a greater volume of air is entrained in salt than in freshwater to generate many more bubbles". If this was true, the salt-water breaking would have to be more severe which is difficult to justify physically.

From the early observations, it was also known that the lifetime of whitecap foaming L_t depends on the water temperature [Miyake & Abe, 1948]. Laboratory experiments of Miyake & Abe [1948] produced a rather strong dependence:

$$L_t \sim \exp(-T_w/25) \tag{3.14}$$

where T_w is the water temperature. Mentionings of the temperature effect are also scattered around later studies [Wu, 1979, 1988, Monahan & O'Muircheartaigh, 1986, Stramska & Petelski, 2003], but no systematic efforts to investigate it have been attempted. This creates an additional uncertainty about the whitecap coverage W in different meteorological conditions, and in this regard it is also necessary to point out what appears to be a persistent confusion about dependence of W on atmospheric stability.

Variations of dependence of W versus U due to the atmospheric stability were foreshadowed in very early studies [Monahan, 1971], were even quantified to some extent later [e.g. Wu, 1979] and are still highlighted now [e.g. Stramska & Petelski, 2003]. It is hard, however, to justify such connection, between the stability of the atmospheric boundary layer and the whitecap coverage of the ocean surface, physically. Wave breaking, whitecap coverage and lifetime of the foam are essentially the water, not the air properties. We see two possible explanations of the correlations, between the whitecap and the stability, which are observed.

First of all, the unstable atmospheric conditions (which signify water being warmer than the lower atmosphere) affect the wind profile. For the steady low boundary layer such profile is described as

$$U(z) = \frac{u_*}{\kappa}\left[\ln\frac{z}{z_0} - \psi\left(\frac{z}{L}\right)\right] \tag{3.15}$$

where z is the vertical coordinate, $\kappa = 0.42$ is von Karman constant, ψ is a function of the Monin-Obukhov length scale L (we refer the reader to the literature on atmospheric physics for more details [e.g. Komen *et al.*, 1994]). Under stable and neutral conditions, the profile is logarithmic and U_{10} wind in (3.5) and τ stress in (3.7), or other relevant wind characteristics are easily found. In unstable conditions, there can be significant deviations from the logarithmic profile because

of the function ψ. These are quite difficult to take into appropriate account, hence the bias occurs in estimates of U_{10}, u_*, τ and in the corresponding dependences. In this case, some correlations between the whitecap coverage and atmospheric conditions can be observed which are, however, due to the bias of surface wind estimates rather than due to dependence of W on stratification of the air.

The second possible explanation is a misinterpretation of some data. For example, Wu [1979] analysed whitecap-coverage data measured independently by Monahan [1971] and by Toba & Chaen [1973] and demonstrated a clear separation of the data obtained in stable, neutral and unstable conditions. In both data sets, for the same wind speeds whitecap coverage on average was higher when the atmosphere was stable, lower when the stratification was neutral and even lower in unstable circumstances. Since, however, a significant range of surface water temperatures was involved (in Monahan [1971] it was from 17.5° to 30.55°), and the surface temperature trend was not removed, it would affect the conclusions. Ordering the stratification as stable, neutral and unstable would correspond, on average, to increasing water temperature, and therefore to decreasing whitecap coverage according to (3.14). This is exactly the trend observed by Monahan [1971] and attributed to the atmospheric stability without ruling out the surface-temperature dependence first.

Further uncertainties of (3.5)-like parameterisations of the coverage W in terms of wind speed U, which may prove essential in some circumstances, have to be highlighted. Again, the early researchers were already aware of them. Monahan [1971] mentions variations of the whitecap coverage as a function of wave fetch and wind duration. These days, it is translated as dependence of W on the second parameter, U/c which characterises inverse wave age (stage of wave development or wind forcing) [e.g. Zhao & Toba, 2001, Stramska & Petelski, 2003, Guan *et al.*, 2007]. Indeed, this should be expected based on apparent physical argument. As it is discussed above, the whitecap coverage depends on the breaking probability and the breaking strength. Both of them depend on the wave age. For example, in a laboratory experiment Babanin *et al.* [2009a,b] demonstrated that, for stronger forcing U/c, the breaking probability is higher whereas the breaking severity is weaker. Thus, the trends are opposite, and therefore their combined effect on the whitecap coverage may not be clearly pronounced, but obviously variations of magnitude of W, at the same wind speed U, but for different development stages U/c, can be expected.

Another essential uncertainty, also pointed out by the early researchers, is due to the presence of biological surfactants. Monahan [1971] mentions "variations in sea water surface tension caused by the occasional presence of organic films [Abe *et al.*, 1963, Garrett, 1967]". Such 'occasional presence' may have a significant impact on regional variations of the whitecap-coverage dependence, because of different biological activity in an ocean region. Stramska & Petelski [2003], for example, conducted observations in a polar area, where amount of dissolved organic material is different to the waters of traditional observations, and concluded that some of historical relationships for W-versus-U would overestimate their observations by a factor as large as 8.

To conclude the brief overview of the early observations of whitecaps, we have to say that, while studies of this property of wave breaking have now spanned more than six decades, many uncertainties remain in parameterisations of the whitecap coverage until today. Given the fact that importance of this oceanic characteristic grows as the means of remote sensing of the ocean develop, it is important to realise these uncertainties and address them. Some of them are linked

with gaps in our understanding of the wave breaking process, and some are not.

3.2 Traditional means (visual observations)

When capacities for measuring and storing surface elevation data became available, further research of wave breaking concentrated on hydrodynamic characteristics of the breaking, rather than on the connections with the wind as in Section 3.1. As far as the wave-breaking part of the measurement is concerned, still, for many year the visual observations remained the most reliable, or sometimes the only means to detect the breaking events. These included manual tagging of breaking waves in the surface elevation records [Weissman *et al.*, 1984, Holthuijsen & Herbers, 1986, Stolte, 1992, 1994, Babanin, 1995] or video-taping of the surface, accompanied by collocated measurements of the waves [Katsaros & Atakturk, 1992, Babanin *et al.*, 2001]. In the laboratory experiments or field observations, the tagging can be performed in real time while observing breaking waves recorded and marking them electronically. In case of the video-taping, such tagging can be done by means of repeated watching the recorded videos, which reduces a possibility of human error.

In any case, the observations deal with visible whitecapping, that is with the Breaking-in-Progress stage of the process (see Section 2.2). Therefore, they mostly concentrated on studies of the breaking probability (see Section 2.5) and dependences of the breaking occurrence on wave, wind and other environmental characteristics.

The first major observation of the kind was by Holthuijsen & Herbers [1986]. In many regards, it was a break-through in experimental studies of wave breaking, particularly in field conditions. One of the authors was watching a wave buoy and "triggered a radio signal each time an active whitecap was seen to pass under the buoy. The signal was recorded synchronously with the buoy signal on one tape in an onshore station, thus identifying breaking waves with an 'on-off' signal". Then wave-by-wave analysis of individual waves was conducted by means of the zero-crossing method. Probability and statistics of wave height, crest height, wave period, steepness and asymmetry of the breaking waves were studied for the first time, dependence of the breaking probability on wind speed was considered.

In particular, it was concluded that "the breaking occurs at wave steepness values much less than the theoretically expected steepness of a limiting wave" (2.46). This issue has been discussed in Section 2.1 above, and we now know that measurements of the wave which already exhibits whitecaps cannot provide estimates of the limiting steepness at the breaking onset.

Other outcomes of the paper, for example, conclusions on the connection of the breaking occurrence with the structure of wave groups remain valuable up-to-date knowledge on the wave breaking. Holthuijsen & Herbers [1986] concluded that the probability of a wave group to have at least one breaker was higher for longer wave groups. In their observations, almost 100% of long groups, i.e. those consisting of 7 waves produced a breaker. Overall, 0.69 of all breaking waves happened within a wave group. Those were breaking close to the centre of wave groups, slightly ahead of this centre. As will be discussed later, such observations are consistent with the present understanding of two-phase behaviour of the wave breaking [see Young & Babanin, 2006a, Sections 5 and 6] and with the asymmetric shape of non-linear waves groups due to the modulational instability [Shemer *et al.*, 2002], which is expected to be the major mechanism responsible for wave breaking in deep water (see Section 5).

Babanin [1995] conducted wave measurements and wave-breaking observations in the field

and laboratory. In the field, the wave probes were resistance staff gauges which recorded the elevations and buoys recorded the surface acceleration. In all the cases, the breaking detection was conducted by means of visual observations and synchronous electronic labelling the breaking events.

Like in Holthuijsen & Herbers [1986], it was concluded that mean steepness of the breaking waves is well below the limiting steepness (2.46) and that the waves usually break close to the centre of wave groups. Unlike in Holthuijsen & Herbers [1986], however, it was found that all the breakers displayed a well-pronounced negative front-to-back asymmetry (1.3) and that a dominant breaker at the top of wave group envelopes is usually accompanied by one or sometimes two subsequent breaking dominant crests. In any case, as mentioned above, both observations deal with the waves already breaking rather than with the breaking onset, and as it is now well-understood in the course of such breaking a wave can go through a broad range of steepnesses, which will be gradually decreasing, and of asymmetries which will tend to oscillate [e.g. Babanin *et al.*, 2007a, 2009a,b, see also Sections 2.1 and 5].

Acceleration measurements by Babanin [1995] demonstrated a very strong asymmetry of time series of the vertical acceleration in the breaking events. While in general oscillations of the acceleration signal are quite symmetric, in the course of breaking the downward acceleration could reach the value of (2.49). This is consistent with theoretical expectations for monochromatic limiting waves [e.g Longuet-Higgins *et al.*, 1963] and with observations of waves which can be treated as quasi-monochromatic [e.g. Liu & Babanin, 2004], but it is significantly less than (2.54) which could be expected for a complicated sea [Longuet-Higgins, 1985].

Babanin [1995] marked conditionally large and small breaking events by electronic tags of different duration which allowed him to research their statistics separately. Together with having measurements of both surface elevation and surface acceleration in the breaking waves, this helped to reveal new features of the wave breaking properties across the spectrum. The large breakers were interpreted as those of dominant waves which belong to the spectral peak region, and the small breakings were related to the equilibrium interval of the spectrum.

Breaking of the energetic waves amounted approximately one third of the total number of breakers which is about half of the percentage measured by Holthuijsen & Herbers [1986]. When the same data were used for further analysis, this ratio was found to depend on the wave development stage [e.g. Banner *et al.*, 2000], so this and above mentioned differences between Holthuijsen & Herbers [1986] and Babanin [1995] observations can perhaps be attributed to the wave age of the observed sea states. The latter study also showed that, while average breaking rates did depend on the wind speed, variations of the dominant breaking occurrence correlated with the running variance of surface elevations. Since such wave variance is mostly determined by the contributions from the spectral peak, this finding demonstrated that properties of the waves themselves, i.e. hydrodynamics rather than the wind, ultimately control the breaking process of dominant waves.

Breaking of small waves, on the contrary, appears to correlate with the running variance of the acceleration. Spectrum of the acceleration is dominated by the high-frequency contributions into the variance [e.g. Babanin *et al.*, 1993]. Thus, the correlation signifies a connection of the small-scale breaking with variations of the level of equilibrium interval in the wave spectra.

Therefore, Babanin [1995] concluded that short-term equilibrium of the wave spectrum tail (i.e. level α in the spectrum shape formulation (2.7)) was supported by changes of the frequency of breaking occurrence of waves that belong to this tail. Breaking of the dominant waves controls

the energy in the spectral peak region, that is the enhancement γ of the peak (2.7). Overall breaking rates were also found to depend on the spectral width which was formulated as

$$\nu = \frac{m_0}{f_p F(f_p)} \tag{3.16}$$

following Belberov *et al.* [1983].

Observations similar to those by Holthuijsen & Herbers [1986], Babanin [1995] have obvious limitations due to the human error when marking rapid and suddenly happening events, and due to physical capability of the observer to only resolve large enough breakers. Holthuijsen & Herbers [1986] "watched the buoy from either a nearby observation tower (~ 100 m from the buoy) or from a nearby ship (~ 50 m from the buoy)". Their estimate is that they could see whitecaps of the minimum size of approximately 15 cm. Babanin [1995] watched the whitecaps occurring either inside of an array of wave staffs or on a drifting buoy. In the first case, the observer was located 16 m directly above the array and could resolve any breaking which produced whitecaps. In case of the buoy, the observer was watching the buoy from a drifting research vessel, some 100 m from the buoy, and had the clear view of the whitecaps down to the size of the buoy (less than a meter [Babanin *et al.*, 1993]).

Such limitations can be overcome to some extent by high-resolution video taping of the wave surface. Having followed such approach, Katsaros & Atakturk [1992] reported a quite unique statistics of micro-breaking. Contrary to many expectations (see Section 2.8), micro-breaking rates in their observations did not appear higher than those for plunging and spilling breaking. An important finding of Katsaros & Atakturk [1992] is that, while the overall amount of plunging/spilling breaking depends on average on the background mean wind speed, the amount of micro-breaking does not. This can now be explained by the cumulative effect of the wave breaking, that is by the fact that small-scale breaking is affected by the breaking of larger waves or modulation due to the larger waves. In such case, the cumulative effect at high frequencies will be such that the induced breaking of the short waves will dominate the breaking caused by inherent reasons. Therefore, breaking rates at small enough scales should be fully determined by behaviour of the longer waves in the system, and will poorly correlate with the background wind [Babanin & Young, 2005, Babanin *et al.*, 2007c]. Other important conclusion of Katsaros & Atakturk [1992] is that, if the breaking statistics is investigated in terms of the wave-generating wind, it will depend on two parameters: the wind speed and the wind forcing u_*/c_p (here, c_p is phase speed of waves at the spectral peak f_p).

Other examples of visual observations and manual tagging the breaking events include investigations by Weissman *et al.* [1984], Stolte [1992, 1994] where the tags were used to develop ad hoc criteria in order to then computerise the subsequent data processing. These and other contact measurements of wave breaking, based on assumed trial-and-error criteria, will be reviewed in Section 3.3 below.

Thus, the traditional visual observations gave a significant boost to understanding, description and parameterisations of the breaking rates in different wind-wave fields. This is, however, a very laborious kind of studies which involve an observer who marks and then counts breaking events by visually monitoring wave probes, where the surface elevations are recorded, and waiting for whitecapping to occur. While the visual observations do not suffer from uncertainties due to empirical thresholds set in 'automated' wave-breaking detection techniques described later in this Section 3, they are nevertheless subject to human error and are too manually intensive and

time consuming to be broadly employed in the wave research.

3.3 Contact measurements

Contact measurements of wave breaking imply instrumentation placed at the air-sea interface where the breaking actually happens. What, however, they should measure? There are vast volumes of records by wave probes sensing surface elevations, velocities and accelerations accumulated over decades, most of them undoubtedly had breaking waves passing over and recorded, but those are impossible to identify without some criteria which would distinguish breaking from non-breaking waves.

A significant number of clever and elaborative attempts and approaches have been tried in this regard. Since the most obvious feature of the breaking is discontinuity of just about every geometrical, physical and even chemical property at the ocean surface, many studies aimed at developing an ad hoc criterion by means of trial and error to detect such a discontinuity. Others have relied on known physical limiters, i.e. limiting Stokes steepness (2.46), limiting acceleration (2.55) or limiting orbital velocity (2.48).

The contact measurements of the wave breaking is an area of research extensively explored and developed over the period of some 30 years, and it is impossible to even briefly mention all relevant studies. Here, we will suggest a review of a small selection of examples in an attempt to illustrate the ongoing experimental effort of the phenomenon which has been resisting such investigations and still remains difficult to approach experimentally.

The field study by Thorpe & Humpries [1980] used a breaker detection scheme based on a jump of the surface slope associated with the leading edge of the breaking region. Following the tradition of whitecap observations, they were seeking a correlation between wind speed and the breaking probability. The data clearly indicated such dependence, but no quantitative relationship was provided.

A similar breaking detection technique was developed by Longuet-Higgins & Smith [1983] who suggested a physical-limiter criterion and were followed by many studies based on this criterion. The authors reasoned that "if a breaking wave passes the recorder, we expect a sudden jump in surface elevation" which has to be detectable because of large values of time t derivative of surface elevation $\partial\eta/\partial t$. To detect the jumps, a wire wave probe was used deployed on a specially designed buoy. The buoy was tested first in the laboratory and then applied in the field to look for the derivative

$$R_t = \frac{\Delta\eta}{\Delta t} = c\frac{\Delta\eta}{\Delta x} = c\tan\theta \tag{3.17}$$

where the discretisation Δ is determined by sampling frequency of the time series, and the limit is defined by the maximal possible inclination of the surface (2.52). The authors argued that if lower values of R_t are set as the criterion for the jump detection circuit, breaking-in-progress will be identified, but caution should be exercised not to have the circuit respond to steep, but non-breaking waves.

Longuet-Higgins & Smith [1983] applied their technique in the field, measurements were conducted for wind speeds from 1 m/s to 14 m/s. At the maximal wind speed, the breaking rates found were of the order of 1% which is consistent with later field observations [e.g. Babanin *et al.*, 2001]. Interestingly, however, they found that histograms of measured surface jumps in

breaking waves did not depend on actual selection of the critical value for R_t (provided, of course, it was high enough). Measured values of R_t often exceeded the maximal theoretical value of

$$\frac{R_t}{c} = 0.586 \tag{3.18}$$

which follows from (3.17), (2.52).

Detection of the surface-elevation jumps in accordance with technique defined by (3.17)-(3.18) was employed for wind-generated waves by Xu *et al.* [1986], Caulliez [2002] in laboratory. Xu *et al.* [1986] measured probability of occurrence, breaking height and breaking duration, their dependence on the wind and their interconnections. The data disintegrated into two distinct groups, the dominant breakers and the second group "probably associated with either the breaking of small waves riding on long waves or other profile irregularities". This is a feature, becoming familiar and having already been mentioned a few times above - the two-phase behaviour of wave breaking in spectral environment (see Sections 5 and 6 for more details). Xu *et al.* [1986] described statistics and dependences for the two groups separately. For the dominant breakers, they found average steepness of $ak = 0.375$. As will be discussed below, since the detection was based on ratio R_t/c exceeding the limit (3.18), this is most likely steepness of waves already breaking rather than a criterion for the incipient breaking as it was interpreted.

Caulliez [2002] found that breaking waves detected in the wave records this way exhibit a self-similar shape with very strong negative asymmetry of $A_s \approx 0.5$ (1.3). Like Longuet-Higgins & Smith [1983], Xu *et al.* [1986], Caulliez [2002] also observed the ratio R_t/c (3.18) exceeding the maximal theoretical value of 0.586. On average, the measured maximal slopes of wavefronts were 45° which is "much larger than 30°, the value predicted for the highest Stokes wave" (i.e. 2.52).

Longuet-Higgins & Smith [1983], Xu *et al.* [1986], Caulliez [2002] interpreted the fact that they found $\frac{R_t}{c} > 0.586$ as measuring 'the waves that are just about to break', 'not actually breaking', 'near-breaking', or in other words incipient breaking or the breaking onset (see Section 2.1). Here, we would disagree with such interpretation. If $\theta_{critical}$ (2.52) defines the maximal possible inclination of the surface for steady waves, then inclination angles of $\theta > \theta_{critical}$ should signify the surface which is unstable and is already breaking. As review of pictures of breaking waves in Section 1 shows, local inclination of surface in the course of breaking can reach almost any angle and perhaps even 90° in a vertically plunging jet. The fact that histograms measured by Longuet-Higgins & Smith [1983] did not depend on the critical value for R_t supports such conjecture: raising the level of R_t did not remove the breakers-in-progress and did not eventually limit the statistics to the incipient breakers only, because the breakers-in-progress exhibited the surface steepness, locally, higher than the limiting Stokes-wave steepness.

Therefore, the techniques developed by Longuet-Higgins & Smith [1983], Xu *et al.* [1986], Caulliez [2002] appear an excellent practical tool to identify and measure properties and statistics of the breaking-in-progress, rather than those for the breaking onset. This supposition is further supported by experimental results of Babanin *et al.* [2007a, 2009a,b] who found that at the breaking onset a wave is nearly symmetric with respect to the vertical, but it inevitably starts leaning forward (develops a progressing negative asymmetry (1.3)) as it begins and continues to break, in accord with measurements of the breaking-wave shape by Caulliez [2002].

Another example of using physical limiters to detect breaking events is a laboratory study of

wind-generated waves by Hwang *et al.* [1989]. The authors employed two limiting criteria for the water waves in order to detect the breaking, i.e. geometric criterion (2.52) and kinematic criterion (2.48), in a comprehensive study intended to investigate the breaking probability, breaking duration and lengthscale, breaking phase with respect to the wave shape, breaking severity and the probability of multiple subsequent breaking within one wave group. The instantaneous local values for the surface slope and the orbital velocity were obtained from the time series of surface elevation by means of Hilbert Transform (see Section 3.7).

Breaking regions were found geometrically similar, with duration of their persistence and spatial extent been proportional to the scale of breaking waves. Such observation served a good experimental support to the dissipation theory by Hasselmann [1974] which has formed the basis for dissipation terms employed in spectral models until now and is only started to be challenged recently, in the light of new experimental evidence (see Section 6).

Interesting observations were done with respect to the breaking phase, which challenged unambiguity of the breaking criteria themselves. According to the authors, "... based on the geometric criterion, the breaking inception is on the downwind side of the wave crest, while the kinematic criterion indicates inception on the upwind side. This delicate difference, although restricted to a narrow region of $\pm 10^{\circ}$ of the wave crest demonstrates that the breaking phenomena described by these two criteria, as well as by other threshold variables, are not exactly the same". Depending on the wind speed, a trend was observed for the breaking moving closer to the crest at higher wind speeds. Since for higher wind speeds, Babanin *et al.* [2009a,b] observed depleted severity, it may be that the phase of wave breaking region relative to wave crest is linked to the breaking strength. Such assumption, however, is a mere speculation at the present stage and need experimental verifications.

Probability of breaking, breaking duration and breaking length were investigated in terms of wind speed. Repeated breaking within wave groups was also found to correlate with the wind, but probability of the repetition in these laboratory observations was quite low compared to field observations [e.g. Donelan *et al.*, 1972, Holthuijsen & Herbers, 1986, Babanin, 1995]. Such probability was about 20% at 16 m/s wind and only around 10% at 7 m/s. The current understanding of the repeated breaking indicates that it is primarily due to behaviour of nonlinear wave groups, i.e. hydrodynamics, rather than the wind. The strong wind, however, can influence the wave grouping and correspondingly the breaking and reduce the breaking severity, and thus decrease or even diminish probability of the multiple subsequent breaking [Babanin *et al.*, 2009a,b]. For laboratory waves, which are always young, wind forcing is usually quite strong even at moderate wind speeds and thus may affect the observed statistics of the repeated breaking.

Estimates of the breaking severity, because they are rare, are most instructive. Hwang *et al.* [1989] evaluated loss of potential energy in terms of ratio $\Delta H/H_{before}$ where $\Delta H = H_{before} - H_{after}$. They found that it is

$$\frac{\Delta H}{H_{before}} = 1 - \frac{H_{after}}{H_{before}} = 30\% \pm 3\%. \tag{3.19}$$

If translated into energy, it gives

$$s = 1 - \frac{H_{after}^2}{H_{before}^2} \approx 50\%. \tag{3.20}$$

Significantly lower were found losses of kinetic energy Q (2.25):

$$s_{kinetic} = \frac{\Delta Q}{Q_{before}} = 20 - 25\%. \tag{3.21}$$

Such difference is qualitatively consistent with recent observations. Young & Babanin [2006a], when comparing spectra of pre-breaking and post-breaking waves, found some 40% of energy lost in the peak region of surface elevation power spectrum in case of dominant breaking, while the peak region of velocity spectrum measured below the wave troughs remained virtually unaltered.

Interesting account of contact laboratory experiment with wind-generated waves was provided by Leikin *et al.* [1995]. It was dedicated to measurements of wave asymmetry A_s (1.3), and although the breaking detection was not conducted, discussion of these results is relevant here.

Leikin *et al.* [1995] found a strong correlation of the asymmetry A_s with inverse wave age u_*/c_p, whereas correlations of skewness S_k (1.2) and steepness ϵ (1.1) with the wind forcing were poor. Thus, they supposed that "the vertical asymmetry of waves is caused by direct wind forcing". At the same time, they conducted bispectral analysis which revealed strong non-linear coupling between the main wave and its harmonics. Therefore, Leikin *et al.* [1995] also concluded that the observed wave system can be treated as mainly the dominant component with its harmonics propagating at the same speed. Normally, such system would have non-zero skewness S_k, but not non-zero on average asymmetry A_s. Therefore, the phase shift between the main component and the harmonics was considered and was found to increase with u_*/c_p and thus explained the growth of vertical asymmetry.

The two conclusions, i.e. the direct influence of the wind on the wave shape and this shape being a result of bound non-linear harmonics, seem contradictory. The first process signifies a strong air-sea interaction, whereas the second one appears a purely hydrodynamic phenomenon. The influence of the wind could perhaps be held responsible for the overall growth of the steepness and consequently the non-linearity, including bound harmonics, but such straightforward reasoning cannot explain the growing phase shift, and most importantly, there was in fact no correlated growth of the wave steepness as a function of wind forcing.

We would suggest a different explanation of the trend observed by Leikin *et al.* [1995]. At high wind forcing there is indeed a strong connection between the wind input into waves and the asymmetry [Agnon *et al.*, 2005]. This connection, however, does not bring about the negative average asymmetry, it only causes correlated oscillations of the input and A_s. In our view, what makes the asymmetry non-zero on average (in formulation of Leikin *et al.* [1995] it is positive rather than negative for waves leaning forward) is the wave breaking whose frequency of occurrence grows towards higher wind speeds, particularly as the measurements by Leikin *et al.* [1995] extend into really extreme conditions.

The range of wind speeds involved in the experiment was $u_* = 0.27 - 1.71$ m/s which, if converted into corresponding winds at standard 10 m height using (3.15), gives $U_{10} \approx 8-48$ m/s. These signify some very high wind speeds. Agnon *et al.* [2005] found that for strongly forced and highly non-linear wind waves, the wind-wave energy transfer, which depends on the mean wind speed, and the wave asymmetry are correlated, and they both oscillate with the same period. Thus, the observed by Leikin *et al.* [1995] connection of magnitude of the asymmetry with the wind speed can be explained through the mechanism of air-sea coupling.

The waves, however, have to become non-linear first, and this comes through the gradual growth of the wave steepness as a result of wind action. According to Agnon *et al.* [2005], the steepness ϵ and skewness S_k also exhibit oscillations correlated with the wind speed, but no direct connection of ϵ and S_k was observed by Leikin *et al.* [1995].

The discrepancy can be explained by the growth of wave breaking occurrence which accompanies the increasing wind speeds. In non-linear wave trains, steepness, skewness and asymmetry all oscillate due to modulational instability [Babanin *et al.*, 2009a,b]. Mean value of A_s remain close to zero unless a wave breaks. The wave always break when it starts leaning forward, i.e. when its steepness and skewness are maximal and the asymmetry $A_s \approx 0$. In the course of the breaking such wave exhibits $A_s < 0$ and at this stage the oscillations of the asymmetry are interrupted. Therefore, if many wave-breaking events take place within a wave record, average asymmetry over such record will deviate towards negative values, whereas maximal values of ϵ and S_k are not affected.

It is also instructive to notice that values of asymmetry A_s in Leikin *et al.* [1995] tend to saturate at $u_*/c_p \geq\sim 1.2$ (their Figure 1a). Since phase speeds of the laboratory waves measured were $c_p \leq\sim 1$ m/s, this translates into the saturation at wind speeds $U_{10} \approx 34$ m/s which is consistent with recent observations both in the field [Powel *et al.*, 2003] and laboratory Donelan *et al.* [2004]. Kudryavtsev & Makin [2007] investigated the latter case and explicitly connected it to wave breaking.

Returning back to the issue of contact measurements of wave breaking, two good examples of trial-and-error method are papers by Weissman *et al.* [1984], Stolte [1992]. As mentioned in Section 3.2, both studies used visual observations in order to develop an ad hoc breaking criterion and further process wave-breaking records automatically.

Weissman *et al.* [1984] were measuring the surface elevations with very thin wire probes and were detecting the breaking waves based on spectral energy in $18 - 32$ Hz frequency band. A wave was regarded breaking if the energy density exceeded some threshold level in the vicinity of crest of a respective wave group. The technique was applied in a fetch-limited field experiment, and breaking statistics at ~ 6 m/s wind was considered. Again, it was found that the mean steepness of breaking waves is well below the Stokes criterion (2.46). While temporal coverage of the breaking was only 1.2%, the relative high-frequency energy in those events was ten times that, i.e. 12%. Such a difference may bear significant implications for interpretations of radar, sonar and other remote sensing signatures of the wave-breaking events.

Stolte [1992] high-passed wave records at 1 Hz cut-off frequency and used the visual observations to deduce empirical criteria: e.g. $+2.5$ cm-jump over 0.31 s to mark the start of a breaker and -1.25 cm over 0.016 s for the breaker's end. Very interesting statistics for the breaker velocity, height, length, momentum, for spectral distribution of the breaking momentum, parameterisations of the total and relative numbers of breaking were obtained. Stolte [1992] also provided an experimental dependence of breaking severity on the wind speed which is quite a unique result.

The contact means for detecting the wave breaking and quantifying the breaking physics do not have to be restricted to measuring the surface elevations or other surface properties only. Lammarre & Melville [1992], Su & Cartmill [1992], Gemmrich & Farmer [1999], for example, developed a technique based on conductivity measurements below the surface. The breaking causes air-entrainment into the water column which is accompanied by a reduction of electrical conductivity. Effectively, the void fraction in the water is detected which signifies and quantifies

breaking events, their probabilities, severity and other properties. Gemmrich & Farmer [1999] defined a wave as the breaking event if the air fraction exceeded 8% in accord with the theory of Longuet-Higgins & Turner [1974]. The method is quite sensitive and accurate, and when used in field experiments it allowed to obtain spectral distribution of the breaking probability [Banner *et al.*, 2002, see Section 5 for details].

Thus, the trial-and-error criteria based on interpretation of one or another kind of discontinuities/jumps caused by the breaking can bring very fruitful and useful outcomes and should not be underestimated. Some of them, however, are very involved and leave a room to uncertainties if are to be repeated. For example, Stolte [1992] admits that his criteria had to be modified for more and for less intensively breaking wave fields. With respect to the Weissman *et al.* [1984] technique, Katsaros & Atakturk [1992] wrote: "Since the threshold, i.e. the absolute value of the measured band energy varies with wind speed (stress), gustiness, underlying long waves, currents etc., it had to be determined individually for each run". Gemmrich & Farmer [1999], who used the void-fraction criterion, pointed out: "While this criterion utilizes a well-defined property of all breaking waves except microbreaking, the definition of a suitable threshold again seems arbitrary and depends on the precise depth of the measurement as well as other factors that we cannot control, such as the vertical gradient of air fraction".

3.4 Laboratory measurements in deterministic wave fields

Laboratory measurements may involve both contact and remote-sensing methods and deal with either random (for example, wind-generated as in Section 3.3) or deterministic wave fields. The principal difference of the latter, with respect to the field observations, is that in such controlled repeatable experiments location of the breaking is known. If so, the necessary measurements of the wave breaking can be planned without having to detect the breaking event first. Such can thus be fine measurements which either require precise positioning of measuring devices or employ delicate high-precision instrumentation, impossible to transport and deploy in the field, for example, Particle Image Velocimetry (PIV).

Rather than just concentrating on passive observations and measurements, in laboratory an experimental effort can create conditions to simulate the breaking by means of a designated physical mechanism, for example by means of superposition of linear waves achieved through use of frequency dispersion [e.g. Cummins, 1962, Davis & Zarnik, 1964, Longuet-Higgins, 1974, Rapp & Melville, 1990, Meza *et al.*, 2000], or a superposition of non-linear waves through amplitude dispersion [e.g. Donelan, 1978, Pierson *et al.*, 1992], evolution of non-linear wave groups [e.g. Melville, 1982, Babanin *et al.*, 2007a, 2009a,b], or simply by artificial means such as concentration of wave energy because of converging channel walls [Van Dorn & Pazan, 1975, Ramberg & Griffin, 1987] or over an obstacle or a submerged shoal [e.g. Manasseh *et al.*, 2006, Calabresea *et al.*, 2008].

Conditions can also be created to exaggerate some wave-breaking features and extend the breaking time in order to study the phenomenon in greater detail. Caution has to be taken to properly scale down the observed and extended features, to clearly realise limits of applicability of the modelled conditions, but potential rewards of such laboratory efforts can be very significant.

In this regards, experiment by Duncan [1981] has to be highlighted whose results were broadly implemented and whose ideas stimulated very many related experiments, applications

and studies [e.g. Phillips, 1985, Melville, 1994, Phillips *et al.*, 2001, Melville & Matusov, 2002, Gemmrich *et al.*, 2008, among many others]. In the experiment, a steady breaker was produced by means of towing a submerged hydrofoil with phase speed of the breaking wave. Profile of the breaking waves, velocity distributions, turbulent wake and other properties of the steady breaker were measured and investigated.

Of particular importance for subsequent studies and applications was Duncan [1981] conclusion that the energy dissipation rate in such breaker can be described by a single independent variable, the wave's phase speed c (see Section 2.6). Thus, the rate of energy loss per unit length of the breaking front is proportional to:

$$S_{ds}(c) \sim \frac{\rho_w}{g} c^5. \tag{3.22}$$

Since in the linear or quasi-linear sense the phase speed translates into frequency/wavenumber, such conclusion signifies existence of a universal spectral function for the wave energy dissipation, and attempts have been undertaken to formulate and quantify such dissipation term [Melville, 1994, Phillips *et al.*, 2001, Melville & Matusov, 2002, Gemmrich *et al.*, 2008, among others].

In reality, however, the breaking is principally unsteady, and this brings about a proportionality coefficient broadly called the breaking parameter b. Measurements within realistic unsteady-breaking conditions in laboratory and in the field saw b varying by 4 orders of magnitude. Some studies pointed out its dependence on wave steepness ak [e.g. Melville & Matusov, 2002, Drazen et al., 2008], others argue that it is not the average steepness (1.1), but rather local variations of the steepness, that is wave slope, crest-to-wavelength ratio, along with other characteristics such as density of the whitecapping foam, relative orbital velocity (with respect to the phase speed) which form such breaking parameter b [Gemmrich *et al.*, 2008].

If we identify a range of open ocean-sea-lake peak frequencies very broadly as $f_p = 0.1 - 0.3$ Hz, then the range of dissipation rates at the spectral peak $S_{ds} \approx 9 \cdot 10^5 - 4 \cdot 10^3$ according to (3.22) which is only two orders of magnitude. That is the predicted range of change of the dissipation based on the Duncan [1981] hypothesis is two orders of magnitude less that the range which can be inflicted by uncertainties brought about by the 'proportionality coefficient' b. Given the fact that the hypothesis (3.22) has been widely exploited in the wave-dissipation literature lately, it should be emphasised that its practical significance appears in fact rather low.

Besides, the connection of dissipation in a breaking wave with its phase speed is clearly not applicable in case of induced breaking, i.e. the breaking of short waves caused by the large waves, whereas such cumulative dissipation tends to dominate at high frequencies [Babanin & Young, 2005, Babanin *et al.*, 2007c]. Therefore, even if the proportionality coefficient in (3.22) could be adequately quantified, the dissipation formulation of this kind, strictly speaking, is only applicable at the spectral peak region or below, where the cumulative effect is negligible.

Generation of deterministic unsteady breaking in the laboratory has been most frequently attempted through focusing the wave energy by using the wave frequency dispersion. The waves are generated mechanically with frequency being linearly decreased and thus the group velocity increased (2.19). As a result, linear superposition of waves in a pre-determined location is achieved [although at the later stages, because of the increasing average steepness in the converging wave packet, some essential non-linear interactions take place, i.e. Brown & Jensen, 2001]. The technique was originally suggested in ship design testing [Cummins, 1962, Davis

& Zarnik, 1964] and was introduced into broad research of wave breaking by Longuet-Higgins [1974], since when it has been employed in numerous laboratory experiments.

The most comprehensive study of this kind is that by Rapp & Melville [1990]. Laser Doppler velocimetry was used to obtain two components of the velocity in the breaking region, but the main wave measuring probes were simple surface piercing resistance wires. Since the method allows to position the breaking location quite precisely, energy losses and other relevant information concerning the breaking can be obtained with only two wave gauges. The technique deals with groups of waves, rather than an individual wave which is breaking, and it was found "advantageous to consider the momentum flux and energy flux loss from the wave packet as opposed to considering individual waves" (see also discussion in Section 2.7).

In Section 2.7 and throughout the text, results of Rapp & Melville [1990] have already been mentioned and discussed with regard to a number of relevant topics. This comprehensive and thorough study represents a benchmark in terms of methodology of laboratory investigations of the wave breaking and in terms of physics of the breaking which is caused by the linear superposition of a number of waves. Some features of such breaking are general, but some are distinctly different if compared with physics of the breaking which occurs, for example, as a result of non-linear evolution of wave groups [Babanin *et al.*, 2009a].

What needs to be additionally highlighted in this Section is the technique of flow visualisation of the breaking region devised by Rapp & Melville [1990]. They performed photographing of propagation and diffusion of dye initially floated on the surface. It was a precursor of the modern flow-visualisation means of the wave motion, such as PIV [e.g. Melville *et al.*, 2002, Oh *et al.*, 2008, Babanin & Haus, 2009], but many results of Rapp & Melville [1990] on subsurface mixing due to a breaking event, such as temporal and spatial measures of the mixing, their connection with wave properties and momentum losses in the course of the breaking, remain state of the art up to date.

The linear superposition technique was employed by Nepf *et al.* [1998], Wu & Nepf [2002] in their laboratory comparison of two- and three-dimensional wave breaking. The experiment was conducted in a wave basin where water fronts were generated by 13 independently programmed and driven paddles. If moved concurrently, the paddles would create a long-crested wave, but the crest could have been tapered laterally, and this was done by applying a cosine window to the signal which controlled the motion of the set of paddles. While the method of converging a wave packet due to phase dispersion was the same as in other tests which used such superposition, the tapering allowed to create short-crested waves and thus investigate the influence of crest's three-dimensionality on the wave breaking.

Here, we would like to point out that short-crestedness and directionality of the waves are often confused and used inter-changeably in the literature, although this is not the same feature. Indeed, if 2D-Fourier-like analysis is applied to two-dimensional wavy surfaces, in case of short-crested waves the outcome will be an angular distribution of wave energy. Such angular distribution, however, will not be a δ-function even if the short-crested waves are strictly unidirectional. Opposite is also true: that is superposition of long-crested waves having come from different directions will be decomposed by the 2D Fourier Transform into a finite-width directional spectrum. This is because Fourier analysis, when applied formally, will treat the former situation also as a superposition of long-crested harmonic waves which they are not, and therefore the wave energy placed by such analysis at oblique angles is just a noise in the Fourier sense due to the short-crestedness.

This may sound as an abstract mathematical argument, but it has a principal physical consequence for the wave breaking. Modulational instability, which can lead to the wave breaking, still exists in two-dimensional wave trains with three-dimensional wave crests, even though the breaking onset is set back from steepness $\epsilon = 0.29$ in strictly 2D waves to $\epsilon = 0.44$ in 2D waves with 3D wave crests [Melville, 1982, Babanin *et al.*, 2009a,b]. The proper directionality, however, can fully suppress the modulational instability and therefore the wave breaking due to this reason, if the directional spreading of wave field is broad enough [Onorato *et al.*, 2009a,b, Waseda *et al.*, 2009a].

In this context, Nepf *et al.* [1998], Wu & Nepf [2002] conducted experiments with short-crested rather than directional waves. Three-dimensional structure of the crest was created by either focusing or diffracting the waves generated separately by the 13 paddles. Surface elevations were measured by an array of six wave gauges deployed on a carriage which could traverse the array to a measurement point near the wave-breaking location. An extensive set of geometric (wave steepness and shape), kinematic (2.48) and dynamic (up-frequency spectral energy shift) criteria were investigated.

It was found that the imposed directionality of the crest could either increase (focusing waves) or decrease (diffracting waves) the wave steepness at breaking onset [as opposed to the lateral modulational instability of the wave crest which increases the steepness at the incipient breaking, e.g. Melville, 1982]. Shape parameters at the breaking were altered in a similar manner. The kinematic and dynamic criteria, on the contrary, were not affected by the crest directionality. Since the dynamic criterion considered is sensitive and difficult to estimate, particularly in the field, it was concluded that the kinematic criterion (2.48) is the most robust property to describe the breaking onset.

Special attention was paid to the severity of breaking in the circumstances. The severity was defined in terms of wave groups (2.31). It was found that "spatially focusing and diffracting wave packets lost 34% and 18% of their energy, respectively, as a result of plunging breakers and lost 12% and 9%, respectively, as a result of spilling breakers. Comparable two-dimensional breakers with the same spectral shape lost 16% for plunging and 12% for spilling".

The breaking strength and its spectral distribution in case of breaking caused by linear focusing, considered by Nepf *et al.* [1998], Wu & Nepf [2002], is very different to the severity distribution in the breaking event caused by amplitude dispersion [Pierson *et al.*, 1992] or by non-linear modulation [Babanin *et al.*, 2009a,b]. The wave superpositions, whether these are due to frequency or amplitude dispersion, concentrate wave energy and thus create a steep wave which then becomes unstable and breaks. A very steep wave can be brought about by a completely different physical mechanism, modulational instability of wave trains. Such instability leads to formation of non-linear wave groups, within which rapid instantaneous concentration of wave energy occurs at some fetch. Location of such event, which results in wave breaking if the concentration leads to formation of a steep enough wave, is repeatable in deterministic experiments, but it is not as precise as that due to the superpositions of waves discussed above. The breaking happens at a particular phase of the non-linear group, close to the top of the group whose envelope is not symmetric, and since the group usually comprises a non-integer number of carrier waves, the exact position of the breaking oscillates [Melville, 1982, Babanin *et al.*, 2007a, 2009a,b].

The oscillation, however, is quasi-periodic and measurements of the breaking onset or of other phases of the breaking events can be conducted by a simple wave probe through recoding

a number of breaking events at the location [Babanin *et al.*, 2007a, 2009a,b]. Since it is believed that the modulational instability may be one of the primary mechanism responsible for wave breaking in ocean wave fields, later in this paper a significant attention will be paid to laboratory experiments dealing with the breaking due to such instability (Sections 5, 6).

3.5 Acoustic methods

Underwater ambient acoustic noise is generated through a number of possible sources such as precipitation, formation of bubbles in saturated condition [e.g. Blanchard & Woodcock, 1957], biological sources [e.g. Chitre *et al.*, 2006], or the breaking waves. In most circumstances, the latter is by far a dominant source [e.g. Thorpe, 1992, Bass & Hey, 1997, Tkalich & Chan, 2002, Manasseh *et al.*, 2006, among many others]. Here, we will describe relation of the ambient sound to wave breaking following Manasseh *et al.* [2006], Babanin *et al.* [2001].

The ambient sound level in the ocean at a given frequency may vary by 20 dB, increasing with the wind speed [e.g. Knudsen et al., 1948, Wenz, 1962, Kerman, 1988, 1992, Ding & Farmer, 1994]. Wind and wave effects are most marked in the $0.1 - 10$ kHz band. The general mechanisms of sound creation in this band are understood, although their inter-relationships are not. Wind pumps energy into the wave spectrum, causing wave growth which can lead to breaking. The whitecapping from a breaker creates bubbles near the surface, and bubbles emit sound. However, it is known that the wind dependence is indirect. It is the hydrodynamic evolution of the waves that determines whether breaking occurs [e.g. Babanin *et al.*, 2001, 2009a,b]. Once breaking happens, it is the primary source of the ambient noise in the ocean [e.g. Kerman, 1988, 1992, Farmer & Vagle, 1988, Felizardo & Melville, 1995]. The wave-breaking bubbles can either generate the sound themselves as described below or can transform pressure fluctuations in the air into acoustic noise in the water [Didenkulov, 1992].

Subdividing the $0.1 - 10$ kHz band allows more detailed explanations. In general, it is above 0.5 kHz that the wind-dependent component to the sound spectrum dominates [Wenz, 1962]. Furthermore, Bass & Hey [1997], Babanin *et al.* [2001] showed that the sound spectrograms due to breakers become evident above 0.5 kHz. Theoretical work [e.g. Meyer, 1989] suggests that the bubble-formation process dominates the acoustic spectrum at frequencies greater than 0.5 kHz. From the basics of bubble acoustics briefly described below, $0.5 - 10$ kHz corresponds to the natural emissions of millimeter-sized bubbles at near-surface depths. Frequencies around $0.1 - 0.5$ kHz are likely to be produced by bubble clouds, not individual bubbles [e.g. Prosperetti, 1988, Lu et al., 1990, Tkalich & Chan, 2002].

It has been well known since the time of Rayleigh [1917], that individual bubbles oscillate volumetrically with a natural frequency that depends on their size [see Leighton, 1994, for a review], suggesting an obvious application to instruments analysing bubbly flows. The simple-harmonic solution to the Rayleigh-Plesset equation describing bubble-acoustic oscillations shows that a single bubble's natural frequency is inversely related to bubble size, according to

$$\omega_0 = \sqrt{\frac{3\gamma_0 P_0}{\rho_w}} \; \frac{1}{R_0}, \tag{3.23}$$

[Minnaert, 1933] where ω_0 is the sound radian frequency, γ_0 is the ratio of specific heats of the gas, P_0 is the absolute liquid pressure and R_0 is the equivalent spherical radius of the bubble.

If the number of bubbles is assumed infinite, continuum approximations based on (3.23) permit overall acoustic properties of a bubbly cloud to be calculated [e.g. Commander & Prosperetti, 1989, Duraiswami et al., 1998]. The acoustic properties of bubbles have been the basis of several oceanographic instruments [e.g. Phelps et al., 1996, Terrill & Melville, 2000] as well as industrial instruments [Duraiswami et al., 1998, Boyd & Varley, 2001, Manasseh et al., 2001] although none are in widespread use. Most systems measure bubble-size distributions, relying on an active principle. Sound is sent into the water and the attenuation or reflection of the resulting signals is interpreted to infer the bubble-size distribution.

However, bubbles also passively emit sound at their natural frequency, that is without being forced by an external sound field. As a bubble detaches from its parent body of gas, it produces an acoustic pulse. This may be due to a sudden compression of the trapped gas as the bubble pinches off [Manasseh *et al.*, 1998]. This 'ringing' of the bubble may last less than 10–20 cycles; for example, for a 2 mm diameter bubble (i.e. 3 kHz natural frequency), the pulse can last less than 10 ms. While any disturbance may cause the bubble to ring, the highest-amplitude sounds are created when a bubble is pinched off [Chen et al., 2003, Vazquez *et al.*, 2005, 2008] or coalesces Manasseh et al. [2008]. Many bubble-creation events occur per second, during processes ranging from filling a glass to wave breaking. Although humans perceive this as a continuous noise, it is due to many discrete, brief events. An individual bubble's pulse becomes briefer as the bubbles are produced more closely to each other; and the frequency of the signal drops during the pulse, with the earliest acoustic cycles being closest to the natural frequency given by (3.23) [Manasseh, 1997]. It was shown by Manasseh et al. [2004] that these effects may be explained by inter-bubble acoustic interactions as the system becomes more 'cloud-like'. Furthermore, sound intensity drops rapidly with distance from the bubbles, which may be considered as monopole sources [Longuet-Higgins, 1989, Leighton, 1994].

These phenomena suggest that a sufficiently short time window triggered on a signal peak often contains data specific to a single, nearby, newly-formed bubble [Manasseh et al., 2001]. This implies that appropriately thresholded acoustic data can generate statistics as a function of time, on both the number of bubbles produced and their size. Detection of the bubbles can be linked to the periods of waves producing them, if the wave records are taken simultaneously, and thus be used to study the breaking probability (see Section 5). The bubble size appears to be an indicator of the breaking severity (see Section 6). Thus, a single device can be employed to obtain and study the wave-breaking energy dissipation. We should note, however, that, like most of other methods described in this Section 3, it has to rely on an empirical threshold.

To summarise the above, acoustic methods of investigation of the breaking can be broadly subdivided into two large groups of studies: active acoustic probing and passive acoustic techniques, and less broadly into research of sound produced by individual bubbles and bubble clouds. The latter subdivision is only less broad as far as the wave-breaking applications are concerned. Physics of oscillations of individual bubbles [Medwin & Daniel, 1990, Lowen & Melville, 1991b, Manasseh, 1997, Manasseh *et al.*, 1998, 2006] and bubble clouds [Carey & Bradley, 1985, Prosperetti, 1985, Tkalich & Chan, 2002, Manasseh et al., 2004] are quite different. Detection and quantification of the wave-breaking effects by means of individual bubbles or their clouds, however, simply implies dealing with different spectral bands of the acoustic noise produced in the course of the breaking.

The subdivision into the active and passive acoustic methods, on the contrary, is essential in wave-breaking studies. There are two basic active techniques employed in this regard. One

of the methods of active acoustic probing makes bubbles or bubble clouds resonate when they are exposed to an external source of sound [e.g. Thorpe, 1992, Farmer *et al.*, 1998, Terrill & Melville, 2000, Gemmrich & Farmer, 2004]. While they resonate at the same frequencies which they emit when being produced or collapse naturally, technically this means presence of sonar in the water which has to be powered and maintained. This limits applications of the technique, particularly in the extreme weather conditions, and on long-term or even regular basis. As a result, such active acoustic methods have been rather extensively employed to investigate oceanic phenomena related to the breaking such as bubble clouds and bubble size distributions, void fraction [e.g. Thorpe, 1992, Farmer *et al.*, 1998, Terrill & Melville, 2000, Gemmrich & Farmer, 2004], but not so much the wave-breaking physics and statistics.

Another active acoustic method, which has been gaining momentum over the past two decades or so, is based on using reflective properties of the water heterogeneities (such as small particles of matter, bubbles or even turbulent vortices) or of the water surface. The former use Doppler shift of the sound reflected by moving inhomogeneities to determine the motion velocity, and the latter simply monitors sound reflected from the surface to measure surface oscillations. The velocity records can be acquired as three-dimensional time series (so-called Acoustic Doppler Velocimeters (ADV)) or as a sequence of spatial slices of one-dimensional velocity fields (pulse-to-pulse coherent Doppler profilers [Dopbeam, Veron & Melville, 1999]). Another type of active acoustic devices of this kind are Acoustic Doppler Current Profilers (ADCP) which, if, for example, positioned at a not-very-deep bottom, can measure velocity time series at a number of points between the bottom and the surface, as well as time series of the surface elevations. ADVs, Dopbeams and ADCPs are manufactured by industry both as research and applied instruments.

Such acoustic velocimeters have been used to investigate velocity fields beneath breaking waves [Doering & Donelan, 1997, Young *et al.*, 2005], to quantify differences in kinetic energy due to wave breaking [Young & Babanin, 2006a], to measure turbulence caused by the breaking, even within the crests of breaking waves [Gemmrich & Farmer, 2004]. Compared to the sonars employed to make the bubble clouds resonate, the Doppler velocimeters have been in much broader use in wave-breaking studies, both in laboratory and in the field. On one hand, this is due to availability of industrially produced battery-operated models of ADVs and ADCPs designed for field use. On the other hand, even laboratory high-precision cabel-powered versions made their way into dedicated field experiments [Veron & Melville, 1999, Gemmrich & Farmer, 2004, Young *et al.*, 2005, Young & Babanin, 2006a].

Among the breaking-detection methods, passive acoustic determination of breaking and its properties have a potential advantage. The instrumentation (hydrophones) is relatively cheap, robust and easy to maintain. The hydrophones are deployed below the surface and are solid-state devices, therefore escaping most of the destructive power of breaking waves. Once deployed, they can be operated on a long-term or regular basis and collect ready-to-process time series.

Passive acoustic measurements have been employed in a number of field observations and laboratory experiments. Their first applications to the wave-breaking studies were by Farmer & Vagle [1988] in the field and by Melville et al. [1988] in the laboratory. Both experiments showed that acoustic signatures of breaking waves can be used to identify the breaking events. Farmer & Vagle [1988] used a single hydrophone and found that the mean distance between the breakers and acoustic strength of the breakers depends on the wind speed.

Ding & Farmer [1994] further advanced the technique. They developed a directional array of hydrophones and a method to track individual breaking events out in the ocean. The directional

array made possible measurements of the phase speed of breaking events, and showed it was related to the spectral scale of breaking waves (the wave period) and therefore to the spectral scale at which the dissipation occurs. Ding and Farmer obtained interesting statistics on the frequency and spacing of breaking occurrences, on breaking duration, dimension and speed, and some temporal and directional spectral characteristics of breaking probability. They showed a number of distributions of the breaking probability as a function of event speeds and event directions (which are analogues of the wave spectrum frequency and direction), but did not attempt to relate the magnitude and shape of the distributions to the wave spectrum and thus to obtain the spectrum of energy dissipation.

Lowen & Melville [1991a] extended and summarised results of the earlier laboratory studies. They used measurements of the acoustic pressure and concluded that duration of the hydrophone signal above a background noise threshold is proportional to the breaking wave period. Their estimates also showed that, albeit small (i.e. $\sim 10^{-8}$ of the dissipated wave energy), the acoustic energy radiated by breaking waves is proportional to the mechanical energy dissipated.

These important findings are illustrated in respective figures of Melville *et al.* [1992]. Onset, impact and duration of the acoustic noise brought about by a breaking event are clearly seen. Acoustic energy emitted in the course of the breaking can be easily quantified.

These results provided a possible method of measuring temporal spectral scales of breaking events, and even the dissipation related to those scales, using a single hydrophone. In a spectral environment, that would potentially provide the breaking probability (Section 2.5) and severity (Section 2.7) and ultimately the spectral distribution of the dissipation (2.20).

In Lowen & Melville [1991a], Melville *et al.* [1992], the waves were made to break by means of dispersive focusing of wave packets, generated mechanically, with a pre-selected central-frequency. The method was effectively developed for a single-wave environment, and determination of the scales and energy losses of breaking waves in complex spectral environment was beyond the scope of the studies.

While showing a certain promise in investigating such an elusive characteristic of the breaking process as wave-energy spectral dissipation, the technique, however, proved inapplicable in the field. This is, mostly, due to much higher levels of the background ambient noise in the field which makes the determination of both duration and energy of the breaking acoustic impact not feasible.

To demonstrate this, in Figures 3.1, 3.2 and 3.3 breakers, detected by repeated viewing of video records, and synchronised wave records are shown. The data were collected during the Lake George field experiment [Babanin *et al.*, 2001, Young *et al.*, 2005]. The first and last breakers of a one-minute segment of record 4 of Table 5.2 (i.e. those occurred in $t = 1$ s and $t = 55$ s) are shown in the captured video images seen in Figures 3.1 and 3.2, respectively. It is clear that these are cases when the crest of a breaking wave is passing through the wave array and over the bottom-mounted hydrophone underneath the array.

Figures 3.3a-d plot time series of the digitised acoustic signal near $t = 1$ s and $t = 55$ s (Figures 3.3c-d are a zoom-in of Figures 3.3a-b). In both Figures 3.3a and 3.3b, there are well-defined peaks in the acoustic noise level associated with the breaking events. This is in qualitative agreement with laboratory results by Melville *et al.* [1992]. In contrast to the laboratory breaking waves, different fractions of energy are apparently lost by field breakers, and therefore the breaking noise impact above the background in situ ambient noise is not always evident in field acoustic time series. For instance, the breaking event that was visually observed at $t = 53$ s is not

Fig. 3.1. Video image of the breaker occurred near $t = 1$ s of the one-minute record shown in Figures 3.3ac and 3.4.

well defined in the time series in Figure 3.3b. It is, however, clearly seen in the corresponding acoustic noise spectrogram in Figure 3.4.

Figure 3.4 shows a spectrogram of this minute of the acoustic record. The spectrogram is a time series of consecutive spectral densities computed over 256 readings of the acoustic signal with a 128 point overlap; the segments were windowed with a Hanning window [see Babanin *et al.*, 2001, for further details]. Values of the spectral density are shown using a logarithmic scale, with darker patches corresponding to higher values (i.e., louder recorded sound levels associated with dominant-wave breakers).

If the temporal resolution of the acoustic signal in Figures 3.3a-b is increased, as in Figures 3.3c-d, other features become apparent. For the breaker occurring in the first second (Figure 3.3c), there is an apparent alteration of the frequency of the sound: the acoustic carrier downshifts in frequency. This is not the case, however, for the breaker at $t = 55$ s (Figure 3.3d), in spite of the fact that the acoustic signature of this breaker has quite a distinct amplitude enhancement above the ambient noise. Nevertheless, both breakers are clearly seen as breaking crests in the spectrogram in Figure 3.4.

Felizardo & Melville [1995] applied passive acoustics techniques of Lowen & Melville [1991a], Melville *et al.* [1992] in the field, where breaking waves of all scales and various dissipation rates can be present at the same time. They argued that the dependence of ambient noise on wind is indirect, which argument signified an essential move away from the decades-long tradition to associate the wave breaking with the wind, toward wave hydrodynamics which drives the physics of wave breaking as we understand it now. They indeed found correlations between the ambient noise level and wave parameters related to the incidence of wave breaking, and also between the total dissipation, estimated in a number of different ways, and the acoustic noise. No attempts to obtain a spectral distribution of the total dissipation were made. It should be men-

Fig. 3.2. Video image of the breaker occurred near $t = 55$ s of the one-minute record shown in Figures 3.3bd and 3.4.

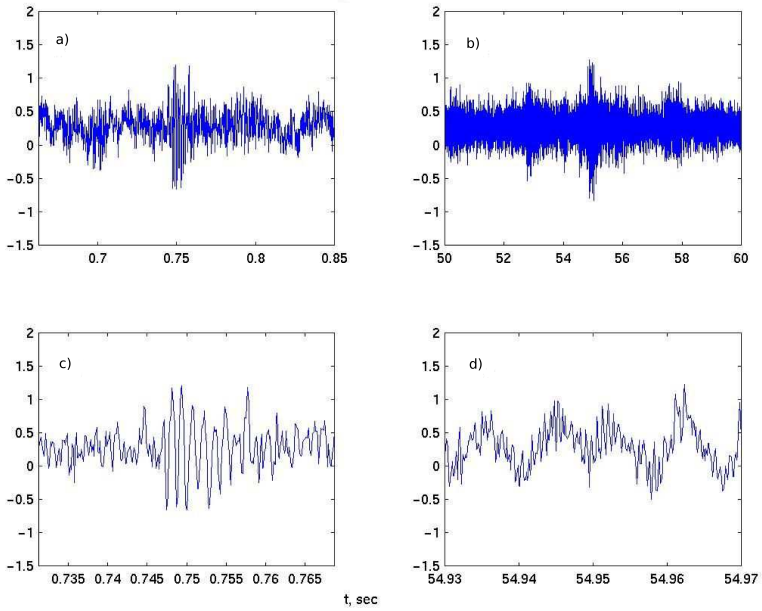

Fig. 3.3. Time series of acoustic signatures of the breakers shown in Figures 3.1 and 3.2. a) and c) Zoom out and zoom in for the breaker in Figure 3.1. b) and d) Zoom out and zoom in for the breaker in Figure 3.2.

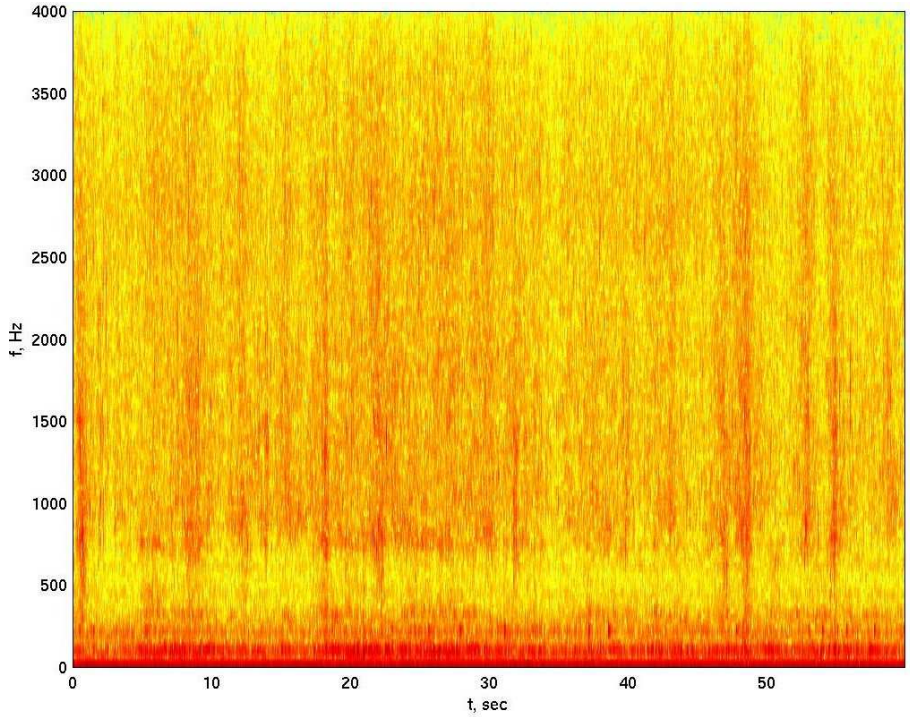

Fig. 3.4. Spectrogram of one-minute record of acoustic noise recorded by a bottom-mounted hydrophone during wave record 4 of Table 5.2. Darker crests correspond to dominant waves breaking. The breaker in $t = 1$ s is depicted in Figures 3.1 and 3.3ac, and the breaker in $t = 55$ s in Figures 3.2 and 3.3bd.

tioned, in addition to the issue of the much larger levels of ambient noise in the field described above, that extending the Lowen & Melville [1991a], Melville *et al.* [1992] approach into the multi-scale wave environment may not be as straightforward as considering the duration of the hydrophone signal above a threshold even if it was clearly determined. The acoustic energy radiated by a breaking event and even the threshold itself [e.g. Babanin *et al.*, 2007b] can be altered owing to multiple breakings nearby, or due to simultaneous breakings of different scales at the measurement spot.

A number of other passive acoustic techniques have been further developed to work on breaking detection and statistics. Bass & Hey [1997], Babanin *et al.* [2001] both used the spectrograms of hydrophone-recorded noise to detect breaking events. As illustrated in Figures 3.1-3.4 above, the identification of distinct crests in the spectrograms, spanning a frequency range from 500 Hz to 4 kHz, appears to be a more reliable means of breaking detection in the complex spectral environment than the integrated ambient noise exceeding a threshold. The spectrogram method, however, can only be applied for the detection of dominant breakers.

Babanin *et al.* [2001] obtained wave-breaking data at experimental site at Lake George near Canberra in south-eastern Australia during 1997-2000. Since the Lake George field experiment will be frequently referred to through the rest of the paper, it is relevant to provide a brief descrip-

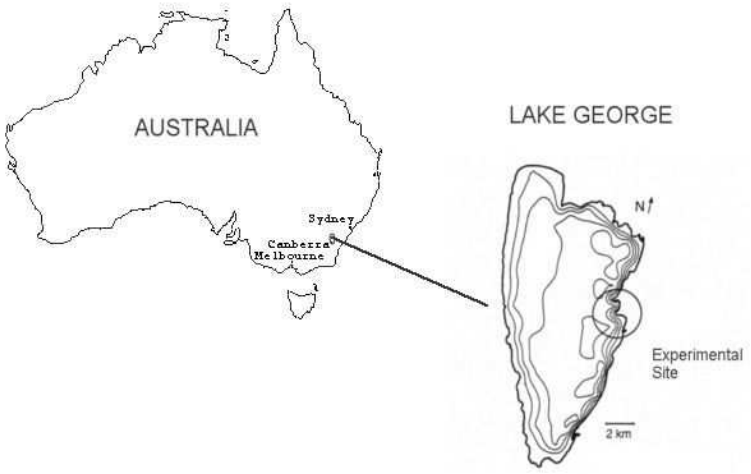

Fig. 3.5. Location of the Lake George field experiment site.

tion of pertinent details here. For further details on the experiment, its layout, instrumentation and measurements, we refer the reader to Young *et al.* [2005].

A contour map of Lake George, shown in Figure 3.5, indicates a simple bathymetry, with the bed sloping very gently toward the eastern shore of the lake. Since its bed form is extremely flat, Lake George is an ideal location to study in situ fetch-limited behavior of wind-generated waves in a constant finite-depth environment.

The predominant wind directions at Lake George are westerly and north-westerly, and therefore the site was located near the eastern shore as seen in Figure 3.5. Under typical meteorological conditions the range of values of inverse wave age U_{10}/c_p and non-dimensional depth $k_p d$ expected at the site were $1.0 < U_{10}/c_p < 3.5$ and $0.7 < k_p d < 2.0$, respectively. At extreme end, wind-wave records at wind forcing as strong as $U_{10}/c_p \approx 8$ were taken [Donelan *et al.*, 2006, Babanin *et al.*, 2007b]. Here, k_p is wavenumber corresponding to the spectral peak, and d is the mean water depth. For linear waves, these experimental conditions are representative of intermediate-depth wind seas.

The experimental site included an observation platform with a shelter to accommodate equipment and researchers during observational periods (see Figure 3.6 for a general view). The platform was located 50 m from shore and was accessible via an elevated walkway. The site was equipped with a comprehensive instrumentation system for the study of finite-depth wind-wave energy sources and sinks. The measurements described here were made from a 10 m long measurement bridge located to the side of the platform. Approximately halfway along the bridge, the water-surface elevations were measured using an array of capacitance gauges (see also Figures 3.1, 3.2). A hydrophone was located directly below the wave probes and sensed the noise generated by individual breaking waves. The water surface around the capacitance array and hydrophone was viewed using a video camera. In addition, the records were electronically 'marked' by an observer who manually recorded visual occurrences of breaking. All the mea-

Fig. 3.6. General view of the experimental site at Lake George. The platform and hut containing logging equipment are shown on the right. The measurement bridge extends toward the left.

surements were synchronised. Using this integrated system, it was possible to inter-relate the visual appearance of the water surface in any sequence of individual video frames and the acoustic signature of breaking waves at that time, together with the wave height properties measured by the directional array at the breaking location.

An anemometer mast, having accommodated three wind probes at 10 m and 5.65 m elevations above the water surface (two cup anemometers measured one-minute mean and two-second gust wind speeds and one wind vane measured wind directions), was erected 10 m from the platform beyond the end of measurement bridge to avoid disturbing the air flow. Another anemometer mast, accommodating five wind probes at four heights closer to the surface (four cup anemometers and a wind vane), was set 6 m to the side of the bridge to ensure undisturbed airflow for these lower anemometers.

A total of 26 records of all the measured variables, relevant for studying the wave breaking, taken during the period in October-December 1997, were processed, and Table 5.2 in Section 5 summarises their parameters. Selection of the records was based only on the requirement of relatively constant wind speed.

The wind speed U_{10} and wind direction were measured very close to 10 m above the water level by the uppermost wind speed and wind direction sensors on the anemometer mast. The wind probes were Aanderaa Instruments wind speed sensor 2740 and wind direction sensor 3590. Slow changes in the water depth in Lake George caused only small variations in the position of the sensors over the surface, and corresponding adjustments in the U_{10} speed were made on the basis of the wind profiles obtained with the anemometer mast.

Relatively young, strongly forced waves with $U_{10}/c_p = 3.3-6.5$ were employed for studying the wave-breaking statistics. Their spectral peak frequencies f_p ranged from 0.33 to 0.50 Hz. The wind speed U_{10} ranged from 8.5 to 19.8 m/s.

Visual detection of dominant wave breaking occurrence is arguably one of the most reliable methods available since it does not require any additional experimental criteria. At Lake George, most wave records were supplemented by videotaped images of the water surface surrounding the wave array. The videotaping allows repeated playback of wave records to establish the breaking statistics by visual means and to verify the results. This visual observation method was used to obtain the breaking statistics.

As mentioned above, the video records were synchronised with the surface elevation records gathered by the array of wave probes. Both the surface elevation sampling and video framing were performed at 25 Hz rate so that there was unambiguous correspondence between each wave height reading and a video image. For the video taping a computer-controllable Panasonic model AG-7350 video recorder (VCR) was used whose time-code generator facility allowed rapid retrieval of particular segments of the recorded wave series corresponding to visually observed breaking events.

The hydrophone output was recorded on the VCR audio channel. The hydrophone had two signal gains, 20 and 40 dB. Normally, for developed wind waves the 20 dB gain was sufficient to detect breaking waves. During data analysis the acoustic signal was sampled at the $8K$ Hz rate and digitised. These synchronised time series of the acoustic signal contain potentially valuable additional information about visually observed dominant wave breakers, particularly in relation to breaker strength.

In Figure 3.4, spectrogram of the first minute of record 4 in Table 5.2 is plotted. The dark crests across almost the entire $4K$ Hz frequency span in the spectrogram are associated with acoustic noise from dominant breaking waves. This was confirmed through repeated viewing of the synchronised video records. For example, the first and last breakers (near $t = 1$ s and $t = 55$ s) detected in the spectrogram in Figure 3.4 are shown in the captured video images seen in Figures 3.1 and 3.2, respectively. It is clear that these are cases when the crest of a breaking wave is passing through the wave array and over the bottom-mounted hydrophone.

After the connection between the spectrogram signatures and the visually observed dominant breakers was established, the acoustic spectrograms were used along with the video records to obtain the wave-breaking statistics (see Section 5.3.1). As a further example, Figure 3.7 shows another spectrogram of breaking occurrences during a 1 min-long segment of record 12 (Table 5.2) when the wind and waves were much weaker and only two isolated breakers occurred within the 1 min record.

Thus, the use of spectrograms rather than acoustic intensity time series is a preferred method for detection of dominant breaking events in the wave field. A similar conclusion was reached by Bass & Hey [1997], who used spectrograms to detect breakers in the natural surf zone. However, the acoustic time series can provide useful physical insights into the breaking process, that is in order to estimate periods of individual breaking waves, the amount of energy lost etc., particularly in circumstances when the background ambient noise is weak like in the laboratory [Melville *et al.*, 1992].

The Lake George wave and breaking data were further used to develop another passive acoustive method, capable of detecting both dominant and small breaking events, as well as their severity [Manasseh *et al.*, 2006]. As described above, individual sound pulses corresponding to the

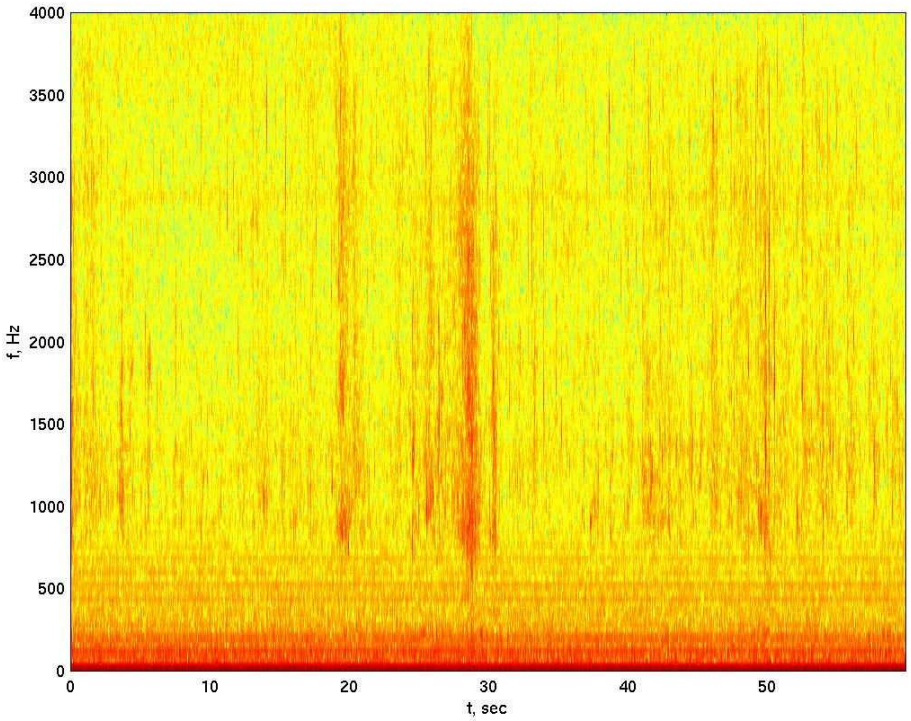

Fig. 3.7. Spectrogram of one-minute record of acoustic noise recorded by a bottom mounted hydrophone during wave record 12 of Table 5.2.

many individual bubble-formations during wave breaking events typically last only a few tens of milliseconds. For details on signal conditioning, pulse processing, determination of optimal trigger level and other elements of analysis, we refer the reader to the original paper. Here, we will mention that with the new technique, each time a sound-level threshold was exceeded, the acoustic signal was captured over a brief window typical of a bubble-formation pulse, registering one count. Each pulse was also analysed to determine the likely bubble size generating the pulse.

Using the time series of counts and visual observations of the video record, the sound-level threshold that detected bubble-formations at a rate optimally discriminating between breaking and non-breaking waves was determined by a classification-accuracy analysis. This diagnosis of breaking waves was found to be approximately 70-75% accurate once the optimum threshold had been determined.

The classification-accuracy analysis detailed in Manasseh *et al.* [2006] ought to be applied in further field experiments, covering a wider range of wind-wave environments than were available in Lake George. If in each future field experiment, synchronised surface video and underwater audio records were made with the same equipment and settings (for example, with the hydrophone the same distance below the surface and the camera the same distance above), the classification-accuracy analysis could be repeated on several datasets from a wider range of sea-

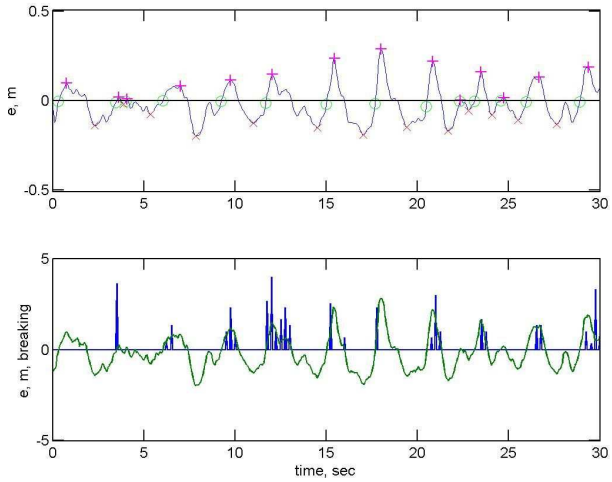

Fig. 3.8. Time series of water elevation. Upper panel: ◯, zero up-crossings; $+$, crests; $\times$, troughs. Lower panel: water elevation with superimposed count of detected bubbles within 0.25 s intervals at the optimal breaking-detection discriminant.

state environments than studied here. If the classification accuracy of 75% is not worsened, it would suggest the discriminant recommended (in sound pressure amplitude at the hydrophone) has a universality.

The method was then used for detailed analysis of wave breaking properties across the spectrum. To obtain wave breaking probabilities of individual waves at different frequencies, a zero-crossing analysis was applied. From the time series of surface elevations, the period of each wave was calculated as follows. Times when the surface elevation crossed the mean or 'zero' level were noted. Two consecutive zero up-crossings were analysed and the time of the troughs preceding and following them were recorded. The difference between the trough times was taken as the period of that wave T, giving its frequency. Figure 3.8 (top panel) shows a 30 s section of the surface elevation data of record 5 (Table 5.2) used to calculate wave frequencies.

In Figure 3.8, limitations of the zero-crossing analysis at small scales are quite obvious. These limitations and other issues with the zero-crossing analysis are discussed in Appendix of Manasseh *et al.* [2006]. A superior alternative for higher-frequency breaking, which also preserves the wave shape contrary to the standard Fourier-based bandpassing procedures, would be a riding-wave removal (RWR) method [Schulz, 2009].

The synchronous passive acoustic wave-breaking data was then combined with the surface-elevation data and the zero-crossing analysis. Such bubble detection events are shown, for the same time series, in the bottom panel of Figure 3.8. Occasional events which would correspond to negative surface elevations were excluded from the analysis to avoid possible ambiguity in detecting wave breakers when those events happened close to wave troughs. For each acoustically-determined breaker, the frequency of the wave at the same time was extracted. The total number of breaking waves $n(f)$ was found for each of the calculated frequencies f.

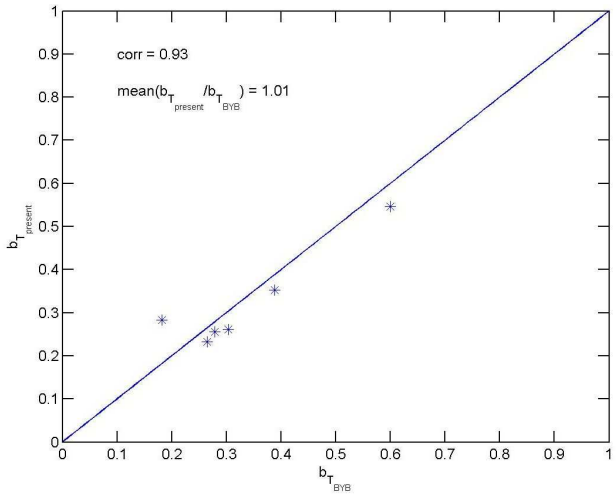

Fig. 3.9. Comparison of dominant breaking probabilities (2.3) obtained by the spectrogram (denoted as 'BYB') and bubble-detection (denoted as 'present') methods.

When applied to real field data, a breaking-probability distribution could thus be obtained, this will be described in Section 5. This is the rate of occurrence of wave-breaking events at different wave scales. Therefore, the method provides spectral distribution of the breaking probability (2.4) rather than the frequency of occurrence of dominant breakers (2.3) like the spectrograms. For the dominant breaking, the two techniques were compared and showed effectively the same breaking count, provided that the assumed dominant frequency band is $\Delta f_p = \pm 0.35 f_p$ (2.8). This comparison is shown in Figure 3.9.

With support from a separate, laboratory experiment, the estimated bubble size was argued to be dependent on the severity of wave breaking and thus to provide information on the energy loss due to the breaking at the measured spectral frequencies. A combination of the breaking-probability distribution and the bubble size can lead to direct estimates of spectral distribution of wave dissipation.

In order to examine the hypothesis that the bubble size is related to the breaking severity, the passive acoustic analysis was applied to data from a laboratory wave-maker. Waves with a frequency of 0.75 Hz and various amplitudes were generated in a flume of width 1.215 m of the School of Civil and Environmental Engineering of the University of Adelaide. The water depth was 225 ± 5 mm above a sandy bottom. A vertical board 45 mm wide and 150 mm deep was placed about 10 m downstream of the wavemaker; its top was 30 ± 3 mm above the mean water level so plunging breakers were forced to form over this barrier. Two capacitance probes measured the instantaneous water elevations, 640 ± 5 mm upstream of the board and 560 ± 5 mm downstream of the board. A hydrophone (Bruel & Kjaer 8103) with a diameter of 9.5 mm was mounted 60 ± 2 mm downstream of the board with its tip 55 ± 2 mm below the mean water level. The probes and hydrophone were approximately in the centre of the flume width. A typical acoustic time series is shown in Figure 3.10.

The acoustic signal was preamplified by a Bruel & Kjaer 2635 charge amplifier set to the

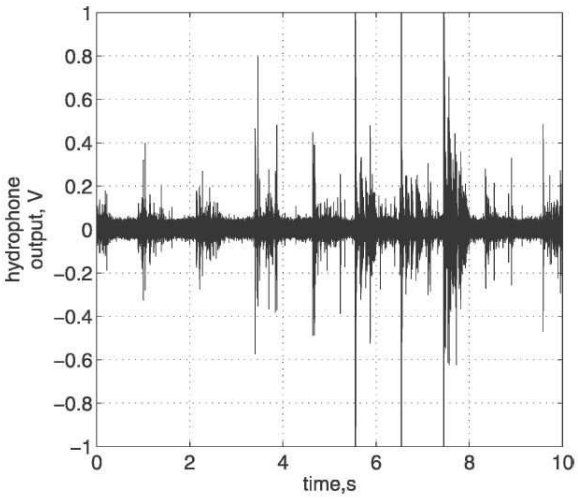

Fig. 3.10. Acoustic time series showing grouping of sound pulses at breaking events. Note that wave frequency is 0.75 Hz so that, with 100% of waves breaking, crests are about 1.33 s apart.

hydrophone's calibration such that $1V$ output represented exactly $100Pa$ sound pressure amplitude. The signal was passed through a 400 Hz unity-gain high-pass filter and digitised at 40 kHz. The pulsewise processing was applied in real time on 5 min of data. Since in this laboratory testing every wave broke, the hydrophone was deliberately placed within a few cm of the bubble-formation zone, so rather than determining the optimum trigger level by classification-accuracy analysis as for field data, the criterion was simply to minimise variance in the processed data while keeping the data collection time per run reasonably brief. Typically, 500-1000 pulses were acquired.

The difference between the water elevations upstream and downstream of the wave-breaker were used to calculate the energy loss (2.23), a parameter assumed to represent the true breaking severity (Section 2.7). The results are shown in Figure 3.11, where the mean local bubble radius R_0 is shown with the 95% confidence interval calculated from the pulsewise processing. It can be seen that there is a clear, though not necessarily linear, increase in R_0 with the loss of energy by the plunging breaker. At higher wave amplitudes than those shown, breaking increasingly occurred prior to the board and between the upstream probe and the board, so those conditions could not be used for the present analysis. While this preliminary result supports the contention that R_0 can be a proxy for local breaking severity, much work is required to determine the true relationship between bubble size and breaking severity under a wider and more realistic range of breaking conditions.

Explicit calibration of the bubble size in terms of breaking strength, that is quantitative parameterisations of the wave energy loss across the spectrum in terms of the bubble size, or spectrum of the bubble sizes produced in the course of wave breaking, is still to be accomplished. Qualitatively, however, the new method signifies a tested technical means for studying spectral wave energy dissipation by non-intrusive remote-sensing passive-acoustic devices.

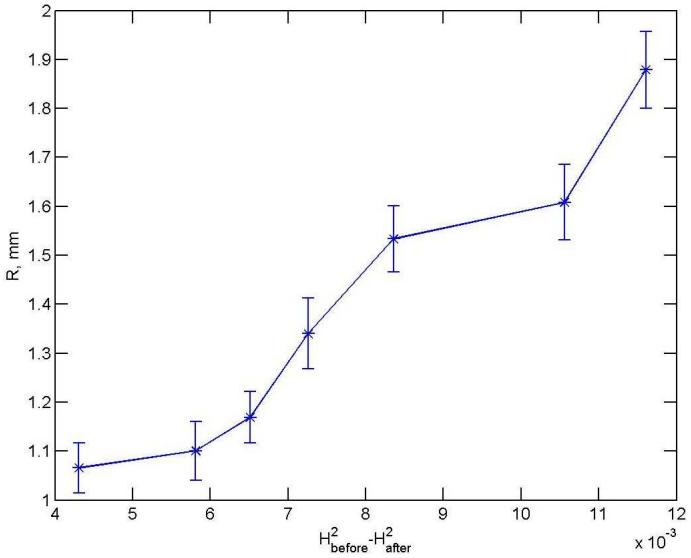

Fig. 3.11. Breaking severity assumed as bubble radius R_0 versus laboratory energy loss (2.23). Vertical bars are for 95% confidence limit on R_0 (denoted as R in the Figure).

Itemised outline of the measurement and analysis procedure was formulated in Manasseh *et al.* [2006] as follows.

1. A submerged hydrophone monitors sound continually;
2. A prior statistical classification-accuracy analysis has determined a sound-pressure threshold optimally discriminating breaking from non-breaking events. When the instantaneous sound pressure exceeds this predetermined level, a very brief pulse of sound is captured, assumed to be due to a single, freshly-formed bubble;
3. The pulse frequency is rapidly measured, and translated into the bubble's radius;
4. Running statistics on the rate of detection of bubbles and the mean bubble size during breaking events are collected;
5. Each detected bubble is linked to the synchronous wave-height record by means of a zero-crossing or RWR analyses, thus determining the period of the wave breaking at the time of the bubble detection and the wave-period distribution of the breaking rate (this procedure is detailed in Section 5 dedicated to the breaking-probability analysis);
6. From the laboratory experiments, the mean bubble size can be related to the wave breaking severity;
7. The rate of occurrence of the breaking events times their severity can be used to estimate wave energy dissipation due to breaking (Sections 2.7, 6);

8. The wave-period distribution of the dissipation rate is obtained (see Section 6).

At the time of writing, the instrumentation and equipment tested by Manasseh *et al.* [2006] only exists as a laboratory version, and its field and yet alone industrial applications are to be developed. Potentially, however, the technique is very promising in this regard. Being the passive technique, it does not involve large levels of power supply and can be operated on batteries. If collocated with surface wave measurements and intended on measurements of wave breaking occurrence and severity, the device only have to record size of bubbles and time when they are generated. Such sequence of double numbers, particularly given the fact that the wave breaking is a relatively rare event, requires minimal amount of electronic memory for data storage. Therefore, a field version of the device is quite feasible if the equipment is enclosed in a water-proof container, with only hydrophone sensing head exposed, and placed below the surface away from direct impact of breaking waves. Such instrument would be possible to use both for dedicated experiments and for long-term observational campaigns autonomously.

In summary, acoustic techniques have consistently showed the ability to detect breaking-event signatures, and therefore the ability to study breaking statistics. The techniques are, in principle, capable of distributing the breaking probability along the spectral scales of the corresponding breaking waves. This could be done in a number of ways. The breakers could be detected and statistics of their periods obtained. According to Lowen & Melville [1991a], Melville *et al.* [1992], the statistics are proportional to the signal duration above the threshold. While this method poses apparent difficulties in the wind-generated wave fields, techniques based on spectrograms of underwater acoustic noise proved successful for detecting dominant wave breaking in such environments. Alternatively, the phase speed of breakers, detected by a directional hydrophone array, could be related to the phase speed of waves with the corresponding frequency [Ding & Farmer, 1994]. A different approach, developed by Manasseh *et al.* [2006], allows to identify breaking waves by means of detecting bubble-formation events collocated with surface waves recorded synchronously.

Furthermore, it appears possible to obtain the distribution of breaking-wave energy dissipation along the spectral frequencies. In laboratory, as Lowen & Melville [1991a], Melville *et al.* [1992] showed, once the breaking event is detected, the energy loss can be estimated by the amount of acoustic energy radiated. In the field, the bubble-detection technique of Manasseh *et al.* [2006] demonstrates a certain promise by relating the bubble size to the breaking strength.

However, no systematic studies have been done of the spectral distributions of the breaking probability, and no advances have been made in obtaining an observation-based spectral distribution of the dissipation [e.g. Babanin *et al.*, 2007c]. This is probably due to difficulties in applying the method of thresholding the integrated-noise-over-background, in the spectral environment of real seas with multiple breaking at various scales. In the real seas, the integrated background noise level will change, depending on wave and wind conditions, thus varying the threshold value [Ding & Farmer, 1994, Babanin *et al.*, 2007b]. Even for stable wind-wave situations, the simultaneous presence of multiple wave scales can cause ambiguity in the detection of breaking events, and moreover in measuring their duration or acoustic energy radiated. Babanin *et al.* [2001] synchronously detected the breakers by passive acoustics and by video recordings in the field, and showed that similar integrated noise above the background sometimes indicated a breaker and sometimes did not.

Manasseh *et al.* [2006] developed a new passive acoustic method of breaking determination

using a single hydrophone. Its key difference from other methods reviewed in this Section was the analysis of very brief pulses which are associated with sound emission by individual bubbles. This method shares both the advantages and some limitations of the other passive acoustic methods. It does rely on a discriminant (threshold) to trigger breaker detection and analysis and any such procedure will inevitably result in errors as discussed. However, the statistical procedures developed by Manasseh *et al.* [2006] would permit a rigorous determination of discriminants from future field data, possibly leading to a universal discriminant.

3.6 Remote sensing

The acoustic techniques described in Section 3.5 are based on non-intrusive measurements and therefore are themselves remote-sensing methods of studying various wave-breaking features and properties. They have been singled out into a separate Section because of a number of practical advantages they appear to provide compared to other remote-sensing means, in this particular area of oceanography.

The current Section is dedicated to radar and optical sensing techniques. Of these, the microwave radar backscattering means have been applied in the wave-breaking studies as often as, and sometimes together with the acoustic methods [see e.g. Melville et al., 1988, Lowen & Melville, 1991a].

The radar active backscatter has been extensively used for remote sensing of the ocean surface with the purpose of detecting, monitoring and studying surface winds, ocean currents and other oceanic features. Large number of laboratory experiments showed that the Bragg scattering mechanism, based on backscatter of the microwave radiation by the surface water waves with wavelengths of the order of a few cm, is the main process to be accounted for in this regard, although variety of other contributing physical mechanisms are possible [e.g. Lowen & Melville, 1991a]. Strength of the reflected signal depends on height of the cm-waves, and due to rapid response of heights of such waves to the environmental forcing, the backscattered signal is a good indicator of activity and strength of the oceanographic phenomena of interest.

It is quite early by comparison with techniques other than visual observations, that it was noticed that the radar backscatter can be used to study the wave breaking. Pigeon [1968], Long [1974], Lewis & Olin [1980], Alpers *et al.* [1981], Kwoh & Lake [1984], Chaudhry & Moore [1984], Keller et al. [1986] all observed strong microwave return, so-called 'sea spikes' in the reflected signal, and associated it with the breaking.

Breaking of very short waves is mostly induced by the long waves (see Section 5.3.2). This can be either due to modulation of short waves by underlying longer waves [e.g. Donelan, 2001], in which case they occur on the front face of the dominant crests, or forced by larger-scale breaking [Young & Babanin, 2006a], in which case it should happen in the wake of large breaking. If the short waves break because they overcome a steepness limit like the dominant waves [i.e. Brown & Jensen, 2001, Babanin *et al.*, 2007b, 2009a,b], then the Bragg scattering due to such height-saturating short waves should be locked to the phase of dominant waves in front of the crest or behind the crest, depending on what effect induces the small-scale breaking.

Microwave backscatter indeed makes this distinction. It is already in the early studies that Alpers *et al.* [1981], Kwoh & Lake [1984] noticed that the Bragg spikes are linked to the steep crests of breaking waves. Kwoh & Lake [1984] further concluded that the Brag scattering is not the only mechanism responsible for the sea spikes at breaking crests. They distinguished

the backscatter from capillary waves generated on the front face of the breaking wave, from the turbulent wake behind the crest [see also Wetzel, 1990] and from the sharp near-breaking crests themselves [see e.g. earlier work of Lyzenda et al., 1983, on the topic of wedge diffraction].

Melville et al. [1988], Jessup *et al.* [1990], Lowen & Melville [1991a], Melville *et al.* [1992], in laboratory and in the field, moved from recognition of the wave-breaking contribution into the radar backscatter to the question of whether these remote-sensing techniques can be used for studying the breaking statistics and physics, and the answer was positive. In this regard, combined laboratory studies of the microwave backscatter and acoustic signature of the breaking are most instructive [Melville et al., 1988, Lowen & Melville, 1991a, Melville *et al.*, 1992].

Such laboratory experiments showed that both reflected microwave power and the radiated acoustic energy correlate with the wave energy dissipation (see also Section 3.5 above). Similarly to the case of acoustic probing, this gives a promise to determine the breaking strength, along with the breaking occurrence/probability. Like in the acoustic case, however, this promise proved so far difficult to realise in the complicated multi-scale oceanic waves fields.

In the laboratory, the main proportion of the backscattered power appeared to precede the acoustic response to breaking. This interesting detail indicates that the radar sensing can be employed for studying the incipient breaking statistics/probability, because the sound signature obviously designates the breaking in progress, the stage of active wave collapse when the white-capping and bubbles are produced (see Sections 2.1, 2.2). Since the onset of breaking is difficult to detect due to absence of distinct visual features, such as whitecapping, this makes the microwave sensing a valuable tool for studying the initial stage of wave breaking, even if in the laboratory.

Another potential application of the microwave radar backscatter is due to its ability to measure Doppler spectrum of the reflected signal, and therefore orbital velocities including those at the breaking onset. The latter has been frequently used as a breaking criterion ((2.48), Section 2.9) and even provides a basis for deducing a dissipation function based on observations of probability distributions of the orbital velocity, but have hardly been a subject of convincing dedicated study and comprehensively measured. In Lowen & Melville [1991a], peak of the Doppler spectrum corresponds to velocity within 10% of (2.48). Lamont-Smith *et al.* [2007] showed that spectral density of this peak and its width depend on the phase velocity of breaking waves, and does not depend on the grasing angle of the radar, and further found that the peak magnitude and the radar cross-section for the breaking waves scale with the radar wavelength λ_{radar}:

$$\sim \lambda_{radar}^{1.5}. \tag{3.24}$$

Application of the technique to dedicated field studies of wave breaking followed. Jessup *et al.* [1990] found that sea-spike contribution to the radar cross-section was $\sim u_*^3$. This suggests that the radar return can potentially be used to measure total dissipation of wave energy (i.e. 3.9).

Smith *et al.* [1996] used differences in the backscattered signal of vertical and horizontal polarisations at low grasing angles to distinguish spilling breaking events. They demonstrated a clear association of wave-breaking occurrence with the group structure of wave fields. A very interesting outcome was an identification of the dispersion relationship of the breaking waves. Smith *et al.* [1996] observed developing seas, and for the young seas the dominant waves are expected to actively break [Banner *et al.*, 2000]. It was found, however, that the dominant breaking frequency is about 25% above the spectrum peak frequency. Even higher levels of upshifting were reported as a result of dedicated wave-breaking microwave radar observations by Stevens

et al. [1996]. This is consistent with the observed shrinkage of individual waves prior to the breaking brought about due to modulational instability, and the corresponding upshift of the wave frequency [Babanin *et al.*, 2007b, 2009a,b, see also Section 5.2].

Hwang [2007] investigated correlation between the dominant breaking and the short-scale breaking based on both radar and acoustic observations. He argues that the radar sensing techniques often process a very large number of breaking events and from these statistics an average length scale of the breakers in wave systems emerges. Based on the sea-spike observations, it is about one order of magnitude shorter than the dominant wavelength of the wave field. Such evidence is very important, particularly because, as discussed above, the microwave backscatter can account for wave breaking not producing whitecapping which is a challenge, if not impossible for other wave-breaking detection techniques (with exception of the infrared sensing method as discussed in this Section below). This observation is consistent with some derivations for the dissipation function [Hwang & Wang, 2004].

Paper by Phillips *et al.* [2001] will be the last mentioned in this radar-probing subsection because it effectively links two major remote-sensing techniques, the radar backscatter methods which have been discussed above and optical observations of the breaking which will be discussed next. It undertook measurements of $\Lambda(c)$, the average length of breaking front per unit area per unit speed interval introduced by Phillips [1985]. Combined with the Duncan [1981] hypothesis (3.22), measurements of $\Lambda(c)$ can provide the total energy dissipation:

$$S_{ds} = \int \frac{b\rho_w}{g} c^5 \Lambda(c) dc. \tag{3.25}$$

The radar measurements were conducted with a very high resolution and the moving sea spikes were clearly distinguishable over background backscatter. Many interesting observations were made. Moderate wind-speed conditions were similar to those observed in the acoustic field experiments by Ding & Farmer [1994] (see Section 3.5). Therefore, comparisons of the acoustic sensing and radar backscatter techniques again could be made, particularly as in both experiments spectral distribution of the breaking occurrence was measured in terms of breaker phase speeds.

Phillips *et al.* [2001] found that their overall breaking statistics was close to that of Ding & Farmer [1994], but the phase speeds of breakers were on average lower (i.e. frequencies higher). While acoustic measurements did detect breaking waves propagating with the spectral peak speed c_p, the radar measurements did not. The fastest radar-measured breakers would propagate with the speed of some $0.6c_p$. As it was discussed above, the microwave backscattering technique identifies breaking events at or close to the breaking onset, whereas the acoustic signature signifies wave breaking well in progress. Thus, the results reported by Phillips *et al.* [2001] are consistent with the notion also mentioned a number of times above that the length (and therefore phase speed) of waves decreases immediately prior the breaking, if the breaking takes place as a consequence of the modulational instability. Therefore, the overall number of incipient breakers and developed breakers should be statistically the same averaged value, but statistically average spectral signature of such breakers, if they are caused by the instability of non-linear wave groups, should not.

Thorough quantitative measurements of breaking fronts, such as actual form of the phase-speed distribution of $\Lambda(c)$ were performed by Phillips *et al.* [2001] for the first time. This kind of measurements proved valuable for obtaining breaking statistics and breaking probability (see

Section 2.5 for definitions). Estimates of the dissipation rates based on (3.25), however, as discussed in Section 3.3, seem to be of limited value, particularly away from the spectral peak.

Apart from its scientific merit, paper by Phillips *et al.* [2001] also provides an important link with optical remote-sensing studies which concentrate on measuring $\Lambda(c)$. Advancements in computer power and storage in recent decades made it possible to automatically process large numbers of digital video-images of the water surface. The propagating whitecaps can be identified and distinguished from the background darker water surface, and therefore statistics of breaking fronts, their propagation speeds and other geometric, kinematic and dynamic characteristics of the areas covered with whitecaps can be investigated by means of analysing video sequences in much the same fashion as the radar imaging. Depending on an observational setup (e.g. aircraft or a close-by experimental tower), the video imaging can be significantly more accurate because of the much smaller footprints of the video pixels compared to the radar cross-sections. Effects of the bubbles entrained by breaking waves on the optical scattering and backscattering coefficients were investigated by Terrill *et al.* [2001].

Melville & Matusov [2002] conducted video recording of wave breaking fronts with the purpose of obtaining both the breaking statistics and the dissipation (3.25). Video imaging was conducted from an aircraft. Statistical estimates for the wave breaking and related ocean-mixing characteristics, as well as for the breaking parameter b were obtained. In the traditional framework of relating the breaking properties directly to the wind, it was found that distribution of $\Lambda(c)$ is proportional to

$$\Lambda(c) \sim U_{10}^3 \exp(-c). \tag{3.26}$$

It was also found that the main impact of the wave-breaking mixing effect comes from short waves which is consistent with observations that most of the wave energy/momentum input, which is supported by the shorter waves in the spectrum, is lost locally [e.g. Donelan, 1998].

Dulov et al. [2002] performed the video recording from an observational tower, combined with collocated records of waves by means of a wave array. Their study was intended on investigation of whitecapping coverage and was outlined in Section 3.1. It highlighted the cumulative effect of wave breaking and clearly demonstrated induced nature of the short-scale breaking. Overall, however, this kind of optical observations of the breaking dynamics are far from being routine or even common.

Among the optical means of remote-sensing, infrared methods of probing the breaking waves are also most promising [Jessup *et al.*, 1997a,b, Jessup & Phadnis, 2005]. Here, we quote Jessup *et al.* [1997a]: "Under most circumstances, a net upward heat flux from the ocean occurs primarily by molecular conduction through a thermal boundary layer, or skin layer, at the ocean surface. As a result, the "skin temperature" at the top of this layer is a few tenths of a degree Celsius cooler than the bulk temperature immediately below the skin layer [Katsaros, 1980, Robinson *et al.*, 1984]".

The wave breaking disrupts the skin layer, exposes the bulk waters to the very surface, and their temperature can be readily detected by the infrared-sensing devices. Thus, the wave breaking process can be quantified in terms of the occurrence of breaking events and areal coverage of the turbulent breaking wake. In this way, the infrared technique can be employed to study not only the breaking statistics and probability, but also all sorts of turbulent subsurface mixing and air-sea interactions due to the breaking, such as heat and gas exchanges [e.g. Jessup *et al.*, 1997b].

The infrared sensing can also be used to remotely investigate the most elusive property of the wave breaking, the breaking strength (Sections 2.7, 6). This strength determines the extent and intensity of the turbulent wake, and therefore the recovery rate of the skin layer, as the breaking wake subsides and the surface cools, correlates with the dissipation rate due to the breaking event [Jessup *et al.*, 1997b].

Thus, the infrared-sensing probing is an all-in-one technique for investigation of the wave breaking and its consequences. It allows to detect the breaking occurrence, to investigate the breaking probability and statistics, to study the breaking severity, the turbulent mixing and air-sea exchanges due to the breaking. Needless to say that it can be used to obtain dynamic properties of the wave breaking, such as $\Lambda(c)$ [(3.25), Jessup & Phadnis, 2005]. It is also applicable to micro-breaking (to which most of the other breaking-study techniques are not), and this is basically how it was started.

So why do we still, more than 10 years after the infrared sensing was introduced, refer to this technique as promising and having a great potential? This question is equally applicable to the other remote-sensing methods described in this Section, and to some extent to the acoustic techniques of Section 3.5. In this regard, it is worth quoting Melville et al. [1988] who investigated both acoustic and microwave-radar signatures of breaking waves and wrote: "Our results imply that these remote sensing techniques ultimately may be used to measure the dynamics of breaking waves, and are not restricted simply to obtaining the statistics and kinematics of breaking". More than 20 years after these words, the remote-sensing methods mentioned have still not made the breaking statistics, kinematics and dynamics well-understood and even well-described.

In this regard, it is perhaps not the researchers who developed the remote-sensing methods of studying the breaking, and not engineers who design the technical means of the sensing techniques are to bear the sole responsibility. The methods are well-developed, proved, tested and validated, and the instrumentations, for example the infrared cameras, are quite sensitive, reliable and no longer very expensive. In our view, it is now the physicists who have to share the blame for the lack of progress. Once there is a clearer understanding of physics, of what oceanic properties and features are to be sought, looked for and measured, the modern technical capabilities, including the remote-sensing techniques, are able to effectively investigate them, address issues and deliver results.

3.7 Analytical methods of detecting breaking events in surface-elevation records

The analytical methods of detecting breaking events in surface elevation records could potentially provide a powerful means to study the wave breaking, or at the very least the breaking statistics and probability. There are vast amounts of wave records accumulated over decades of wave observations and measurements, and most of them undoubtedly have the breaking events embedded.

And such analytical techniques do exist, but like almost everything else related to the breaking they have to rely on empirical criteria and therefore are semi-empirical rather than strictly theoretical methods. The theoretical approaches have to be able to deal with non-linear and highly non-stationary, non-homogeneous and sporadic events, which the breaking waves are, in continuous wave time/space series and aim at detecting discontinuities or spikes within the time series or their derivatives such that they can be attributed to the breaking.

A comprehensive overview of the methods for non-stationary analyses is provided by Huang

et al. [1998]. They consider the spectrograms, the wavelet analysis, the Wigner-Ville distribution, the evolutionary spectrum, the empirical orthogonal function expansion and other methods, with particular attention to the Hilbert Transform. Out of these, the spectrograms have been used to find the breakers in records of underwater acoustic noise [Bass & Hey, 1997, Babanin *et al.*, 2001, Section 3.5], Phase-Time Method based on the Hilbert Transform was shown successful in detecting deep-water laboratory breaking under a variety of conditions [Zimmermann & Seymour, 2002], and the wavelet method has actually been applied and proved successful in detecting wave breaking and quantifying the breaking statistics in surface-elevation time series [e.g. Liu, 1993, Mori & Yasuda, 1994, Liu, 2000, Liu & Babanin, 2004]. Here, we will follow Liu & Babanin [2004] when describing the wavelet applications.

Over the past three decades, the wavelet data analysis emerged as some alternative to the Fourier Transform. One of its distinguishing features is capability to analyse time varying signals with respect to both time and scale, which provides a link to capturing rapid changes of dynamic properties of the wave surface and associating them with the breaking processes. This kind of extension of the Fourier analysis is particularly effective when using continuous wavelet transform with the complex-valued Morlet wavelet [Farge, 1992, Liu, 2000] that practically provided a local energy spectrum for every data point of the time series. One of the earlier successful applications of this kind towards studies of wave spectral properties was done by Donelan *et al.* [1996] where a method of non-stationary analysis of directional spectra was developed and shown to be able to obtain instantaneous wave-propagation directions, amplitude and phase of a spectral frequency component, as well as wavenumber-related time-dependent information.

With respect to the wave breaking, Mori & Yasuda [1994] considered that there is a sudden surface jump and interpreted it as a shock wave and then defined a shock wavelet spectrum, using discrete wavelet transform and the Meyer [1989] wavelet to detect occurrences of such surface jumps. They verified their method on laboratory mechanically-generated waves which were breaking randomly, and found a good detection rate. The use of discrete scales and the ratio of two adjacent wavelet coefficients as a criterion for breaking detection, however, lacks clear physical meaning for the process.

Liu [1993] used continuous wavelet transform and the complex-valued Morlet wavelet to obtain a time-frequency wavelet spectrum that effectively provided a localised frequency energy spectrum for each data point in a given time-series. This spectrum can then be used to define an average wave frequency ω, and thus combine with the local wave amplitude a, to obtain a local surface acceleration $a\omega^2$ which would be compared to a given limiting fraction γ of gravitational acceleration g to define the breaking event (2.55).

The classical concept of studying the wave breaking process led to various usages of a limiting value of wave steepness beyond which the continuous surface cannot sustain [e.g. Longuet-Higgins, 1969, see also Sections 2.9, 3.2, 3.3, 3.8]. Thus, for example, the wave surface will break when its downward acceleration exceeds the limiting fraction γ (2.55, see also (2.49)-(2.54)).

As mentioned in Section 2.9, the difficulties of applying the acceleration criterion to the real sea waves are the uncertain value of γ and the fact that the natural wave fields are multi-scaled. Because of the latter, the quantity on the left-hand side of (2.55) cannot be readily calculated from a time series of wave data. If it was possible to estimate this quantity, then such simple familiar notion could be readily used to identify breaking waves in the time series. It is, however, not immediately clear how to pertinently resolve the local amplitude a and the instantaneous

frequency ω from the measured time series $\eta(t)$ of real multi-scaled seas.

Liu [1993] suggested to use the time-frequency wavelet spectrum, $W_\eta(\omega, t)$, to obtain the instantaneous values of effective wave amplitude a and frequency ω from time series of surface elevations $\eta(t)$ as

$$W_\eta(\omega, t) = \frac{1}{C_\psi} \left| \int_{-\infty}^{\infty} \eta(\tau) |\omega|^{1/2} \psi^*[\omega(\tau - t)] d\tau \right|^2 \tag{3.27}$$

where $C_\psi < \infty$ is the admissibility condition and the function ψ is the mother wavelet. Here, we use the Morlet wavelet given by

$$\psi(t) = \frac{1}{\pi^{1/4}} (e^{-imt} - e^{-m^2/2}) e^{-t^2/2} \tag{3.28}$$

with $m = \pi\sqrt{2/\ln 2}$ chosen to fit the wavelet shape.

Once a localised frequency spectrum at each time moment t_i is known:

$$\Phi_i(\omega) = [W_\eta(\omega, t)]_{t=t_i}, \tag{3.29}$$

then for each $t = t_i$ we can define, based on that spectrum, characteristic wave amplitude and frequency at the measurement point. In other words, it replaces the localised spectrum by an equivalent characteristic monochromatic wave.

As the characteristic frequency, average frequency σ (Rice, 1954), was chosen:

$$\sigma_i = \left[\frac{\int_{\lambda_L \omega_p}^{\omega_n} \omega^2 \Phi_i(\omega)\, d\omega}{\int_{\lambda_L \omega_p}^{\omega_n} \Phi_i(\omega) d\omega} \right]^{1/2} \tag{3.30}$$

where ω_p is the localised frequency at the local energy peak, ω_n is the cut-off frequency, and λ_L is a number which Liu [1993] introduced to denote the start of the frequency range covering the wave breaking process. We generally carried cut-off frequency up to 2.5 times the peak frequency. The value of λ_L generally lies between 0 and 2. $\lambda_L = 1$, for example, means that we expect waves of peak frequency and higher to be breaking and therefore disregard contribution of those below ω_p into determination of the characteristic wave.

For the local instantaneous amplitude a, Liu [1993] used $a_i = \eta(t_i) - \overline{\eta}$ in an initial application. Another approach was employed in Liu & Babanin [2004] which was based on considering the case of a simple monochromatic wave that has an acceleration $A\sigma^2 \cos(\omega t + \varphi)$, in order to infer that an appropriate characteristic amplitude at local instantaneous time t_i should be given as

$$a_i = A_i \cos(p_i). \tag{3.31}$$

Here, the local amplitude A_i is obtained from the analytic envelope signal of $\eta(t_i)$ by means of Hilbert transform:

$$A_i = |\mathrm{Hilbert}(\eta_i)|, \tag{3.32}$$

and the local phase p_i can be obtained from the wavelet spectrum $W_\eta(\omega, t)$.

In order to get the phase information of the time series, the mother wavelet to be used should necessarily be a complex one such as the Morlet wavelet shown above. So the calculation of the phase is given as

$$p(\omega,t)=\tan^{-1}\left\{\frac{\Im\left[W_\eta(\omega,t)\right]}{\Re\left[W_\eta(\omega,t)\right]}\right\} \tag{3.33}$$

and thus the local phase p_i can be obtained from averaging the local wavelet phase spectrum at each $t=t_i$ over the same range between $\lambda_L\omega_p$ and ω_n.

Sample results of the average frequency and local amplitude as obtained from (3.30) and (3.31) respectively, using $\lambda_L=1$ (that is waves of the peak frequency and above are expected to break [Babanin *et al.*, 2001]), are shown in the bottom and middle panels of Figure 3.12 for the Lake George waves. There remains to be determined the limiting fraction γ as the threshold for wave breaking that can be rendered through assimilation with measured data.

Liu & Babanin [2004] tested the breaking-detection approach suggested by Liu [1993] and determined the factor γ on the basis of field data. The data were obtained under a variety of wind-wave conditions in deep water in the Black Sea and in a finite-depth environment in Lake George, Australia. The two data sets included time series of surface elevations, with breaking waves marked. Both had been extensively used to study the breaking statistics, and detailed descriptions of the breaking detection procedure as well as of relevant environmental conditions are given in Babanin [1995], Babanin & Soloviev [1998a], Banner *et al.* [2000], Babanin *et al.* [2001]. The Lake George field experiment was also described in Section 3.5, and here we will only summarise relevant details of the Black Sea data set and observations.

The Black Sea is a large enclosed water body, extending some 1200 km west-east and more than 400 km north-south (Figure 3.13). Most of the sea is over 1000 m deep, and therefore wind waves develop in ocean-like conditions. The major difference, compared to the ocean, is the rareness of appearance of swell in the Black Sea because of its enclosed location, and absence of strong surface currents. This makes the Black Sea a convenient site for field observations of deep-water waves in their relatively pure state, not perturbed by wave-swell and wave-current interactions.

Four wind wave records analysed by Liu & Babanin [2004] with the purpose of developing the wavelet-based breaking-detection procedure were taken from an oil rig situated on the 30 m-deep sea shelf in the northwest region of the Black Sea (Figure 3.13). Fetch and depth environment constituted ideal deep-water development conditions, with peak frequencies $f_p=0.16-0.27$ Hz (wavelengths $\lambda_p\approx 20-60$ m), significant wave heights $H_s\sim 1$ m, wind speeds $U_{10}=8.7-10.7$ m/s and mature-wave development stages of $U_{10}/c_p=1-1.7$. A brief summary of relevant wind-wave properties is summarised in the last four records of Table 5.1.

The waves were recorded by an array of high-precision wire wave gauges, deployed beyond the zone perturbed by the platform legs. The breaking events were labelled electronically by an observer (see also Section 3.2). The observer located 16 m above the wave probe array monitored one of the wave probes and triggered a signal whenever a whitecap of any size occurred at the probe. The signal was recorded synchronously with the wave data. An example of wave record with breaking waves marked as vertical bars was shown in Figure 2.2. The waves propagate at a speed of 8 m/s, and thus it is difficult for the observer to place the marks precisely. So the marks, even though they are short, only indicate the presence of breaking waves and not an exact position of whitecapping over the wave phase.

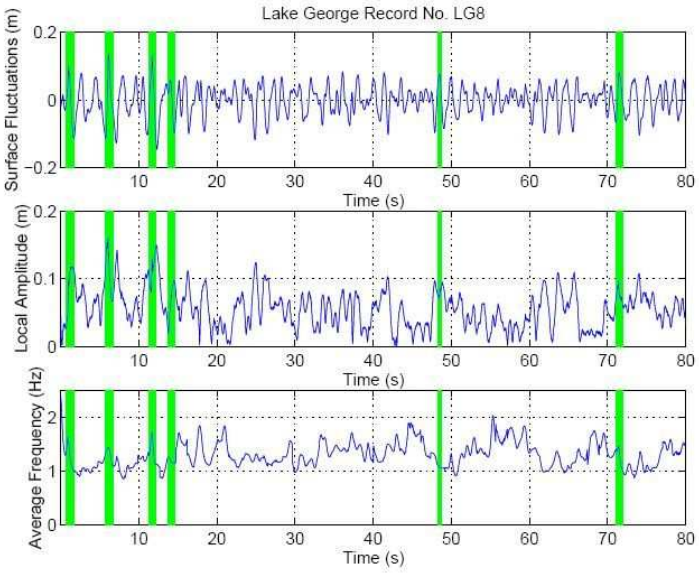

Fig. 3.12. Lake George sample results. Vertical bars indicate breaking events. (top) Surface elevations. (middle) Instantaneous amplitude a (3.31). (bottom) Instantaneous spectrum-average frequency σ (3.30).

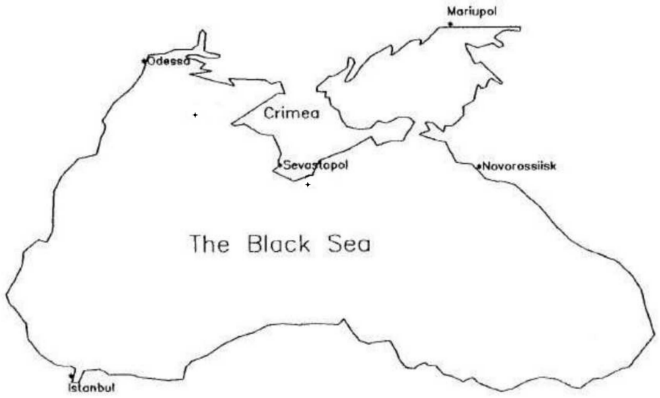

Fig. 3.13. Location of research platforms in the Black Sea (pluses).

Another set of wave breaking was recorded from a research vessel in the Black Sea and the Mediterranean Sea by means of an accelerometer buoy. Wave measurements by this buoy are described in Babanin *et al.* [1993] and environmental conditions during the measurements are given in Table 5.1 (see also Section 5.2). Again, the observer watched the buoy from the vessel and triggered the signal to register the passage of a whitecap over the buoy. Both the ship and the buoy were drifting, the buoy being deployed far beyond the zone perturbed by the ship and

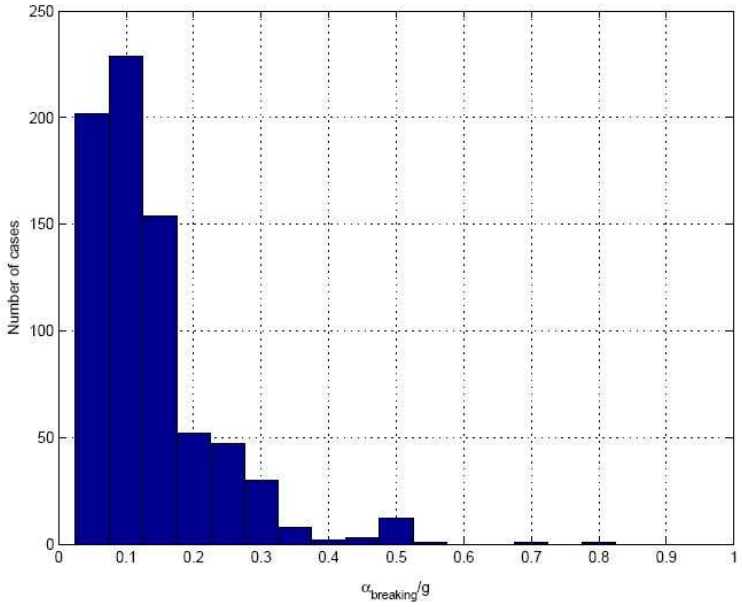

Fig. 3.14. The Black Sea data. Histogram of $\alpha_{breaking}/g$ where $\alpha_{breaking}$ is the $a_{downward}$ acceleration in waves detected as those breaking ((see (2.49), (2.54), (2.55)).

connected to the ship by a long loose cable. The observer was about 10 m above sea level, allowing a clear view of whitecaps with scales down to the size of the buoy (less than a meter). This set of data was used to obtain the histograms of maximal acceleration in the breaking wave (Figure 3.14) and to support the breaking criterion (2.55) in terms of the surface accelerations employed by the wavelet breaking-detection procedure.

In finite depths, the waves become steeper, and for the same frequency ω, the amplitude a of waves in (2.55) will change. Therefore, to verify consistency of the criterion γ obtained for the wavelet procedure on the basis of deep-water measurements, a finite-depth data set was also employed by Liu & Babanin [2004]. These were data recorded during the Lake George experiment described in Section 3.5 above.

To reliably measure the wave breaking and associated effects, a number of independent but integrated techniques were employed in Lake George [see also Young *et al.*, 2005]. The data used by Liu & Babanin [2004] were wave recordings taken by wave resistance probes, and breaking detections were performed by means of bottom pressure probes [Donelan *et al.*, 2005]. The breaking waves generate enhanced pressure at high frequencies, and boosts of this pressure were detected by the pressure probes mounted at the base of the resistance probes. Successful detection of the breaking events by the probes was verified with the synchronised video records. The pressure signal was smoothed by applying a running-average filter.

An example of such a wave record with the bottom-pressure indicated breaking events marked as vertical bars is shown in the upper panel of Figure 3.12. Data records used by Liu & Babanin [2004] were taken during the last stage of the Lake George study when the lake become very shal-

low (see Table 3.1). Therefore, these records, if compared to the deep Black Sea, represent the other end of wave development – bottom-limited and strongly wind-forced waves, under winds of $U_{10}/c_p = 4.7-7.5$, with peak frequencies $f_p = 0.53-1.32$ Hz (wavelengths $\lambda_p = 0.9-3$ m), and significant wave height H_s about 0.1 m.

In Liu & Babanin [2004], the determination of the limiting fraction γ in deep water was based both on direct measurements of surface acceleration in the breaking waves (Figure 3.14) and on comparisons of ability of the measurements and the wavelet breaking-detection technique to provide the same breaking statistics. Feasibility of the approach was then verified by means of predicting the shallow water γ on the basis of knowledge of the deep-water limiting fraction. A reality check was also discussed.

It has always been obvious from general reasoning that once the wave collapse is in progress, the downward acceleration of the water particles on the breaking crest will be determined by a ratio γ in connection with the centrifugal acceleration of the particle and gravitational acceleration g. The exact measure of γ, however, remained elusive. As it was mentioned in this Section above, in studies which may already be regarded classical [i.e. Longuet-Higgins *et al.*, 1963, Snyder *et al.*, 1983] it has been enacted generally as $\gamma = 0.5$, although indirect inference of the acceleration based on laboratory [Hwang *et al.*, 1989] and field measurements [Holthuijsen & Herbers, 1986] indicate that value of γ should be 0.4 or even lower.

In the Black Sea, some of the breaking waves were measured by an accelerometer, and therefore direct estimates of maximal acceleration $\alpha_{breaking}$, which is the $a_{downward}$ acceleration in waves detected as those breaking ((see (2.49), (2.54), (2.55)), for such a wave are available. Histogram of distribution of these estimates for 742 breaking events is shown Figure 3.14.

To define the limiting fraction γ, we are interested in maximal detected value of accelerations $\alpha_{breaking}$. While being on a breaking wave, the accelerometer was not necessarily located at a point of maximal acceleration, i.e. if it was riding a breaker-in-progress (see Section 2.2), and therefore not all the events depicted in Figure 3.14 are indicative of the limiting acceleration sought after to find γ.

As it can be seen from histogram in Figure 3.14, $\alpha_{breaking}$ values of up to $0.8g$ were detected, although the number of those events is very low and their statistics is poor. Occasional high values of the acceleration could have been registered if the accelerometer was shaken by, for

Tab. 3.1. Summary of the Lake George data used. U_{10} is the wind speed at 10 m height, k_p is the peak wavenumber, $a = H_s/4$ is the standard-deviation wave amplitude, d is the water depth.

Record No.	U_{10}, m/s	k_p, rad/m	a, m	d, m
4	6.6	7.2	0.013	0.31
8	11.9	2.3	0.039	0.32
9	12.0	2.1	0.034	0.29
10	8.1	3.1	0.019	0.33
11	10.6	2.2	0.020	0.32
14	7.1	5.6	0.015	0.27
15	7.3	2.5	0.016	0.28

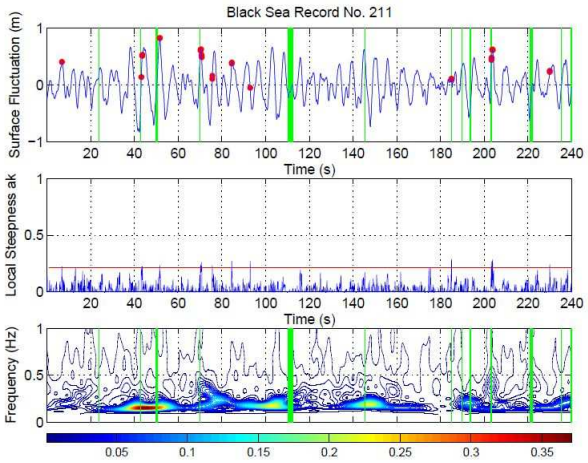

Fig. 3.15. (top) Comparing breaking events detected from the wavelet approach in dots with a Black Sea measurement (see last four records in Table 5.1) in vertical bars. (middle) Local steepness ak. The straight line shows $\gamma = 0.2$, the chosen threshold value. (bottom) Instantaneous wave spectra in relative units (shading scale below). The horizontal axis is the time axis, same as in the top two panels.

example, direct hit by a plunging breaker jet or by a jerk of the cable connecting the buoy to the mother ship. The histogram shows that continuous distribution with reliable statistics of $\alpha_{breaking}$ led to an $\alpha_{breaking}/g \approx 0.3$, and we shall use this as a reference value for γ in deep water. Limiting fraction γ in shallow water is expected to be different due to reasons to be discussed below.

Following the supposition inferred in Liu [1993], Liu & Babanin [2004] persisted to finding the pertinent values for λ_L and γ used to detect wave-breaking events based on a wavelet approach. Amidst the redundant choices and combinations of the values of λ_L and γ, they settled on a plausible and practical approach: to match, as closely as possible, the number of breaking waves estimated from the wavelet approach for a time series with the number of the measured breaking waves. In so doing for each available time series data set, they were able to resolve a rational γ value from a given λ_L value. A physically sound value of λ_L, in turn, can be chosen on the basis of knowledge of the lower bound of frequency scale of waves which are expected to break. This knowledge is available for both deep-water breakers [e.g. Banner *et al.*, 2000] and finite-depth breakers [Babanin *et al.*, 2001].

The top panels of Figures 3.15 and 3.16 present results of the applications of this approach to the same sample cases in the Black Sea and Lake George as shown in Figures 2.2 and 3.12 respectively. The results were obtained for $\lambda_L = 1$. With measured breaking waves marked by vertical bars, breaking events detected by the wavelet approach are shown by the dots. For reference, the Figures also include plottings of corresponding local steepness ak in the middle panel with resolved γ value plotted as the horizontal line, and the corresponding contours of wavelet spectrum displayed in the lower panel.

An examination of the results indicates that the wavelet approach along with the measure-

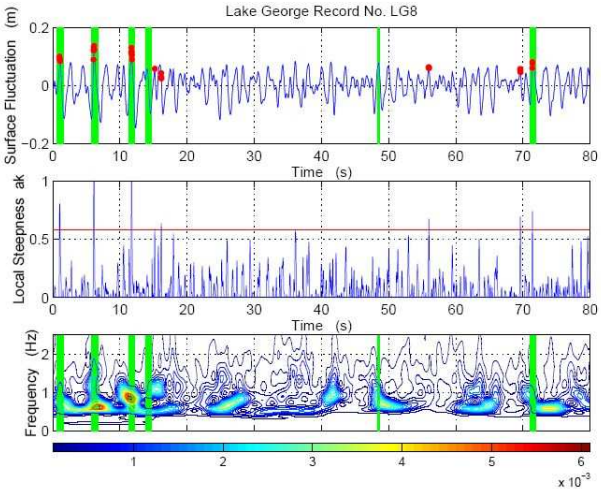

Fig. 3.16. (top) Comparing breaking events detected from the wavelet approach in dots with a Lake George measurement (see Table 3.1) in vertical bars. (middle) Local steepness ak. The straight line shows $\gamma = 0.2$, the chosen threshold value. (bottom) Instantaneous wave spectra in relative units (shading scale below). The horizontal axis is the time axis, same as in the top two panels.

ments are generally successful in capturing breaking wave events at many occasions, although at some other occasions one of them fails to detect a breaker while the other indicates that the breaking occurred. Since the measurement is also basically an approach on capturing breaking events, so the latter is not unexpected as both the measurement and the wavelet approaches should be anticipated as relevant to different phases of wave breaking (see discussion in Sections 2.2-2.4).

Overall, it was expected that both the breaking measurements and the wavelet approach detect the same breaking events only at the developing stage of the breaking phases. The incipient breakers will be detected by the wavelet method and will not be detected by the measurements, and the subsiding breakers, on the other hand, will be detected by the measurements whereas the wavelet method will fail to pick them up. Relative duration of the different breaking phases was discussed in Section 2.4.

As one might have expected in general, there are breaking cases the wavelet approach captured, there are breaking cases the wavelet approach did not capture, and there are cases when the approach anticipated breaking but it was not confirmed by the observed whitecaps. They are all attributes of the wave breaking phases. Therefore, for individual breakings, perfect matching between the measurement and the detection from the wavelet procedure cannot be expected. Matching the total breaking percentages was used. Results of γ value assessments for different λ_L's based on applying the matching breaking percentage approach to the Black Sea and Lake George data are given in Tables 3.2 and 3.3 respectively.

Another interesting insight provided by the wavelet method pertains to relation between the wave breaking and wave groupiness. Donelan *et al.* [1972], followed by a number of experimental and analytical studies [e.g. Holthuijsen & Herbers, 1986, Babanin, 1995, Babanin *et al.*,

2007a, 2009a,b, among others], reported that majority of the breaking events take place within the group structure close the peak of group envelope, although field observations indicated that an essential proportion of the breakings also occurred outside the distinct wave groups [Holthuijsen & Herbers, 1986, Babanin, 1995]. Figures 3.15-3.16 show that breaking does happen beyond the obvious groups of dominant waves and the instantaneous spectra plotted in these Figures indicate why this may be the case.

Once the limiting acceleration criterion (2.55) is applied to the instantaneous wave (3.30)-(3.33) which is characteristic of the instantaneous wave spectrum shown in the bottom panels of Figures 3.15-3.16, occurrence of the breaking event will depend on the product of the characteristic amplitude a and the characteristic average frequency σ squared. Peak of the envelope of dominant waves will give rise to the amplitude a, but not to the frequency σ. If the amplitude rise results in overshooting the threshold value (2.55), the wave will break at the wave group crest. If, however, deformation of the instantaneous spectrum leads to rise of the average frequency σ, this will indicate wave breaking far from the envelope crest and in fact may happen outside of a visible wave group. Such events can be seen around the 70^{th} and the 205^{th} seconds of the Black Sea record in Figure 3.15 where the second higher-frequency peak appears in the instantaneous spectrum and shifts up the average frequency: respective breakers are detected by both

Tab. 3.2. Adapted γ values from Black Sea data.

Rec. No.	$\lambda_L = 0.8$	$\lambda_L = 0.9$	$\lambda_L = 1.0$	$\lambda_L = 1.1$	$\lambda_L = 1.2$	$\lambda_L = 1.3$	$\lambda_L = 1.4$
211	0.1800	0.1940	0.2150	0.2630	0.2950	0.4100	0.6200
238	0.2050	0.2230	0.2550	0.3300	0.4350	0.6400	0.8000
242	0.2878	0.3070	0.3650	0.4750	0.6280	0.8750	1.1000
244	0.2690	0.2950	0.3500	0.4750	0.6780	0.9200	1.2000
Mean	0.2354	0.2547	0.2963	0.3857	0.5090	0.7113	0.9300
Std. Dev	± 0.0512	± 0.0549	± 0.0728	± 0.1066	± 0.1770	± 0.2354	± 0.2676

Tab. 3.3. Adapted γ values from Lake George data.

Record No.	$\lambda_L = 0.8$	$\lambda_L = 0.9$	$\lambda_L = 1.0$	$\lambda_L = 1.1$
4	0.3480	0.3825	0.4800	0.8170
8	0.4540	0.4900	0.5820	1.0500
9	0.4600	0.5150	0.6700	1.2355
10	0.2900	0.3280	0.4350	0.7680
11	0.3180	0.3500	0.4250	0.6690
14	0.2855	0.3180	0.4050	0.7070
15	0.4370	0.4820	0.5820	0.9730
Mean	0.3704	0.4094	0.5113	0.8885
Std. Deviation	± 0.0779	± 0.0838	± 0.1006	± 0.2059

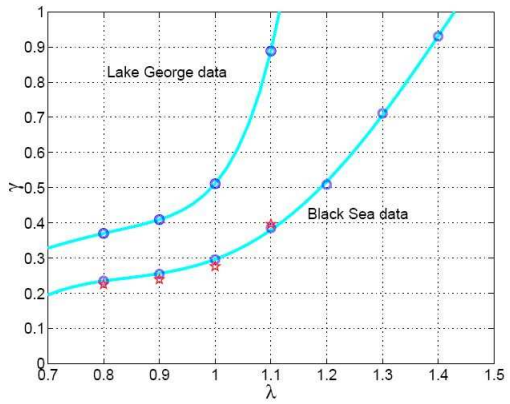

Fig. 3.17. The $\lambda_L - \gamma$ graph. Circles indicate data from Tables 3.2 and 3.3. Stars show conversion of the finite-depth γ according to (3.34)-(3.37).

the measurements and the wavelet method.

The secondary peak is a rather permanent feature of shallow-water spectra, and the Lake-George spectra in particular. Therefore, one would expect the wave breaking to occur more frequently beyond obvious group structure at finite depths, and to occur more frequently in general. The first expectation is supported by Figure 3.16 where many breakers are associated with the rising instantaneous secondary peaks, and the second expectation relates to the known fact that breaking rates are much higher in the finite depths compared to the deep water [e.g. Babanin *et al.*, 2001].

Mean values of γ shown in Tables 3.2 and 3.3 plotted versus the corresponding λ_L yield two distinctive and smooth $\gamma - \lambda_L$ curves for shallow (Lake George) and deep (Black Sea) water conditions. The curves are shown in Figure 3.17.

While the clear distinction between the shallow and deep water conditions is not unexpected, it presents a tangible challenge for an analytical and physically sound interpretation of these results. Previously, we postulated that the limiting downward acceleration is determined by balance of the gravitational and centrifugal forces. Therefore, the difference of the two curves should be possible to explain if we take into account the difference of the centrifugal accelerations for deep water (a_{deep}) and finite depth ($a_{shallow}$) waves of the same frequency ω. Conspicuously, this can be obtained if we consider what happens at the wave crest.

We expect that wave surface breaks once it can no longer sustain itself for some reason and we surmise that, whenever it happens, the downward acceleration at the surface must have exceeded some threshold level we wish to resolve. Effective downward acceleration of the real physical particles at the crest is the difference between gravitational acceleration and centrifugal acceleration caused by the motion of the particle along its orbit. The latter is given by $\omega^2 R$, where R is the radius of curvature of the motion of a particle on the breaking crest:

$$\frac{a_{deep}}{a_{shallow}} = \frac{\omega^2 R_{deep}}{\omega^2 R_{shallow}} = \frac{R_{deep}}{R_{shallow}}. \tag{3.34}$$

Here, R_{deep} and $R_{shallow}$ are now radii of curvature at the highest points of wave orbits con-

figured as circles in deep water and ellipsoids in finite depth. The curvature of two-dimensional curve defined by $y = y(x)$ function is

$$\frac{1}{R} = \frac{\frac{d^2y}{dx^2}}{\sqrt{\left[1 + \left(\frac{dy}{dx}\right)^2\right]^3}}. \tag{3.35}$$

Now, in deep water we have

$$R_{deep} = a \tag{3.36}$$

where a is the local wave amplitude. For the shallow water with water depth d it can be shown that

$$R_{shallow} = a \left\{ \frac{\cosh^2 [k(d+a)]}{\sinh [k(d+a)] \sinh(kd)}. \right\} \tag{3.37}$$

In essence, the orbits in shallow water are horizontally extended so that the centrifugal accelerations are larger for the same values of amplitude a and frequency ω, and thus the effective reduction of downward acceleration is smaller which in turn leads to larger γ for the shallow water cases. Clearly, a correction can be obtained from the ratio of $R_{shallow}/R_{deep}$. Applying this formulation to the four γ values of Lake George data at λ_L values of 0.8, 0.9, 1.0 and 1.1 in Figure 3.17 successfully adjusted them back to the deep-water cases as shown by the plottings of the four open stars.

The significance of this result extends further than merely resolving the differences of the two curves. Our ability to bring together the two distinctly different results, obtained from explicitly different wave environments, by applying the principles of physics, shows that the wavelet breaking detection approach based on the limiting-acceleration concept has a clear physical meaning rather than being just a technical measure. It allows us to apply a single approach to both deep and shallow waters and thus to translate derived parameters of γ and λ_L from one environment into another.

It is also of interest to note that based on the Black Sea acceleration measurement, as shown in Figure 3.14, we have picked a reference value of $\gamma = 0.3$. Now in Figure 3.17, the deep water $\gamma - \lambda_L$ curve based on the Black Sea breaking wave measurements leads γ to be 0.3 at $\lambda_L = 1$. Thus, $\lambda_L = 1$ would be another appropriate reference value to use, particularly as in Figure 3.17 this value also corresponds to transition of the translated finite depth γ's (stars) from underestimating to overestimating their deep-water counterparts. It is certainly consistent as with the deep-water observations based on the same Black Sea data [Banner *et al.*, 2000] as with the finite-depth study based on the Lake George data [Babanin *et al.*, 2001] which both concluded that the peak waves do break. A more refined analysis may require to introduce a wave-age dependence for λ_L as, according to Banner *et al.* [2000], the peak waves do not break if the waves are old enough and thus $\lambda_L > 1$ may be expected in such circumstances.

Now that a feasible rational approach was devised, a reality check, i.e. final count of the breaking waves was performed. To make an assessment of the performance of the approach, the γ values for $\lambda_L = 1$ were taken (Tables 3.2 and 3.3) and applied to the two available data sets in order to test the resulted breaking event matchings between the wavelet-approach detection

and the measurements. The results of these final counts of the breaking cases were shown in Figure 2.4 and discussed in Section 2.4.

Thus, the wavelet transform provides an opportunity to look at each individual wave crest in a time series of wave data and assess whether or not it might be a breaking wave. In Liu & Babanin [2004], the approach showed to be able to produce the same breaking statistics as field measurements of wave-breaking conditions based on detection of whitecaps at a fixed point of observations.

The Liu & Babanin [2004] approach uses the classical limiting downward-acceleration concept, developed primarily for monochromatic waves [e.g. Longuet-Higgins, 1969]. With wavelet transform as a time-frequency analysis method, this concept can now be extended to spectral waves when an instantaneous wave spectrum is replaced by an instantaneous characteristic wave (3.30)-(3.33), and applied to actual sea-wave measurements. The results can be interpreted through the basic wave physics and a limiting value of the acceleration was obtained from available field measurements. The approach is applicable to both deep-water and finite-depth environments.

3.8 Statistical methods for quantifying the breaking probability and dissipation

The statistical methods of quantifying the breaking probability and whitecapping dissipation, described in this Section, do not actually deal with direct and even indirect detection and measuring the breaking events as such. Based on some assumptions and, as it is usual in the wave-breaking studies, on some theoretical/empirical criteria, they try to interpret statistical properties of the wave fields in order to figure out a contribution of breaking waves to this statistics. It is argued that these properties prior to the breaking (or rather in absence of breaking) are known theoretically, and therefore the differences observed are due to the breaking. In this regard, such statistical methods do not deal with either detection or the measurement of wave breaking, which is the topic of this Section 3, but we thought it would be logical to place their brief description in the current Section because these methods do appeal to measurements of the waves and, based on these measurements, infer the breaking probabilities and severity, like the other methods described in this Section do.

The first analytical approach of this kind was a probability model suggested by Longuet-Higgins [1969] and further developed by Hua & Yuan [1992], Yuan *et al.* [1986, 2008, 2009]. All of these studies used the Gaussian distribution of surface elevations to predict the appearance of wave heights exceeding the limiting steepness of Stokes wave (2.46), or its limiting orbital velocity (2.48), or its limiting acceleration at the crest (2.49). In this regard, the models are based on sound physical principles.

Statistical approaches to the surface elevation, or wave-height, or wave-crest probability distributions are now a textbook subject and we refer to such books for details [e.g. Young, 1999, Holthuijsen, 2007]. The surface elevation is often treated as having normal/Gaussian probability distribution, and although obvious deviations from such distributions are reported [e.g. Babanin & Polnikov, 1995], the Gaussian probability density function is a reasonable approximation across a broad range of statistical wave applications.

For a Gaussian process with narrow-banded spectrum, which is what the spectrum of surface

waves is, the probability density function of wave heights $p(H)$ has Rayleigh distribution:

$$p(H) = \frac{H}{4m_0} \exp\left(-\frac{H^2}{8m_0}\right). \tag{3.38}$$

Thus, a probability that wave height H is greater than, for example, some limiting height H_{lim} is

$$P(H > H_{lim}) = \int_{H_{lim}}^{\infty} p(H)dH = \exp\left(-\frac{H_{lim}^2}{H_{rms}^2}\right) \tag{3.39}$$

where

$$H_{rms}^2 = 8m_0. \tag{3.40}$$

Now, for any given wave field with significant wave height H_s (2.38), probability of occurrence of waves exceeding, for example, the Stokes limiting wave steepness (2.46) can be estimated. In a similar fashion, in terms of the wave amplitude $a = H/2$, can be estimated probabilities of occurrence of waves exceeding a threshold acceleration (2.55) or limiting orbital velocity (2.48).

Longuet-Higgins [1969] investigated probability of waves having acceleration greater than the limiting downward acceleration for Stokes waves (2.49). Such waves were assumed to break until the wave height is reduced back to the limiting value, and the difference was attributed to the dissipation. Deductions were done for a narrow spectrum in order to obtain the dissipation of wave energy as a function of the spectrum, that is effectively an essential component of this probability model were assumptions made with respect to the breaking severity.

Yuan *et al.* [1986] extended the theory of Longuet-Higgins [1969] by removing the restriction of narrow-banded spectrum. Hua & Yuan [1992] further argued that the breaking does not stop once the wave steepness reached down the Stokes limit (2.46), and applied a similar probability model to investigate the wave-breaking dissipation by assuming that the lower limit of wave height in the course of breaking is determined by the mean value at a particular frequency derived from the Phillips [1958] equilibrium spectrum. In all cases, the dissipation was found to be a linear function of the wave spectrum.

More recently, as was discussed in Sections 3.2, 3.7 above, it was argued that the breaking waves do not necessarily have the (2.49) acceleration [Holthuijsen & Herbers, 1986, Hwang *et al.*, 1989, Liu & Babanin, 2004]. In addition, once they are breaking they do not stop at the Stokes limiting steepness but may keep losing energy until their steepness is well below the Stokes limit and even below the wave mean steepness [Liu & Babanin, 2004, Babanin *et al.*, 2009a,b, Figure 2.3]. Therefore, even though conceptually attractive, the probability models, as they have been derived, so far are not well justified quantitatively.

Yuan *et al.* [2008] continued the probability-function limiting-value approach, by using a modification of the kinematic criterion (2.48), that is by assuming that the waves at the tail of the probability distribution cannot exist if their surface orbital velocity exceeds the wave phase speed, which is the limiting velocity of the Stokes wave. An essential new ingredient of their model is the surface wind-drift velocity, which modifies (increases) the speed of water particles at the wave crest and thus promotes the breaking.

Yuan *et al.* [2009] combined this probability model with further empirical and analytical argument and applied it to investigating oceanic properties related to the breaking, such as energy

loss, both potential and kinematic, whitecap coverage (see also Section 3.1) and breaking entrainment. They continued on and compared expressions obtained with field observations to find satisfactory agreements.

A different class of probability models were developed over the years to target probability of breaking occurrence, rather than the breaking strength as in the studies described above [e.g. Longuet-Higgins, 1975b, 1983, Houmb & Overvik, 1976, Nath & Ramsey, 1976, Tayfun, 1981, Huang *et al.*, 1983, 1984, Ochi & Tsai, 1983, Snyder & Kennedy, 1983, Papadimitrakis & Huang, 1988]. They usually employ the comparing of probability functions of some properties of the wave systems, sometimes ad hoc properties, and refer to empirical criteria for such comparisons, rather than to physics explicitly. Since the wave measurements are most often conducted as time series of surface elevations, majority of the probability models employed joint probability distributions of wave height H, and wave period T rather than wavelength or wavenumber.

As an example of such model, which does not have a narrow-band spectrum limitation, we will describe the probability model of Ochi & Tsai [1983]. They used T^2 which can be converted into wavelength or wavenumber by means of linear dispersion relationship (see 2.17, 2.51), and therefore probability of occurrence of waves exceeding the Stokes limit (2.46), (2.51) or other limiting steepness can be estimated. Ochi & Tsai [1983] argued that, based on their laboratory observations, the Stokes limiting-steepness criterion (2.51) is too high and the waves will actually break if

$$H \geq 0.020 g T^2. \tag{3.41}$$

They concluded that (2.51) is applicable to what they called regular waves, and the irregular (or spectral waves) have to obey the limit (3.41). From what we know about the wave breaking now, this difference can perhaps be explained in physical terms.

If the waves break due to modulational instability, they do not follow the simple regular/irregular notion because shortly before the breaking onset their steepness reaches up the Stokes limit (2.46) whereas their wavelength shrinks and the period is reduced accordingly. The reduction of the period as observed by Babanin *et al.* [2007a, 2009a,b] is some 10-15% which is in perfect accord with the difference between (2.51) and (3.41) observed by Ochi & Tsai [1983].

Ochi & Tsai [1983] continued on to derive the prediction formula (3.41) by using a joint probability distribution of wave excursion and associated time interval of a non-narrow-band random process. They subdivided the wave breakings into two types, those whose excursion crosses the zero line (i.e. effectively dominant breaking) and those whose excursion is above the zero line (i.e. short waves breaking near the crest of the dominant waves). Ochi & Tsai [1983] found that the second type of breaking is approximately 27% of the first type.

Significance of this study is hard to overestimate. Because the model was intended for a non-narrow-band process, it can be applied both at the spectrum peak which has a characteristic bandwidth and at the spectral tail which does not. This is a very essential advantage as the present understanding of wave breaking indicates two-phase physics of the phenomenon: inherent breaking of dominant waves, determined by their narrow-banded nature, and induced breaking of short waves (see Sections 5, 6). The Ochi & Tsai [1983] results point out to a general steepness threshold for both phases of the wave breaking, which is consistent with the present understanding that the waves break because they reach a limiting steepness regardless the nature of physical processes which led to this steepness being achieved (see comments in Section 2.9).

The relative fraction of the short-scale breakers of 27%, however, appears very low and in this regard the Ochi & Tsai [1983] probability model perhaps would need a further revision.

Unrealistic also is the conclusion that no breaking is expected unless the significant wave height is greater than 4 m. Mathematically, the most important result of the Ochi & Tsai [1983] model is the outcome that breaking probability depends on the shape of wave spectrum and that the fourth moment of the spectrum is the main parameter in this regard.

A probability model of a different kind was proposed by Snyder & Kennedy [1983]. They introduced an artificial 'breaking variable' and then considered statistics of this variable and its relation with the wave directional spectrum. The variable was set equal to 1 inside a whitecap and 0 outside, the whitecap having both horizontal and vertical extents. Defining the whitecapping volume was done in terms of other variable which had a dynamic threshold which would indicate a breaking. A number of further assumptions were done with respect to the dynamic variable, one of which was that it has a maximum at the free surface.

To clarify this reasoning in physical terms, we should simply say that the acceleration was eventually used as the dynamic variable. If it was over some threshold limit, the point of the wave body in space and time was regarded breaking and the breaking variable was set to 1. Then, mapping of the whitecapping surface was done in terms of geometric moments of this variable. Further on, the dynamic variable (acceleration) was related to the wave spectrum, and thus the statistics of the breaking variable in terms of its moments was connected to this spectrum.

A number of very insightful conclusions regarding the breaking probability were obtained with this model. It was found that this probability, and a whitecap coverage, are a function of the ratio between *rms* acceleration and its critical level. The probability appeared a simple inverse function of the wave fetch, and interestingly the cross-wave scale of whitecaps was concluded to be greater than the down-wave scale. The presence of breaking water at some point had certain positive and negative correlations with some phases of other waves in the wave train: for example, if a wave crest was breaking, there was a tendency for successive crests to also break.

Some of the outcomes, however, indicate limitations of the method. Thus, it was concluded that the whitecaps should travel with the speed appropriate to their scale. Such finding is of course perfectly consistent with expected behaviour of waves breaking due to inherent reasons, but not of the induced breaking, i.e. breaking of short waves forced near crests of dominant waves. Obviously, one cannot blame the model for not reproducing what it was never designed to reproduce, but this fact outlines important constraints of such models. Since the induced breaking is expected to dominate at small scales (see Section 5), this means that in practical terms the Snyder & Kennedy [1983] approach is restricted to some range of frequencies around and above the spectral peak. Snyder & Kennedy [1983] in fact had a self-imposed cut-off of some $5f_p - 10f_p$, due to divergence of the integral of the acceleration spectrum which they relied on. This cut-off is actually in reasonable agreement with the limits which indicate dominance of the induced breaking [Babanin & Young, 2005, Babanin *et al.*, 2007c].

To bypass the integration of probability densities for the acceleration, the technique was further tested by means of Monte Carlo simulations of the vertical accelerations [Kennedy & Snyder, 1983]. Additional interesting finding of this statistical study was that "the propagation velocity of the whitecap was typically 45% of the phase velocity associated with the frequency of peak energy". Kennedy & Snyder [1983] further conjectured that "while this velocity is close to the group velocity, the similarity between the two velocities is probably coincidental, as there appears to be no reason to believe that group velocity is a pertinent parameter. The low velocity

of the whitecaps probably reflects the importance of higher frequency wave components to the breaking process". Both the conclusion and the conjecture now find experimental support [e.g. Gemmrich *et al.*, 2008].

Snyder *et al.* [1983], the final paper in the series of Snyder & Kennedy [1983], Kennedy & Snyder [1983] was intended to provide experimental support to the probabilistic model and its rich set of interesting and important conclusions, and to experimentally estimate the key parameter of the model, i.e. threshold value of the downward acceleration. A field experiment was conducted in order to measure the statistical geometric properties of whitecaps, by means of synchronised photographing the breaking waves and recording them with an array of wave probes. Many theoretical findings of the statistical model were confirmed, with the most important conclusion being that the threshold acceleration should correspond to the theoretical limit for monochromatic Stokes waves (2.49), i.e. $0.5g$. The authors cautiously warned that "this conclusion is less than definite because our analysis is limited to wave components with frequencies less than twice the frequency of the spectral peak". Since, as was discussed above, from practical point of view the model is basically designed for dominant waves anyway, the uncertainty is not too essential and the limit perhaps reflects well the critical level suitable for this kind of models.

To summarise the overview of probability methods and models, we have to conclude that they of course do not deal with individual breaking events like other approaches described in this Section 3, but appear extremely capable in quantifying statistical characteristics of the breaking waves in the overall surface-wave field. This should not come as a surprise as, unlike many or even most of the empirical breaking detection techniques, they refer to limiting surface properties based on fundamental physical grounds. In most cases those are limiting steepness, orbital velocity or downward acceleration, or their derivatives (see Section 2.9) which signify definite conditions such that beyond these conditions the water surface cannot sustain itself and collapses. One can argue that water surface may become unstable even before it reaches these limiting conditions, but ultimately the wave certainly cannot persist without breaking after. Therefore, although quantitative conclusions of the probability models perhaps need revision, particularly those which try to predict the dissipation as described above, such statistical models are very sound and promising in physical and theoretical sense.

4 Fully non-linear analytical theories for surface waves and numerical simulations of the wave breaking

The previous Section was dedicated to experimental methods of detecting the wave breaking, quantifying the breaking probability and severity, and measuring effects related to the breaking, including the wave energy dissipation. In the next section, it is logical to describe theoretical methods of describing wave-breaking physics or phenomena leading to the breaking.

While the experimental oceanography produced abundant variety of techniques and approaches to detect and measure the breaking, the theories capable of dealing with the wave breaking are few. These should not be confused with analytical methods intended to detect the breaking events in surface-wave records (Section 3.7) or with the statistical methods of quantifying the breaking probability and strength (Section 3.8). Both such groups of the analytical techniques are placed into experimental Section 3 for a good reason – they principally rely on empirical criteria.

Another significant group of analytical approaches, dealing with the dissipation due to breaking, rather than with the breaking as such is also not included in this Section. Some of these models are based on assumptions intended to interpret pre-breaking or post-breaking properties of the waves, rather than on working with physics leading to the breaking or driving the breaking and its consequences. Others attempt to deduce the dissipation from differences between wave-evolution predictions done by means of kinetic and dynamic equations. In any case, these are indirect techniques which do not depict the wave breaking event explicitly.

In this regard, here we will consider as a wave-breaking theory an analytical method which is able to describe evolution of non-linear waves to the point/moment of the breaking onset, or even beyond, without relying on empirical criteria, or assumptions yet to be proved, or some interpretations of wave properties which supposedly allow to reveal wave-breaking impacts provided those would take place or have already taken place. In this Section, we will refer to wave theories based on first principles.

We conditionally label them fully non-linear analytical theories for surface waves, as opposed to wave theories which are based on first principles, but then involve further assumptions. Typical example of the latter are the perturbation theories based on employing some 'small parameter', usually wave steepness (1.1). Theories which rely on small steepness, or even on finite steepness are indeed also non-linear, and they do depict non-linear effects, including some very important non-linear characteristics of wave shape, wave fields and wave dynamics, but they can hardly be expected to adequately attend to the problem of wave breaking where the steepness of individual wave is by definition ultimately extreme. As an illustration of this point we can refer to Figure 1.2 where the Stokes wave obtained by the perturbation-analysis means does exhibit such non-linear feature of wave shape as skewness S_k, but fails to reproduce another non-linear property, the vertical asymmetry A_s which is an integral part of shape of breaking waves.

Chalikov-Sheinin (CS) model [Chalikov & Sheinin, 1998, 2005] was mentioned in Section 1.2 as such approach which is capable of reproducing the asymmetry A_s of deep-water waves. In very simple terms, this model is based on solution of Euler equation, the fundamental equation of hydrodynamics, the law of Newton applied to fluids in absence of friction force. The model does not involve any assumptions on wave steepness magnitude, and in this regard we will call it fully non-linear. Analytical solutions of fully non-linear equations and boundary conditions so far have not proved feasible, and therefore the existing fully non-linear approaches are

numerical models. There are several such models, and it is their accuracy, stability and ability to integrate the evolution equations in space and time without accumulating numerical errors, that differentiate them and distinguish from one another. We will give a brief overview of the fully non-linear models, based primarily on the CS example, following largely Babanin *et al.* [2007a, 2009a,b].

4.1 Free surface at the wave breaking

Numerical computations of non-linear surface waves have previously been undertaken based on solutions of the potential flow equations [e.g. Watson & West, 1975, Longuet-Higgins & Cokelet, 1976, West *et al.*, 1987] and with a Cauchy-type integral algorithm [Dold & Peregrine, 1986, Dold, 1992]. Both schemes have no limitation in terms of wave steepness, and both were capable of simulating the initial phase of wave breaking (the later stages are rotational and remain extremely difficult to simulate directly). More recently, a method based on a Taylor expansion of the Dirichlet-Neumann operator was developed by Craig & Sulem [1993]. The capabilities of this method were illustrated by computing the evolution of modulated wave packets and a low-order approximation of a Stokes wave for relatively short periods of time. We should point out that this appears to be a principle limitation of all the above schemes: for a steep wave field, they have only been used for simulations of relatively short time/space evolution. These approaches could not be applied to longer periods of time because none of them appear to provide conservation of integral invariants (mass, energy, horizontal momentum).

A numerical scheme for direct hydrodynamical modelling of two-dimensional non-linear gravity and gravity-capillary waves was developed by Chalikov & Sheinin [1998][see also Chalikov & Sheinin, 2005, Chalikov, 2005, 2007]. This approach is based on a non-stationary conformal mapping, which allows the equations of potential flow with inclusion of a free surface to be written in a surface-following coordinate system. This transformation does not impose any restriction on the shape of the surface, except that it has to be possible to represent this surface in terms of a Fourier series. An analogous approach was developed by Dyachenko et al. [1996].

Let us consider periodic two-dimensional deep-water waves whose dynamics is described by principal potential equations. Due to the periodicity condition, the conformal mapping for infinite depth can be represented by the Fourier series [see details in Chalikov & Sheinin, 1998, 2005]:

$$x = \xi + \sum_{-M \le k < M, k \neq 0} \eta_{-k}(\tau) \exp(k\zeta) \vartheta_k(\xi), \tag{4.1}$$

$$z = \zeta + \sum_{-M \le k < M, k \neq 0} \eta_k(\tau) \exp(k\zeta) \vartheta_k(\xi); \tag{4.2}$$

where x and z are Cartesian coordinates, ξ and ζ a conformal surface-following coordinates, τ is time, η_k are coefficients of the Fourier expansion of free surface $\eta(\zeta, \tau)$ with respect to the new horizontal coordinate ζ:

$$\eta(\zeta, \tau) = h(x(\zeta, \xi = 0, \tau), t = \tau) = \sum_{-M \le k \le M} \eta_k(\tau) \vartheta_k(\zeta), \tag{4.3}$$

ϑ_k denotes the functions

$$\vartheta_k(\xi) = \begin{cases} \cos k\xi & \text{for } k \geq 0, \\ \sin k\xi & \text{for } k < 0 \end{cases} \tag{4.4}$$

and M is truncation number.

Non-traditional presentation of the Fourier Transform with the definition (4.4) is, in fact, more convenient for computations with real numbers, such as $(\vartheta_k)_\xi = k\vartheta_{-k}$ and $\sum(A_k\vartheta_k)_\xi = -\sum kA_{-k}\vartheta_k$. So, the Fourier coefficients A_k form a real array $A(-M : M)$, thus making possible a compact programming in Fortran90. Such presentation can be generalised for three-dimensional case.

Note that the definition of both coordinates ξ and ζ is based on Fourier coefficients for surface elevation. It then follows from (4.1) and (4.2) that time derivatives z_τ and x_τ for Fourier components are connected by a simple relation:

$$(x_\tau)_k = \begin{cases} -(z_\tau)_{-k} & \text{for } k > 0, \\ (z_\tau)_k & \text{for } k < 0. \end{cases} \tag{4.5}$$

Due to conformity, the Laplace equation retains its form in (ξ, ζ) coordinates. It is shown in Chalikov & Sheinin [1998, 2005] that the potential wave equations can be represented in the new coordinates as follows:

$$\Phi_{\xi\xi} + \Phi_{\zeta\zeta} = 0, \tag{4.6}$$

$$z_\tau = x_\xi G + z_\zeta F, \tag{4.7}$$

$$\Phi_\tau = F\Phi_\xi - \frac{1}{2}J^{-1}(\Phi_\xi^2 - \Phi_\zeta^2) - z, \tag{4.8}$$

where (4.7) and (4.8) are written for the surface $\zeta = 0$ (so that $z = \eta$, i.e. the surface elevation), J is the Jacobian of the transformation:

$$J = x_\xi^2 + z_\xi^2 = x_\zeta^2 + z_\zeta^2, \tag{4.9}$$

G is an auxiliary function:

$$G = (J^{-1}\Phi_\zeta)_{\zeta=0}, \tag{4.10}$$

and F is a generalisation of the Hilbert transform of G, which for $k \neq 0$ may be defined in Fourier space as

$$G_k = \begin{cases} -F_{-k} & \text{for } k > 0, \\ F_k & \text{for } k < 0, \end{cases} \tag{4.11}$$

actually following from (4.5). Above, Φ is the velocity potential (and Φ_ζ is the derivative of the potential with respect to the 'vertical' coordinate ζ at the surface), z represents the shape of the surface.

Equations (4.6) – (4.11) are written in non-dimensional form with the following scales: length L, where $2\pi/L$ is the (dimensional) horizontal wavenumber, time $L^{1/2}g^{-1/2}$ and the velocity potential $L^{3/2}g^{-1/2}$ (g is the acceleration of gravity). Capillar effects and external pressure were not taken into account in this formulation. Note that the adiabatic equations for surface

waves outside the capillary interval are self-similar: they are invariant over length scale L, what makes the numerical approach very effective and allows for broad interpretations.

The boundary condition assumes vanishing vertical velocity at infinite depth

$$\Phi_\zeta(\xi, \zeta \to -\infty, \tau) = 0. \tag{4.12}$$

Solution of the Laplace equation (4.6) with boundary condition (4.12) yields to Fourier expansion which reduces the system (4.6) – (4.8) to a one-dimensional problem:

$$\Phi = \sum_{-M \le k \le M} \phi_k(\tau) \exp(k\zeta) \vartheta_k(\xi), \tag{4.13}$$

where ϕ_k are Fourier coefficients of the surface potential $\Phi(\xi, \zeta = 0, \tau)$. Eqs. (4.6) – (4.8), (4.10) and (4.11) constitute a closed system of prognostic equations for the surface functions $z(\xi, \zeta = 0, \tau) = \eta(\xi, \tau)$ and the surface velocity potential $\Phi(\xi, \zeta = 0, \tau)$. For more detailed descriptions of the analytical and numerical model, we refer to Chalikov & Sheinin [1998, 2005].

Remarkably, this new formulation is also simpler than the original set of equations since the non-linear conformal coordinate transformation removes a number of non-linear terms. For the stationary case, this method coincides with the classical complex variable method [e.g. Crapper, 1957], and an efficient numerical scheme (CS) for this was developed by Chalikov & Sheinin [1998]. Note that this scheme is more precise than the popular surface integral scheme [Dold, 1992]. As mentioned above, the Dold scheme as well as all schemes based on truncated equations (like those of West *et al.* [1987] and Craig & Sulem [1993]) do not conserve energy without some artificial means. Thus, they are only acceptable for short-duration processes (as indicated by Dold [1992], Chalikov [2009]). In addition, compared to the CS scheme, the surface integral method is cumbersome: a complete set of its equations occupy several pages. For the CS scheme, the equations take 3 lines and the core of the numeric scheme takes 11 lines in Fortran90.

The accuracy of this scheme was demonstrated by a long-term simulation of very steep Stokes waves ($ak = 0.42$). The stability of Stokes waves has been a subject of many speculations. The reality is quite simple: Stokes waves are always unstable to any disturbances, but the rate of development of the instability depends on the amplitudes of the perturbations and their phases. In general terms, a Stokes wave is unstable if it has any perturbation from the pure Stokes form. In the CS case, 11 decimal places of precision and a 4th order Runge-Kutta scheme were sufficient to simulate the propagation of a virtually undisturbed Stokes wave for up to one thousand periods [e.g. Chalikov, 2007].

The conformal mapping even made it possible to reproduce the initial stages of the breaking process where the surface ceases to be a single-valued function. It should be mentioned that the Dold [1992] scheme is also capable of achieving this, but with special smoothing and regularisation. The CS model, however, has a number of important advantages: (1) comparison with an exact solution showed that the scheme has extremely high accuracy; (2) it preserves integral invariants; (3) it is very efficient: its computation time scales as $M \cdot \log(M)$ where M is the number of modes, whereas the Dold scheme scales as M^2; (4) the scheme demonstrates stability over millions of time steps (thousands of periods of the dominant wave). This scheme is able to reproduce a non-linear concentration of energy in physical space resulting in wave breaking and potentially in the appearance of freak waves. In the CS model, the wave model is also coupled with an atmospheric boundary-layer model.

4.1.1 Simulating the evolution of non-linear waves to breaking

For the purposes of studying the wave breaking, the model's ability to reproduce wave evolution without limitations in terms of steepness or duration of propagation is crucial. For this reason, the CS model was chosen in Babanin *et al.* [2007a, 2009a,b] for detailed numerical simulations of physical characteristics of strongly non-linear waves leading to the onset of breaking. Before, the CS model was extensively verified and tested [Chalikov & Sheinin, 1998, 2005] and used in a number of strongly non-linear applications [e.g. Chalikov, 2005, 2007]. It was then additionally checked in terms of its capacity to model non-linear wave features associated with wave breaking.

As mentioned above, one of essential checks for a wave-breaking model is its ability to describe wave asymmetry with respect to the vertical axis. Definitions of the asymmetry A_s (1.3) and skewness S_k (which is asymmetry with respect to the horizontal axis (1.2)) are given in Figure 1.2 and Section 1.2. Capacity of CS model in this regard is demonstrated in Figure 2.1 where a transient steep wave dynamically develops very large asymmetry and skewness.

In numerical simulations of the fully non-linear evolution of steep two-dimensional waves to the point of breaking, we will concentrate on three physical properties featuring non-linearity, i.e. wave steepness, skewness and asymmetry, and their inter-relationships. We will then try to reproduce and investigate these properties in a laboratory experiment with two-dimensional waves (Section 5.1.1). If these properties are indeed linked to wave breaking, but the percentage of breaking waves is small, as it usually is [e.g. Babanin *et al.*, 2001], then examination of average steepness, skewness or asymmetry is likely to be of little use. Therefore, the numerical analysis here will be dedicated to non-linear properties of individual waves.

In Figure 4.1, development of an unforced wave (no wind) to the point of breaking is shown. The wave shown had the Initial Monochromatic Steepness $IMS = 0.16$ and is regarded as moderately steep in terms of the modulational instability. This moderate steepness will allow a reasonably long evolution before breaking occurs. Therefore, the simulation will produce a general, rather than detailed picture to begin with (the time scale is expressed in wave periods, i.e. the wave breaks after 82 periods).

As seen in the Figure, the steepness of individual waves stays reasonably constant for a significant number of periods ($\sim$30), before it starts oscillating noticeably. The magnitude of the oscillation increases significantly beyond the 60^{th} period, and from this point grows rapidly until the simulation ceases (wave breaks) after the 80^{th} period mark.

Similar behaviour is exhibited by the skewness and asymmetry. The simulation starts from a Stokes wave of $S_k = 0.18$ and $A_s \approx 0$. It is informative to note that prior to breaking, the magnitude of the skewness oscillation is so large that at times the wave even becomes negatively skewed (i.e. the trough is deeper than the crest). At the termination of the simulation, however, $S_k \approx 1$, that is the crest is twice is high as the trough (1.2). In Section 5.1.1, it is shown that laboratory waves asymptote to this value of skewness at the onset of breaking. The asymmetry also oscillates through the simulation and reaches the experimentally observed breaking magnitude of $A_s \sim 0.5$ [i.e. Caulliez, 2002].

Therefore, the inherent instability of non-linear waves leads to a breaking even in the absence of wind forcing. In such a scenario, the wave cannot gain energy to grow on average. However, the instability causes gradually-increasing instantaneous distortions of the wave shape, such that at some point the water surface can apparently no longer sustain the wave profile, and collapses. It should be noted that comparisons of such numerical simulations with experiments can only

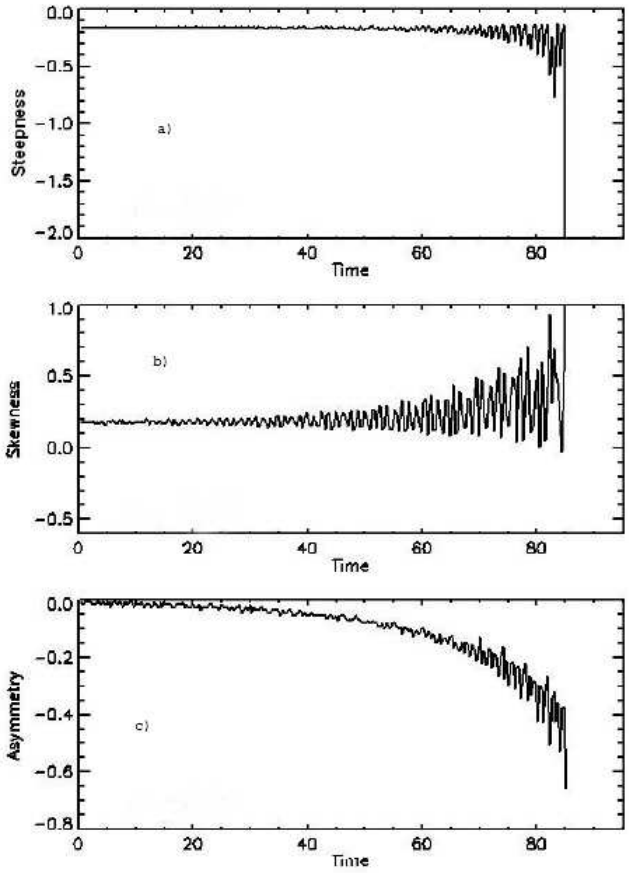

Fig. 4.1. Numerical simulation of evolution of a wave with $IMS = 0.16$ to the point of breaking (no wind). Time scale is in wave periods. (top) Wave slope (steepness where minus sign signifies the forward slope); (middle) skewness; (bottom) asymmetry.

be qualitative. At the initial stages of development, the necessary instability modes, if they are absent, should grow from the continuous background noise. Such noise is suppressed in a discretised numerical model, particularly if the model is very precise.

Figure 4.2 shows the simulated evolution of the non-linear wave properties to the point of breaking in the presence of wind forcing. As above, in each set of three panels the top panel shows the evolution of individual wave steepness, middle panel – wave skewness, and bottom panel – asymmetry. Three sets of subplots correspond to three wind-forcing conditions: $U/c = 2.5$ (moderate forcing), $U/c = 5.0$ (strong forcing) and $U/c = 10.0$ (very strong forcing) where U is a characteristic wind speed (the model is non-dimensional and therefore there is no standard 10 m height and respective wind U_{10}). The initial steepness chosen is $IMS = 0.26$, which should lead to a faster evolution to breaking onset. No initial modulations were imposed. Note

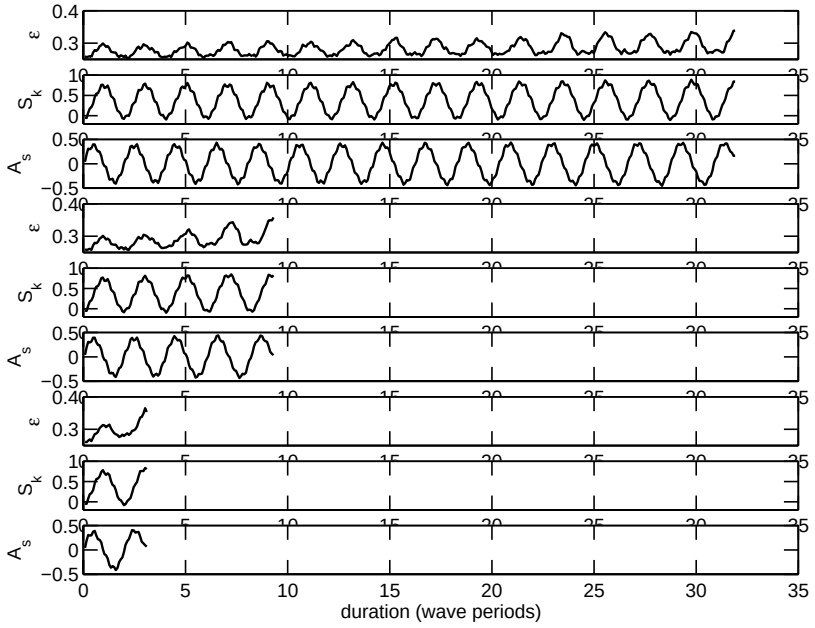

Fig. 4.2. Simulations of steepness (first panel), skewness (second panel); asymmetry (third panel) of the wave of $IMS = 0.26$ as it evolves from the initial conditions to the point of breaking. Top three panels: $U/c = 2.5$; middle three panels: $U/c = 5.0$; bottom three panels: $U/c = 10.0$.

that the minimum value plotted on the steepness scale is $\epsilon = 0.25$ and not zero, and that the simulation starts from a harmonic wave with $S_k = A_s = 0$.

The most obvious feature of the simulations is the oscillations of the values of steepness, asymmetry and skewness. These are not the waves that are shown in the Figure, these are the characteristics of wave non-linearity evolving in physical space.

The top three panels correspond to a moderate wind-forcing condition of $U/c = 2.5$. Under such a wind, it takes approximately 32 wave periods to reach the point of breaking. Oscillations of wave steepness begin immediately and the wave reaches a steepness of $\epsilon = 0.3$ (first maximum) within one period which then relaxes back to $\epsilon = 0.26$ (first minimum) within the next wave period. The period of the modulation is equal to twice the wave period. During each oscillation, the steepness relaxes back to almost $\epsilon = 0.26$ (magnitude of the last steepness trough before breaking is $\epsilon = 0.269$). With the wind energy input imposed, however, the maxima of instantaneous steepness keep growing and reach a value of $\epsilon = 0.34$ at the point which is interpreted as incipient breaking by the model.

The skewness and asymmetry oscillate with the same double-wave period, but without a noticeable increase in magnitude of the oscillation. For example, the value of $S_k = 0.84$ of the skewness at breaking is repeatedly reached by the wave in its progress without breaking. Therefore it appears that the local steepness, if anything, defines the breaking. Visually, skewness is in phase with the steepness oscillations, and it relaxes back to zero when the steepness is

minimal.

The oscillations of asymmetry are apparently shifted in phase with respect to steepness and skewness. The asymmetry oscillates about zero in the range $A_s = \pm 0.45$ which means that the waves are periodically tilted backward and forward. When steepness (skewness) is maximal, asymmetry is zero, i.e. the wave is symmetric with respect to the vertical. If the point of maximum steepness (skewness) is passed without breaking, the asymmetry becomes negative. That is, the wave begins to lean forward. If this point signifies the breaking onset, the wave is apparently still continuing to tilt forward, and this explains why all the breaking waves exhibit negative asymmetry. The negative asymmetry thus is not an indication of the breaking but is rather an indication of the modulation phase at which breaking-in-progress may or may not occur.

The second set of three panels correspond to wind forcing of $U/c = 5.0$. Whilst such forcing is quite strong, and therefore the steepness growth rate is much faster than above, apart from the steepness growth almost all the other breaking and non-breaking properties of the non-linear evolution remain similar to the previous test. The wave steepness, skewness and asymmetry oscillate with the same period and their phase shifting pattern is qualitatively the same, steepness ($\epsilon = 0.36$) and skewness ($S_k = 0.82$) values at breaking are close to those of the above test, asymmetry at breaking approaches zero. Thus, it can be again concluded that it is some critical value of local steepness rather than anything else which defines the breaking onset.

It is interesting to note that, according to known results on wave amplification by wind, the wave growth increment at non-extreme conditions should be approximately a quadratic function of the wind [e.g. Donelan *et al.*, 2006]. If indeed there is some critical steepness signifying breaking onset, then doubling the wind speed in numerical tests should lead to this limiting value being reached four times as fast. This conjecture produces a result close to that simulated: the duration of the evolution to breaking has now been reduced from 32 to 9 wave periods (almost 4 times).

A further doubling of the wind input, as shown in the bottom set of three panels, led to another reduction of the evolution duration - from 9 to 3 periods. This is again consistent with Donelan *et al.* [2006] who showed that at very strong winds the relative wave growth slows down. The other patterns of the wave non-linear evolution appear unaltered. The whole picture again points to the critical local steepness as the parameter responsible for the onset of the water surface collapse. The maximum values of steepness $\epsilon = 0.36$ and skewness $S_k = 0.83$ are almost the same as previously. These values also demonstrate that the instantaneous effect of the wind on the breaking onset is negligible. The wind forcing of $U/c = 10.0$ is now very strong, but this wind is still not capable of pushing the wave over and reducing, even marginally, the critical steepness at breaking.

Let us summarise observations made with this instructive Figure 4.2. Values of steepness, skewness and asymmetry oscillate at a frequency half that of the carrier wave. While the simulation begins with both skewness and asymmetry zero (sinusoidal wave), the sinusoidal wave immediately turns into a Stokes wave, but shape of this wave oscillates, and it is only at a particular phase of these oscillations that the wave shape is clearly that of the Stokes wave again: at the point of maximal skewness, the wave is symmetric. As the skewness is decreasing or growing, the asymmetry is also changing, that is the wave is tilting forward (negative asymmetry) or backward (positive asymmetry). S_k and A_s oscillate between their maximum and minimum values, but remain bounded, their maximum and minimum do not increase in magnitude if the initial steepness is already large enough. In contrast, the oscillations of the steepness progressively

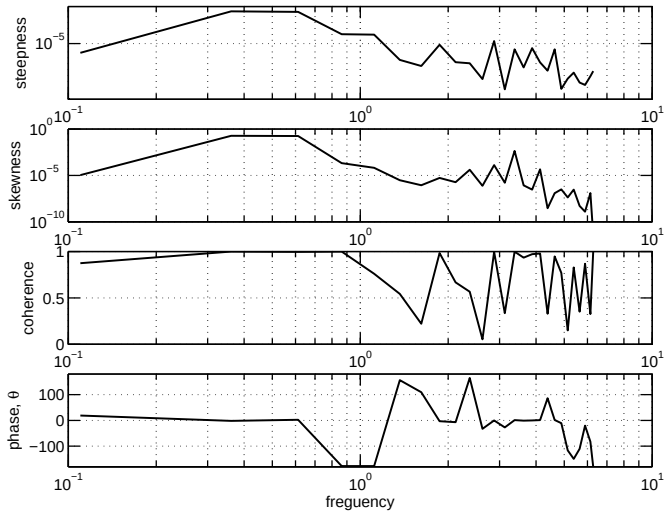

Fig. 4.3. Numerical simulations (see Figure 4.2). Dimensionless wave period is 1. Co-spectra of running steepness and skewness for waves of $IMS = 0.26, U/c = 2.5$. (top panel) Steepness spectrum. (second top panel) Skewness spectrum. (second bottom panel) Coherence spectrum. (bottom panel) Phase spectrum (in degrees).

grow in amplitude until a point is reached where breaking takes place. It is therefore evident from Figure 4.2 that it is the steepness which is the limiting parameter for the breaking to occur.

The coherence and phase relationships of steepness, skewness and asymmetry, outlined qualitatively above, are analysed in Figures 4.3 and 4.4. Figure 4.3 compares spectra of running instantaneous steepness ϵ (1.1, top subplot) and skewness S_k (1.2, second subplot), their coherence (third subplot) and phase (bottom subplot). Since the time scale of the simulations is dimensionless (i.e. presented in terms of wave periods), the frequency scale is expressed in inverse wave periods. Therefore, as expected from the visual examination of Figure 4.2, the peak of the steepness/skewness modulation occurs at twice the wave period (0.5 of the inverse wave period). This frequency dominates the spectrum. The spectral density decreases very rapidly away from the peak.

The peak is rather broad and covers a range of frequencies of $0.4 \div 0.6$ of inverse wave periods. The coherence of the steepness and skewness oscillations in this range is 100%, as could have been expected for numerical simulations of the theory with a model of such high precision. The phase shift between the dominant oscillations of steepness and skewness is zero, as was observed visually. Thus, the steepness and skewness are in phase, and the maximum steepness is achieved at the same instant as the maximum skewness.

Similarly, Figure 4.4 compares the co-spectra of running instantaneous skewness S_k (1.2) and asymmetry A_s (1.3). Again, the broad peak of the asymmetry spectrum falls in the $0.4 \div 0.6$ range of inverse wave periods. Spectra of skewness and asymmetry are almost perfectly coherent, with a phase shift of about 90° (asymmetry is leading). The latter means that the asymmetry reaches its positive maximum (i.e. wave is tilted backward) when skewness is approximately

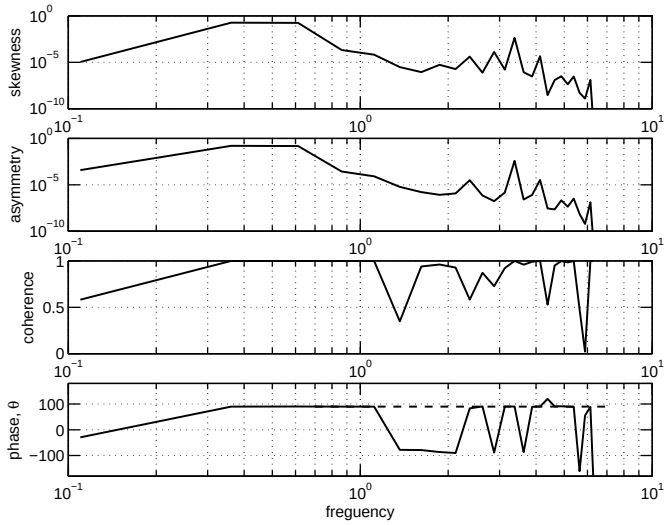

Fig. 4.4. Numerical simulations (see Figure 4.2). Dimensionless wave period is 1. Co-spectra of running skewness and asymmetry for waves of $IMS = 0.26, U/c = 2.5$. (top panel) Skewness spectrum. (second top panel) Asymmetry spectrum. (second bottom panel) Coherence spectrum. (bottom panel) Phase spectrum (in degrees), positive phase means asymmetry is leading. Dashed line shows 90° phase shift.

zero (wave crest and trough are of equal magnitude) and the local steepness is half-way through rising from its minimum to the maximum value in an oscillation. From the positive maximum, the asymmetry begins to decrease and reaches zero half a wave period later (quarter of the period of the oscillation) - i.e. the wave becomes symmetric with respect to the vertical. At this point, steepness and skewness are at their maximum, and it is at this point that the wave may break. Whether the wave breaks or not, the asymmetry will keep decreasing into negative values (wave is tilting forward), while the steepness/skewness start subsiding in quadrature with the asymmetry. It is interesting to look at this moment from a point of view of an observer who encounters the breaker: he sees a very tall crest which begins to break with the water mass falling down from the top and at the same time the front face is growing steeper as the wave is learning forward - obviously a very dangerous situation.

To briefly summarise the intermediate conclusions: we can speculate that a two-dimensional non-linear wave will break when, due to inherent modulations of its height, it will reach some limiting steepness. The skewness and asymmetry also oscillate, in phase and in quadrature with the steepness respectively. In the simulations, however, they do not appear to exhibit some specific limiting value at the point of breaking.

We shall now conduct a similar set of numerical simulations for a wave with initially half the steepness $IMS = 0.13$ (Figures 4.5 and 4.6). A very strong forcing of $U/c = 10.0$ is applied in order to achieve breaking in a reasonably short period of time.

The three panels in Figure 4.5 show the time evolution of individual wave steepness (top), skewness (middle) and asymmetry (bottom) as in Figure 4.2 above. The wave steepness in the top subplot grows under the $U/c = 10.0$ wind forcing so rapidly that its oscillations are barely

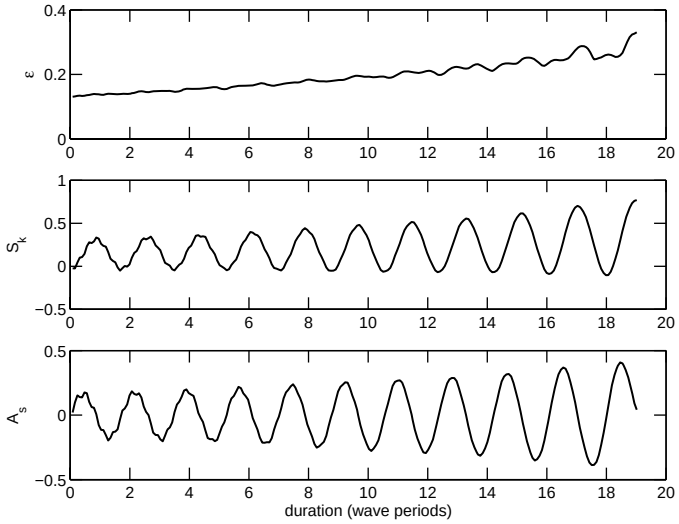

Fig. 4.5. Simulations of steepness (first panel), skewness (second panel); asymmetry (third panel) of the wave of $IMS = 0.13, U/c = 10.0$ as it evolves to breaking.

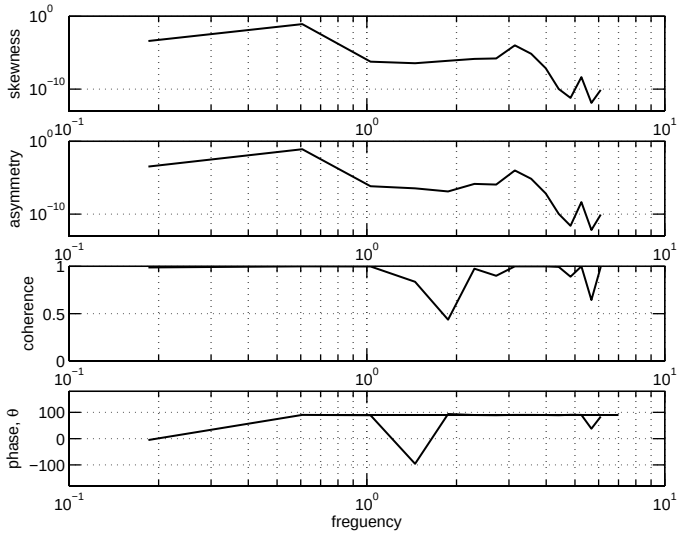

Fig. 4.6. Numerical simulations (see Figure 4.5). Dimensionless wave period is 1. Co-spectra of running skewness and asymmetry for waves of $IMS = 0.13, U/c = 10.0$, 19 wave periods to breaking. (top panel) Skewness spectrum. (second top panel) Asymmetry spectrum. (second bottom panel) Coherence spectrum. (bottom panel) Phase spectrum (in degrees), positive phase means asymmetry is leading. Straight line shows 90° phase shift.

visible over the strong mean trend. The value of steepness $\epsilon = 0.33$ at the point of breaking, similar to the previous tests, supports the concept of a limiting breaking-onset value. Compared with same wind forcing in Figure 4.2, it now takes much longer (19 wave periods versus 3) to achieve this steepness, but as soon as it is reached, the wave breaks.

It is instructive to observe the behaviour of the skewness and asymmetry of these initially much less steep waves (bottom two panels). Since non-linearity is now obviously weaker, it could have been expected that the oscillations would start from much smaller magnitudes of $S_k = 0.33$ and $A_s = 0.18$. They do eventually grow to maxima of $S_k = 0.77$ and $A_s = 0.41$ similar to values observed previously. These may be indicative of limiting values of the wave skewness and asymmetry, but they are obviously not a breaking criterion, as in the previous test they did not lead to the breaking unless the limiting steepness was also reached.

Co-spectra of running skewness and asymmetry of the $IMS = 0.13$ wave are shown in Figure 4.6. Their values are quite similar to those for the case of $IMS = 0.26$ in Figure 4.4 above, but it is noticeable that the peak at half the inverse wave period is now narrower and the coherence is stronger across almost the entire frequency band. Apparently, the stronger non-linearity tends to somewhat randomise the wave-shape oscillations (Figure 4.4). The obvious decrease in the coherence between one and two inverse wave periods still requires an explanation.

Figure 4.7 shows a composite set of fetch-versus-steepness dependences for different values of wind forcing $U/c = 1 - 11$. The fetch is expressed in dimensionless terms of number of wavelengths to the breaking at a particular $IMS = ak$.

As shown in Babanin *et al.* [2007a], wave with no superimposed wind forcing and $IMS < 0.1$ will never break, even though they will exhibit oscillations of steepness, asymmetry and skewness similar to those shown in Figures 4.1, 4.2, 4.5. Evolution of such waves is not plotted in the Figure, and in fact we do not plot $IMS < 0.17$ because such development to breaking is too slow for the purpose of demonstration. The upper limit of steepness included is $IMS = 0.28$ as waves with $IMS > 0.3$ will break immediately, within one wavelength/period. Between these two limits, the dimensionless distance to breaking decreases with increasing IMS.

Figure 4.7 allows the estimation, based on the numerical simulations with the CS model, of when a two-dimensional wave breaks. For example, it will take a wave of $IMS = 0.24$ six wavelengths to reach the point of breaking under $U/c = 8.5$, seven wavelengths under $U/c = 8.0$, eleven wavelengths under $U/c = 7.5$. If wind forcing is reduced significantly, i.e. $U/c = 3.0$, such a wave will only break after 31 wavelengths. Under the same wind forcing, the wave will break faster if its IMS is greater. That is, at the forcing of $U/c = 3.0$, but $IMS = 0.26$, it will take 15 wavelengths to reach the point of breaking, and at $IMS = 0.27$ only 9. Quantitative application of these strictly two-dimensional numerical results may be limited, but as it will be shown in Section 5.1.1, qualitatively this picture agrees well with the experiment.

4.1.2 Simulation of the breaking onset

The potential model is not suitable for investigation of the breaking in progress. At such stage, the wave can hardly be regarded irrotational [see e.g. Gemmrich & Farmer, 2004]. Therefore, in the numerical experiments described, the CS model was only employed to simulate development of the steep waves from some initial (mostly uniform) conditions to the breaking onset which signified a wave grown beyond a certain stability limit. In the numerical simulations, a wave was regarded as breaking if the water surface became vertical at any point. This was discussed in

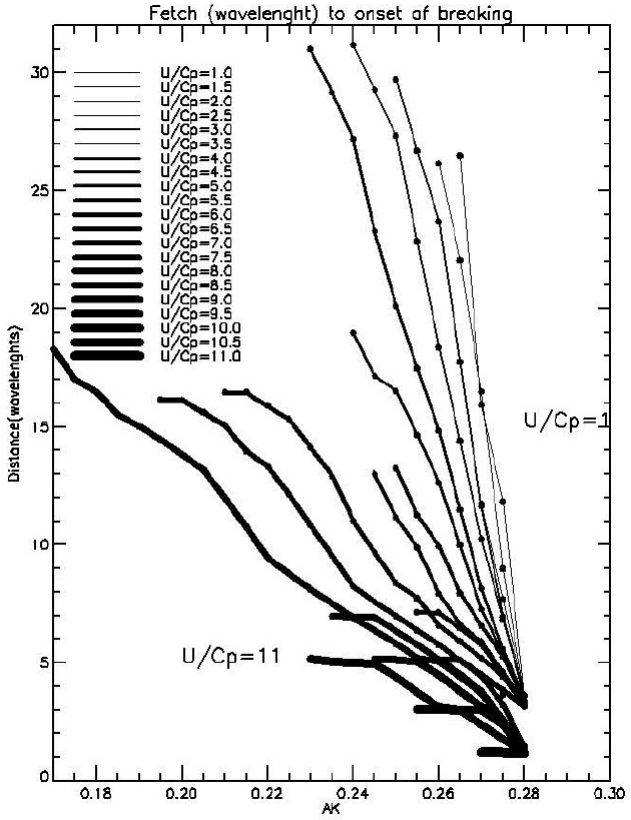

Fig. 4.7. Numerical simulations, number of wave lengths to the breaking versus $IMS = ak$; different wind forcing U/c.

Section 2.1, where the criterion for terminating the run was also formulated (2.1).

Nevertheless, it is important to consider non-linear characteristics of the wave at this final stage of numerical simulations, as they will represent the asymptotic properties of the incipient breaker. Figure 4.8 shows wave profiles prior to breaking at the point when the wave of $IMS = 0.26$ reached its maximum values of negative asymmetry (left panel) and maximum of its skewness/steepness (right panel). Note that these points are separated by three quarters of the oscillation period. Non-linear evolution of this wave has been analysed in Figure 4.2 of Section 4.1.1 above. As in Figure 4.2, cases of $U/c = 2.5, 5.0$ and 10.0 are shown.

The shape of the wave in the left panel corresponds well to the common notion of a breaker. Its negative skewness of $A_s = -0.42$ (for all the three winds) is high by all standards [e.g. Caulliez, 2002]. As indicated by Figure 4.2, however, this is not an incipient breaker yet. This wave will continue to develop to the shape shown in the right panel, as also demonstrated in Figure 4.2.

In the right panel, what is interpreted within the model as incipient breaking is shown. If

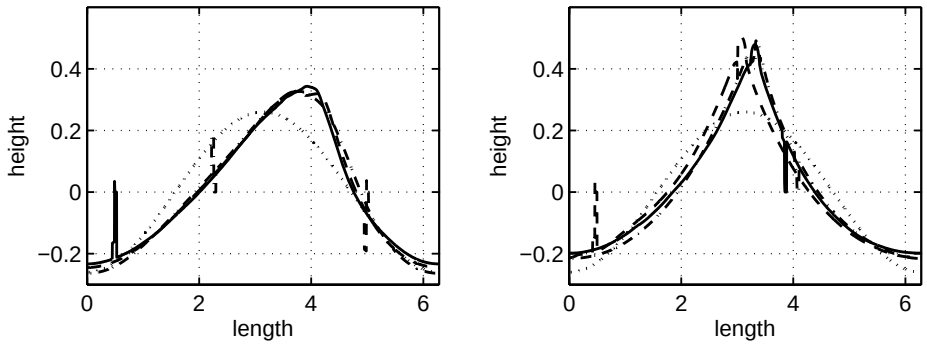

Fig. 4.8. Numerically simulated wave shape prior to breaking. Waves propagate from left to right. (left) minimal (maximal negative) asymmetry A_s (1.3); (right) maximal skewness/steepness S_k/ϵ (1.2)/(1.1). $IMS = 0.26, U/c = 2.5$ (solid line), 5.0 (dashed line), 10.0 (dash-dotted line). Initial wave is shown with dotted line.

compared with the dashed profile of initial wave, one can see that the trough is flatter, the crest is much sharper.

Both in the left and right panels, wave profiles evolved significantly from the initial harmonic wave shown by the dashed line. Despite the fact that the evolution occurred under very different wind-forcing conditions, and took very different times to reach the breaking point, the magnitudes of the asymmetry ($A_s = -0.42$), skewness ($S_k = 0.84, 0.82, 0.83$) and steepness ($\epsilon = 0.34, 0.36, 0.36$), as well as the profiles of the three waves, are virtually identical. This highlights again the important role of the hydrodynamic mechanism in redistributing the wave energy and forming the non-linear wave profile, whereas the wind appears to serve merely as the source of energy to the wave system.

The statistical properties obtained by means of CS model for such incipient breaking are shown in Figure 4.9. Note that steepness/skewness and asymmetry are measured at the different phases of the last prior-to-breaking oscillation. This is done at the points in time when the wave reached its maximum values of negative asymmetry or skewness/steepness respectively. These points are separated by three quarters of the oscillation period (see Figure 4.2 above). The estimates shown in Figure 4.9 were obtained from a comprehensive set of numerical runs covering a range of initial steepness $IMS = 0.10 - 0.30$ and wind forcing $U/c = 0 - 11$. The steepness is shown in terms of $kH = 2\epsilon$.

Since we identified the steepness as a possible reason for wave collapse, it is most interesting to investigate the limiting values of kH. The data points cluster (top subplots), although the scatter is noticeable: $kH = 0.75 - 0.85$ with some outliers reaching values above 0.9. The mean value of the limiting steepness is $\epsilon \sim 0.4$, which is very high, particularly considering that the value of local slope near the crest is even higher than this mean value. Dyachenko & Zakharov [2005] specifically investigated shape of the incipient breaker with a high-resolution version of fully non-linear model similar to that of CS [Dyachenko et al., 1996]. They found a remarkable agreement of the limiting steepness with the Stokes limiting-steepness criterion (2.46). Shape of the wave, however, is different to that of the Stokes wave with the crest pointed at 120° angle

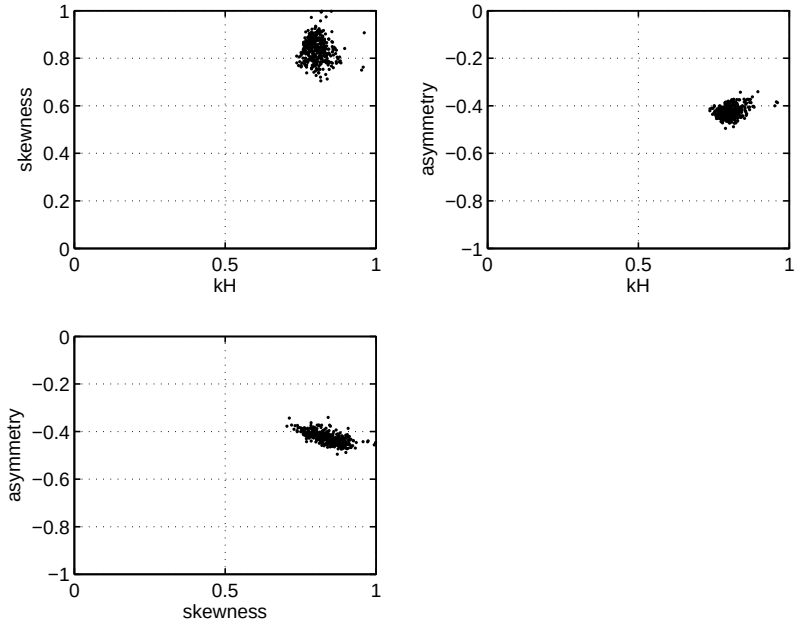

Fig. 4.9. Numerically simulated incipient breaking. (top left) skewness versus steepness; (top right) asymmetry versus steepness; (bottom) asymmetry versus skewness.

[Stokes, 1880]. What is most encouraging is that such outcome of the numerical simulations finds full experimental support (see Section 5.1). At such magnitudes of the water surface slope, the surface may simply collapse because of gravity, depending on the velocity field in the water. If so, the role of the instability which led to the occurrence of these waves is not in the causing wave breaking as such, but rather in simply producing a very steep wave.

As indicated previously, skewness and asymmetry are not breaking criteria, but they do have limiting values (see Figure 4.2). In Figure 4.9, the incipient-breaking skewness is scattered in the range of $S_k = 0.7 - 1$ (top left) and the asymmetry in the range from $A_s = -0.35$ to -0.5 (bottom). Within the scatter, there is no dependence of one property on the other, except a possible negative correlation between the steepness and asymmetry in the bottom panel. The latter result is supported by Figure 4.2, but is not necessarily a feature of approaching breaking onset: a larger negative asymmetry is likely to be followed by a greater skewness even in absence of breaking.

4.1.3 Influence of wind and initial steepness

The role of the wind in the wave breaking has already been mentioned several times throughout the paper. It is apparently very important in growing the wave steepness (i.e. Figures 4.2, 4.5, 4.7). Once a wave is becoming steeper, the instability mechanism is leading it to the breaking sooner. If waves are initially below the threshold $\epsilon = 0.10$, they will not break at all, despite modulations, unless wind forcing raises the steepness above the threshold.

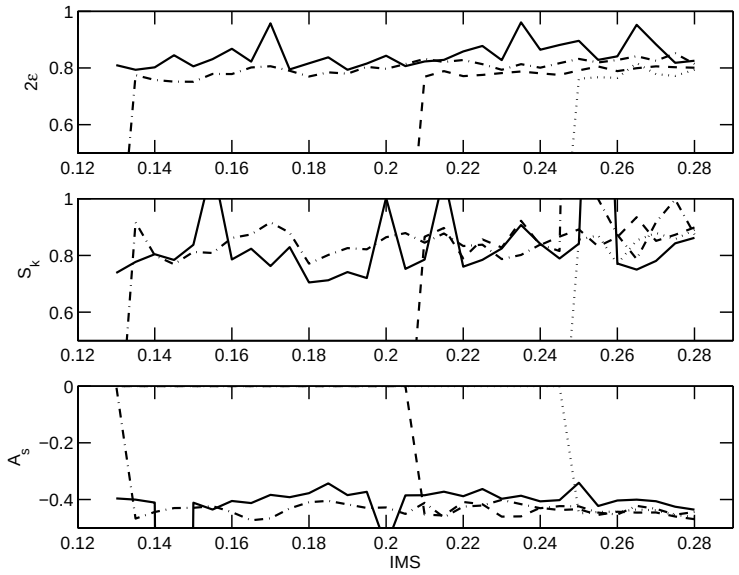

Fig. 4.10. Simulations of incipient breaking. (top panel) steepness 2ϵ (1.1); (middle panel) skewness S_k (1.2); (bottom panel) asymmetry A_s (1.3) - versus IMS for $U/c = 3$ (dotted line), 5 (dashed line), 8 (dash-dotted line) and 11 (solid line).

In this Section 4.1.3, we will discuss the capacity of the wind to instantaneously affect the breaking onset. That is: can the wind push a steep wave over and thus reduce the limiting steepness at breaking? Due to the very large density difference between the water and the air, such a possibility seems low. This conjecture is supported by Figures 4.2, 4.5. The large scatter of the limiting steepness values in Figure 4.9 above, however, needs investigation.

In Figure 4.10, the non-linear features of the incipient breaker are shown as a function of IMS for a variety of wind-forcing conditions. Note that the simulation was run within a limited number of wave periods (i.e. a simulation was stopped after some 400 wave periods regardless whether the wave has reached the breaking onset or not). Thus, in these numerical experiments, for different wind-forcing situations waves stop breaking at different IMS (e.g. for $U/c = 3$, the waves do not have enough time to break if $IMS < 0.25$).

The limiting steepness at breaking onset 2ϵ (1.1) in the top subplot is plotted verus IMS for $U/c = 3$ (dotted line), 5 (dashed line), 8 (dash-dotted line) and 11 (solid line). The incipient-breaking steepness grows both for higher IMS and stronger wind forcing. The latter is particularly counter-intuitive. Even though the growth is marginal, the four lines clearly separate and therefore instantaneous steepness at breaking appears to be somewhat larger at stronger winds.

The skewness and asymmetry of the incipient breakers (middle and bottom panels) do not exhibit a dependence on IMS or wind forcing except at extreme forcing of $U/c = 11$. At such winds, the skewness is somewhat lower (the wind flattens the wave crests) and the wave is slightly less tilted. Thus, it is only at extreme conditions that the wind is capable of influencing the wave shape at breaking and even then the effect is only marginal.

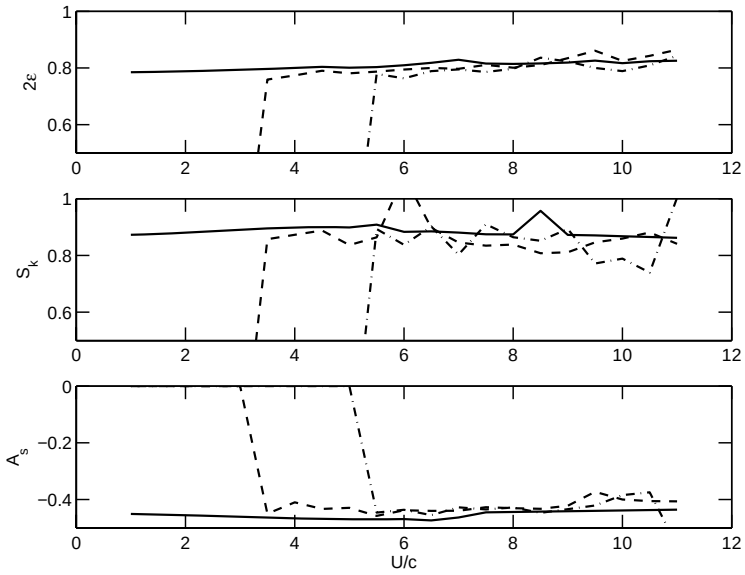

Fig. 4.11. Simulations of incipient breaking. (top panel) steepness 2ϵ (1.1); (middle panel) skewness S_k (1.2); (bottom panel) asymmetry A_s (1.3) - versus U/c for $IMS = 0.20$ (dash-dotted line), 0.24 (dashed line) and 0.28 (solid line).

The same properties of the incipient breaker are plotted versus U/c for three different IMS values of 0.20, 0.24 and 0.28 in Figure 4.11. The value of $IMS = 0.28$ is extreme and the wave grows to the limiting steepness almost instantaneously - within $1 - 3$ periods (see figure 4.7). Note that the simulation was again run for a limited number of wave periods. As a result, in the case of $IMS = 0.20$, for example, the waves do not have enough time to break if $U/c < 5$.

Apart from the relatively weak growth of the limiting steepness as a function of wind in the top panel (as previously noted), the skewness (middle) and asymmetry (bottom) panels exhibit another marginal feature. For the critical initial steepness of $IMS = 0.28$, both skewness and asymmetry magnitude at breaking are, for all wind forcing cases, greater than the respective values at less steep initial conditions.

Thus, the numerical simulations of the breaking onset reveal some marginal effects which the wind forcing and initial-steepness conditions have on the onset of breaking. Some of these effects are only noticeable at extreme winds and critical initial steepness.

Therefore, the wind plays a dual role in this process. Firstly, it accelerates the growth of individual wave steepness. In the simulations shown in Figure 4.2, doubling the wind speed resulted in the wave growing to its critical height almost four times faster. Secondly, the wind can affect the limiting wave shape, but this effect was found to be small and only relevant at very strong wind forcing $U/c > 10$ [see also Babanin *et al.*, 2009a].

To finalise Section 4.1, based on the numerical simulations of initially monochromatic steep two-dimensional irrotational waves by the fully non-linear model, it can thus be summarised that there are breaking-onset criteria in terms of free surface. First, there is a threshold Initial

Monochromatic Steepness for the wave train. If IMS is greater than this value,

$$IMS \approx 0.1, \tag{4.14}$$

then according to simulations based on the CS model a breaking will always occur. Even if the wave is initially sinusoidal and linear, the non-linear evolution of the wave will ultimately lead to the breaking. The distance to breaking will be a function of this initial steepness [Babanin *et al.*, 2007a, see also Section 5]. The second criterion is the steepness of an individual wave at the breaking onset. As seen in Figures 4.2 and 4.9, there appears to be a limiting value of such steepness of

$$2\epsilon \sim 0.8. \tag{4.15}$$

Therefore, the fully non-linear model is sufficiently self-consistent to describe evolution of the steep wave train from initial conditions which have no indication of any singularity in the system, all the way to the incipient breaking. It also provides quantitative characteristics both for the wave train, in which the breaking will occur, and for the individual wave, which will break. Thus, such modelling allows us to move from mathematical abstractions to physical reasoning and verify the theoretical conclusions by experimental means. Such verification will be discussed in Section 5.

4.2 Kinematics of the breaking onset

The review of the fully non-linear modelling of wave evolution to the breaking should also attend to the family of kinematic/dynamic criteria obtained by means of the Dold-Peregrine (DP) model. They were mentioned in Section 2.9 as rate of change of the local mean wave energy density/ the rate of change of the momentum flux averaged over half a wavelength/ the local average mean energy flux to the energy maximum in the wave group [the sequence of papers by Banner & Tian, 1998, Song & Banner, 2002, Banner & Song, 2002, Song & Banner, 2004, Banner & Peirson, 2007], and received a considerable discussion lately.

These papers are consecutive parts of a single study and subsequently rely on respective previous results. Thus, the main target of the experiment by Banner & Peirson [2007] was verification of the numerical kinematic breaking criteria suggested by Song & Banner [2002], and in the course of events Banner & Peirson [2007] used the model employed in Banner & Tian [1998], Song & Banner [2002], Banner & Song [2002], Song & Banner [2004] in order to substitute some data which could not be retrieved from their experiment.

Before going into details, we should point out that even if the proposed kinematic/dynamic subsurface diagnostics was valid, it can hardly be regarded general. In all five papers the authors used imposed sidebands, or a combination of waves, to start the modulation. This is not a natural but an artificial modulation. When the sidebands are enforced, it is them that will grow, whereas if they are not imposed, i.e. a steep wave is allowed to evolve naturally, the modulation starts itself and resonant sidebands are selected from the background noise. This physics was described, for example, in Lake & Yuen [1978]. Since the sidebands imposed in the sequence are not necessarily those which would be selected naturally, there is no fundamental ground to believe that the Banner & Tian [1998] or Song & Banner (2002) criteria, i.e. measure of wave energy/momentum convergence rate, has a general quantitative and perhaps qualitative value.

It should also be mentioned that in the CS Chalikov & Sheinin [1998, 2005] approach described in Section 4.1 the wave model is coupled with the wind through a turbulent atmospheric model. Banner & Song [2002] also tried to introduce wind forcing, but this is done in the framework of a DP model, through employing dynamical boundary conditions by means of an empirical parameterisation. Use of an empirical parameterisation in an analytical model is a disadvantage, particularly as it is well-known that this parameterisation is not applicable in the case of wave breaking [e.g. Babanin *et al.*, 2007b].

The kinematic criterion for breaking onset was obtained numerically, first by Banner & Tian [1998] as a rate of change of the momentum flux beneath the surface, and was later formulated as a non-dimensional measure of wave energy convergence rate δ in Song & Banner [2002]. It is also employed in this form by Banner & Peirson [2007].

We should point out that breaking criteria formulated as a rate of change of the momentum flux beneath the surface or a non-dimensional measure of wave energy convergence rate do not actually deal with a free-surface property, which ultimately leads the wave to loss of stability and collapse. In practical terms, it is not possible to measure any of the two criteria for any applied purpose in realistic circumstances directly, particularly given the fact that the measurement has to be done in the wave-following coordinate system. As discussed below, Banner & Peirson [2007] were not able to achieve this even in a dedicated academic laboratory experiment.

Indeed, even if such measurement was possible, such a criterion can hardly be converted into a measure of surface-wave spectral densities. Thus, it would be of limited use in spectral modelling of wave-energy dissipation, in wave forecasting and other typical applications requiring knowledge of wave-breaking.

From a physical point of view, the value of the rate of energy convergence can hardly indicate any concrete meaning so far as the wave breaking as such is concerned, i.e. physical collapse of the water surface. So what happens to the surface, and why does the crest plunge or spill if the rate of energy convergence below the surface is such and such? In fact, this criterion becomes meaningful only if we translate its formulation into a "wave is becoming too steep and surface becomes unstable", or "orbital velocity of water particles on the crest exceeds wave phase speed", or a similar formulation for the water-surface properties/behaviour. In this regard, if the mentioned criteria were true, they refer to the fluid dynamics which accompanies the breaking, but not the one which causes it.

The numerical computations by means of a DP model suffer from a number of limitations as discussed in Section 4.1 above. In summary, it has a limited accuracy, does not preserve integral invariants, and its stability over time depends on the primary wave steepness. As a result, it cannot integrate steep waves over long periods. Most of the simulations in Banner & Tian [1998], Song & Banner [2002] are done for remarkably low initial steepnesses, close to the limit of $\epsilon_0 = 0.1$. In fact, based on the precise CS model, this limit was established as an initial monochromatic steepness below which the breaking *does not* occur and was confirmed experimentally [Babanin *et al.*, 2007a]. But in simulations by Banner & Tian [1998], Song & Banner [2002], the waves *do* break having such initial steepness. Thus, the results of Banner & Tian [1998], Song & Banner [2002] on the threshold value of ϵ_0 have inconsistencies if compared with experiment. This highlights the inaccuracy of the DP scheme when it comes to quantitative predictions, and demonstrates its limited capacity in predicting the breaking onset and perhaps the misleading role of imposed wave groups. Additionally, the very low range of the initial steepnesses employed by Banner & Tian [1998], Song & Banner [2002] in practice appears too

marginal to be of a general applicability value.

It is not, however, only numerics, which makes quantitative and even qualitative outcomes of Banner & Tian [1998], Song & Banner [2002], Banner & Song [2002], Song & Banner [2004] problematic. The numerics can be improved if, for example, a CS scheme was employed. But it is the underlying physics which makes quantitative kinematic analysis of the breaking onset, based on a potential two-dimensional model, impossible, coupled with questionable mathematics in the sequence of papers.

Before going into detail, we remind ourselves that science is built upon a systematic proposal and subsequent criticism of theories, and to their credit Banner and co-workers were among the first to propose a dynamic criterion for breaking in terms of energy/momentum fluxes in the water. In drawing attention to weakness in their modelling our intention is to set the stage for others to develop a more robust theory.

We will start with the physics. For a detailed discussion of differences between two-dimensional modelling and real waves, even quasi-two-dimensional waves in wave tanks, we refer the readers to Babanin *et al.* [2007a, 2009a]. Here, we will only briefly mention the two most important items. First, waves in a wave flume, though not directional, still develop three-dimensional features at their crests if $\epsilon > 0.29$. This is a well-known experimental fact [e.g. Melville, 1982, Waseda & Tulin, 1999]. These features stabilise the wave and delay the breaking onset. In Babanin *et al.* [2007a, 2009a], it was shown that indeed in simulations by means of CS model the waves of $\epsilon > 0.29$ broke within one period, whereas laboratory waves could proceed without an immediate breaking even at $\epsilon > 0.4$. This key difference cannot be captured in a two-dimensional model and makes accurate quantitative estimates of any breaking onset in terms of wave energy convergence rate or alike impossible in principle..

Second is the wave-induced turbulence [e.g. Gemmrich & Farmer, 2004, Babanin, 2006, Babanin & Haus, 2009, Gemmrich, 2009]. The irrotational DP scheme (as well as CS scheme on that matter) does not model turbulence, whose intensity level rapidly increases near the breaking onset, and therefore it is not capable of producing quantitatively accurate values of the rate of change of the momentum flux or the wave energy convergence rate or any other description of the velocity field.

Therefore, we have to conclude that the capacity of the numerical simulations of the breaking onset and the underwater velocity field within the approach adopted by Banner & Tian [1998], Song & Banner [2002], Banner & Song [2002], Song & Banner [2004] is limited in principle, and any criteria obtained in this way could only be regarded approximate, if valid. This validity, however, may be questionable due to serious mathematical issues.

Banner & Tian [1998] and the subsequent publications assign a single linear wave

$$\eta = a\cos(x) \tag{4.16}$$

as initial condition in the periodic domain $[0, 2\pi]$. Simultaneously, they impose a disturbance of the kind

$$\eta' = \epsilon a \left\{ \cos\left[\left(1 + \frac{1}{N}\right) x - \phi\right] + \cos\left[\left(1 - \frac{1}{N}\right) x - \phi\right] \right\} \tag{4.17}$$

where $\epsilon = 0.1, \phi = \pi/4$ and N is the number of waves in the imposed modulation. The problem is that the wavenumbers of the disturbances, i.e. $1+1/N$ and $1-1/N$, are not integer and cannot fit the periodic domain. This is a non-periodic disturbance in a periodic domain.

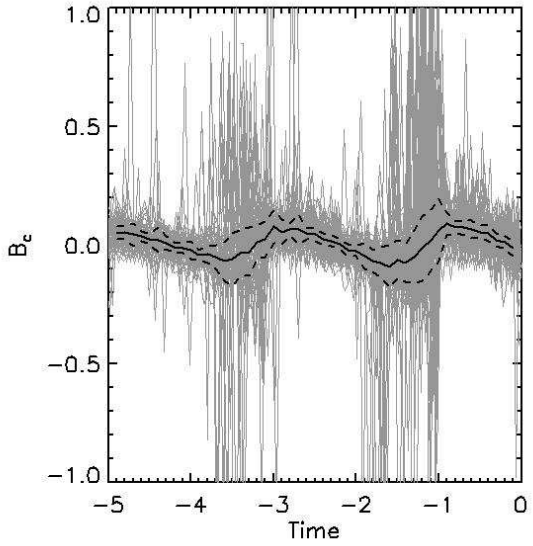

Fig. 4.12. Pre-breaking evolution of the criterion δ (4.19) [Song & Banner, 2002], denoted here as B_c, versus time in wave periods. 0 signifies the breaking onset. The Figure is a private communication from Dmitry Chalikov.

To make the formulation right, one can use the following carrier wave

$$\eta = \frac{a}{N}\cos(Nx). \tag{4.18}$$

Then, disturbances with wavenumbers of $N+1$ and $N-1$ will provide the same wavenumber ratio as in (4.17), but all the waves will remain periodic.

Thus, in summary, it is difficult in principle to expect the numerical simulations in Banner & Tian [1998], Song & Banner [2002], Banner & Song [2002], Song & Banner [2004] to produce accurate physical values to quantify the breaking onset. Most importantly, however, the formulations used in these simulations is inconsistent mathematically. Indeed, as it will be demonstrated in Figure 4.12 below, the 'diagnostic' parameter δ does not show the singularity prescribed by simulations of Song & Banner [2002] and in fact exhibits some reduction when a wave is approaching the breaking onset.

The experiment conducted by Banner & Peirson [2007], however, was intended to test just that: the breaking criterion δ derived in the numerical model, and was concluded a success. Such an obvious contradiction needs some re-analysis.

To conduct the verification, the experiment had to measure the surface elevations and associated subsurface velocity field which, however, was not done. Banner & Peirson [2007] write that they intended to use a PIV system for this purpose, but it proved not feasible.

Instead, to obtain the depth-integrated kinetic energy density, surface elevations were measured and converted into potential energy. In non-linear, and in particular in extremely non-linear

circumstances such as the breaking onset, the relationship between the two is not known. Therefore, the kinetic energy was obtained from the measurements of potential energy by means of Song & Banner [2002] model simulations. Kinetic energy densities were inferred from potential energy densities "based on their relative magnitudes as determined in Song & Banner [2002]".

Thus, it appears that the uncertainty loop was closed: the criteria of Song & Banner [2002] were calibrated by means of the Song & Banner [2002] model itself. Since the proportion of the kinetic and potential energy in the experiment was not measured, but was assumed the same as in the numerical simulation, the non-dimensional convergence rate of the total energy in the wave tank and in the model emerges the same. The 'agreement' of the model and the experiment is in fact remarkably good, but that appears to be an imposed result.

To further verify validity of the convergence rate δ as a breaking indicator, simulations were performed with adiabatic version of CS model. This was done by Dmitry Chalikov on request of the author of the paper. The series of experiments conducted by Song & Banner [2002] (their eq.1) were basically repeated, but they were corrected for the periodicity of disturbances. The carrier wave mode with amplitude a_p was placed at wavenumber k_p, where k_p changed in the range of 3-10, and steepness $a_p k_p$ was in the range of 0.085-0.185. Then, 160 long-term simulations were carried out up to the point of breaking or up to non-dimensional time $t = 500$ which corresponded to 138-252 periods of the carrying waves. Disturbances with amplitudes $0.1a_p$ were assigned at wavenumbers $k_p + 1$ and $k_p - 1$. Number of modes was $M = 2000$ and number of grid points $N = 8000$, which provided a sufficient accuracy of approximation. A criterion for terminating a run was defined by the first appearance of a non-single value of surface η (2.1).

In principle, it is possible to continue the integration for a short period of time after the moment defined by (2.1), but details of this stage of the wave breaking are not well described by a potential model as discussed above. It is important to emphasise that after the moment when the criterion (2.1) has been reached, the solution never returns to stability: the volume of fluid crossing the vertical $x(i)$ rapidly increases. Up to this moment, conservation of the sum of potential and kinetic energy, of horizontal momentum and of the volume in the CS model was excellent. Therefore, the onset of breaking is defined with a very good accuracy, and it does not depend on resolution. We should note that in Banner & Tian [1998], Song & Banner [2002], Banner & Song [2002], Song & Banner [2004], Banner & Peirson [2007] this issue is not discussed or even mentioned. And this is a very important issue, particularly if some quantitative criteria are considered. As mentioned above, the DP scheme employed in this sequence of papers is not conservative, and the deviations increase as the waves grow steeper.

In the described tests conducted by means of the CS model, out of the total of 160 runs, 146 were terminated by breaking, and the rest, corresponding to smaller steepnesses, were stopped. As we know, if initial steepness in the wave train is below some threshold, the modulational instability will never eventuate in a breaking event [Babanin *et al.*, 2007a]. Each run was saved, and the post-processing was applied to the last period of evolution, terminated by the breaking.

At each run shown in Figure 4.12 below, the pre-breaking trough-to-crest wave was defined in the range between its two consecutive troughs with coordinates $X_{f_{min}}$ (front trough) and $X_{b_{min}}$ (rear trough). The Figure shows evolution of the Song & Banner [2002] criterion

$$\delta = \frac{1}{\omega_p \overline{E}} \frac{d\overline{E}}{dt} \tag{4.19}$$

denoted here as B_c. Song & Banner [2002] and other papers of this series omit details on how they detected the wave and its length, but in any case behaviour of δ in Figure 4.12 does not demonstrate any similarity to their predictions. Here, $\overline{E}$ is sum of potential and kinetic energies averaged over the wave length $X_{f_{min}} - X_{b_{min}}$. As seen, the characteristic does not change significantly, does not exhibit singularity, and on the contrary systematically decreases when approaching the breaking onset.

Thus, we have to conclude that the kinematic/dynamic set of criteria of the type of the convergence rate δ (4.19) do not appear to be indicating a breaking onset when verified by means of CS model. As discussed above, in any case practical applicability of such criteria is low because they are difficult if not impossible to measure in most of realistic circumstances. Potential models are not expected to perform particularly well in this regard anyway, due to turbulence generated at pre-breaking stages. In any scenario, free-surface based criteria should be regarded as generic, with the subsurface indicators being secondary, as it is the surface of the wave which collapses in a breaking event.

5 Wave breaking probability

As already mentioned in Section 2 dedicated to definitions of wave properties and phenomena related to wave breaking, the breaking probability, or as it is also often called breaking rates or frequency of breaking occurrence is one of the most important statistical characteristics of wave fields which contain the breaking events. Technical definitions for the breaking probability are given in Section 2.5.

Together with the breaking severity (Sections 2.7, 6), the probability defines the wave-energy dissipation due to wave breaking. Knowledge of such dissipation is required across a broad range of wave-related applications, with the wave forecast being the most frequent and obvious, and therefore the breaking occurrence has enjoyed a key attention within the wave-breaking studies.

Experimental and statistical techniques of the breaking-probability studies have been discussed in detail in Section 3, and theoretical approaches in Section 4. As described in these Sections, in the past parameterisations of the breaking rates in terms of environmental characteristics usually relied on wind speed or its derivatives. In this paper, we argued that, although the wind of course essentially responsible for formation of fields of wind-generated waves, its capacity to directly trigger or even affect a breaking event is only marginal, and even then can only be noticed at very strong wind forcing. The breaking mainly happens due to hydrodynamic phenomena, that is due to processes in the wave train itself. Therefore, as far as the wave-breaking probability is concerned, the wind influence is indirect and parameterisations have to be done in terms of properties of wave fields. In this Section, we will concentrate on the latter approach and will describe the hydrodynamics which controls the wave-breaking occurrence and rates.

In Section 5.1, we start from breaking events which develop within trains of initially monochromatic waves due to modulational instability of such wave trains. While the frequency of breaking occurrence depends gradually on the initial monochromatic steepness, there is a steepness threshold below which the breaking does not happen. Such threshold is of key importance, both for monochromatic and spectral wave fields, and will be scrutinised in Section 5.2. Breaking in wave fields with continuous spectral distribution of wave scales will be discussed in Section 5.3, which is subdivided into further subsections. Wave spectrum usually has a narrow and sharp peak, and the physics of breaking of the dominant waves, which correspond to the spectral peak and exhibit pronounced group-modulated structure (Section 5.3.1), is essentially different to that of waves which are relatively shorter compared to the dominant waves and whose breaking may be induced by larger and longer waves (Section 5.3.2). In directional wave fields, the very existence of the modulational instability is an issue. Since the real waves are directional with exception of swell which has low steepness and does not break anyway, this issue is of significant importance for the wave breaking and will be discussed in a separate Section 5.4. Finally, wind-forcing effects will be described in Section 5.5.

5.1 Initially monochromatic waves

In Section 4.1, numerical simulations of the breaking development within initially monochromatic wave trains were described, conducted by means of CS models. Results of the simulations were further used in a laboratory experiment to verify the model's ability to predict the breaking onset and to parameterise the breaking probability for such waves [Babanin *et al.*, 2007a, 2009a,b].

Although it has already been mentioned a number of times above, it should be emphasised again that comparisons of the numerical simulations of non-linear wave evolution with the laboratory experiments can only be qualitative. Firstly, no matter how sophisticated the model is, it is still a simplification of the physical environment and disregards or possibly suppresses some natural features. One such feature is the three-dimensionality of wave motion. Even in the quasi-two-dimensional environment of the wave tank, some directional characteristics may play an essential role. For example, Melville [1982] showed that for steepness $\epsilon > 0.3$, the wave crests develop a crescent-shaped perturbation and this three-dimensional instability manifests itself in a more complicated way compared to the strictly two-dimensional case. This has a significant consequence for the numerical simulations. The two-dimensional CS model predicts immediate breaking onset for $\epsilon > 0.29$ whereas in the laboratory experiments of Melville [1982] such waves become short-crested but can persist without breaking for some time.

Another significant difference between the laboratory and model is the continuous nature of modes in the experimental environment, even if those modes are only minor background noise, and the discrete nature of numerical modes. It is important to understand that at the initial stages of development, the necessary modulational modes should grow from the continuous noise. If the modes are not imposed, some sidebands naturally appear from the background and are expected to be defined by the ratio of characteristic wave steepness $\epsilon = ak_0$ to spectral bandwidth $\Delta\omega/\omega_0$, where k_0 and ω_0 are some characteristic wavenumber and angular frequency respectively, and a is the mean amplitude at this wavenumber:

$$M_I = \frac{\epsilon}{\Delta\omega/\omega_0}. \tag{5.1}$$

This ratio was shown important in the original studies of instabilities of weakly modulated trains of monochromatic carrier waves of small amplitudes [e.g. Yuen & Lake, 1982]. Here, we denote this ratio as M_I (Modulational Index).

Evolution of wave trains described in this Section mainly deals with slowly-modulated two-dimensional monochromatic waves. Such wave trains are subject to modulational instability which is commonly termed Benjamin-Feir instability after the work of Benjamin & Feir [1967]. Many authors point out, however, that it was first discovered by Lighthil [1965] who established the growth rate for this instability in the limit of very long modulation. The growth rate was proportional to the wavenumber of the modulational perturbation which result has obvious physical limitations if applied to short waves (large wavenumbers). The general description for behaviour of the growth rate was found by Zakharov [1966] before Benjamin & Feir [1967], but in English-language literature the papers were published independently in the same year [Zakharov, 1967]. Feir [1967] was the first to observe the modulational instability in the experiment and Zakharov [1968] further developed and summarised its theory.

The Benjamin-Feir instability was developed for nearly-linear waves, and in this paper dedicated to wave breaking the waves even initially are not of the small amplitude. Therefore, analogy of the observed empirical modulational interplay with the small-amplitude near-monochromatic theoretical phenomenon should be treated with caution and we will avoid the term of Bejamin-Feir instability. Here, M_I signifies the fact that the wave steepness and length of wave modulation (or number N of waves in the modulation), where

$$\frac{1}{N} \sim \frac{\Delta k}{k_0}, \tag{5.2}$$

are not independent quantities, i.e. steeper waves will correspond to fewer waves in a modulation. Thus, if non-linear waves are allowed to evolve naturally, they will form groups where N is not a free parameter, but will be defined by the initial steepness ϵ (1.1).

Therefore, as mentioned above, in the experiment we expect the necessary resonant modes to naturally develop from the background turbulent noise. These modes, however, can be suppressed or even prohibited in a discretised numerical model. In such circumstance, the waves, even if they are steep Stokes waves, will propagate for an indefinitely long period without breaking.

If the model is constructed so as to allow multiple modes, another numerical feature still distinguishes the model from nature. The background noise, the source of the necessary modes dictated by M_I, cannot be completely reduced to zero in nature. In a digitised medium it can, however, be made very small. For example, in the CS numeric scheme, the 11^{th}-order decimal accuracy is employed. Such accuracy is essential for precise simulations, but since it is the only source of noise in the system, it can obviously slow down the development of the initial modes. As is sometimes done in numerical simulations [e.g. Dold & Peregrine, 1986, Banner & Tian, 1998, Song & Banner, 2002], the modes can be deliberately introduced as initial conditions. Such an approach was not, however, employed in the simulation described in Section 4.1, since in this scenario M_I of the system is pre-defined rather than formed naturally, and wave development to the breaking may be altered. Other implication of the numerical modelling, essential for the present discussion, have been already considered in Sections 2.1, 4.1 above.

The laboratory experiment described in Babanin *et al.* [2007a, 2009a,b] was conducted at the ASIST wind-wave facility at RSMAS, University of Miami (`http://peas.rsmas.miami.edu/groups/asist`). The tank is a stainless-steel construction with a working section of 15 m $\times$ 1 m $\times$ 1 m. Its programmable fan is capable of generating centreline wind speeds in the range of 0 to 30 m/s. Immediately downstream of the fan, extensive flow-straightening devices are installed to condition the air flow and introduce appropriately scaled turbulence. Values of wind speed further used here will be those of U_{10}, i.e. extrapolated to the 10 m height.

ASIST includes a fully-programmable wave maker able to produce both monochromatic waves and waves with a predefined spectral form. These waves are dissipated at the opposite end of the facility by a minimum-reflection beach. The ASIST beach design had been a subject of a special research project. A gently-sloping (10 degrees) grid of 2.5 cm-diameter acrylic rods is used. A perforated acrylic plate is placed beneath the rods to split wave orbital velocities into multiple turbulent jets to increase viscous dissipation. The energy of the reflected component is approximately 5-10% of the incident energy depending on the initial wavelength.

In the experiment described, monochromatic deep-water two-dimensional wave trains were generated by the wave paddle. The water depth was held at 0.4 m, thus providing deep-water conditions for the wave frequencies involved. With a tank length of 13.24 m, surface elevations were recorded at 4.55 m, 10.53 m, 11.59 m and 12.56 m from the paddle. For each record, the initial monochromatic steepness (IMS) was varied in such a way that the waves would consistently break just after one of the wave probes. In this way, the dimensional distance to breaking (and therefore the breaking probability), wave train properties immediately prior to breaking and detailed properties of the incipient breaker could be measured. Note that this breaker is a result of natural non-linear wave evolution, rather than being forced or simulated by means of, for example, coalescing linear wave packets. The fact that breaking could be predicted and controlled by manipulating IMS only is a strong corroboration of the numerical model.

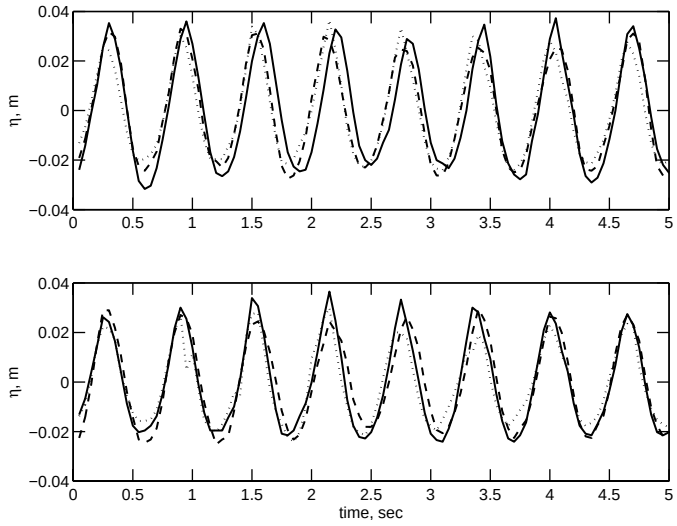

Fig. 5.1. Time series of surface elevations η measured at the first wave probe. (top panel) Waves of $U/c = 0$ and $IMF = 1.6$ Hz for different IMS: 0.31 (solid line), 0.25 (dashed line), 0.23 (dotted line). (bottom panel) Waves of $IMS = 0.23$ and $IMF = 1.6$ Hz under different wind forcing: $U/c = 0$ (solid line), $U/c = 1.4$ (dashed line), $U/c = 11$ (dotted line).

In Figures 5.1 and 5.2, time series of surface elevations η at the first and the second wave probes are shown. All the waves in these time series are generated with the same Initial Monochromatic Frequency $IMF = 1.6$ Hz, but with different initial steepness IMS and wind forcing U/c, as indicated.

At the first probe (Figure 5.1), 4.55 m from the wavemaker, the waves are still near-monochromatic, with only marginal modulation due to developing instabilities and perhaps some parasitic modes present in the tank (i.e. non-potential part of the oscillations generated by the paddle, seiches etc.). The latter, if present, is part of the background noise from which the necessary modulational modes will grow in Figure 5.2, as dictated by M_I (5.1).

The top subplot of Figure 5.1 has zero wind forcing. Waves with three different $IMS = 0.31$ (solid line), 0.25 (dashed line) and 0.23 (dotted line) are shown. Differences other than those due to the initial wave height are hardly distinguishable.

In the bottom subplot, waves of $IMS = 0.23$ are plotted with no wind forcing (solid line, for cross-reference with the top panel), $U/c = 1.4$ (dashed line) and a very strong wind of $U/c = 11$ (dotted line). The effect of the wind on the profile of the mechanically-generated wave is not noticeable at this first probe, except for the extreme forcing case, where wind-generated ripples are visible in the time series.

The wave profiles look very different at the second probe, 10.53 m from the paddle, some 10 wavelengths downstream (Figure 5.2). In all the cases, breaking has still not occurred. Waves in the top three panels evolve without wind forcing, and in the bottom subplot waves are shown strongly forced ($U/c = 11$).

The top subplot shows initially very steep waves of $IMS = 0.31$. By the time they reach

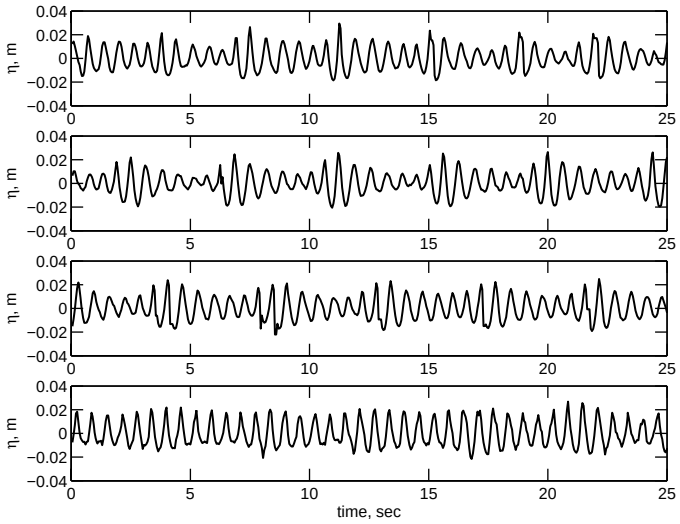

Fig. 5.2. Time series of surface elevations η measured at the second wave probe, $IMF = 1.6$ Hz. (top panel) $IMS = 0.31, U/c = 0$. (second top panel) $IMS = 0.25, U/c = 0$. (second bottom panel) $IMS = 0.23, U/c = 0$. (bottom panel) $IMS = 0.23, U/c = 11$.

probe 2, they have developed into a very strongly modulated group of 6 waves. Less initially steep waves ($IMS = 0.25$, second subplot) evolve into a more elongated modulated group of some 7 waves. Even less steep waves ($IMS = 0.23$, third subplot) evolved into a subsequently weaker modulated group of approximately 7.5 waves (15 waves in two modulations). Note that no initial modulation was introduced (see Figure 5.1). This interesting observation is, however, not unexpected and is in full qualitative agreement with the discussion above: i.e. if M_I for the system does not change, a larger initial steepness should lead to fewer waves in the modulation which results from the Benjamin-Feir-like instability.

The effect that the wind forcing has on the modulation is demonstrated in the bottom subplot of Figure 5.2. Here, very strongly wind-forces mechanically-generated waves of $IMS = 0.23$ are plotted (see the third subplot for comparisons with waves of the same IMS evolving without wind forcing). Whilst the number of waves in the modulation did not seem to change, the depth of the modulation R changed dramatically:

$$R = \frac{H_h}{H_l} \tag{5.3}$$

where R is height ratio of the highest H_h and the lowest H_l waves in the group. The difference in modulation depth is 1.6 times – it changed from $R = 2.1$ down to $R = 1.3$.

It was observed that this change also led to a very significant reduction in the breaking severity (see Section 6 below). The severity (energy loss in a breaking event, see Section 2.7 for definitions) is a very important breaking property as, along with the frequency of breaking occurrence (breaking rate) discussed in this Section 5, it defines the energy dissipation in a wave field.

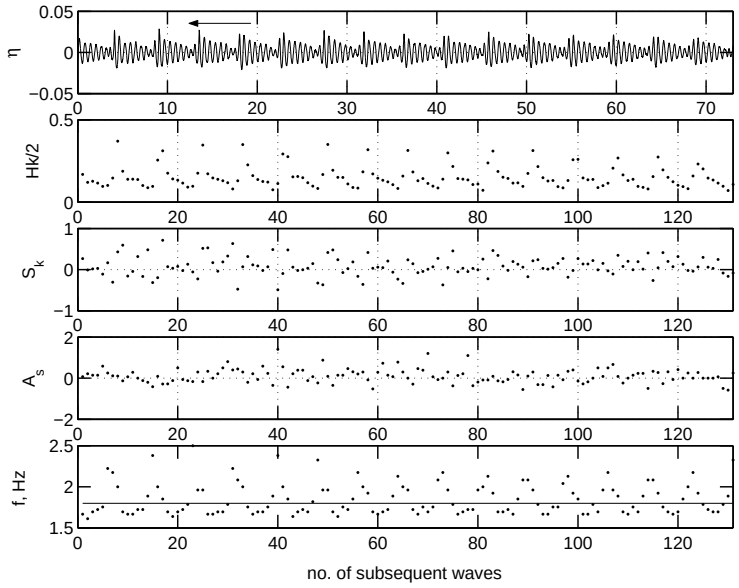

Fig. 5.3. Segment of time series with $IMF = 1.8$ Hz, $IMS = 0.30$, $U/c = 0$. (top panel) Surface elevation η. (second top panel) Rear-face steepness ϵ (1.1). (medium panel) Skewness S_k (1.2) (rear trough depth is used). (second bottom panel) Asymmetry A_s (1.3). (bottom panel). Frequency (inverse period). $IMF = 1.8$ is shown with solid line. The waves propagate from right to left.

5.1.1 Evolution of non-linear waves to breaking

Non-linear evolution of two-dimensional laboratory waves to breaking will now be investigated in a fashion similar to the numerical study of Section 4.1. We will be mainly interested in what happens in the physical wave field rather than in Fourier space. Also, we will deal with individual waves, rather than with average non-linear properties of the wave ensemble. The non-linear characteristics of interest (i.e. individual wave steepness, skewness and asymmetry), will be obtained by means of zero-crossing selection and analysis of individual waves. In addition to these three characteristics, we will scrutinise the behaviour of the period (frequency) of individual non-linear waves. This feature was not obtained in dimensionless numerical simulations, but in the laboratory it appears to be quite variable, even in the train of waves of initially uniform frequency. The effect of such local-frequency variation is significant for the breaking-onset study since, when wave-height growth is accompanied by a synchronous reduction of wave period, this has a combined impact on the local wave steepness.

Figure 5.3 shows a wave record with an initial monochromatic frequency $IMF = 1.8$ Hz and an $IMS = 0.30$, with no wind forcing. It should be noted that there is a conceptual change in the frame of reference compared to the numerical-model results. In the case of the model, a single wave was followed as it approached the point of breaking. Here, observations are made at a single point as a succession of wave passes. One can approximately move from the fixed frame of reference in Figure 5.3 to the moving frame by considering the waves shown propagating from

right to left, as indicated by the arrow in the figure.

The top panel in Figure 5.3 shows the measured water surface elevation η as a function of time (horizontal axis). Interpreting this as a wave moving from right to left shows that, within each wave group, the maximum value of the water-surface elevation gradually decreases and then suddenly increases until a point, where breaking occurs. The saw-tooth shape of the wave envelope once again indicates the modulational instability as the mechanism behind this behaviour of the non-linear wave train [e.g. Shemer & Dorfman, 2008]. The point of breaking was located immediately after the probe at a distance of 10.73 ± 0.1 m from the wave maker. Each successive wave passing the wave gauge was analysed to determine its steepness, skewness, asymmetry and frequency, which are shown in the four panels of Figure 5.3.

The major features seen in the numerical model are confirmed by the laboratory data. The incipient breaking waves are the steepest waves in the wave train, with the steepness oscillating in a periodic fashion. Skewness and asymmetry also oscillate, but behave in a less ordered fashion. However, at the point of breaking skewness is positive (i.e. peaked up) and asymmetry is small (i.e. only slightly tilted forward). A feature which could not be determined from the numerical model is that there is also a modulation in the frequency. At the point of breaking the frequency increases rapidly, further increasing the steepness and hastening the onset of breaking.

5.1.2 Measurements of the breaking onset

Measurements of physical properties of the breaking onset due to modulational instability is a most intriguing task. Whilst the properties of waves breaking due to focusing the coalescing packets have been described in great detail previously [e.g. Rapp & Melville, 1990], physical characteristics of breaking resulted from the non-linear wave evolution have rarely been measured.

As the location of the breaker can be controlled by varying the IMS at the wavemaker, the waves were made to break immediately after a wave probe and thus the properties of incipient breakers could be directly measured. Figure 5.4 shows the four steepest incipient breakers. A slight variation of the recorded height of the breakers is visible here and was also the case in Figure 5.3. There are two reasons for this variation in height. Firstly, there is some low-frequency modulation of the wave-group amplitude which can be either natural or an artifact of the tank. Secondly, there was a ± 10 cm variation of the observed breaking location. This variation in the breaking position could have been due to a non-integer number of waves in the modulation. These reasons were not investigated in detail as they did not influence our main results. In any scenario, transition of the wave to the incipient-breaking stage is very rapid and difficult to capture precisely. Therefore, we chose the highest breakers for examination, as those are apparently closest to breaking onset.

Typical features of waves just prior to breaking can now be analysed. The nearly-breaking wave is the highest and most skewed, but is almost symmetric. The two waves immediately preceding and following the breaker are asymmetric: the preceding wave is tilted backward (positive asymmetry) and the following wave is tilted forward (negative asymmetry). The preceding wave is smaller than the following wave, and, at least in these observations, the preceding trough is shallower. This may be a key feature to distinguish the linear-focusing breaking onset from the modulational-instability breaking, as the former is not expected to exhibit uneven front and rear troughs. Thus, the boat which climbed the front face of the breaker, would then fall into the very

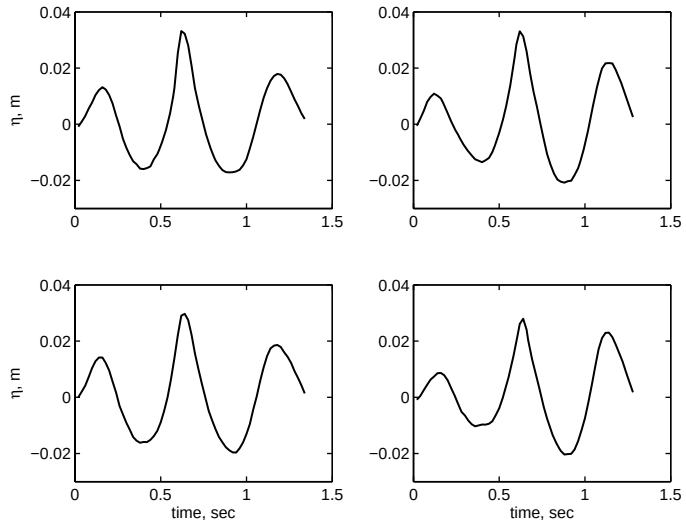

Fig. 5.4. $IMF = 1.8$ Hz, $IMS = 0.30$, $U/c = 0$. Four steepest incipient breakers (from top left to bottom right).

deep trough followed by an even steeper wave front.

Figure 5.5 shows one, five, twenty and fifty steepest breakers in consecutive panels. Note that no normalisation was applied and the waves are plotted as they appear in physical space, from the front zero-crossing of wave preceding the breaking to the rear zero-crossing of the following wave. Despite this, the pictures are remarkably similar even in the subplot with 50 waves and this prompts a universality of such incipient-breaker shapes. The quantitative characteristics of these waves are further scrutinised in Figures 5.6-5.12.

Figure 5.6 shows data for the five steepest breakers. The analysis is at first limited to these steepest cases as wave quantities close to the breaking point change rapidly, as shown in Figure 5.3. These steepest cases are considered to be on the point of breaking. According to the numerical simulations, the steepness seems to be the single robust criteria for breaking. For the 20 steepest breakers (see further Figure 5.7), steepness was confined to the narrow range $Hk/2 = 0.37$ to 0.44, whilst skewness was scattered over the wide range $S_k = 0$ to 1 and asymmetry $A_s = 0.8$ to -0.4. Considering only those waves at the point of breaking, however, as in Figure 5.6, shows a clearer trend. The steepness appears to approach an asymptotic limit of

$$\frac{Hk}{2} \approx 0.44, \tag{5.4}$$

which may represent an absolute steepness limit. We should point out that this limit is remarkably close to the theoretical steady limiting steepness of $ak = 0.443$ (2.46), i.e. the Stokes limit $H/\lambda = 1/7$ (2.45). It is also in excellent agreement with the dedicated fully non-linear simulations of the breaking onset (see Section 4.1). The skewness at the breaking point asymptotes the value of

$$S_k \approx 1 \tag{5.5}$$

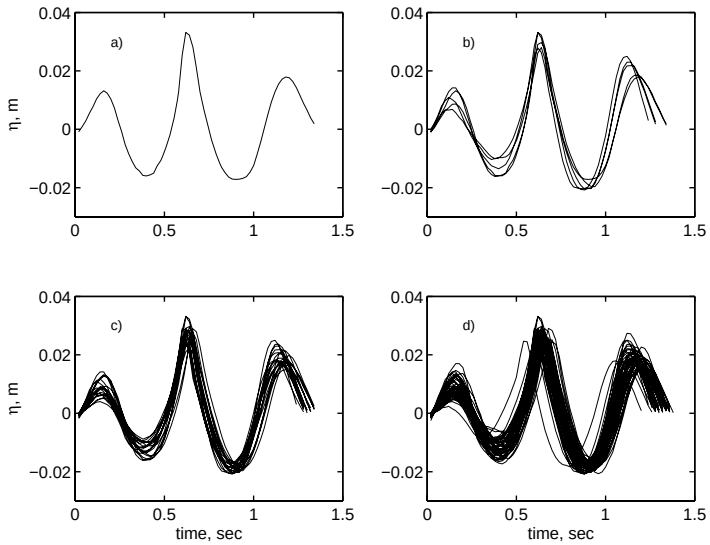

Fig. 5.5. $IMF = 1.8$ Hz, $IMS = 0.30$, $U/c = 0$. (top left panel) The steepest incipient breaker. (top right panel) Five steepest incipient breakers. (bottom left panel) Twenty steepest incipient breakers. (bottom right panel) Fifty steepest incipient breakers.

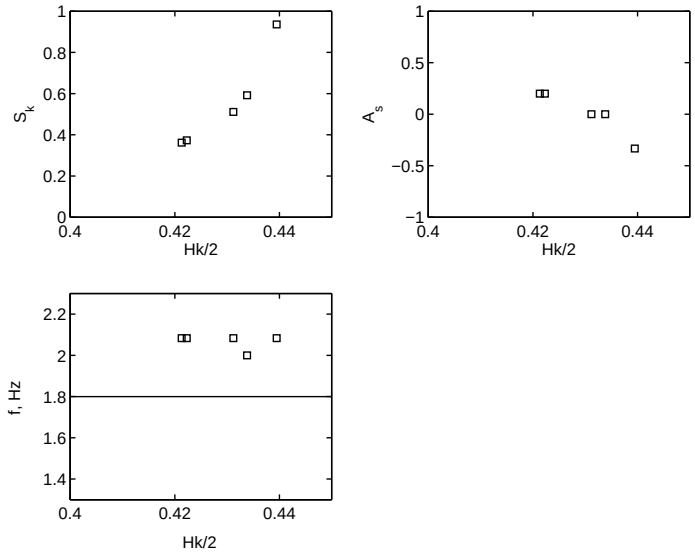

Fig. 5.6. Laboratory statistics for the incipient breakers (5 steepest waves). $IMF = 1.8$ Hz, $IMS = 0.30$, $U/C = 0$. (top left panel) Skewness versus steepness. (top right panel) Asymmetry versus steepness. (bottom panel) Frequency (inverse period) versus steepness. $IMF = 1.8$ Hz is shown with the solid line.

which means that the crest is twice as high as the trough (1.2). Values of asymmetry (1.3) in the imminent breaker are transitional rather than definite.

Such an observation is very important because it signifies that the waves break once they achieve the well-established state beyond which the water surface cannot sustain its stability. It is postulated that the other geometric, kinematic and dynamic criteria of breaking, explored in the literature (see Section 2.9), are indicative of a wave approaching this state, but are not a reason or a cause for the breaking. As this limit is approached, the skewness increases very rapidly and immediately after the limit is reached the asymmetry becomes negative (i.e. the wave starts tilting forward at the point of breaking).

In this regard, it is necessary to highlight that, although the limit (5.4) replicates the Stokes limiting steepness (2.45)-(2.46), the dynamical non-linear waves we observe here should not be unambiguously identified as the Stokes waves. They do exhibit positive skewness (1.2) on average, but this skewness goes through oscillations to an extent of waves periodically becoming almost sinusoidal (Figures 4.2, 5.3). And although their average vertical asymmetry (1.3) is zero, it oscillates too, and for most of the time the wave is actually asymmetric. Also, the crest geometry is far from the steady pointy 120° corner flow (2.47), and is likely to be driven by crest instabilities characteristic of very steep waves [Longuet-Higgins & Dommermuth, 1997, Longuet-Higgins & Tanaka, 1997]. A good illustration of the differences between the stationary Stokes wave and a transient wave at the breaking onset is Figure 1.2. In the measured breaking-onset Figures 5.4-5.5, the crest instability is actually visible (the tip of the crest is leaning forward).

It should be mentioned, even if in passing, that the limiting steepness of standing waves at breaking is different to that of the propagating waves. In a series of analytical studies it was identified as

$$\frac{Hk}{2} \approx 0.69, \tag{5.6}$$

[Penney & Price, 1952, Schwartz & Fenton, 1982] or

$$\frac{Hk}{2} \approx 0.61, \tag{5.7}$$

[Okamura, 1986]. Dynamics of the standing waves will not be further discussed in the present paper.

Various quantitative characteristics of waves propagating to their breaking are analysed in Figures 5.7 – 5.12. Figure 5.7 shows a comprehensive set of statistics of the properties of the 20 highest incipient breakers and their relationship with the preceding and following wave. The first (top left) subplot is similar to the statistical plot of numerically simulated skewness versus steepness in Figure 4.9. Remarkably, values of limiting local steepness, the property which was revealed by the model as the likely indicator of breaking is in the same range as was predicted in numerical simulations: $2\epsilon \approx 0.8$. For a real wave, even if two-dimensional, such steepness is extremely high. Noting that the mean steepness is $\epsilon \approx 0.4$ and that near the crest the wave is even steeper, it is not surprising that the wave is on the point of collapse.

The skewness of the 20 highest waves in the first subplot scatters from almost 0 to almost 1. As indicated in the simulational Section 4.1, we would expect the skewness to also have a limiting value. Clearly, however, such a limit is not a very robust breaking characteristic. Also in the top

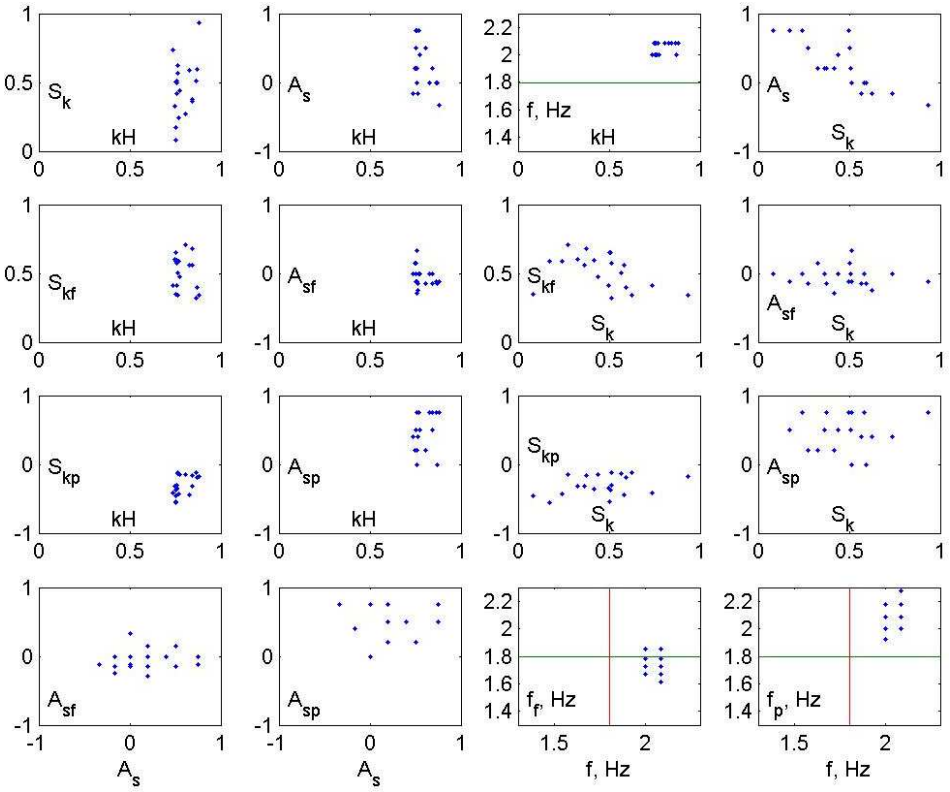

Fig. 5.7. Laboratory statistics for the incipient breaker (20 steepest breakers). $IMF = 1.8$ Hz, $IMS = 0.30$, $U/c = 0$. (top left panel) Skewness versus steepness. (top line, second left panel) Asymmetry versus steepness. (top line, second right panel) Frequency (inverse period) versus steepness. $IMF = 1.8$ Hz is shown with solid line. (top line, right panel) Asymmetry versus skewness. (second top line, left panel) Skewness of the following wave versus steepness of the breaker. (second top line, second left panel) Asymmetry of the following wave versus steepness of the breaker. (second top line, second right panel) Skewness of the following wave versus skewness of the breaker. (second top line, right panel) Asymmetry of the following wave versus skewness of the breaker. (second bottom line, left panel) Skewness of the preceding wave versus steepness of the breaker. (second bottom line, second left panel) Asymmetry of the preceding wave versus steepness of the breaker. (second bottom line, second right panel) Skewness of the preceding wave versus skewness of the breaker. (second bottom line, right panel) Asymmetry of the preceding wave versus skewness of the breaker. (bottom line, left panel) Asymmetry of the following wave versus asymmetry of the breaker. (bottom line, second left panel) Asymmetry of the preceding wave versus asymmetry of the breaker. (bottom line, second right panel) Frequency of the following wave versus frequency of the breaker. $IMF = 1.8$ Hz is shown with solid lines. (bottom right panel) Frequency of the preceding wave versus frequency of the breaker. $IMF = 1.8$ Hz is shown with solid lines.

row of subplots, asymmetry is scattered from $A_s = -0.33$ to $A_s = 0.75$ (second panel), with a possible dependence of S_k on A_s in the fourth panel, consistent with the numerical simulations

(Figure 4.9).

A robust property of the breaking, in the third panel, is the wave frequency. The scatter of this property is small, with all the values falling into a range $f = 2 - 2.08$ Hz $= 1.11 - 1.16IMF$. Thus, the wave clearly reduces in length prior to collapse. We should mention that the measured steepness $\epsilon = kH/2$ is the physical rear-face steepness, and therefore the effect of period contraction has already been accounted for.

In the second row of plots, the skewness of the wave following the incipient breaker (first panel) and its asymmetry (second panel) are much less scattered than the skewness and asymmetry of the breaker itself: $S_k = 0.32 - 0.70$, asymmetry changes from $A_s = -0.29$ to 0.33. In the Figure, subscript 'f' signifies the following wave and subscript 'p' preceding wave. We have already discussed the double-breaking in observational Section 3, which means that this following wave will break soon after the incipient breaker. Thus, its physical shape is not random and should exhibit some characteristic properties leading to breaking. The skewness and asymmetry of the following wave, however, do not correlate with the skewness and asymmetry of the breaker (third and fourth panels of the second row, first panel of the bottom row).

In the third row, the skewness of the wave preceding the breaker is even less scattered: $S_k = -0.55$ to 0.12 (first panel). Remarkably, it is essentially negative, i.e. rear trough of the preceding wave is always deeper than its crest. The asymmetry $A_s = 0$ to 1.33 is never negative (a couple of large $A_s = 1.33$ values are offscale in the second panel and not shown), that is, this wave is tilted backward. There is no correlation of skewness and asymmetry of this preceding wave with those of the near-breaker (last two panels of the third row, second panel of the bottom row). Thus the three waves, surrounding the breaking event, tend to exhibit some quasi-universal form, but variations of their shape are not correlated with each other, which means that these shape distortions are random. Therefore, it is not the mean characteristics of the observed shapes, but rather their limiting values should asymptote the universal form parameters. These were analysed for the highest breakers in Figure 5.6.

The last two subplots in the bottom right corner show the local frequency of the following f_f and preceding f_p waves versus the frequency of the breaker f_b. $IMF = 1.8$ Hz is shown with two solid lines. The local frequency was found to be a robust characteristic for the incipient breaker above, and we can expect a reasonable correlation of these properties. Although f_f and f_p are more scattered than f_b the correlation is present. In the last panel, all the data points are in the second quadrant and thus the preceding wave is decreasing in length along with the incipient breaker. In the second last panel, the points are on average in the fourth quadrant. Therefore, while the incipient breaker is decreasing in length, the following wave is actually longer than its initial value defined by $IMF = 0.18$ Hz. Since we know that the double-breaking will likely occur, i.e. this following wave will break shortly after the current breaker, then it should now be shrinking rapidly. Thus, some very active physics must be involved in the short time scale evolution of this set of very non-linear waves.

Figure 5.8 further provides similar detailed analysis of the shape of the wave following the incipient breaker. Note that this wave will break shortly after the current incipient breaker and therefore, whatever its properties are now, they are progressing towards breaking. In the Figure, kH, S_k, A_s, f are properties of the currently analysed wave. As above, subscript 'p' preceding wave.

The steepness $2\epsilon = 0.28 - 0.57$ is on average about half the steepness of the incipient breaker (first subplot). Since this wave is still the second largest in the modulated group, this fact

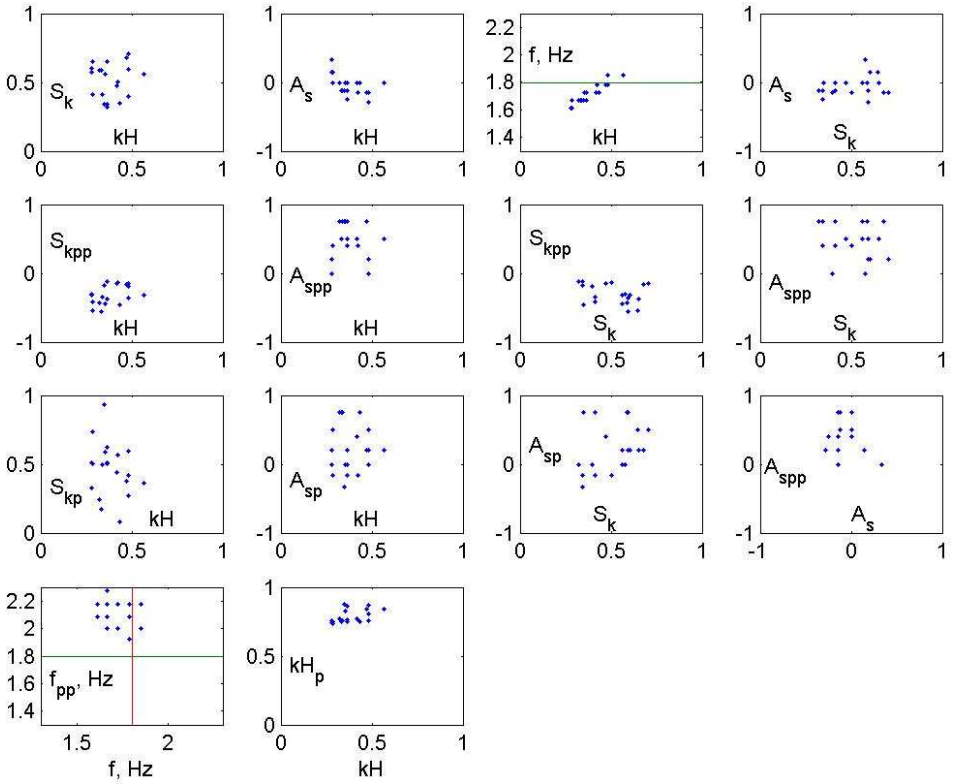

Fig. 5.8. Laboratory statistics of the wave following the incipient breaker (20 steepest breakers). $IMF = 1.8$ Hz, $IMS = 0.30$, $U/c = 0$. (top left panel) Skewness versus steepness. (top line, second left panel) Asymmetry versus steepness. (top line, second right panel) Frequency (inverse period) versus steepness. $IMF = 1.8$ Hz is shown with solid line. (top line, right panel) Asymmetry versus skewness. (second top line, left panel) Skewness of the wave preceding the breaker versus steepness of the wave following the breaker. (second top line, second left panel) Asymmetry of the wave preceding the breaker versus steepness of the wave following the breaker. (second top line, second right panel) Skewness of the wave preceding the breaker versus skewness of the wave following the breaker. (second top line, right panel) Asymmetry of the wave preceding the breaker versus skewness of the wave following the breaker. (second bottom line, left panel) Skewness of the breaker versus steepness of the wave following the breaker. (second bottom line, second left panel) Asymmetry of the breaker versus steepness of the wave following the breaker. (second bottom line, second right panel) Asymmetry of the breaker versus skewness of the wave following the breaker. (second bottom line, right panel) Asymmetry of the wave preceding the breaker versus asymmetry of the wave following breaker. (bottom line, left panel) Frequency of the wave preceding the breaker versus frequency of the wave following the breaker. $IMF = 1.8$ Hz is shown with solid lines. (bottom line, right panel) Steepness of the breaker versus steepness of the wave following the breaker.

highlights how much higher is the incipient breaker. The ranges of skewness $S_k = 0.32 - 0.70$ and asymmetry $A_s = -0.29$ to 0.33 have been mentioned above, here they do not appear to correlate with the steepness (first and second plots) or with each other (fourth plot).

There is a 94% correlation between the steepness and local frequency (third subplot), the frequency grows as steepness increases. Whilst this following wave is on average longer than IMF, it crosses the IMF value at approximately $2\epsilon = 0.5$ and continues to decrease in length:

$$f = 1.7\epsilon + 1.39. \tag{5.8}$$

If this expression is extrapolated to the ultimate frequency value of $f = 2.08$ of the breaker in the third subplot of Figure 5.7, it yields $2\epsilon = 0.81$, which is approximately the value of steepness observed for this incipient breaker. This result should be interpreted as confirmation of the fact that the wave following our breaker is in a state of transition towards its own breaking onset.

In the second row of plots and the last plot of the third row, steepness, skewness and asymmetry of the waves preceding and following the breaker are all plotted versus each other. They all appear uncorrelated, in contrast to the steepness, skewness and asymmetry of the breaker and steepness of the following wave (respectively, first and second subplots of the third row and the last subplot at the bottom). There is also no correlation between the frequencies of the preceding and the following waves (first bottom subplot). Thus, we conclude that perturbations/distortions of the shape of the wave following the breaker do not correlate with distortions of the other two waves in the set of 20 steepest breakers. There is only strong correlation between shape changes within the wave itself, i.e. its steepness and frequency, which indicates its state of transition to limiting breaking steepness.

In Figure 5.9, these properties are analysed for the wave preceding the breaker. Since many cross-correlations have already been analysed, this figure only has three rows of plots. This wave will not break imminently, but is a part of the obviously inter-connected double-breaking and appears to 'disappear' after the double-breaking (see Figure 6.2). Therefore, some of its properties and cross-properties are different to those obtained for the breaker and pre-breaker. As before, in this Figure kH, S_k, A_s, f are properties of the currently analysed wave, subscript 'f' signifies the following wave, i.e. S_{kff} is skewness of the wave following the following wave.

The wave is still steep, although its steepness $2\epsilon = 0.27 - 0.49$ is lower compared to the other two waves (first panel). Unlike them, it is negatively skewed (trough is deeper than crest, first plot) and tilted backward (positive asymmetry, second plot). It is very short, even if compared with the incipient breaker, but its local frequency is more scattered: $f_p = 1.92 - 2.27$. There is no noticeable correlation between these properties of the wave itself, as well as between its steepness, skewness and asymmetry and those of the breaker (bottom three plots) and the wave following the breaker (first three plots in the second row). It is only in the last subplot of the middle row that a marginal correlation (68%) may be identified between the steepness of this wave and the skewness of the incipient breaker. As have been discussed above, this skewness is transient and is expected to asymptote to some value at the point of breaking (see Figure 5.6). This correlation may be an indication of some interaction between the breaker and the wave preceding it which will very soon lead to dissipation of the preceding wave (Figure 6.2). The issue of the interaction between the breaker and preceding wave, however, may be of significance and may even hold a key to the downshifting observed in Figures 6.1-6.2. This point needs further investigation.

In Figures 5.10 – 5.12 asymptotic, rather than statistical properties of the incipient breaker are considered. Three subplots in the top raw of Figure 5.10 were zoomed in and scrutinised in Figure 5.6 and are repeated here for consistency of comparisons with other Figures and analysis of other wave-shape characteristics. In these three Figures, the characteristics of the 5 steepest

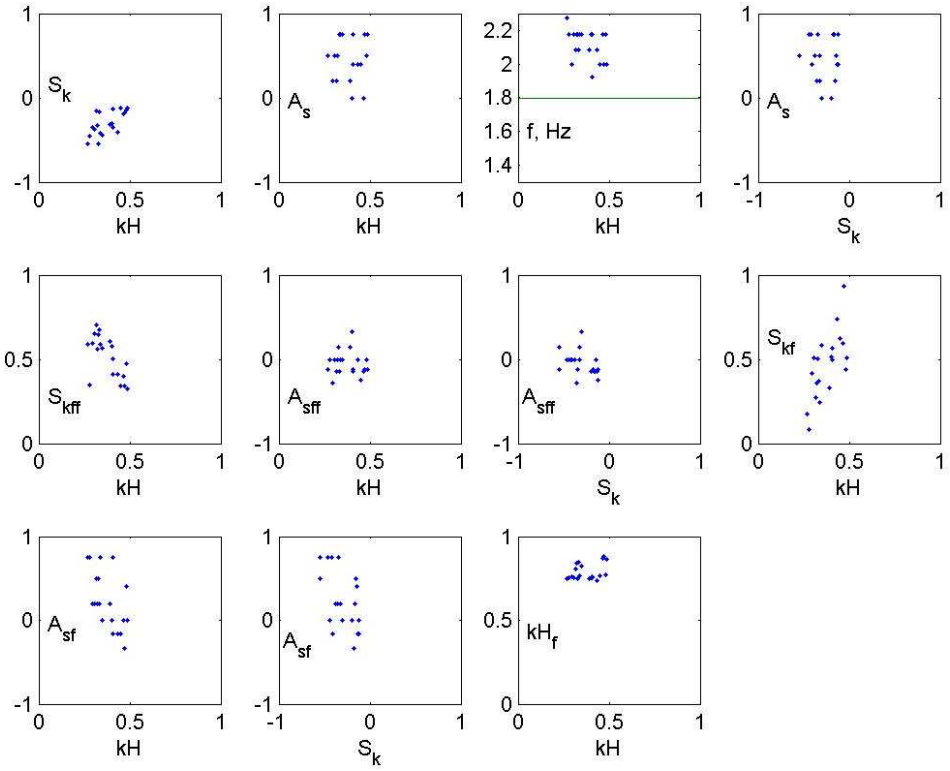

Fig. 5.9. Laboratory statistics of the wave preceding the incipient breaker (20 steepest breakers). $IMF = 1.8$ Hz, $IMS = 0.30$, $U/c = 0$. (top left panel) Skewness versus steepness. (top line, second left panel) Asymmetry versus steepness. (top line, second right panel) Frequency (inverse period) versus steepness. $IMF = 1.8$ Hz is shown with solid line. (top line, right panel) Asymmetry versus skewness. (middle line, left panel) Skewness of the wave following the breaker versus steepness of the wave preceding the breaker. (middle line, second left panel) Asymmetry of the wave following the breaker versus steepness of the wave preceding the breaker. (middle line, second right panel) Asymmetry of the wave following the breaker versus skewness of the wave preceding the breaker. (middle line, right panel) Skewness of the breaker versus steepness of the wave preceding the breaker. (bottom line, left panel) Asymmetry of the breaker versus steepness of the wave preceding the breaker. (bottom line, second left panel) Asymmetry of the breaker versus skewness of the wave preceding the breaker. (bottom line, right panel) Steepness of the breaker versus steepness of the wave preceding the breaker.

waves are plotted. As discussed above, transition to breaking happens very rapidly, and breaking onset and its location may be somewhat modulated due to, for example, uneven number of waves in the non-linear oscillations. Thus, we would expect that it is the highest waves measured that would be closest to the ultimate limiting characteristics of the incipient breaker and its following and preceding counterparts.

In Figure 5.10, as the steepness limit is approached, the skewness increases very rapidly (first subplot) and the asymmetry starts to decrease and becomes negative (subplots 2 and 4), i.e. the

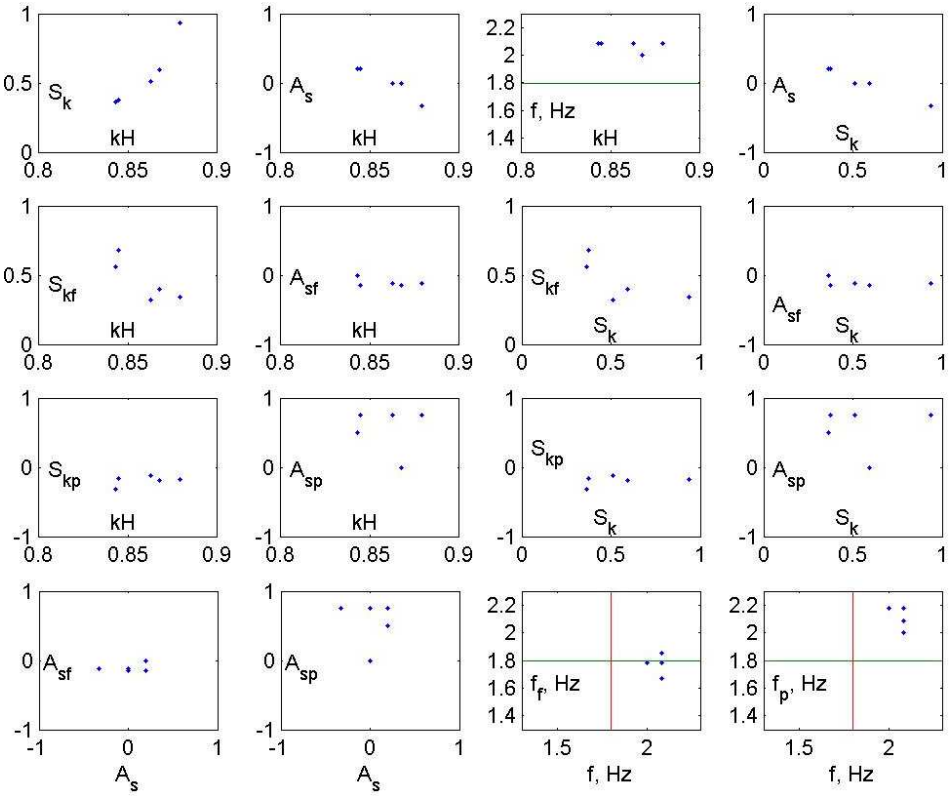

Fig. 5.10. As in Figure 5.7, for 5 steepest breakers.

wave starts tilting forward at the point of breaking. The latter conclusion slightly differs from what was simulated numerically with the CS model (see Section 4.1) where the wave started tilting forward after the point of maximum steepness was passed. Thus, the model simulates the very late stages of the breaking onset with some deviation, which is not unexpected.

We will not discuss scatter, correlations and cross-correlations of the five steepest breakers in Figures 5.10, 5.11 and 5.12 in great detail as this largely repeats relationships observed in Figures 5.7, 5.8 and 5.9. We will only highlight correlations which were marginal within the 20-wave statistical plots and only become visible in the asymptotic plots.

In Figure 5.11, for the waves following the 5 steepest breakers, some dependence of skewness on steepness can be identified (first subplot). This could be expected since this wave is developing towards breaking. Its asymmetry is almost zero (second and fourth subplots). This fact indicates some interaction between the breaker and this wave. Apparently, as the breaker asymptotes its point of collapse, shape of the following wave does not appear random, but is almost perfectly symmetric and therefore is somehow locked with the shape of the incipient breaker. The dependence of the local frequency on steepness, which was noticed previously, is now very clear (third subplot).

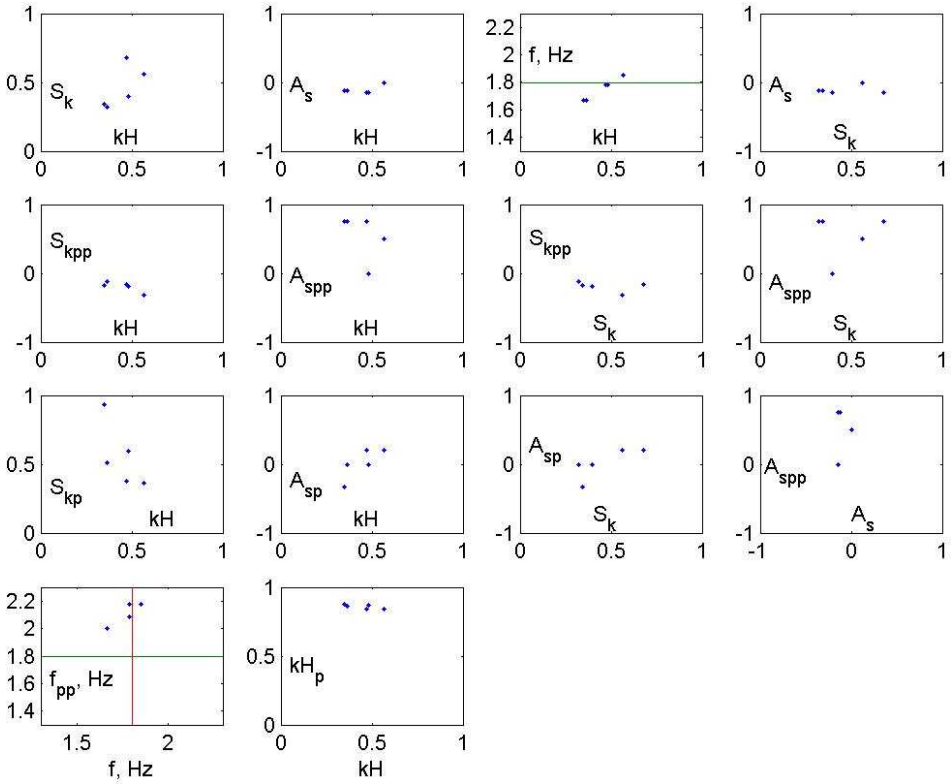

Fig. 5.11. As in figure 5.8, for 5 steepest breakers.

Some marginal dependences between skewness and asymmetry of the breaker and steepness and skewness of the following wave (first three subplots of the third row) are visible. The frequencies of this wave and the wave preceding the breaker are also correlated, which tend to increase together (bottom left subplot). Also correlated are the skewness of this wave and steepness of the wave preceding the breaker (first subplot in the middle row of Figure 5.12), asymmetry of the breaker and steepness of the preceding wave (first subplot in the bottom row of Figure 5.12). Together with the correlation of skewness of the breaker and steepness of the preceding wave noticed before (last subplot of the middle row), these properties likely indicate active interactions between the three waves, one of which is now at the point of breaking.

5.1.3 Laboratory investigation of wind influence

Following the same approach as in the numerical simulations in Section 4.1, we now investigate the influence of wind on the non-linear wave evolution and breaking onset. The wind has been shown to play multiple roles in the wave evolution to breaking. At larger scales, the wind generates waves and pumps energy into the waves, increasing their steepness and thus leads to more frequent breaking. At moderate wind conditions, doubling the wind speed resulted in the

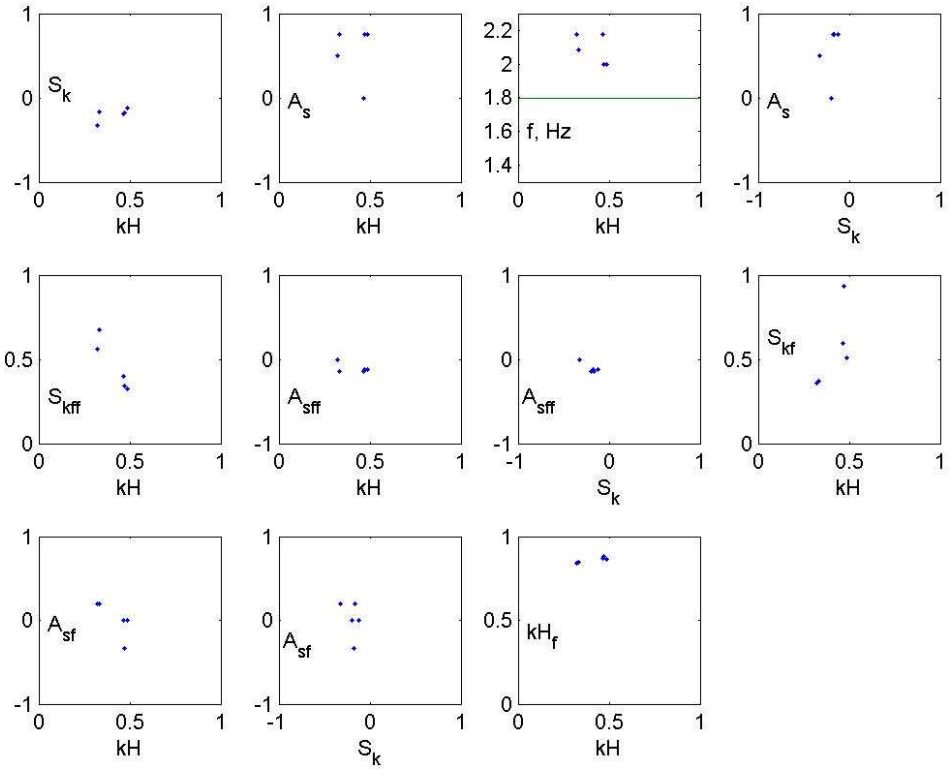

Fig. 5.12. As in figure 5.9, for 5 steepest breakers.

breaking occurring four times faster (e.g. Figure 4.2). Instantaneously, at the point of breaking onset, the capacity of the wind to push the wave over and thus affect the onset is small, even if the wind is very strong and the wave is very steep (Figures 5.14-5.16). At medium scales, however, the wind was observed to change the depth R (5.3) of the modulation of already existing waves and in this way to alter the severity of the breaking (Figures 6.2-6.3).

Figure 5.13 is similar to Figure 5.3, but moderately-strong wind forcing of $U/c = 3.9$ is now applied to the mechanically generated waves. Note that $IMF = 1.5$ Hz is different to $IMF = 1.8$ in figure 5.3. This is done in order to have incipient breakers, as before, at the probe 2 where data is recorded. With the wind superimposed, the waves of $IMF = 1.8$ Hz, $IMS = 0.30$ would break before this probe (see discussion in Section 4.1 and Figure 4.2).

In Figure 5.3, the modulation depth (5.3) $R = 4$ whereas in the current Figure 5.13 $R = 2.9$, i.e. difference in the modulation depth is 1.4 times. Thus, we observe the expected feature of smearing of the modulation by the wind.

This smearing is reflected in all the other non-linear properties shown in the Figure. Steepness (second panel), skewness (third panel) and asymmetry (fourth panel) are intentionally plotted at the same vertical scale as those in Figure 5.3 even though their range of oscillations is now noticeably reduced. Because of the IMF change, the scale of the frequency plot (bottom) could

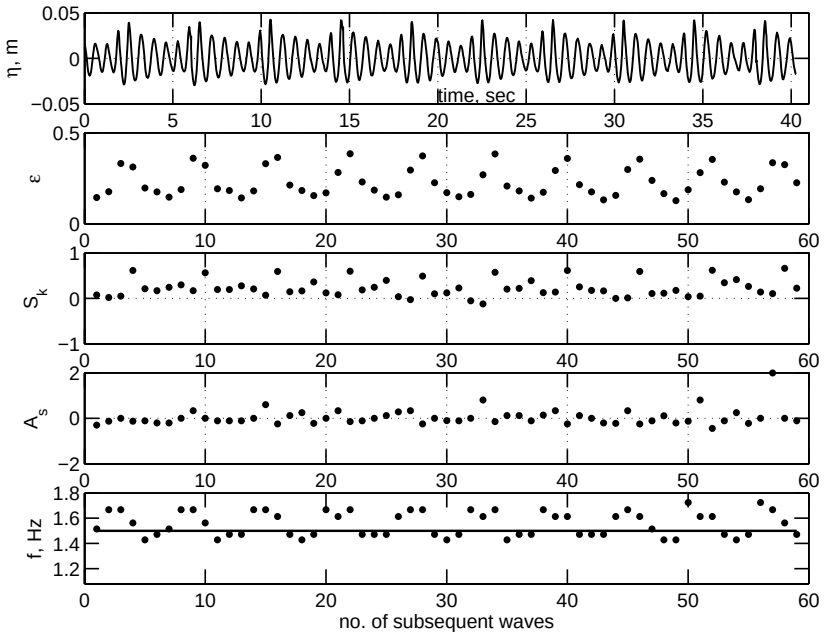

Fig. 5.13. As in figure 5.3, with wind forcing. Segment of time series with $IMF = 1.5$ Hz, $IMS = 0.30$, $U/c = 3.9$. (top panel) Surface elevation η. (second top panel) Rear-face steepness ϵ (1.1). (medium panel) Skewness S_k (1.2) (rear trough depth is used). (second bottom panel) Asymmetry A_s (1.3). (bottom panel). Frequency (inverse period). $IMF = 1.5$ is shown with solid line.

not be left the same, but scale limits were kept proportional to those in Figure 5.3. Reduction of the local frequency oscillations, moderated by the wind, is also apparent.

The major features of the breaking onset in the presence of wind forcing are shown in Figures 5.14, 5.15 and 5.16. Visually, the breakers in Figure 5.14 did not qualitatively change compared to those in Figure 5.5 with no wind. Quantitative properties, however, were altered by the wind.

In Figure 5.15, analogous to the no-wind Figure 5.7, the statistics of a comprehensive set of properties for the 20 highest incipient breakers and their links to the preceding and following wave is shown. Quantitatively, for the 20 waves approaching breaking, the wind influence generally brought more order to their shapes, as the scatter of almost all the properties is reduced and the marginal dependences became clearer. Qualitatively, the wind changed the shape of the preceding wave which is now not skewed negatively on average (first subplot in the third raw) and increased the steepness of the following wave from $\epsilon = 0.19$ to $\epsilon = 0.27$ on average (not shown).

With regard to the asymptotic shape of the breaker, the wind in Figure 5.16 has a scattering rather than stabilising influence. In this Figure, analogous to Figure 5.10, characteristics of the 5 steepest waves are plotted in the presence of wind. Apparently, at these very last pre-breaking stages, the wind is capable of modifying the wave, which is about to loose its stability, and to

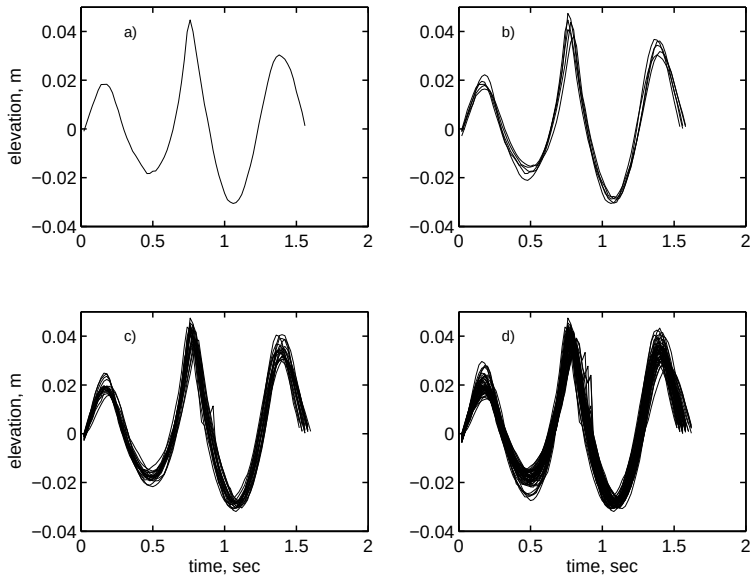

Fig. 5.14. As in Figure 5.5, with wind forcing. $IMF = 1.5$ Hz, $IMS = 0.30$, $U/c = 3.9$. (top left panel) The steepest incipient breaker. (top right panel) Five steepest incipient breakers. (bottom left panel) Twenty steepest incipient breakers. (bottom right panel) Fifty steepest incipient breakers.

somewhat randomise its characteristics.

In the first subplot of the top row, the limiting skewness is plotted versus limiting steepness. Skewness no longer approaches 1, but steepness extends beyond the $2\epsilon = 0.88$ limit and reaches $2\epsilon = 0.97$. The asymmetry is no longer negative, that is, the breakers do not tilt forward. Frequency remains a robust property and stays in almost the same range of $f = 1.11 \div 1.19\, IMF$.

Therefore, while the breaking is mainly a hydrodynamic process, wind, if present, does influence the incipient breaking. As was noticed in the numerical simulations, this influence is small, but it is noticeable and diverse – from the shape-stabilising effect when approaching breaking onset to the shape-randomising effect at the point of breaking.

5.1.4 Distance to the breaking

As mentioned earlier in this Section, distance to breaking in a train of steep initially monochromatic waves can be controlled by varying IMS and therefore can be predicted. Based on the laboratory measurements, such predictions are summarised in Figure 5.17 (top), which shows the non-dimensional distance to breaking $N = x_b/\lambda$ as a function of IMS, where x_b is the dimensional distance to breaking. A range of values of IMS are shown, along with cases with and without wind forcing. As expected, the addition of wind forcing reduces the non-dimensional distance to breaking. However, this reduction is not so great that the data points deviate markedly from the functional relationship between N and IMS, the non-linear effects obviously dominate over the wind forcing.

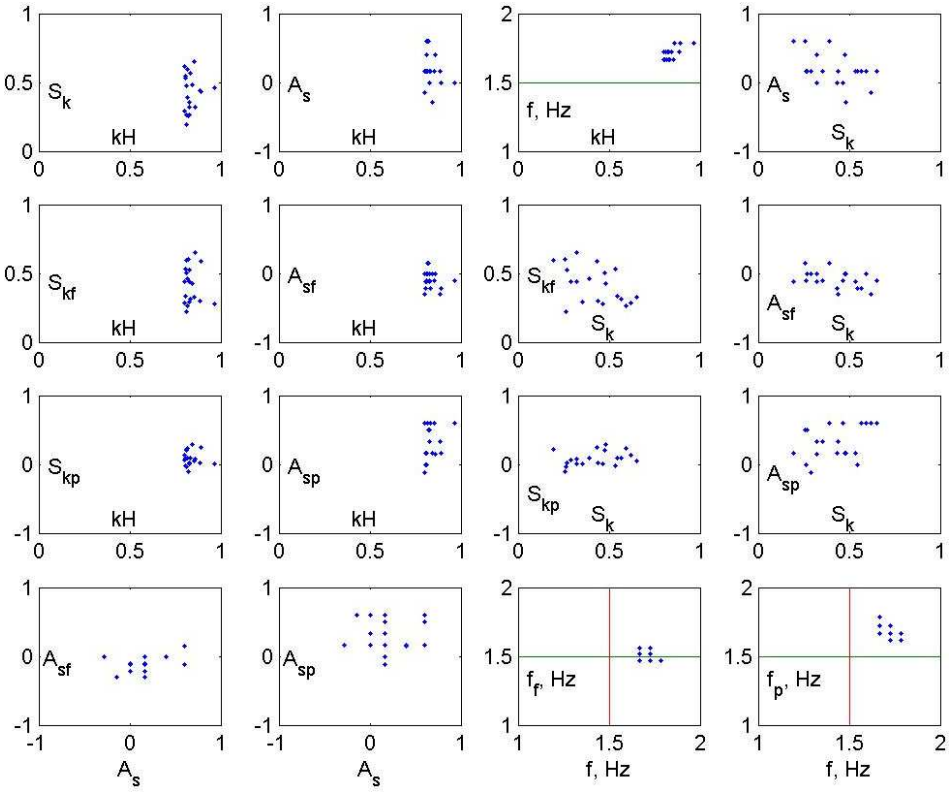

Fig. 5.15. As in figure 5.7, with wind forcing. $IMF = 1.5$ Hz, $IMS = 0.30$, $U/c = 3.9$. Laboratory statistics for 20 steepest incipient breakers.

In accordance with the numerical simulations, for each wave length an increase of its initial steepness resulted in the breaking occurring closer to wavemaker. In dimensionless terms, this dependence was parameterised as follows:

$$N = -11 \, \mathrm{atanh}[5.5(\epsilon - 0.26)] + 23, \text{ for } 0.08 \leq \epsilon \leq 0.44. \tag{5.9}$$

Consistent with the model results, the formula imposes two threshold values of IMS. For $\epsilon > 0.44$, the wave breaks immediately (compared to $\epsilon = 0.3$ for the two-dimensional model - see discussion of modelling limitations in the beginning of Section 5) and if $\epsilon < 0.08$ the wave, in the absence of wind forcing, will never break (compared to $\epsilon = 0.1$ for the model).

In Figure 5.17 (top) two points (squares) are shown which were derived from Figs. 1 and 2 of Melville [1982] for comparison. The two measurements in Melville [1982] were conducted for initially uniform wave trains, their initial steepness and approximate dimensionless distance to breaking being known. Although recorded under different conditions, these points agree very well with the above parameterisation and provide strong support for laboratory results presented here.

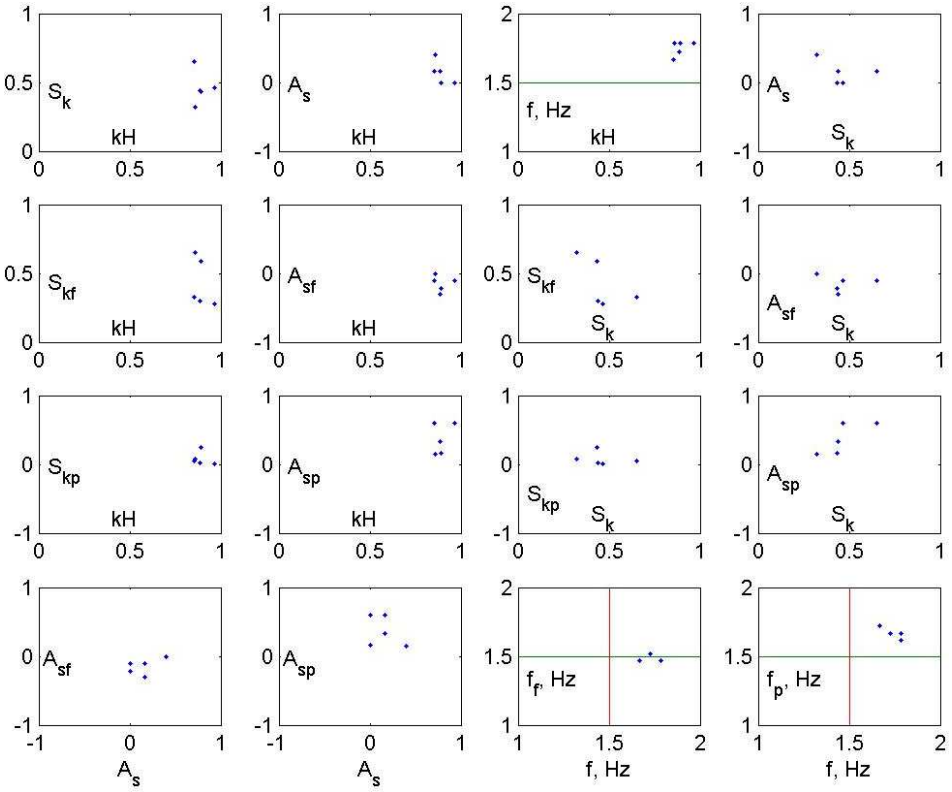

Fig. 5.16. As in figure 5.10, with wind forcing. $IMF = 1.5$ Hz, $IMS = 0.30$, $U/c = 3.9$. Laboratory statistics for 5 steepest incipient breakers.

The relationship (5.9) potentially provides a means of predicting the onset of breaking in the open ocean, although some further modification is required for application to such a case. In a field situation, the notion of an initial monochromatic steepness does not exist. Besides, the waves will be three-dimensional, and the modulational mechanism will be combined with wind forcing, current shear, superposition of dispersive spectral waves, modulation due to linear wave groups, among other relevant features. However, the above analysis suggests that should waves reach some critical steepness then they will ultimately break. It does not matter whether this limiting steepness occurred due to sustained wind forcing, wave group modulation or other means, as long as the limiting value is reached.

Clearly, the breaking process is associated with individual waves, and hence a local measure of the steepness of each wave is the desired quantity. For applications (e.g. in a wave-prediction model), such time-domain information is impractical and a spectral or average value of the steepness of the wave field is the only possible quantity available.

A further complication in comparing available field data with predictions of the current parameterisation is due to the fact that the relationship (5.9) predicts the probability of incipient

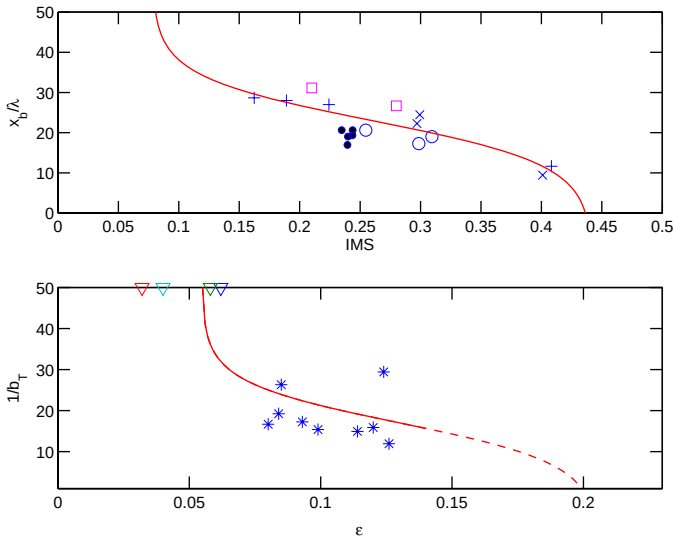

Fig. 5.17. Parameterisation of the breaking probability. (top panel) Laboratory data. Number of wave lengths N to breaking versus IMS. No wind forcing: $\circ$ – $IMF = 1.6$ Hz; x – $IMF = 1.8$ Hz; $+$ – $IMF = 2.0$ Hz. Filled circles represent $IMF = 2.0$ Hz, with wind forcing applied. Squares are data points derived from Melville [1982]. The parameterisation (5.9) is shown with solid line. (bottom panel) Field data. Inverse breaking probability b_T, measured by visually detected whitecaps, versus the peak spectral steepness ϵ_{peak} denoted as ϵ. Triangles signify measured $b_T = 0$. The line identifies the approximation (5.23) (the dotted part is the extrapolation based on parameterisation of Babanin *et al.* [2001]).

breaking, whereas in the field it is impossible to directly measure whether a wave is an incipient breaker or not. At best, we can measure quantities which result from the breaking process. Common measures of this type include the acoustic signature of breaking waves or surface whitecap coverage. Although these quantities are indirect measures, they are related to the breaking process. However, a breaking wave emits an acoustic signature and forms whitecaps over a substantial part of its period, and therefore the probability of encountering such sound or whitecaps would be higher than the probability of breaking onset (see Section 2.4 above).

Given the uncertainties, comparison of the present parameterisation of the breaking probability (5.9) with field data can only be qualitative at this stage, as the quantities being compared are not identical. This is done in Figure 5.17 (bottom), but will be discussed in detail in Section 5.3 after the probability dependences for spectral waves are introduced.

5.2 Wave breaking threshold

In the numerical simulations of Section 4.1 and the laboratory experiments of Section 5.1, breaking threshold was established in terms of the Initial Monochromatic Steepness of initially uniform train of steep waves [Babanin *et al.*, 2007a, 2009a]. According to the numerical simulations, if

IMS is less than

$$IMS_{threshold} = 0.1 \tag{5.10}$$

the wave train will exhibit all the non-linear behaviour described in Section 4.1, including oscillations of the steepness, skewness and asymmetry, but will never break. This is because in the course of the modulational evolution of non-linear groups no wave will grow to reach the limiting steepness (2.46). Therefore, the threshold (5.10) does not signify any new kind of non-linear behaviour of wave system, but merely the magnitude of the modulation. In this regard, the modulational instability may lead either to a breaking wave, if the limit (2.46) achieved, or to a high non-breaking wave. The latter may even qualify as a freak (rogue) wave if, by definition, its height satisfies the criterion

$$H_{freak} \geq 2.2 H_s, \tag{5.11}$$

but its steepness is still below the limiting steepness.

In Banner *et al.* [2000], Babanin *et al.* [2001], a similar physical threshold was established for dominant waves in a continuous wave spectrum. This was done on the basis of two deep-water and a finite-depth data sets. The deep-water sets included the Black Sea data (see Section 3.7) and Lake Washington observations [Katsaros & Atakturk, 1992], and the finite-depth measurements were those conducted at Lake George (see Section 3.5). Overall range of the dominant frequencies involved as a result was very broad: $f_p = 0.2 - 0.4$ Hz for the Black Sea, $f_p > 0.5$ Hz for Lake Washington, and $f_p = 0.3 - 0.5$ Hz for Lake George. Also, two deep-water data points from the Southern Ocean were included with $f_p < 0.1$ Hz. The ten-meter reference wind speed U_{10} ranged from 3 to 20 m/s, and the dimensionless depth of Lake George – from deep water down to values of $k_p d = 0.7$ [see Young & Babanin, 2006b].

The Black Sea data are tabulated in Table 5.1. The experimental arrangement involved visual surveillance of waves passing over a wave probe, with collocated breaking events labelled electronically by an observer. With this data, it was possible to investigate the distribution of breaking probability with respect to the distance from the spectral peak. The first 9 records (Table 5.1) were obtained in 1993 from the research vessel "Professor Kolesnikov" (henceforth PK) operated by the Marine Hydrophysical Institute (MHI) in Sebastopol.

The PK wave data were recorded using an accelerometer buoy, as described by Babanin *et al.* [1993]. Briefly, the buoy diameter was 0.58 m and its operational bandwidth was $0.08 - 1.0$ Hz, which easily covered the wave frequencies of interest. It was deployed around 100 m from the ship to avoid any interference between the ship and the wind and wave fields. Record lengths of 34 min to 68 min were acquired using a sampling frequency of 4 Hz. Observer watched the buoy from the vessel and triggered an electronic signal to register the passage of a whitecap over the buoy. This signal was recorded synchronously with the buoy data. The observer varied the duration of the electronic label according to the geometrical size of the whitecap, providing an approximate indication of individual breaker dimensions for future analysis. The observer was about 10 m above sea level, allowing a clear view of whitecaps with scales down to the size of the buoy. The environmental data collected simultaneously included 10-minute averages of the 10 m wind speed and direction, measured by a standard Russian M63-MP anemometer on the ship's bow, together with mean water and air temperature data.

The first 7 records were obtained with the ship anchored about 3.2 to 6.4 km offshore the relatively flat West Coast of the Crimea. Quite young, strongly forced, fetch-limited waves with

$U_{10}/c_p = 2.7 - 4.1$ were observed. Their spectral peak frequencies f_p ranged from 0.3 to 0.44 Hz. The wind speed U_{10} ranged from 11.7 to 15.0 m/s. Records 16 and 18 were gathered from the drifting vessel during the same PK cruise in the Eastern part of the Mediterranean Sea, during which older waves were observed approaching full development, with $U_{10}/c_p = 0.9$ and 1.15. Their rather low observed peak frequencies of 0.16 Hz and 0.17 Hz corresponded to 8.4 m/s and 11.2 m/s wind speeds respectively.

The last four wave records were recorded from an oil rig situated 60 km offshore in the north-west region of the Black Sea in horizontally uniform water of 30 m depth. They are the deep-water records which have been extensively used in wavelet analysis of the wave breaking and were described in Section 3.7 above. The complete environmental data set included one-minute averaged wind speeds, five-minute averaged surface current speed and direction measurements at three-hour intervals as well as water and air temperatures recorded every three hours [see Babanin, 1988]. To avoid possible air-flow distortion by the platform, an M63-MP anemometer was deployed on a tower 42 m above sea level, well above the deck buildings. The drag-coefficient dependence of Large & Pond [1981] was used to estimate the 10 m wind speed from the observed data.

The surface-elevation time series with labelled individual breaking events were analysed to determine individual breaker properties and breaking statistics. The accelerometer data series from the PK cruise were segmented to reduce the effects of low-frequency trends and integrated twice prior to analysis. With shorter waves riding on longer ones, occasional confusion could occur as to which wave scale was actually breaking, but since dimensional information on the individual whitecaps was available from the label length, it is believed that uncertainties of this type were not essential.

The Lake Washington data set described by Katsaros & Atakturk [1992] represents a short-wave extreme of natural deep-water wind waves. These short fetch-limited waves were generated by light winds. For this data set, U_{10} ranged from 3.4 m/s to 6.8 m/s, with peak wave frequencies $f_p = 0.55$ Hz to 0.75 Hz and wave development stages of $U_{10}/c_p = 1.5$ to 2.5. The waves were measured by means of a wire wave gauge, with breaking events recorded by a video camera observing the wave gauge. A detailed analysis provided the number of plunging, spilling and micro-scale breakers for each of the sixty-six 17-minute-long records. For the breaking-probability analysis, available plunging and spilling breaker statistics was combined to quantify the breaking waves in the spectral-peak band.

The finite-depth wave-breaking data were obtained at the experimental site at Lake George near Canberra in south-eastern Australia (Figure 3.5) during October-December 1997. These data were described in detail in Section 3.5 (see also Table 5.2). The two South Ocean data points were added to extend the probability study to very long waves, see Banner *et al.* [2000].

As mentioned above, Banner *et al.* [2000], Babanin *et al.* [2001] concentrated on the breaking statistics of dominant waves. This statistics was investigated and the dominant breaking probability was parameterised in terms of average spectral-peak steepness. The significant mean wave steepness given by

$$\epsilon_{significant} = \frac{H_s k_p}{2} \tag{5.12}$$

contains some contribution from the higher-frequency components, which is irrelevant from the point of view of evolution of dominant-wave groups to the breaking. Therefore, the significant

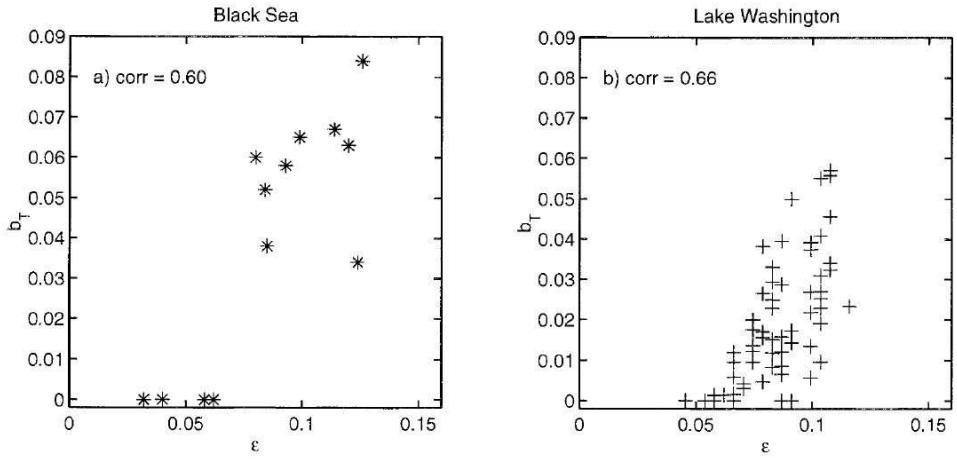

Fig. 5.18. Observed dominant wave-breaking probability b_T (2.3) versus the dominant wave steepness ϵ (5.13) for two diverse field sites (a) Black Sea data (*) (b) Lake Washington data (+). The legend shows the correlation coefficient based on a linear fit.

steepness of the spectral peak was introduced:

$$\epsilon_{peak} = \frac{H_p k_p}{2}, \tag{5.13}$$

where

$$H_p = 4\sqrt{\int_{0.7f_p}^{1.3f_p} F(f)df}, \tag{5.14}$$

i.e. the dominant waves were assumed to have frequencies within $\pm 30\%$ vicinity of the spectral peak (see (2.6) and discussion in Section 2.5). Intrinsically, ϵ_{peak} is an appropriate parameter as it provides a direct measure of non-linearity of the dominant waves. Huang [1986] previously used a similar parameter, the significant wave slope, in his modelling of breaking influence on upper ocean dynamics. Values of ϵ_{peak} for the data records of the present paper are given in Tables 5.1 and 5.2.

Figure 5.18 shows the number of breakers per wave period as a function of the dominant wave steepness ϵ_{peak} (5.13) which is denoted as ϵ in the Figure, for the Black Sea data (left panel) and Lake Washington data (right panel). Two conclusions may be drawn from these results. Firstly, these figures show that steeper dominant waves have higher breaking probabilities and these are well-correlated with the spectral peak steepness parameter ϵ_{peak}. Secondly, there is strong visual evidence of a threshold value for ϵ_{peak} around 0.05–0.06 that determines whether dominant wave breaking occurs or not. This level is consistent with the threshold level of $\epsilon = IMS \sim 0.1$ (5.9)-(5.10) reported by Babanin *et al.* [2007a] on the basis of numerical simulations and laboratory experiment, once this is converted to an equivalent root-mean-square measure.

The finite-depth Lake George breaking probability is tabulated in Table 5.2 and plotted in Figure 5.22a. As can be seen in this Figure, the Lake George data are consistent with the ϵ_{peak} threshold observed for deep-water data in Figure 5.18. Therefore, the value of

$$\epsilon_{peak_{threshold}} = 0.055 \tag{5.15}$$

can be adopted as a universal wave-breaking threshold for dominant spectral waves, applicable both in deep water and in finite depths.

Thus, presence of the wave-breaking threshold is established both for monochromatic wave trains and spectral waves. The threshold represents some characteristic mean steepness value. Whether this is a uniform two-dimensional wave train or a spectral three-dimensional directional wave field, this characteristic value signifies whether evolution of the train will result in a breaking event or events, or not. In the spectral sense, the threshold as described here is established for dominant waves.

For shorter waves of the spectral tail, such threshold is impossible to define unambiguously, in terms of a characteristic steepness similar to (5.13)-(5.14), because there is no characteristic bandwidth at the broad-banded spectral tail (see also discussion in Section 2.5). Breaking threshold, however, does exist at the smaller scales too, as the wave-breaking dissipation clearly exhibits thresholded behaviour in terms of spectral density of the wave steepness [see Babanin & Young, 2005, Babanin *et al.*, 2007c]. It will be discussed in Section 5.3.2 in the context of breaking probabilities for the spectral waves and its value is given by (5.32).

Therefore, a characteristic breaking threshold always exists and bears a principal significance in wave-breaking dynamics and statistics. Breaking probability will depend on the characteristic steepness or its equivalent, but only if it exceeds the threshold value, and the probability appears to depend on the excess above the threshold steepness rather than on the steepness itself (see Sections 5.1.4 and 5.3.1).

From the point of view of non-linear hydrodynamics of wave trains/fields, however, this threshold does not signify any fundamental transition from one type of behaviour to another. As mentioned in the beginning of this Section with respect to two-dimensional trains, the non-breaking trains, with their characteristic steepness being below the threshold (5.10), will exhibit all the same non-linear dynamic features as the breaking trains (except for the breaking itself of course). The breaking/non-breaking segregation is not because of a transition to a different underlying physics of the wave evolution, but due to ability/non-ability of the non-linear wave system to produce individual waves which exceed the limiting steepness (2.46).

Differences between the breaking threshold (5.10), (5.15) and breaking criterion (2.46) should be emphasised and stressed at this stage. The threshold is a mean steepness of the wave train/field, whereas the criterion is a limiting steepness for individual waves in this train/field. That is if the mean steepness is above (5.10), (5.15), there will appear individual waves reaching up the steepness of (2.46). Therefore, individual waves can be steeper than (5.10)/(5.15), but that does not warrant an eventual breaking unless the mean steepness exceeds this level. Once these individual waves will break, the mean steepness may fall below the threshold and the breaking will stop. High individual waves will still be produced, but they will not be reaching the limit and will not be breaking unless there is an input of energy into the wave system (e.g. wind input in the field or mechanical generation of waves in the laboratory).

5.3 Spectral waves

Now that the meaning of the breaking threshold is understood (Section 5.2 above), breaking probability of spectral waves, i.e. waves with continuous distribution of energy along different wave periods/lengths and different directions can be analysed. While it is tempting to extend an analogy of the distance-to-breaking (which, with some caution, can be interpreted as breaking probability) of the monochromatic trains, parameterised in Section 5.1.4, to the spectral waves, this is not a straightforward exercise because amplitudes and therefore steepness of waves with specific wavenumber are not defined in the continuous-spectrum environment. Even less straightforward such notion is at the spectral tail where there is no even a characteristic bandwidth which can be employed to produce a definition of a characteristic steepness similar to that for the spectral peak (5.13)-(5.14).

Therefore, in Section 5.3.1, we start from parameterising the spectral-peak breaking probability first, following Banner *et al.* [2000], Babanin *et al.* [2001], and will then attempt the analogy with monochromatic wave trains (Figure 5.17) for these dominant waves of continuous-spectrum wave fields. In Section 5.3.2, breaking probability of relatively short waves (i.e. short with respect to the waves at the spectral peak) will be discussed.

5.3.1 Breaking probability of dominant waves

As defined in Section 2.5, breaking probability b_T (2.3) for the spectral dominant waves will be considered as the mean passage rate past a fixed point of dominant wave-breaking events per dominant wave period. The dominant waves are taken within the spectral band of $0.7f_p$ to $1.3f_p$ (2.6), which contains spectral components determining the group structure of the dominant wave field. Measurements of b_T require averaging over a large number of wave groups since the breaking process is characterised by long-period intermittencies [e.g. Donelan *et al.*, 1972, Holthuijsen & Herbers, 1986, Babanin, 1995, Babanin *et al.*, 2009a].

As discussed in Section 3 above, previously wave breaking properties such as breaking probability, whitecap area coverage etc. had been assumed to have a primary dependence on the wind speed U, the dependence ranging from linear up to the fourth power according to different authors. In Figure 5.19, breaking probabilities for two data sets are plotted against the wind speed U_{10}. These are the Black Sea data (Table 5.1, first panel) and Lake Washington data [Katsaros & Atakturk, 1992, second panel]. It is seen in these panels of Figure 5.19a and b, that in isolation the Black Sea data and the Lake Washington data correlate rather well with U_{10}. When these two data sets are plotted together in Figure 5.19c, however, they are seen to have distinctly different offsets. Two additional data points obtained from analysis of the Southern Ocean video records [see Banner *et al.*, 2000] show yet another dependence on U_{10}. Therefore, it is an obvious conclusion that it is not possible to establish a common dependence of the dominant wave-breaking probability on U_{10}. While for individual data sets such dependence can be a good fit to the data, there is no universal direct dependence of the wave-breaking probability on the wind speed.

In Figure 5.20, the breaking probability is plotted against another plausible wind-forcing parameter, the inverse wave age U_{10}/c_p denoted as $2\pi\gamma$ in this Figure:

$$\gamma = \tilde{f}_p = \frac{U_{10} f_p}{g} = \frac{1}{2\pi}\frac{U_{10}}{c_p}\,. \tag{5.16}$$

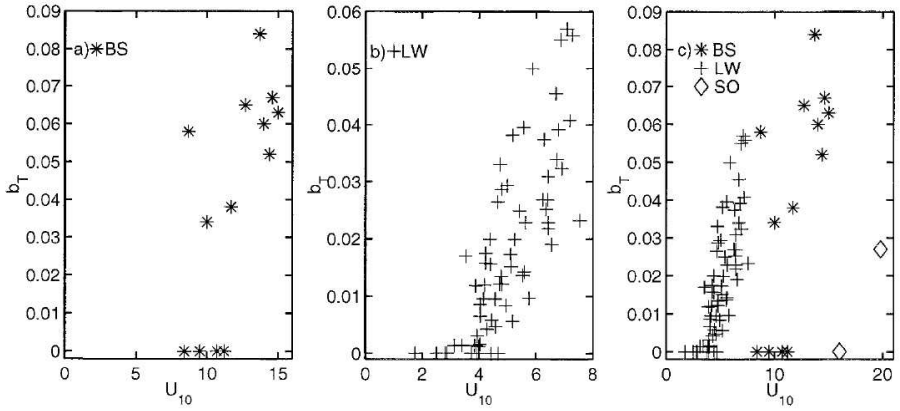

Fig. 5.19. Observed dominant wave breaking probability b_T against U_{10} wind speed for three diverse field sites (a) Black Sea data (*) (b) Lake Washington data (+) (c) composite of the Southern Ocean data (diamonds) with (a) and (b).

Here, it is seen that the individual data sets have similar offsets, but exhibit quite different rates of change of the breaking probability as a function of the wave age. Therefore, the wind forcing does not appear a universal breaking-probability property either, although it provides a relevant secondary parameter as will be seen below.

Thus, Figures 5.19–5.20 support the argument made throughout this paper that the wind's influence on the wave breaking is indirect and, unless the wind forcing is very strong, mainly comes through the slow increase of the wave steepness which is then linked to faster non-linear hydrodynamic processes which may lead to the breaking. Correspondingly, the parameterising of breaking probability by means of wind-speed characteristics is not feasible in general case and has to be done in terms of wave-related properties. For the dominant waves, spectral-peak steepness ϵ_{peak} (5.13)-(5.14) was suggested and successfully used as such parameter (see Section 5.2, Figure 5.18 and Eq.(5.15)).

The above-mentioned wind forcing γ (5.16) and shear-current influences were further shown to have a marginal effect on the dominant-wave breaking and therefore they were employed in the breaking parameterisation through secondary-importance parameters (see also Figure 5.20 for dependence of b_T on γ). For the shear current, the parameter introduced was

$$\Delta = \frac{u_s}{u_0} = \frac{0.01U_{10}}{\epsilon c_p}, \tag{5.17}$$

the ratio of the wind-induced surface current u_s to maximum orbital velocity u_0. The drift-current velocity was adopted from Babanin [1988] as

$$u_s \sim 0.01U_{10}, \tag{5.18}$$

and the maximal orbital velocity was used that of a linear surface-gravity wave with height equal to the peak wave height (5.14)

$$u_0 = \epsilon_{peak} c_p. \tag{5.19}$$

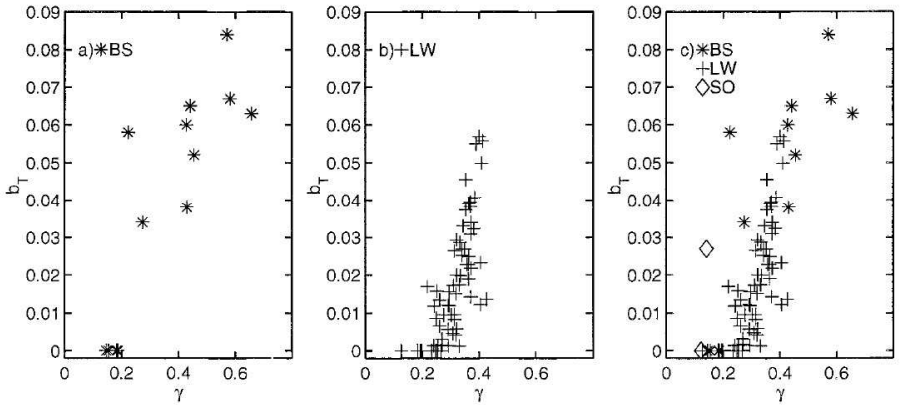

Fig. 5.20. Observed dominant wave breaking probability b_T versus wind-forcing parameter U_{10}/c_p, denoted as $2\pi\gamma$ in this Figure, for three diverse field sites (a) Black Sea data (*) (b) Lake Washington data (+) (c) composite of the Southern Ocean data points with (a) and (b).

The Black Sea and Lake Washington breaking-wave data sets, plotted in Figure 5.21a, b for the b_T-versus-Δ dependence, show that the breaking fraction increases with the shear parameter, although with a far lower visual correlation than seen for the peak steepness. Also, the existence of a shear threshold is not as evident as with the steepness. These indicate the secondary role of vertical shear as outlined above.

For the Lake George data set these marginal influences, as well as the primary dependence on ϵ_{peak} (5.13), are demonstrated in Figure 5.22a, c and d. Since waves observed at Lake George were affected by bottom proximity, ratio H_s/d was also used as a parameter to characterise finite-depth effects on the wave-breaking statistics (Figure 5.22b). In the final parameterisation (5.20), the secondary properties were introduced as perturbation terms of the form $1+\gamma, 1+\Delta$ and $1+H_s/d$, which makes their effect negligible when the parameters are small. For example, H_s/d reduces to zero when the water becomes deep or when the waves vanish, and in such circumstances the parameter will have no effect on the overall dependence of breaking probability b_T on steepness ϵ_{peak}. We note that extrapolation of the expression (5.20) into conditions when γ, Δ or H_s/d are very large has to be done with caution as such extrapolations would take the dependence beyond the range of actual experimental data used to obtain the parameterisation. Values of b_T, Δ, γ, and H_s/d are shown in Table 5.1 for the Black Sea and Table 5.2 for Lake George respectively.

For the data sets, combined from the Black Sea, Lake Washington and Southern Ocean data points (deep water) and Lake George measurements (finite depth), dependence of the spectral peak breaking probability b_T on the composite parameter is shown in Figure 5.23. The data sets agree very well, and the correlation coefficient of 0.89 is very high, particularly if we take into account the diversity of the data used. The exponent is approximately quadratic in the final proposed parameterisation of

$$b_T = 6.16^{+1.91}_{-1.46}[(\epsilon_{peak} - 0.055)(1 + H_s/d)(1 + \Delta)(1 + \gamma)]^{1.94^{+0.15}_{-0.12}}, \tag{5.20}$$

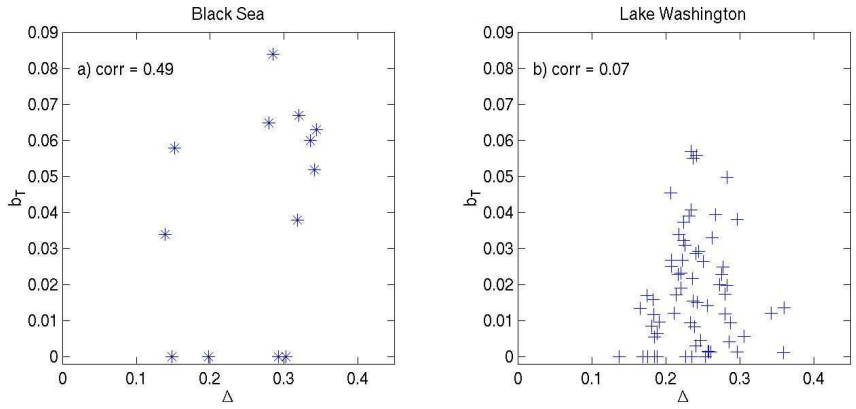

Fig. 5.21. Observed dominant wave breaking probability b_T (2.3) versus surface shear parameter Δ (5.17) for two diverse field sites (a) Black Sea data (*) (b) Lake Washington data (+). The legend shows the correlation coefficient based on a linear fit.

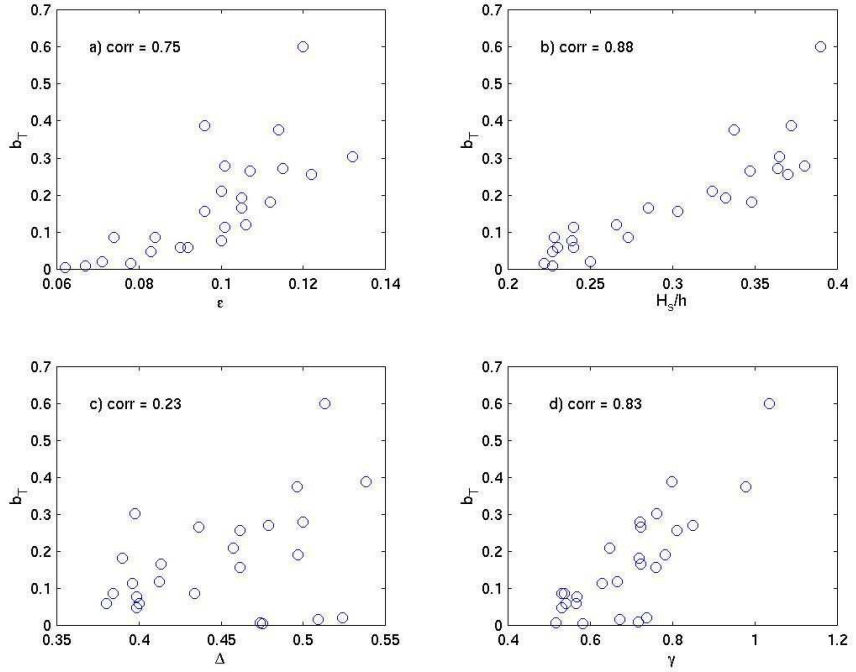

Fig. 5.22. Lake George dominant-wave breaking probability b_T versus (a) steepness ϵ_{peak} (5.13), (b) bottom interaction parameter H_s/d, (c) shear stress parameter Δ (5.17), and (d) non-dimensional peak frequency γ (5.16). The legend shows the correlation coefficient based on a linear best fit for each case.

where 90% confidence limits are shown.

For practical purposes, when information on the wind forcing and shear is not available, a simplified parameterisation can be used, in terms of wave and water-depth characteristics only:

$$b_T = 85.1^{+37.9}_{-26.2}[(\epsilon_{peak} - 0.055)(1 + H_s/d)]^{2.33^{+0.25}_{-0.21}}. \tag{5.21}$$

This dependence is shown in Figure 5.24 and provides a reasonable linear correlation of 0.81 within the range of the data available.

Now, the comparison of this dominant-waves spectral breaking probability with the distance-to-breaking of the monochromatic wave trains (5.9) can be conducted. The breaking process is an individual-wave phenomenon, whereas for applications some spectral value of the steepness is needed. Therefore, establishing a link between parameterisations of the breaking probability in terms of individual-wave steepness and in terms of spectral steepness, even if approximate, has a significant practical value.

As discussed in Section 5.1.4, since the quantities are not identical, comparison of the parameterisation (5.9) with field data can only be qualitative. In order to conduct the comparison, the Black Sea dataset of Babanin *et al.* [2001] was considered. Based on visual observations of whitecapping, this dataset provides information on the probability of breaking b_T of dominant waves (see Table 5.1). Dominant waves are defined in the spectral sense as those having frequencies near the spectral peak frequency f_p, i.e. $f = f_p \pm 0.3 f_p$ (2.6). In the present context, b_T can be approximately related to the non-dimensional distance to breaking N by

$$b_T \approx 1/N. \tag{5.22}$$

Tab. 5.1. Summary of Black Sea data used for the breaking-probability analysis. Here, f_p is the spectral peak frequency, H_s is significant wave height, U_{10} is wind speed at 10 m, ϵ_{peak} is the significant steepness of the spectral peak, $\Delta_{shear} = u_s/u_o$ is the shear parameter defined by ratio of the surface drift u_s to wave orbit u_o velocity, $\tilde{f}_p = \frac{U_{10} f_p}{g} = \frac{1}{2\pi}\frac{U_{10}}{c_p}$ is the non-dimensional peak frequency or the parameter of the inverse wave age, and b_T is the spectral peak breaking probability (2.3).

Run	f_p, Hz	H_s, m	U_{10}, m/s	ϵ_{peak}	Δ_{shear}	$\tilde{f}_p$	b_T
6	0.36	0.39	11.7	0.085	0.318	0.430	0.038
7	0.34	0.49	12.7	0.099	0.280	0.441	0.065
9	0.30	0.53	14.0	0.080	0.336	0.428	0.060
10	0.31	0.54	14.4	0.084	0.341	0.455	0.052
11	0.44	0.38	15.0	0.120	0.344	0.657	0.063
13	0.39	0.45	14.6	0.114	0.320	0.581	0.067
14	0.41	0.45	13.7	0.126	0.285	0.571	0.084
16	0.17	1.19	8.4	0.062	0.148	0.146	0
18	0.16	1.32	11.2	0.058	0.198	0.183	0
211	0.16	0.83	9.5	0.032	0.303	0.154	0
238	0.17	0.89	10.7	0.040	0.293	0.186	0
242	0.27	0.99	10.0	0.124	0.139	0.274	0.034
244	0.25	0.88	8.7	0.093	0.152	0.224	0.058

Figure 5.17 (bottom) shows $1/b_T$ as a function of the peak spectral steepness (5.13). An approximation to the data shown in the Figure, consistent with the functional form of relationship (5.20) between N and IMS is

$$\frac{1}{b_T} = -10\text{atanh}(13.3(\epsilon_{peak} - 0.13)) + 17, \text{ for } 0.055 \leq \epsilon_{peak} \leq 0.205. \tag{5.23}$$

The lower limit (no breaking if $\epsilon_{peak} < 0.055$) is obtained from the experimental data [Banner *et al.*, 2000, Babanin *et al.*, 2001] and the upper limit ($\epsilon_{peak} = 0.205$) is obtained by extrapolating

Tab. 5.2. Summary of Lake George data used for the breaking-probability analysis. Here, f_p is the spectral peak frequency, H_s is significant wave height, U_{10} is wind speed at 10 m, ϵ_{peak} is the significant steepness of the spectral peak, $\Delta_{shear} = u_s/u_o$ is the shear parameter defined by ratio of the surface drift u_s to wave orbit u_o velocity, $\tilde{f}_p = \frac{U_{10} f_p}{g} = \frac{1}{2\pi}\frac{U_{10}}{c_p}$ is the non-dimensional peak frequency or the parameter of the inverse wave age, d is water depth and b_T is the spectral peak breaking probability (2.3).

	Run	f_p, Hz	H_s, m	U_{10}, m/s	ϵ_{peak}	Δ_{shear}	$\tilde{f}_p$	H_s/d	b_T
1	311501.oc7	0.48	0.21	11.0	0.078	0.509	0.672	0.222	0.016
2	311615.oc7	0.48	0.17	8.5	0.059	0.474	0.517	0.178	0.007
3	311638.oc7	0.49	0.17	9.4	0.062	0.475	0.581	0.183	0.005
4	311757.oc7	0.42	0.35	17.1	0.114	0.496	0.977	0.337	0.375
5	311823.oc7	0.36	0.45	19.8	0.120	0.513	1.035	0.410	0.600
6	311845.oc7	0.33	0.40	15.0	0.096	0.538	0.797	0.372	0.388
7	311908.oc7	0.35	0.37	12.9	0.101	0.500	0.721	0.380	0.279
8	311930.oc7	0.38	0.34	12.8	0.107	0.436	0.723	0.347	0.265
9	311958.oc7	0.39	0.33	11.5	0.100	0.457	0.646	0.324	0.210
10	312021.oc7	0.40	0.39	13.7	0.132	0.397	0.761	0.365	0.303
11	312048.oc7	0.37	0.37	13.1	0.112	0.390	0.718	0.348	0.182
12	312111.oc7	0.40	0.25	9.3	0.074	0.434	0.536	0.290	0.087
13	312207.oc7	0.48	0.20	8.5	0.083	0.399	0.532	0.227	0.047
14	312232.oc7	0.50	0.22	9.0	0.100	0.399	0.568	0.239	0.077
15	312254.oc7	0.49	0.22	9.1	0.092	0.380	0.565	0.240	0.058
16	312316.oc7	0.49	0.21	8.6	0.084	0.384	0.532	0.228	0.086
17	312339.oc7	0.50	0.21	8.6	0.090	0.400	0.541	0.230	0.060
18	010004.no7	0.52	0.22	9.8	0.101	0.396	0.629	0.240	0.113
19	010030.no7	0.48	0.24	10.7	0.106	0.412	0.665	0.266	0.119
20	010055.no7	0.46	0.26	11.8	0.105	0.414	0.723	0.285	0.165
21	010140.no7	0.43	0.28	12.6	0.096	0.461	0.759	0.303	0.157
22	010204.no7	0.40	0.31	13.3	0.105	0.497	0.782	0.332	0.192
23	010226.no7	0.40	0.35	13.9	0.122	0.461	0.810	0.370	0.257
24	010248.no7	0.39	0.35	14.8	0.115	0.479	0.850	0.364	0.271
25	151238.de7	0.48	0.19	11.1	0.067	0.573	0.716	0.227	0.009
26	151301.de7	0.45	0.21	11.8	0.071	0.524	0.737	0.250	0.021

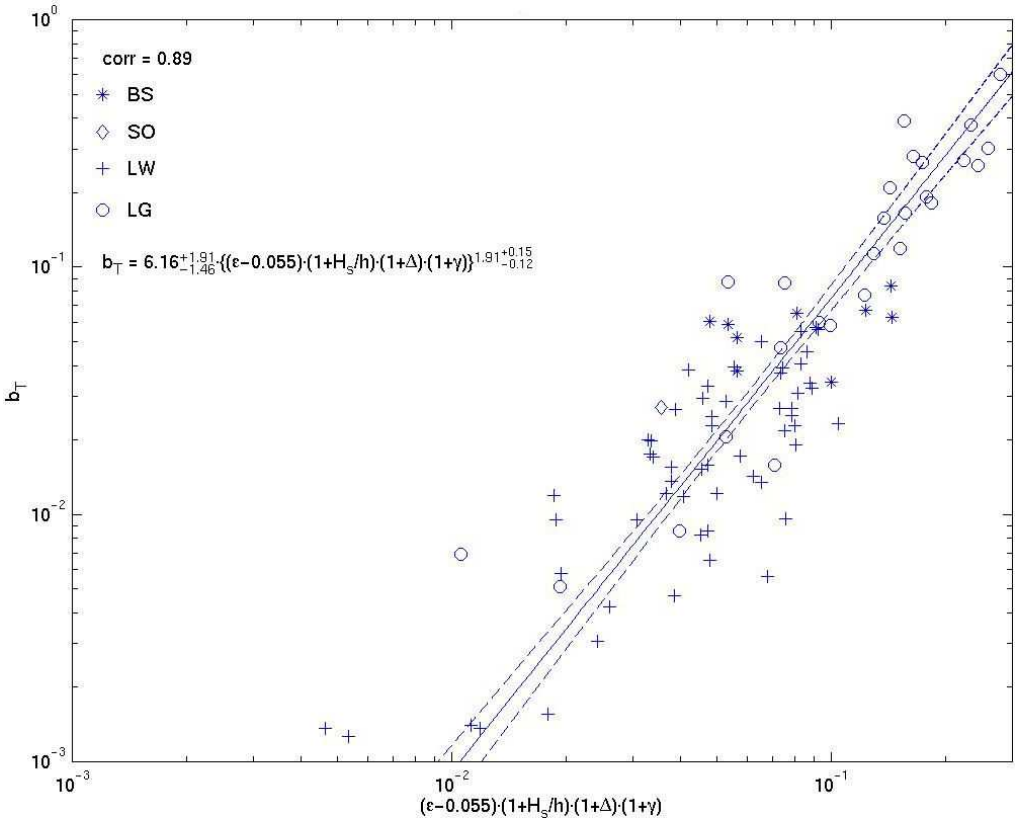

Fig. 5.23. Combined log-log plot of the observed dominant-wave breaking probability b_T versus the modified significant peak steepness adjusted for the water-depth, wind-forcing and shear-current influences. Four diverse field sites are shown: Black Sea (BS), Southern Ocean (SO), Lake Washington (LW) (all deep water), and Lake George (LG) (finite depth). The legend shows the correlation coefficient based on a linear best fit in the log-log domain together with the parameterisation (5.20) and the $\pm 90\%$ confidence limits.

the parameterisation developed in Babanin *et al.* [2001] to the 100% breaking condition.

Thus, we conclude that the distance before breaking occurs, which is related to the breaking probability, is a function of the background mean wave steepness in the wave train/field. In the latter case, this concept/analogy can only be applied to the dominant waves. Other potential method of estimating the breaking rates of dominant waves, based on measurements of ensemble-average asymmetry (1.3) in the wave trains, without having to actually detect the breaking events, will be discussed in Section 5.4 below, see eqs. 5.43, 5.44. Breaking of relatively short waves, i.e. waves of scales smaller than the dominant waves, will be discussed in the next Section 5.3.2.

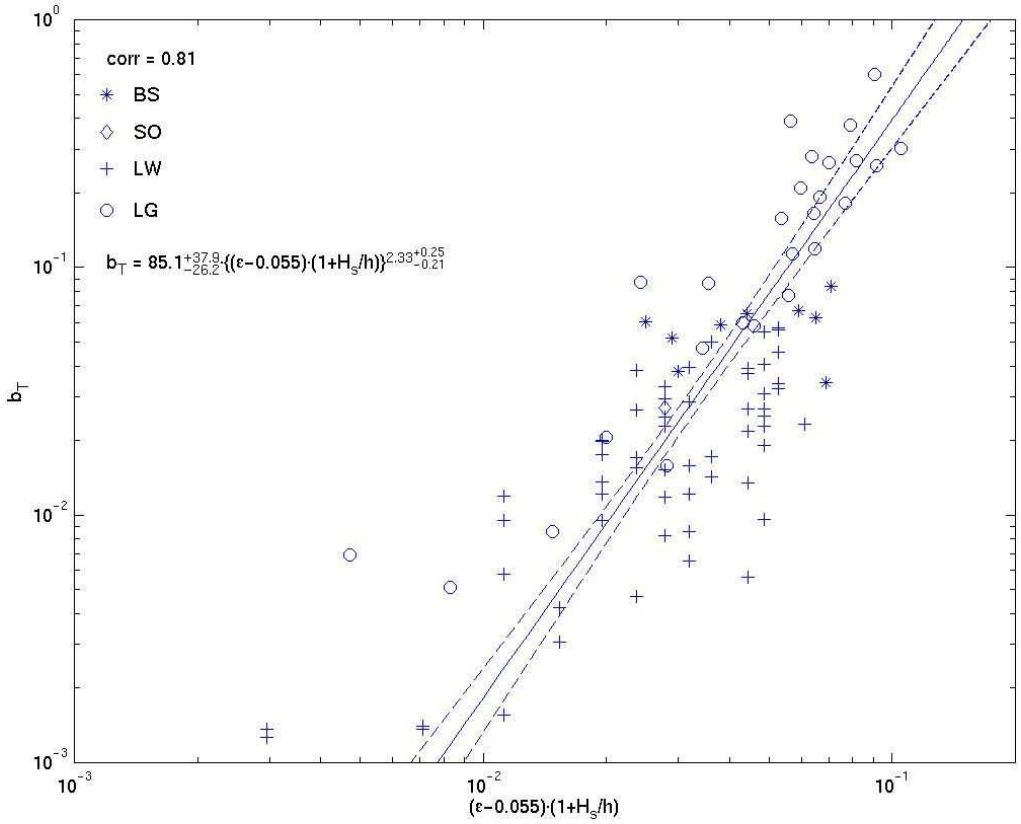

Fig. 5.24. Combined log-log plot of the observed dominant wave breaking probability b_T versus the modified significant peak steepness adjusted for the water depth $(\epsilon - 0.055)(1 + H_s/h)$ (5.21). Four diverse field sites are shown: Black Sea (BS), Southern Ocean (SO), Lake Washington (LW) (all deep water), and Lake George (LG) (finite depth). The legend shows the correlation coefficient based on a linear best fit in the log-log domain together with the parameterisation and the $\pm 90\%$ confidence limits.

5.3.2 Breaking probability of small-scale waves

Lately, frequency distribution of the breaking probability $b_T(f)$ (2.4) has been a sought after function [e.g. Ding & Farmer, 1994, Phillips *et al.*, 2001, Banner *et al.*, 2000, 2002, Melville & Matusov, 2002, Gemmrich, 2006]. There is an expectation in the wave-modelling community that, once some universal function for $b_T(f)$ is obtained, such parameterisation will provide a major step forward towards an experimental, rather than speculative dissipation function.

Breaking of small-scale waves, however, apart from inherent reasons such as modulational instability or linear focusing, can be affected by longer waves. As a result, parameterisation of the breaking rates at some short-wavelength is problematic, if not impossible in terms of steepness of those short waves or spectral density at the respective wavelength. Here, as the short/small-scale we mean waves with temporal and spatial scales smaller than those of the dominant waves in a

wave field.

There is a number of ways in which the long waves can affect the breaking of shorter waves. One of them is modulation of the train of the short waves riding the underlying large-scale waves. The latter compress the short-wave lengths at their front face and extend those at the rear face. As a result, the front-face small waves become steeper and frequently break [Donelan, 2001]. In absence of the underlying long waves, the breaking due to the regular reasons would be much less frequent.

Another reason is breaking of the large waves [Banner *et al.*, 1989, Tulin & Landrini, 2001, Manasseh *et al.*, 2006, Young & Babanin, 2006a]. This is how Tulin & Landrini [2001] describe the short waves in such circumstance: "As we have observed in our large wind-wave tank, the growth of these waves is much effected by the existence of breaking energetic waves, which not only modulate the microbreakers, but virtually eliminate them as the microbreaker train is overcome by the energetic breaker at the peak of the wave group. It would seem, observing this striking phenomenon, that it is the action of the energetic breakers which causes the microbreakers to disappear, and that they begin growing again from very short waves. Their eventual length is thus determined by the effective fetch between energetic breakers."

The quoted observational description is helpful in many regards. First of all, while it is mentioned in definite terms that the short waves are eliminated, it is not explicitly said that these microwaves actually break too. In principle, they can be dissipated without breaking, because of interaction, for example, with the turbulent wake of the large breaker [e.g. Banner *et al.*, 1989]. In this regard, it is difficult if not impossible to separate the small-scale breaking and small-scale wave-energy dissipation.

The quote also points out that, in presence of frequent large breaking, for the short waves the induced breaking/dissipation dominates. Indeed, the small-scale waves only exist between the large breakers and their breaking/dissipation is determined by their effective fetch between such breakers, regardless physics which would drive them to the breaking inherently. This is the so-called cumulative effect, very important for the spectral dissipation of wind waves. This effect signifies the fact that breaking/dissipation of short waves of a certain small scale above the peak in the wave spectrum is determined by the integral of the wave spectrum below this scale, rather than by the value of the spectral density at this particular frequency/wavenumber [Babanin & Young, 2005, Manasseh *et al.*, 2006, Young & Babanin, 2006a, Babanin *et al.*, 2007c].

Quantitative observations, and particularly parameterisation of the breaking probability of the short spectral waves are not very many. This is primarily due to difficulties of detecting the small breaking and of separating the dominant breaking and small breaking, particularly as the latter is often correlated or even linked to the large breaking as mentioned above.

One of the first clear experimental evidences of the spectral distribution of the breaking events was provided by Gemmrich & Farmer [1999] in terms of rate of occurrence of breaking events with different phase speeds. Banner *et al.* [2000] showed results on frequency distribution of the breaking probability based on information gathered in the Black Sea data set. 2121 individual breakers of the 13 records listed in Table 5.1 were analysed. The sampling frequency of 4 Hz allowed us to compile frequency distributions for the breakers as histograms over the range from f_p to twice the peak frequency $2f_p$. Binning of breaking event probabilities was carried out for $\pm 15\%$ constant percentage wavenumber bands centred on $k_p, 1.35k_p, 1.83k_p, 2.48k_p$ and $3.35k_p$, thereby covering the wavenumber range k_p to $4k_p$ or equivalently, the frequency range f_p to $2f_p$.

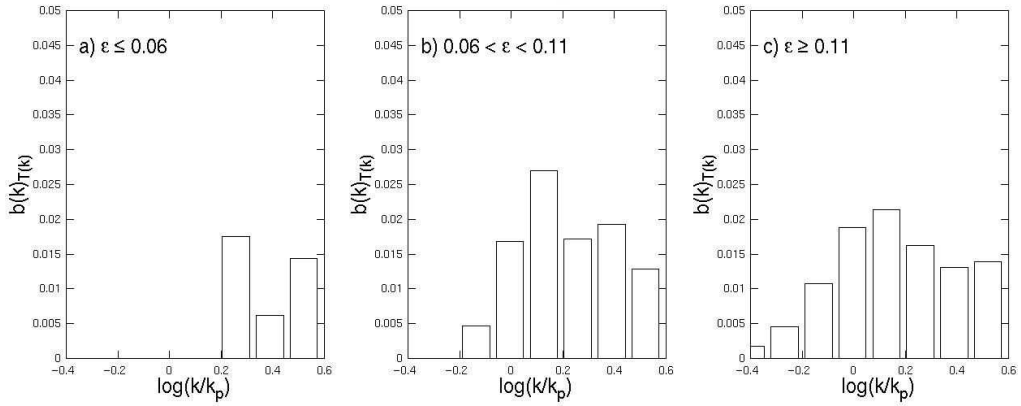

Fig. 5.25. The shift towards the spectral peak of the histogram of the breaking probability as a function of the mean steepness in each $\pm 15\%$ relative wavenumber bin. (a) for $\epsilon_{peak} < 0.06$ (corresponding to well-developed seas) breaking occurs well above the spectral peak. For the steeper seas in (b) $0.06 < \epsilon_{peak} < 0.11$ and (c) $\epsilon_{peak} > 0.11$, the histogram peak moves towards the spectral peak.

Figure 5.25 shows how the peak of the breaking probability distribution shifts from well above the spectral peak to close to the spectral peak as the dominant wave slope ϵ_{peak} increases. This is consistent with the findings of Ding & Farmer [1994] who found from their relatively old wind-sea conditions that the mean breaking event speed is considerably smaller than the phase speed of the dominant wind seas. It also follows the trend reported by Gemmrich & Farmer [1999], who observed that the peak of the normalised breaking frequency distribution was located well above the spectral peak frequency for typical mature wind seas.

While negligible breaking is observed at the spectral peak for the wave fields with $\epsilon_{peak} < 0.06$, the wave breaking occurs at higher wavenumbers (Figure 5.25a). If the peak steepness $0.06 < \epsilon_{peak} < 0.11$ is higher, the wave breaking histogram moves closer to the spectral peak (Figure 5.25b), and even below the peak at $\epsilon_{peak} > 0.11$ (Figure 5.25c).

For standard unimodal spectral shape, which occurs under simple wave-development condition, e.g. JONSWAP spectrum (2.7), the peak steepness ϵ_{peak} can be related to the wind forcing or inverse wave age U_{10}/c_p. That is, for young waves, frequent breaking of the dominant waves is expected, whereas old dominant waves will not be breaking at all. As mentioned above, this is consistent with other observations [i.e. Ding & Farmer, 1994, Gemmrich & Farmer, 1999], but it has to be kept in mind that generally speaking the breaking parameter ϵ_{peak} is not unambiguously related to the wave age. Waves of the same nominal wave-development stage U_{10}/c_p may have quite different values of ϵ_{peak} due to a variety of circumstances, for example due to presence of swell which is quite typical for the open oceans. These could lead to different breaking probabilities at the spectral peak and different breaking frequency distributions.

In Banner *et al.* [2000] and later in Banner *et al.* [2002], attempts were made to draw a dependence, similar to (5.20) through a selection of frequency bins at scales smaller than the spectral peak. Since there is no characteristic bandwidth at these small scales, a selection of different Δf in (2.5) were applied in order to define a characteristic spectral steepness ϵ in those

spectral bins. Even then, adjustments to the shape of the spectral windows and to the threshold values had to be made. Since parameterisation (5.20) is quadratic in terms of the wave steepness, it should be expected linear if expressed through some spectral-density measure.

In this regards, two issues have to be clarified here. Absence of the characteristic bandwidth away from the spectral peak is not a merely technical question, this is a physical problem. As mentioned above, the modulational instability mechanism cannot be active in the broad-banded process which the small-scale waves are. Even if the induced-by-long-waves breaking of short waves is disregarded, this means that physics of the breaking at the shorter scales is altered compared to the dominant waves.

The induced breaking, however, cannot be disregarded as it is significant already close the spectral peak and apparently becomes dominant at higher frequencies/wavenumbers. In Manasseh *et al.* [2006], the bubble-detection method described in Section 3.5 was applied to the Lake George wave-breaking data in order to estimate the breaking probability at wave frequencies beyond the spectral peak, and to obtain the distribution of breaking probability $b_T(f)$ (2.4) with wave frequency. To do that, the number of waves at each frequency $N(f)$ was redefined. As discussed in Section 2.5, if the waves are counted by the zero-crossings, the resulting count $N_c(f)$ will be less than the nominal reference count $N(f)$ given by (2.13), because in real seas, waves of periods different to $1/f$ will occupy some part of the record. The breaking probability b_T used by Manasseh *et al.* [2006] was defined as

$$b_T(f) = \frac{n(f)}{N_c(f)}, \tag{5.24}$$

where $N_c(f)$ is the number of waves counted by the zero-crossing analysis within the bandwidth

$$f = f_c \pm 0.1 f_p, \tag{5.25}$$

with the set of central frequencies being

$$\frac{f_c}{f_p} = 0.8,\ 1.0,\ 1.2,\ 1.4,\ 1.6,\ 1.8,\ 2.0. \tag{5.26}$$

Shown in Figure 5.26 is the wave power spectrum created from the surface-elevation data, and the breaking probability, b_T as a function of wave frequency for a 19.8 m/s wind speed (rec. 5 of Table 5.2). The breaking distribution in the top panel of Figure 5.26 was normalised so that it matches the spectral density at the peak frequency. This was done purely to make comparison of the two curves easier. The $b_T(f)$ curve in the bottom panel is bracketed by two lines which are the calculated 95% confidence intervals on $b_T(f)$ [Walpole & Meyers, 1978]. Although the b_T curve only covers a fraction of the frequency spectrum, it is clear that the downward trend in breaking probability with wave frequency is statistically significant.

Figure 5.27 presents more derived analysis made possible by the passive acoustic method. Even though this Figure was only intended by Manasseh *et al.* [2006] to demonstrate the potential of the passive acoustic method, it is worth pointing out some apparent features of the breaking-probability frequency distributions which had hardly been examined experimentally before.

In this Figure, distributions of $b_T(f)$ (5.24) are plotted versus relative frequency f/f_p for records 5 through 11 of Table 5.2, which correspond to different wave spectra developed under different wind speeds. In Lake George's bottom-limited environment, well-developed and even

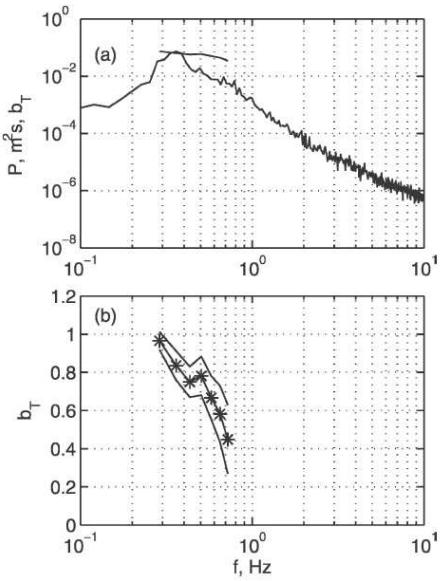

Fig. 5.26. Wave power spectrum and breaking probability versus wave frequency f. a) Wave power spectrum $P(f)$. Normalised breaking probability from the bottom subplot is also shown; b) Wave-breaking probability $b_T(f)$ (5.24).

fully developed waves can be still strongly forced [Young & Babanin, 2006b] and therefore are expected to break at the spectral peak.

Out of the six wave records analysed, only the first one (19.8 m/s mean wind speed), corresponds to full development for the given water depth [Young & Babanin, 2006b]. Therefore, although the waves are strongly forced, the wave spectrum will not develop further: the total wave energy will not grow and the spectral peak will not shift to lower frequencies. Since both the wind and the non-linear interactions keep pumping energy into those lower frequencies, it must be rapidly dissipated at these scales due to interaction of the longer waves with the bottom and subsequent breaking. This is seen from the upper curve in the top panel of Figure 5.27: nearly 100% breaking is measured for frequencies below the spectral peak.

Breaking rates $b_T(f)$ normalised by their respective spectral densities $P(f)$ are shown in Figure 5.27, bottom panel. At the spectral peak, these normalised breaking rates merge together very clearly, but they stay separated both above and below the peak. Thus, if there is a linear or quasi-linear dependence of b_T on $P(f)$, it would only be applicable at the spectral peak. Away from the spectral peak other influences make the dependence of b_T on $P(f)$ non-linear or affect this dependence in another way.

This uncertainty was investigated, based on the Lake George measurements, by Babanin & Young [2005], Babanin *et al.* [2007c]. They attempted to draw an analogy with findings of Banner *et al.* [2000], Babanin *et al.* [2001] for the spectral peak and sought a dependence of the breaking probability at different frequencies as a function of the so-called saturation density at

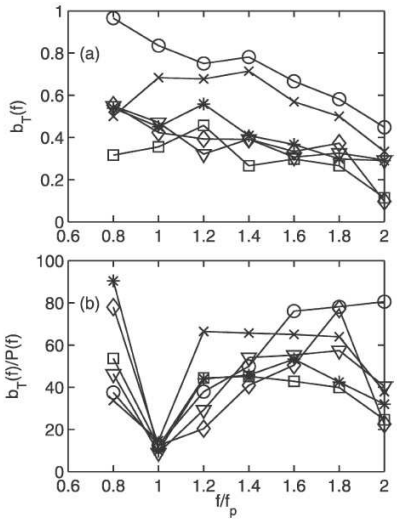

Fig. 5.27. Breaking probabilities versus wave frequency f normalised by the peak frequency f_p. a) $b_T(f)$ (5.24); b) b_T normalised by the spectral density $P(f)$. Squares: $12.8m/s$; *: $12.9m/s$; ∇: $13.2m/s$; diamonds: $13.7m/s$; $\times$: $15.0m/s$; circles: $19.8m/s$. The records are from Table 5.2.

that frequency, a spectral analogue of the squared wave steepness introduced by Phillips [1984]:

$$\sigma_{Phillips}(f) = \frac{(2\pi)^4 f^5 F(f)}{2g^2}. \tag{5.27}$$

In Babanin & Young [2005], Babanin *et al.* [2007c], the saturation $\sigma(f)$ was normalised by a directional spreading parameter:

$$\sigma(f) = \sigma_{Phillips}(f) A(f). \tag{5.28}$$

Here, $A(f)$ is the integral characteristic of the inverse directional spectral width introduced by Babanin & Soloviev [1987, 1998b]:

$$A(f)^{-1} = \int_{-\pi}^{\pi} K(f,\theta) d\theta \tag{5.29}$$

where θ is the wave direction, $K(f,\theta)$ is the normalised by its maximum-value directional spectrum:

$$K(f,\theta_{maximum}) = 1. \tag{5.30}$$

Normalisation by the directional spreading was brought in by Banner *et al.* [2002], who also investigated breaking probability across the frequency as a function of the saturation spectrum. The normalisation seemed needed in order to explain why the wave-breaking threshold which they observed is not universal in terms of the saturation density values. As will be shown below,

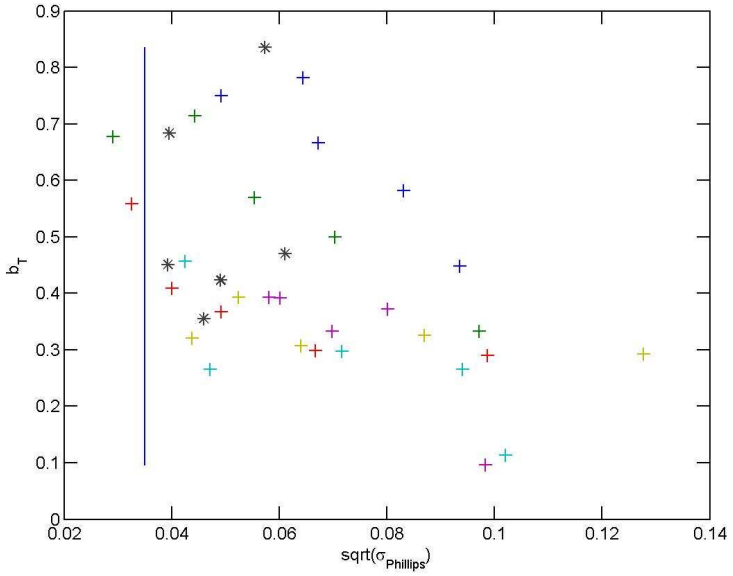

Fig. 5.28. Breaking probability $b_T(f)$ (2.4) versus saturation parameter $\sqrt{\sigma_{\mathrm{Phillips}}(f)}$. Asterisks denote spectral peak points. Threshold $\sigma_{\mathrm{Phillips}} = 0.035$ is shown with the solid line.

results of Banner *et al.* [2002] must have been influenced by the cumulative effect and the directional normalisation is in fact not necessary. In Babanin & Young [2005], Babanin *et al.* [2007c], values of A were

$$A(f) \approx 1, \tag{5.31}$$

and therefore the normalisation did not impact the value of the universal threshold significantly. In principle, however, its estimate had to be revisited.

In Figure 5.28, the revisited plot of the breaking probability $b_T(f)$ (2.4) versus $\sqrt{\sigma(f)_{Phillips}}$ instead of $\sqrt{\sigma(f)}$ is shown. $\sqrt{\sigma_{Phillips}}$ rather than $\sigma_{Phillips}$ is used to provide a qualitative analogy with Figures 5.22-5.25 where spectral steepness ϵ was employed. Asterisks denote the spectral peak values, crosses are all the other data points from the frequency range (5.26). Based on such figure, Babanin & Young [2005], Babanin *et al.* [2007c] concluded that the saturation (5.27)-(5.28) is not the most suitable parameter for wave-breaking dependences. It is not possible to draw a general dependence through the data cloud in the Figure with any degree of certainty. The saturation is the firth moment of the spectrum, and any variations of the spectral shape, particularly at higher frequencies, cause large scatter of this characteristic.

As a threshold property, however, the saturation produced quite a robust value. When tuned in the spectral model [Babanin *et al.*, 2007d], the threshold was chosen as

$$\sqrt{\sigma(f)_{threshold}} = 0.035, \tag{5.32}$$

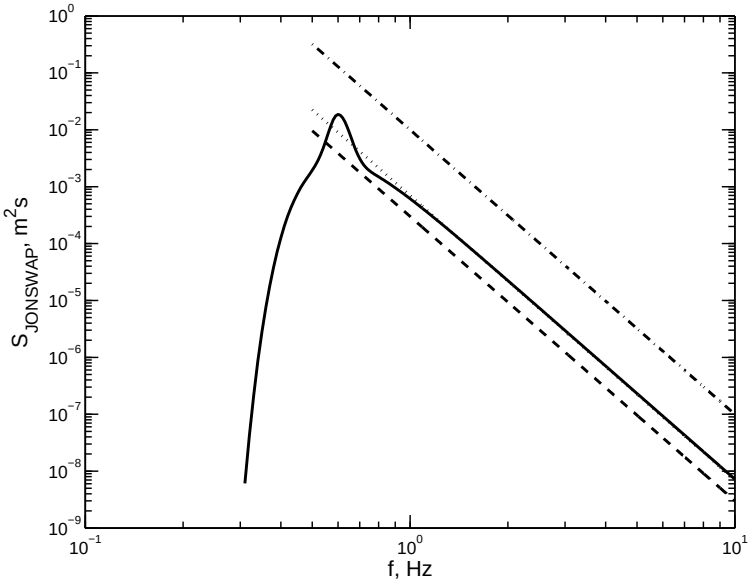

Fig. 5.29. Illustration. JONSWAP spectrum (2.7) is shown with solid line (peak enhancement of $\gamma = 7$ is chosen for clarity), zero breaking saturation level with dashed line, 5% breaking level with dotted line and 100% breaking level with dash-dotted line. The breaking limits are drawn qualitatively for illustration purposes only and must not be used for estimates.

with only a few outliers below this value, which is, in Figure 5.28, also suitable as the revised threshold $\sqrt{\sigma(f)_{Phillips_{threshold}}}$.

Since a universal dimensionless saturation-threshold value $\sigma_{threshold}$ can be established, the dimensional threshold can then be obtained at every frequency:

$$F(f)_{threshold} = \frac{2g^2}{(2\pi)^4} \frac{\sigma(f)_{threshold}}{A(f)f^5}. \tag{5.33}$$

Meaning of the dimensional threshold is illustrated in Figure 5.29.

In Figure 5.29, JONSWAP spectrum parameterisation (2.7, solid line) and arbitrary breaking limits are used for illustration purposes, but real spectra and breaking threshold exhibit similar behaviour [Babanin & Young, 2005, Babanin *et al.*, 2007c, Babanin & van der Westhuysen, 2008]. The dashed line indicates the dimensional threshold (5.33), and the dash-dotted line is the ultimate spectral limit in the saturation terms i.e. the spectral density cannot physically reach over this limit because steepness of waves will be such that all the waves will be breaking [Babanin *et al.*, 2007c]. If the spectral density drops below the dashed level, there will be no breaking in the wave field, but unless the waves are swell or forced by very light winds, they normally do exhibit some breaking. The spectrum drops below this limit in its front face which signifies the obvious knowledge that waves, which are longer than the dominant ones in the wind-wave spectrum, do not break.

Therefore, wave spectra exist between these two lines. The dotted line indicates 5% breaking

rate. As it is known, at typical moderate deep-water conditions breaking rates are of the order of a few percent [e.g. Babanin *et al.*, 2001, also Figure 5.23]. Thus, in a typical wave spectrum, the spectral density corresponding to the small/short waves is somewhat above the dimensional threshold (5.33), approximately at the position indicated by the dotted line in Figure 5.29. This means that inherent breaking in trains of such waves is active, and the rate of such inherent breaking is determined by the degree of excess of the real spectrum above the dashed threshold level at each frequency. The induced breaking, however, alters such simply-derived breaking rates and in fact tends to dominate at smaller scales away from the spectral peak.

Let us try to apply the threshold value (5.33) to experimental data in order to test the breaking probabilities in different frequency bins in dimensional terms. Indeed, while the overall scatter in Figure 5.28 is prohibitive, data points for the spectral-peak bin (asterisks) exhibit a reasonable correlation as a function of the saturation spectrum. In Figure 5.30, the Lake George data, in a search of the dependence of $b_T(f)$ on wave spectrum $F(f)$, are separated into narrow spectral bins

$$f_i = f_p + 0.2if_p \pm 0.1f_p \tag{5.34}$$

with $i = 0, 1, ...4$, i.e. starting from the spectral peak. Only records with breaking rates in excess of 2% across all the frequencies were chosen to avoid bias due to zero-breaking contributions when the rates are low. A Riding Wave Removal (RWR) procedure [Schulz, 2009] was used to identify periods of the breaking waves. The standard zero-crossing analysis becomes naturally noisier towards higher frequencies when the riding shorter waves may not necessarily cross the mean level. The RWR technique works, once the bubble detection signals a breaking, by finding the shortest riding waves first, and then removing all of them from the signal before re-processing the signal to look for the next largest riding waves.

At the spectral peak (first panel), consistent with the two-phase behaviour of the breaking/dissipation discussed above, dependence in terms of the wave spectrum is linear:

$$b_T \approx 2(F - F_{threshold}). \tag{5.35}$$

If, however, this dependence, as shown with solid lines in subsequent subplots, is applied to the breaking rates at higher frequencies, it exhibits a progressively larger underestimation. Such result is fully consistent with our expectations that follow from the documented cumulative behaviour. Inherent (linear) dependence of the wave breaking rates on the spectrum excess should be present at each frequency. However, at every next frequency away from the spectrum, the contribution of the induced breaking (due to waves breaking at lower frequencies) has to become progressively larger. (It should also be kept in mind that dependence (5.35) is dimensional, and the dimensional values of $F(f)$ decrease away from the spectral peak).

What happens if the cumulative effect is disregarded, as it is now in most of breaking/dissipation parameterisations? As seen in in Figure 5.30, it would still be possible to draw a linear dependence in each frequency bin, but at every subsequent frequency such dependence will become steeper and the intersect will move further from the origin (i.e. the threshold value will be growing). This is exactly what was done, for example, in Banner *et al.* [2002].

In the case of Figure 5.30, the universal threshold value has been already subtracted at the bottom scale, and therefore all the dependences have to go through the zero. If we now try to fit a best power function at each frequency, this will result in a quadratic function at $f = 1.2f_p$,

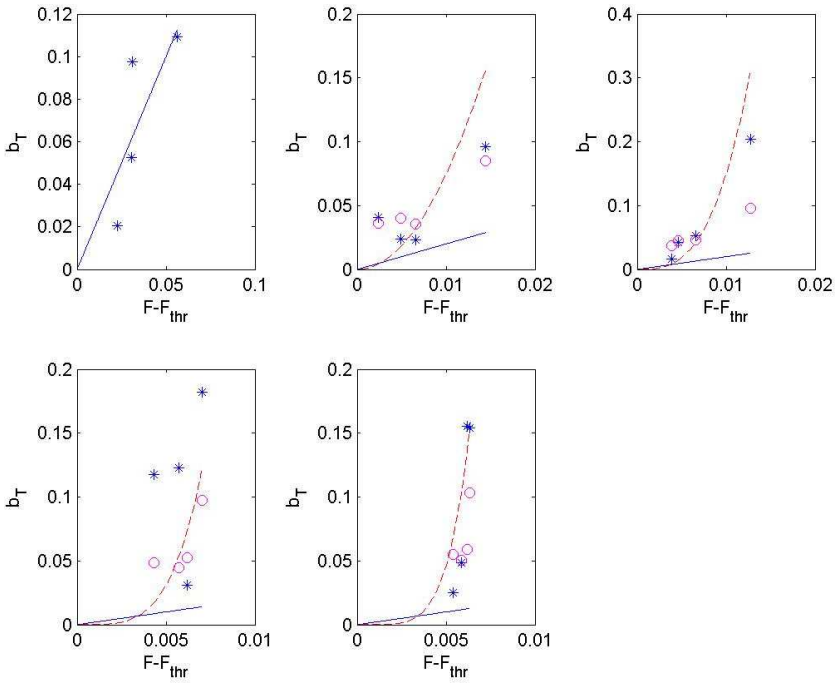

Fig. 5.30. Breaking probabilities (from left to right) for frequencies of $f_p, 1.2f_p, 1.4f_p, 1.6f_p, 1.8f_p$ in the $\pm 0.1 f_p$ frequency range. Solid line in all plots identifies the linear dependence obtained in the first panel. Dashed lines, from left to right, are $b_T \sim (F - F_{threshold})^2, b_T \sim (F - F_{threshold})^3, b_T \sim (F - F_{threshold})^4, b_T \sim (F - F_{threshold})^5$. Circles in the higher-frequency bins are estimates of the breaking probability based on accounting the cumulative effect (5.37).

a cubic function at $f = 1.4f_p$, a fourth power at $f = 1.6f_p$, and a fifth power at $f = 1.8f_p$ as shown in the Figure.

Thus, fitting some functions expressed in terms of local spectral density at each frequency can be done across the spectrum as a matter of tuning, but as a matter of physics such approach appears to be misleading. Moreover, fitted once the dependences will not necessarily work for another wave spectrum, where amount of induced breaking is different. In our view, there are no simple algebraic dependences for the spectral breaking/dissipation, and integral functionals have to be employed to account for the cumulative contributions across the spectrum. A parametric form which accounts for such functional was suggested for the wave-breaking dissipation function S_{ds} (2.21) by Babanin & Young [2005], Young & Babanin [2006a], Babanin *et al.* [2007c,d]:

$$\begin{aligned} S_{ds}(f) &= -a_1 \rho_w g f \left[F(f) - F_{threshold}(f)\right] A(f) \\ &- a_2 \rho_w g \int_{f_p}^{f} \left[F(q) - F_{threshold}(q)\right] A(q) dq. \end{aligned} \tag{5.36}$$

Here a_1 and a_2 are experimental coefficients yet to be comprehensively estimated [Young &

Babanin, 2006a, Tsagareli, 2009].

It should be reminded that S_{ds} is not a function for the breaking probability only, but is a dissipation function which combines contributions of the breaking probability and breaking severity (see (2.20)-(2.21) for definitions and Sections 2.7 and 6 for discussions). With that in mind, it is clear how the breaking probability at smaller scales can be described mathematically.

Function (5.36) accommodates both the threshold behaviour and the cumulative effect. Inherent breaking is depicted by the first term on the right-hand side of (5.36), and the cumulative term by the second. Close to the spectral peak the first term dominates, and at the spectral peak the inherent breaking is the only breaking mechanism as the integral in the second term is zero. Away from the peak, the integral grows and, while the inherent breaking may persist throughout, the cumulative term will rapidly increase and become the dominant cause of the breaking at higher frequencies. These higher-frequency breaking rates are in fact influenced by the induced breaking already as close to the peak as $1.2f_p$, this can be seen in Figures 5.27 and 5.30.

Now, to prove that it is the cumulative effect which is working in Figure 5.30, at each higher-frequency bin of (5.34) the cumulation was estimated based on the spectral-peak wave-breaking approximation (5.35), i.e.

$$b_T(f_i) = 2\sum_{i=0}^{N}\left[F(f_i) - F(f_i)_{threshold}\right]. \tag{5.37}$$

Expression (5.37) implicitly assumes two things with respect to the higher frequency breaking: that is, an induced breaking at a high frequency occurs every time when a lower-frequency breaking takes place, and the inherent high-frequency breaking is driven by the same law as the spectral-peak breaking (5.35). The first assumption is true for the the wave-breaking dissipation [Young & Babanin, 2006a], but as have been discussed right above such dissipation is not exactly the same property as the breaking probability. For the breaking probability, the two assumptions need to be further verified, but we will use them here for the cumulation-feasibility check.

The (5.37)-estimated data points are shown in Figure 5.30 with circles. With the amount of uncertainty involved, they agree remarkably well with the measurements and with the local-in-frequency-space dependences which fit these measurements, and therefore provide a very strong corroboration of the cumulative effect, which in fact was estimated here in a quite simple way defined by (5.37).

Other mathematical and physical expressions for the cumulative terms are possible of course [e.g. Donelan, 2001], but one way or another these breaking-probability functions/parameterisations have to include integral functionals, rather than be a function of spectral density or other distributed property local in frequency/wavenumber space. The cumulative term has a principal importance, particularly as the contribution of the inherent breaking becomes so small at shorter scales that it renders little connection between $b_T(f)$ and wave spectrum $F(f)$ to an extent that the inherent breaking can in fact be neglected.

5.4 Directional waves and changes to the frequency-directional spectrum of waves due to breaking

Waves on the ocean surface are directional, i.e. three-dimensional, and this is their principal feature. Apart from cases of pure swell, which appears indirectional and even monochromatic but

due to its low steepness has little relevance as far as the wave breaking is concerned, the oceanic wind-generated and wind-forced waves are characterised not only by continuous distribution of their energy along temporal/spatial (or frequency/wavenumber) scales, but also along directions θ [see e.g. (5.29)-(5.30) and Donelan *et al.*, 1985, Babanin & Soloviev, 1987, 1998b].

This is obviously true with respect to all the other wave-related scale-distributed properties and characteristics, including the wave-breaking probability, severity and the dissipation term. These functions are spectra, i.e. describe distribution of the respective properties along frequencies/wavenumbers, and should describe the distribution along directions too. That is the breaking probability in (2.4), technically speaking, should be:

$$b_T(f,\theta) = \frac{n(f,\theta)T}{t} = \frac{n(f,\theta)}{N(f,\theta)} \tag{5.38}$$

and the dissipation in (2.20)

$$D(f,\theta) = b_T(f,\theta)E_s(f,\theta). \tag{5.39}$$

Here, $n(f,\theta)$, for example, is a number of breaking crests in the frequency bin $f \pm \Delta f$ and directional bin of $\theta \pm \Delta\theta$.

Little is known about these breaking-related directional distributions, to such an extent that the dissipation function $S_{ds}(f,\theta)$ (2.24) in wave forecast models is routinely treated as an isotropic function. It is hard to imagine an isotropic energy sink, however, where all the other acting spectral sources have quite defined directional distributions, and there are experimental evidences that the dissipation term is also anisotropic and perhaps even bimodal.

Spectrogram method developed by Babanin *et al.* [2001] and described in Section 3.5 was used by Young & Babanin [2006a] to investigate difference between pre-breaking and post-breaking wave spectra. Such difference, when attributed to the breaking, should clarify spectral contribution of the breaking, including directional distribution of such contribution.

For the analysis, a wave record with an approximately 60% dominant-breaking rate was chosen (record 5 in Table 5.2). This was as close as possible to a 50% rate which would mean that half of the time waves within a single stationary record were breaking and half of the time waves were recovering from the breaking loss. The 50% division of the record into breaking/non-breaking parts enabled Young & Babanin [2006a] to estimate spectra of breaking and non-breaking waves with similar confidence limits. The waves were stationary (scatter of 1 min standard-deviation surface elevation, relative to the 20 min mean, was less than 10%, with no drift of the mean) under steady $U_{10} = 19.8$ m/s wind, with peak frequency $f_p = 0.36$ Hz and significant wave height $H_s = 0.45$ m. The parameterisations of Young & Verhagen [1996], Young & Babanin [2006b] were used to verify that the waves were fully developed in the bottom-limited environment with the measured depth of $d = 1.1$ m. The wave record was 20 min-long and was segmented into 5 breaking parts and 4 non-breaking parts.

In this strongly-forced situation, approximately half the waves were actively breaking. It was assumed that those waves not breaking, had recently done so, having lost their energy in the breaking process. Such assumption seems reasonable in this highly-forced but steady-in-the-mean environment and the analysis which follows is predicated on this assumption.

Models of wind waves, both physical and numerical, implicitly accept a double-scale approach to the wave field [see e.g. Melville, 1994, Lavrenov, 2003]. This implicit assumption is

important for correct interpretation and treatment of the wave breaking, and we shall discuss it here referring to the Radiative Transfer Equation (Section 2.10) which is routinely employed in the wave spectral modelling.

At long scales of thousands of wavelengths and periods, the waves are assumed to be evolving. In a general case, at this scale the left-hand side derivative in (2.56) is positive as the waves grow under wind forcing. If the wave field is stationary and characterised by constant-depth (or deep) conditions, the evolution along the wave fetch is described by the advective term on the left-hand side of (2.56) which is small (less than 5% according to Donelan [2001]) compared to the wind input S_{in} and the dissipation S_{ds} on the right-hand side. The energy transfer across the spectrum due to the non-linear term S_{nl} becomes essential at the scales of thousands and tens of thousands of wave periods [Hasselmann, 1962, Zakharov, 1968]. In our case of a stationary fully-developed constant-depth wave environment, the full derivative is zero and the right-hand-side terms of (2.56) are balanced.

At medium scales of hundreds of wavelengths, the wave fields are usually assumed to be stationary and homogeneous. Time/space series of surface elevation in such waves are used to obtain statistically reliable estimates of wave spectra in experiments, and spectra of this averaging scale are used in wave forecast and research spectral models. Such models have been reasonably successful and this, to some extent, justifies the assumption.

Indeed, the small advective terms and S_{nl} are not capable of bringing about significant changes to the wave spectrum at such time scales. For the dissipation term controlled by wave breaking, however, the scale of hundreds of waves is not small. For example, laboratory experiments on unsteady deep-water breaking by Rapp & Melville [1990], Babanin *et al.* [2009a] show that the breaking is a rapid process of the same order of magnitude in time as the wave period and may cause a major energy loss from the wave group where the breaking occurs. If, within the measurement time-span of hundreds of waves, each wave breaks even once, changes to the spectrum will be significant. Such dramatic losses of energy, however, are not observed at these time scales since the breaking rates are typically not very large [Holthuijsen & Herbers, 1986, Babanin *et al.*, 2001, among others] and, at this time scale, the wind input is apparently capable of restoring the mean spectrum after breaking. This also means that, at this time scale, energy input by the wind is a slower process than the energy loss from breaking, as the energy is input to every wave in the field, whereas it is only lost from a small fraction of the breaking waves.

There are points of view that the spectral models based on the medium-scale averaging of the wave fields may have reached their limit in accuracy with which they can simulate realistic wave-generation and growth conditions [e.g. Liu *et al.*, 1995]. This can be, in part, due to the fact that they average out variations of the wave field at scales of several waves (wave group scale). It is this shorter-scale group structure which plays a major role in intermittent wave breaking [Donelan *et al.*, 1972, Holthuijsen & Herbers, 1986, Babanin, 1995, Banner *et al.*, 2000, Babanin *et al.*, 2007b, 2009a] and modulation of the wind stress [Skafel & Donelan, 1997]. There is modulation of the surface roughness at even shorter scales of dominant waves [Hara & Belcher, 2002, Kudryavtsev & Makin, 2002] and over breaking waves [Babanin *et al.*, 2007b], and disregarding this effect in models of wave growth can lead to underestimation of the growth rate parameter by a factor of $2-3$ when compared to measured values [see Donelan *et al.*, 2006, for a discussion]. The spectral equation (2.56) is not designed for applications at such time scales of individual waves and wave groups.

What happens at the scales of dozens of waves or a hundred waves? In the case of ordinary

weak-in-the-mean breaking conditions, there should be not much variation in properties at this scale. In the case investigated here, the strongly-forced and frequently-breaking dominant waves come in alternating breaking and non-breaking trains from 4 to 120 dominant waves long. The breaking waves are, on average, significantly higher and steeper than those not breaking [Holthuijsen & Herbers, 1986]. It is expected therefore that there will be a noticeable difference between the spectra calculated over breaking-wave train segments and the spectra over non-breaking segments.

Since breaking is the only major process to contribute to the rapid dissipation at this time scale (the bottom friction is relatively small and also relatively constant across the breaking/non-breaking segments), the difference can be attributed to dissipation due to the breaking of the dominant waves in the spectrum (as the spectrogram method is able to detect the breaking of dominant waves only - see Section 3.5). This difference will constitute a non-zero term on the right hand side of (2.56). The main assumption, which was discussed and supported in Young & Babanin [2006a], is that the difference can be attributed to the partial derivative only and the advective term is small. An assumption regarding the advective term was needed as it was not possible to directly estimate its value. The waves were measured using a spatial array of wave probes with the largest separation of 30 cm between the probes [Young *et al.*, 2005]. At such distances, spectral difference along the wave fetch (between the probes) was negligible and could not be detected with a reasonable degree of confidence. Thus, to determine the spectral energy loss due to dominant breaking, it was assumed that it should be sufficient to measure differences between spectra of breaking and non-breaking waves based on measurements of time series at a point.

This difference will be a lower-bound estimate of the dissipation due to breaking. The approach treats the segments of breaking waves as a sequence of incipient breakers. In fact, waves breaking at the measurement point already exhibit some whitecapping and therefore they have already lost some energy prior to arriving at the measurement point. The broken waves in the non-breaking sequence are already gaining energy from the wind, but this energy is still not sufficient, on average, to bring them to the breaking point. Therefore, the energy difference between the breaking-onset and the just-broken waves should in fact be somewhat larger than the one actually measured by this segmenting method.

Additionally, it should be pointed out that the breaking waves are at the same time receiving energy from the wind. This means that the wind-input rate is still slower compared to the dissipation, but wave-growth rates and breaking-dissipation rates are now comparable and differ only by a factor of $2-3$. This interesting observation indirectly supports the conclusion made in Donelan *et al.* [2006] that the wave-growth rates depend on the wave steepness.

To summarise the segmenting approach described here, we would mention again that, in the wave record with 60% dominant breaking rate, the trains of dominant breakers are treated as sequences of incipient breakers and the trains of non-breaking waves as sequences of waves which have just broken. This should lead us to a lower-bound estimate of the dominant-breaking impact across the spectrum. Thus, there will be multiple segments of wave record, from half-a-minute to a few-minutes long, used to obtain spectra based on these individual segments. The spectra obtained for the breaking segments and those obtained for the non-breaking segments will then be averaged separately in order to produce reliable estimates of the *incipient-breaking* spectrum and of the *post-breaking* spectrum.

As mentioned above, the spectrogram method developed by Babanin *et al.* [2001] will be

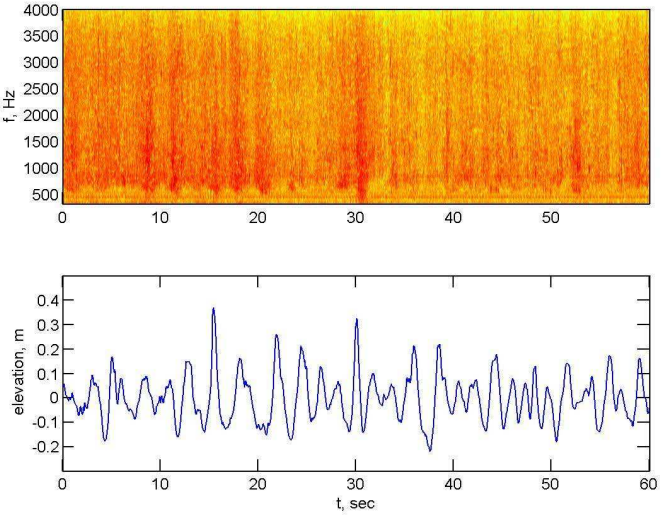

Fig. 5.31. (top panel) Spectrogram of acoustic noise of one minute of the record. Dark crests are associated with breaking waves. (bottom panel) Synchronous surface elevation record.

used to segment the wave records. Spectrograms of the acoustic noise recorded by hydrophone clearly demonstrate patches of enhanced and lowered noise level, which were shown to be associated with breaking activity of dominant waves at the wave-measurement spot above the hydrophone (Section 3.5). For example, in Figure 5.31 the first 35 seconds would be an *incipient-breaking* segment and the last 25 seconds - a *post-breaking* segment.

Thus, a mean *incipient-breaking* spectrum $F_i(f)$ and a mean *post-breaking* spectrum $F_p(f)$ were obtained within the record with nearly 50% breaking rate. The two spectra are shown in Figure 5.32. There is a clear difference between the spectra, with $F_p(f)$ having consistently lower spectral density as one would expect. Confidence limits are very small, and overall the spectra of broken waves lie below 95% confidence limits of the spectra of breaking waves. The higher order moments also exhibit interesting substantial differences:

$$\begin{array}{rcl} S_{k_i} & = & 0.45, \\ S_{k_p} & = & 0.31, \\ A_{s_i} & = & -0.186, \\ A_{s_p} & = & -0.017, \\ K_i & = & 3.34, \\ K_p & = & 2.96. \end{array} \tag{5.40}$$

Here, K_i and K_p are respectively *incipient-breaking* and *post-breaking* kurtosis

$$K = \frac{m_4}{m_0^2}. \tag{5.41}$$

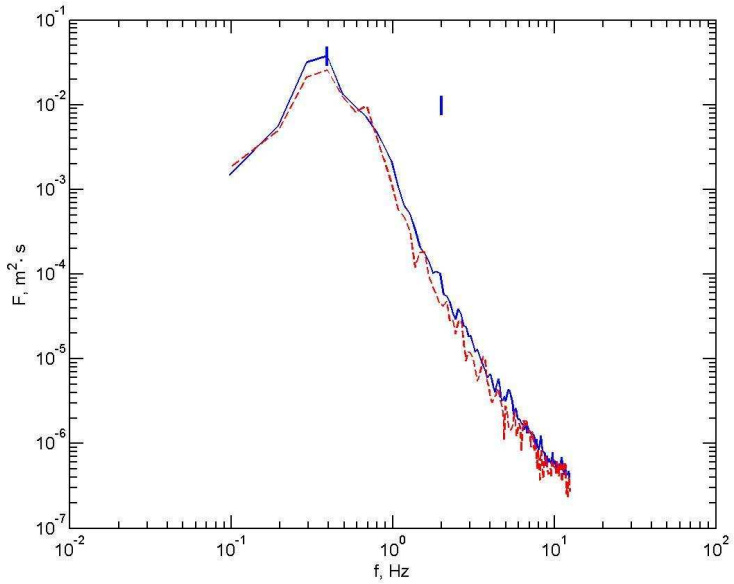

Fig. 5.32. Mean power spectrum of *incipient-breaking* (solid line) and *post-breaking* (dashed line) waves. 95% confidence limits are shown.

According to Wikipedia (`http://en.wikipedia.org/wiki/Kurtosis`), "In probability theory and statistics, kurtosis... is a measure of the "peakedness" of the probability distribution of a real-valued random variable. Higher kurtosis means more of the variance is due to infrequent extreme deviations, as opposed to frequent modestly-sized deviations". For a Gaussian-distributed variable, which the surface-wave elevations are often assumed to be, there should be

$$K = 3. \tag{5.42}$$

This is the case for the broken waves in (5.40), but the *incipient-breaking* trains obviously exhibit the extreme deviations, which again highlights the connection of the breaking events with the wave-group structure.

The non-breaking waves in this strongly-forced steep-wave situation have quite high skewness (1.2), but the breaking waves are even more skewed. Note that these are ensemble-average values which makes them particularly high. There is a possibility that, because of the difference in skewness between breaking and non-breaking waves, there will be a difference in surface orbital velocities and therefore in Doppler shifts between the breaking and non-breaking segments. These effects were estimated and found negligible.

The difference for the vertical asymmetry (1.3) is remarkable: non-breaking waves are, approximately, symmetric, whereas their breaking counterparts show very large mean negative asymmetry (i.e. the waves are on average tilted forward). Since, as have been discussed in Section 5.1.1, at the very point of the breaking onset the individual wave-to-break is nearly

symmetric, the negative asymmetry indicates the obvious fact that the waves measured in the *incipient-breaking* trains are already breaking (they were detected through their whitecapping in the first place). Since, however, the average asymmetry here is an ensemble-average, its distinctly negative value for the trains with many breaking waves has an important implication.

Indeed, if the waves do not break, their asymmetry still goes through the oscillations, that is the waves periodically tilt forward, then recover the symmetric shape and tilt backward (see Sections 4, 5.1, Agnon *et al.* [2005]). On average, however, the asymmetry of such trains should be zero, as it certainly is in the *post-breaking* train (5.40). When the waves start breaking, they tilt forward and then do not appear to recover their symmetric form, at least not until the breaking is ceased and a new cycle of the wave re-development starts. Therefore, wave trains which contain the breaking waves will have negative-on-average asymmetry, depending on how many breakers are embedded into the record. Thus, proper calibration of the breaking probability in terms of ensemble-average wave-train asymmetry should allow to estimate wave-breaking rates in such trains without actually having to observe and detect the breaking events, at least for the dominant waves. This has been a long-standing problem, i.e. judging on the wave-breaking rates in vastly available records of surface-wave elevations. Based on linear interpolation of (5.40), we can suggest that

$$\begin{cases} A_{s_{0\%breaking}} & = 0, \\ A_{s_{100\%breaking}} & = -0.2, \end{cases} \tag{5.43}$$

that is

$$b_T = -5A_s. \tag{5.44}$$

The spectral difference is quantified in the bottom subplot of Figure 5.33, where the ratio of the two spectra is plotted as a function of frequency f. The top subplot duplicates Figure 5.32 to make comparisons easier. Clearly, the loss of spectral density, following the breaking of dominant waves, is spread across almost the entire frequency range. Although there is considerable noise, the longer wave scales appear more affected by the dominant breaking, than the shorter scales of $f > 5f_p$. It is possible that these shorter scales recover from the breaking impact at a time scale of a few tens of dominant periods (shorter than the averaging period of the spectra shown here). It is also possible that the broadband impact of the dominant breaking becomes less effective at high frequencies. The strongest attenuation is observed for waves in the $3f_p - 5f_p$ range. The mean energy loss across the full measured spectrum is approximately 20%.

It has to be emphasised here that, even though the short waves do also break as discussed in Section 5.3.2 above, the observed broadband difference of the two spectra is due to the dominant breaking. The inherent breaking of short waves, which would naturally occur in the absence of background dominant breaking, would not be detected by the segmenting method. Such breaking will randomly take place on a time scale shorter than the segment length. As a result, such smaller-scale breaking will happen in all segments and the resulting differences in the energy between the segments will not identify breaking at this scale. Therefore, any differences in the high-frequency parts of the spectra are linked to the dominant breaking, rather than to any other processes occurring at the higher frequencies.

It should be pointed out that the observed spectral difference is effectively the indicator for spectral dissipation, rather than for the breaking probability only, regardless what an actual phys-

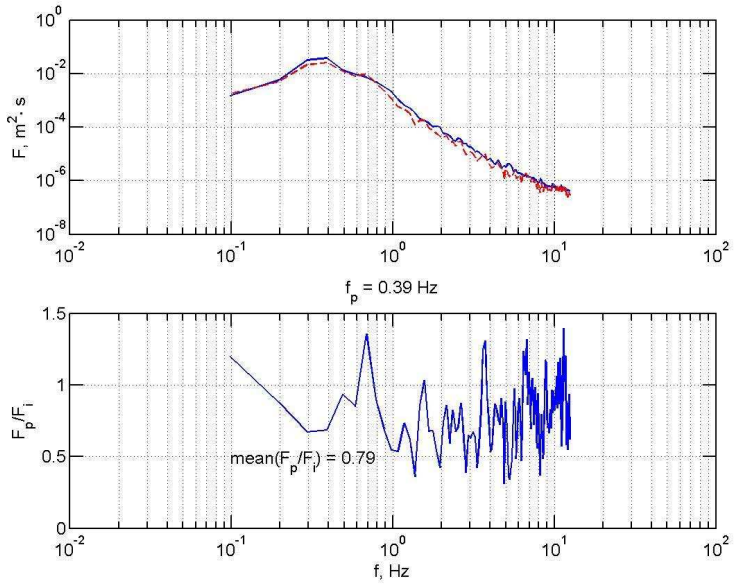

Fig. 5.33. (top panel) Mean power spectrum of *incipient-breaking* (solid line) and *post-breaking* (dashed line) waves. (bottom panel) Ratio of the spectra shown in top panel.

ical cause for such high-frequency dissipation is: i.e. whether this is an enhanced level of high-frequency breaking, or an enhanced level of turbulent-viscosity dissipation at high frequencies, or both. This is equally true with respect to the directional spectra and directional distribution of the dissipation discussed below. Figures 5.32, 5.33, however, demonstrate the cumulative effect for the wave-energy dissipation, similar to the cumulative effect for the wave breaking shown in Section 5.3.2.

The conjecture that the difference/dissipation between the observed spectra in Figures 5.32, 5.33 is due to dominant breaking required quantitative verification. Measurements of the total dissipation in the water column beneath the surface waves were used for this purpose. Estimates obtained by means of such measurements are not necessarily more accurate than the estimates obtained in Young & Babanin [2006a] by the segmenting method, but the first approach is quite well established and provided a good reference value for the new results.

The volumetric rate of total turbulent kinetic energy dissipation ϵ_{dis} can be obtained from the Kolmogorov inertial subrange of the velocity spectrum in the water [e.g. Terray *et al.*, 1996, Veron & Melville, 1999]. If the velocity spectrum $V(f)$ exhibits a

$$V(f) \sim f^{-\frac{5}{3}} \tag{5.45}$$

Kolmogorov interval, the level of this interval depends on the dissipation ϵ_{dis}:

$$V(f) = \frac{7}{110} 2^{\frac{4}{3}} \Gamma\left(\frac{1}{3}\right) \left(\frac{8\epsilon_{dis}}{9\alpha} \frac{u_{rms}^{orb}}{2\pi}\right)^{2/3} f^{-\frac{5}{3}} \tag{5.46}$$

where u_{rms}^{orb} is the *rms* orbital velocity and $\alpha \approx 0.4$ is Heisenberg's constant [Veron & Melville, 1999]. The larger is the dissipation rate ϵ_{dis}, the higher will be the Kolmogorov interval of the spectrum $V(f)$.

ϵ_{dis} is the dissipation rate per unit of volume, and to obtain the total dissipation in the water column per unit of area, D_a one needs to integrate $\epsilon_{dis}(z)$ over the water depth z from the surface $z = 0$ to the bottom $z = d$:

$$D_a = \int_0^d \epsilon_{dis}(z) dz. \tag{5.47}$$

To perform the integration, either continuous measurements of the $\epsilon_{dis}(z)$ profile or its parameterisation as a function of depth are required. Knowledge of the parameterisation is obviously preferable as it enables estimation of the total dissipation on the basis of a single-depth measurement of the spectrum (5.46).

There is, however, no general agreement on the parameterisation of the vertical dissipation distribution $\epsilon_{dis}(z)$. In the classical theory of the boundary layer over a solid wall, ϵ_{dis} is a simple function of the distance z to the wall:

$$\epsilon_{dis}(z) \sim z^{-1} \tag{5.48}$$

[see e.g. Landau & Lifshitz, 1987]. Early measurements in the boundary layer beneath the wavy surface found the ϵ_{dis}-depth distribution to be consistent with this wall-layer theory [Arsenyev *et al.*, 1975, Dillon *et al.*, 1981, Oakey & Elliott, 1982, Jones, 1985, Soloviev *et al.*, 1988]. More recently, however, both by direct and indirect means it was shown that, at least at strong wind forcing, the dissipation ϵ_{dis} close to the water surface may exceed the wall-layer values by up to two orders of magnitude [Agrawal *et al.*, 1992, Melville, 1994, Drennan et al., 1996, Terray *et al.*, 1996]. Terray *et al.* [1996] and Drennan et al. [1996] parameterised the vertical dissipation profile as

$$\epsilon_{dis}(z) = \begin{cases} const & z < H, \\ \sim z^{-2} & z \geq H. \end{cases} \tag{5.49}$$

Based on considerations of the expected total wind input which should match the total dissipation, it was found that H approximately scales with significant wave height H_s as

$$H = 0.6 H_s \tag{5.50}$$

[Terray *et al.*, 1996, Drennan et al., 1996]. Later refined studies of Soloviev & Lukas [2003], Gemmrich & Farmer [2004] confirmed the existence of enhanced near-surface turbulence due to breaking, but pointed out that the scaling H of the constant-dissipation level is still an issue.

At Lake George, turbulence spectra $V(f)$ were measured by Acoustic Doppler Velocimeters (ADV) as described by Young *et al.* [2005] in greater detail. Under reasonably strong wind forcing, such spectra exhibited distinct Kolmogorov intervals as shown in Figure 5.34. The vertical profile of these turbulence spectra is plotted in the Figure. The ADV was traversed down from the surface in 10 cm increments and the six 20 min-averaged spectra shown in Figure 5.34 were recorded at 10 cm, 20 cm, 30 cm, 40 cm, 50 cm and 60 cm from the mean water level, respectively. The wind was steady in speed and direction over the two-hour time period of measuring the profile, $U_{10} = 9.7$ m/s on average, with a maximum of 10.9 m/s and a minimum

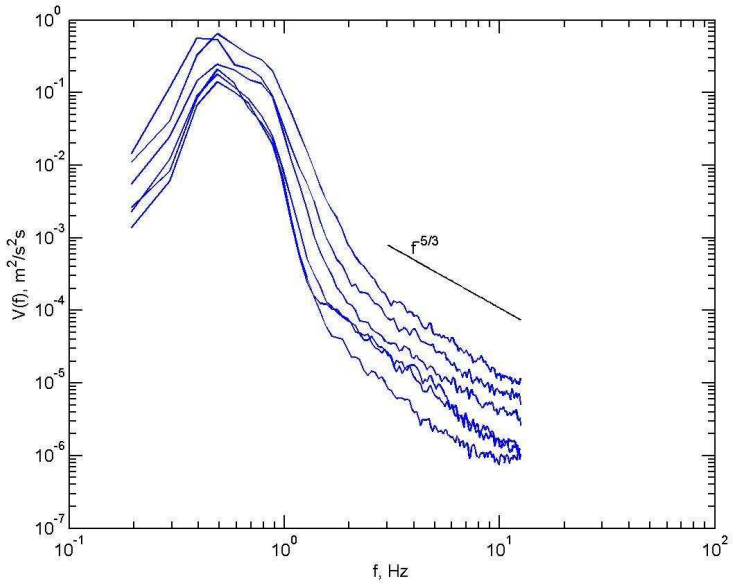

Fig. 5.34. Velocity spectrum $V(f)$ measured at 10 cm, 20 cm, 30 cm, 40 cm, 50 cm and 60 cm distances from the surface for a 9.7 m/s mean wind speed (the more energetic spectra are closer to the surface). The Kolmogorov interval slope of $f^{-\frac{5}{3}}$ is shown.

of 8.3 m/s. The more energetic spectra shown in Figure 5.34 were recorded closer to the surface, with the energy level decaying with depth.

Dissipation rates ϵ_{dis} obtained on the basis of such spectra using (5.46) are shown in Figure 5.35. This Figure plots ϵ_{dis} as a function of z in dimensionless form

$$\frac{\epsilon_{dis}\kappa z}{u_{*_w}^3} = function\left(\frac{gz}{u_{*_w}^2}\right) \tag{5.51}$$

where u_{*_w} is the friction velocity in the water, $\kappa \approx 0.4$ is the von Karman constant, and the mean water level is now treated as the wall. Wall-law scaling is applied to the dissipation ϵ_{dis} and height-of-fully-developed-waves scaling is applied to the distance-to-the-surface z [see Agrawal *et al.*, 1992, Melville, 1994]. For boundary layers over solid walls, such scaling of the dissipation would give values of

$$\frac{\epsilon_{dis}\kappa z}{u_{*_w}^3} = 1 \tag{5.52}$$

shown by the vertical line in the figure. The enhancement of the dissipation rates compared to the wall layer is obvious. Maximal values of the enhancement are up to 200 times greater than the wall-layer magnitude (even greater than those in Agrawal *et al.* [1992] where they were up to 70 times).

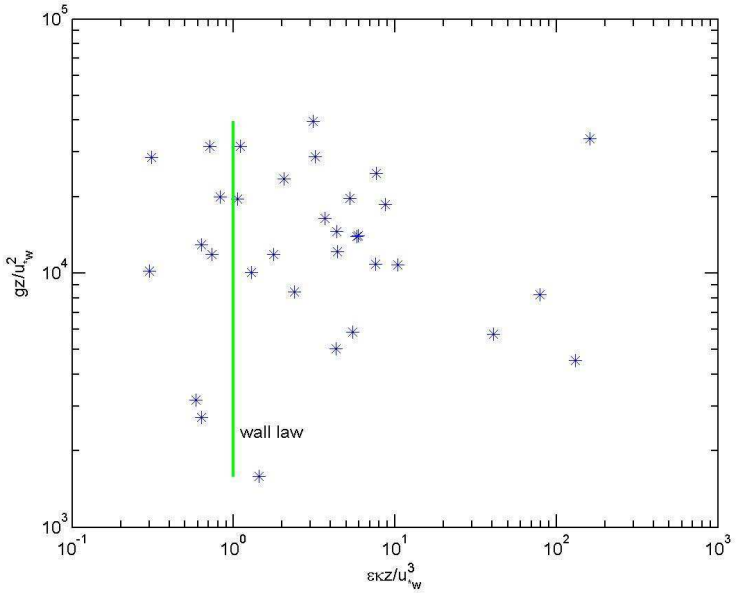

Fig. 5.35. Dissipation ϵ_{dis} (denoted as ϵ in this Figure) versus distance-to-the-surface z in the wall-layer coordinates. The vertical line represents the dissipation level in the boundary layer over a solid wall.

Dissipation of energy of wind-generated waves in the finite-depth water column, that is in the Lake George conditions, consists of two parts: turbulent kinetic energy dissipation D_a (5.47), which would occur in the deep water as well as in finite depths, and dissipation per unit area due to bottom friction B_a. The total dissipation T_a

$$T_a = D_a + B_a \approx I_a \tag{5.53}$$

should match the wind energy input per unit area I_a for steady wind-wave conditions. Technically speaking, some of the wave energy dissipated from the waves does not necessarily convert into the turbulence and may be spent on, for example, work against buoyancy forces when the bubbles are entrained into the water in the course of wave breaking. Such amount, however, is never greater than 50%, usually much less [Melville *et al.*, 1992], and therefore a reasonable match indicated by (5.53) has to be expected.

In order to verify which of the parameterisations, (5.48) or (5.49) is to be used for the integration (5.47) in general case, Babanin *et al.* [2005] estimated and compared B_a, D_a and I_a. For that, a set of records for which the wind input I_a was directly measured [Donelan *et al.*, 2006] was chosen for the analysis. B_a was estimated by means of physical modelling of the respective wave conditions in a laboratory flume with the bottom covered with Lake George mud [Babanin *et al.*, 2005], and the ADV-obtained ϵ_{dis} were integrated over the depth using both (5.48) and (5.49).

The vertical profile of ϵ_{dis} for the Figure 5.34 spectra is shown in Figure 5.36. The profile is very close to quadratic and therefore parameterization (5.49) was first used to estimate the

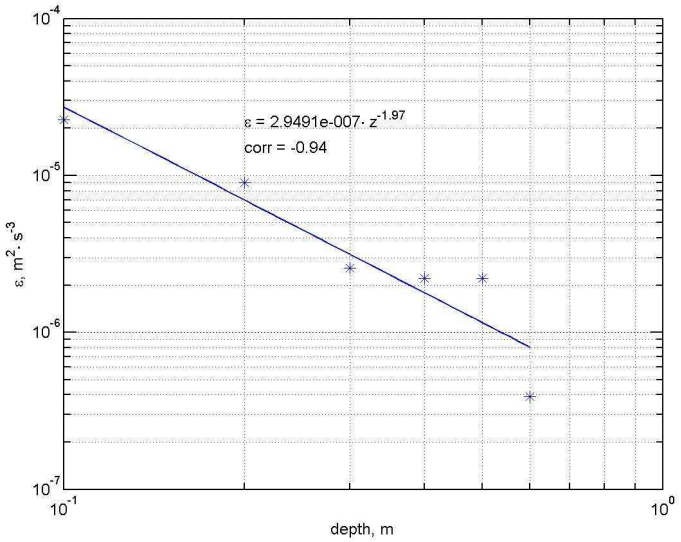

Fig. 5.36. Dimensional profile of dissipation ϵ_{dis} (denoted as ϵ in this Figure) versus distance-to-the-surface z, obtained from the turbulence spectra shown in Figure 5.34. The line of best fit and its correlation coefficient are shown.

dissipation D_a.

The corresponding total dissipation T_a (5.53) is plotted versus the total wind input I_a in Figure 5.37. The data separate into two groups. For records with wind speed $U_{10} < 7.5$ m/s (five points on the left), the total dissipation is significantly overestimated. It is, however, somewhat underestimated for the winds $U_{10} > 7.5$ m/s (points on the right).

Figure 5.38 shows the total dissipation T_a (5.53) plotted versus the total input I_a, while dissipation D_a (5.47) was estimated on the basis of the wall-layer distribution for ϵ_{dis} (5.48) as was suggested by a number of authors mentioned above. Dissipation for the light-wind points now matches the wind input quite well, whereas the dissipation at winds $U_{10} > 7.5$ m/s is greatly underestimated.

An obvious conclusion to be drawn is that the volumetric rate of total turbulent kinetic energy dissipation ϵ_{dis} is distributed according to the $\sim z^{-1}$ law (5.48) for waves generated by light winds and as $\sim z^{-2}$ (i.e. similar to predictions of (5.49)) for waves under stronger winds. Since the inverse-quadratic dissipation has always been associated with wave breaking, such the conclusion is consistent with observations that the breaking does not occur for waves forced by light winds of $U_{10} \lessapprox 5 - 7$ m/s.

Finally, to provide a better agreement between the dissipation and the energy input of the strong-wind points in the top panel, the scale for H in (5.49) had to be adjusted. To obtain the $H = 0.6H_s$ scale in (5.49), Terray *et al.* [1996] had to rely on an inferred wind-input rate. Babanin *et al.* [2005] used the total wind input I_a measured, and the comparisons led to a conclusion that the constant-dissipation layer does not reach below $H = 0.4H_s$. The outcome is

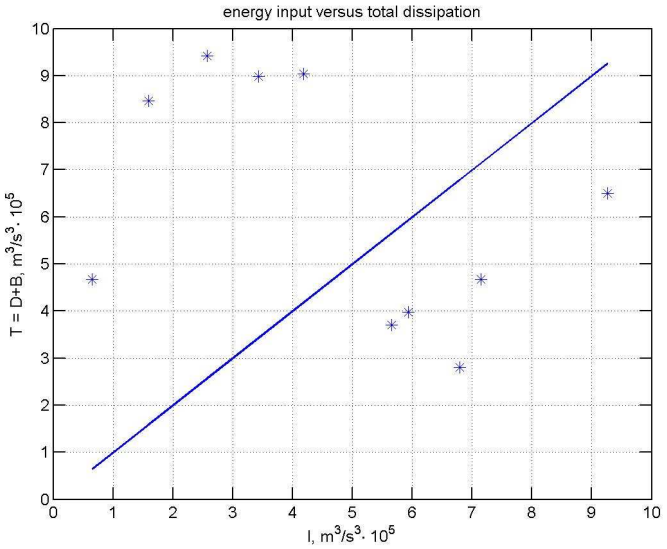

Fig. 5.37. Total dissipation in the wave water column T_a (5.53) versus measured total wind input I_a (denoted as T and I, respectively). Parameterisation (5.49) is used for integrating D_a in (5.47) at $z > 0.6H_s$.

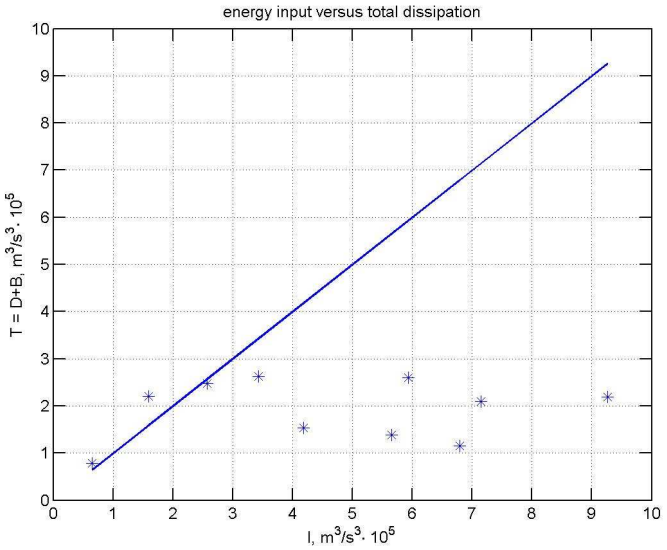

Fig. 5.38. Total dissipation in the wave water column T_a (5.53) versus measured total wind input I_a (denoted as T and I, respectively). Parameterisation (5.48) is used for integrating D_a in (5.47) at $z > 0.6H_s$.

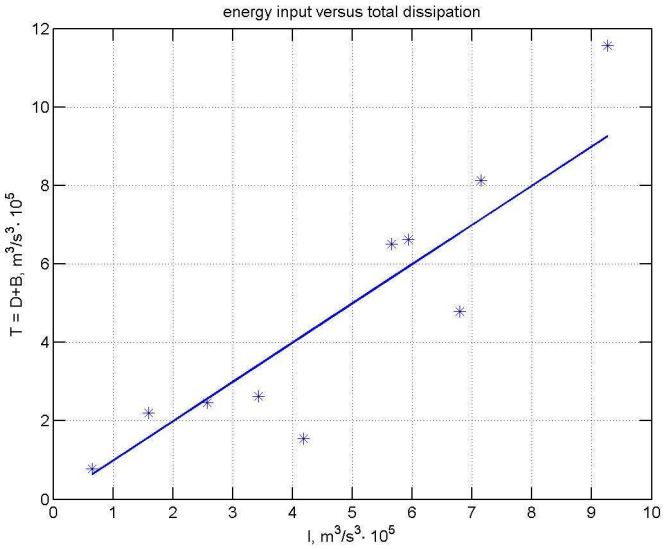

Fig. 5.39. Total dissipation in the wave water column T_a (5.53) versus measured total wind input I_a (denoted as T and I, respectively). Parameterisation (5.54) is used for integrating D_a in (5.47).

shown in Figure 5.39 and the resulting parameterisation for the dissipation rate ϵ_{dis} is now as following:

$$\epsilon_{dis}(z) = \begin{cases} const & z \leq 0.4H_s, \\ \sim z^{-1} & z > 0.4H_s, U_{10} < 7.5 \text{ m/s}, \\ \sim z^{-2} & z > 0.4H_s, U_{10} \geq 7.5 \text{ m/s}. \end{cases} \tag{5.54}$$

Therefore, the inverse-quadratic dissipation profile (5.54) for the strong-wind Lake George records was adopted. During the wave record analysed in the segmenting exercise described here, ADV measurements synchronised with the wave and sound recordings were carried out at a distance of 20 cm from the surface at the location of wave array. ADV velocity spectra of *incipient-breaking* and *post-breaking* periods are shown in Figure 5.40. The orbital velocities of waves around the peak, unlike the peak spectral densities of the power spectra in Figures 5.32, 5.33, do not appear to differ significantly. The levels of the Kolmogorov intervals at higher frequencies of the two spectra, however, are essentially different. At these frequencies and at the 20 cm depth, the turbulent velocities apparently dominate the orbital velocities. The difference between Kolmogorov intervals can be attributed to the loss of energy from across the wave spectrum seen in Figures 5.32, 5.33. The total dissipation estimated from the velocity spectra and the wave spectra should match:

$$D_{a_i} - D_{a_p} = g \cdot \int_f \overline{(\frac{F(f)_p - F(f)_i}{\Delta t})} df \tag{5.55}$$

where Δt is the time difference between the mean time points of subsequent breaking and non-

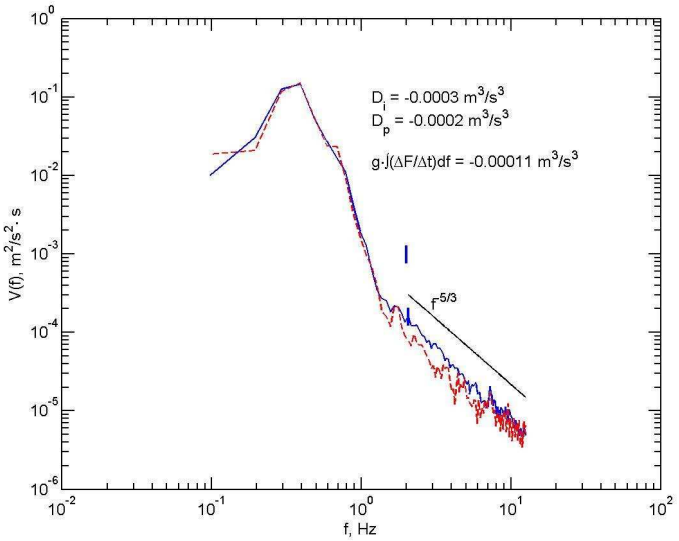

Fig. 5.40. Mean velocity spectrum of *incipient-breaking* (solid line) and *post-breaking* (dashed line) waves. The Kolmogorov interval slope of $f^{-\frac{5}{3}}$ is shown. The text demonstrates values of respective total dissipation rates D_a (5.47, denoted as D in this Figure) and the integral of spectral dissipation seen in Figure 5.32. 95% confidence limits are shown.

breaking segments and the overline represents the ensemble average. Here, the spectral dissipation term will be multiplied by g:

$$S_{ds}(f) = g \cdot \frac{\Delta F(f)}{\Delta t} \tag{5.56}$$

rather than being used as

$$S_{ds}(f) = \frac{\Delta F(f)}{\Delta t}. \tag{5.57}$$

following its formulation in (2.56). This is done to match the dimensions of dissipations D_a and $\int_f S_{ds}(f)df$.

Based on the data shown in Figure 5.40 and using (5.47), under the incipient dominant breakers the dissipation rate per unit of area is $D_{a_i} = -0.0003$ m^3/s^3, and under the broken dominant waves it is $D_{a_p} = -0.0002$ m^3/s^3. The latter, of course, should not be zero in the absence of dominant breaking because dissipation due to breaking of waves of all other scales persists. The difference

$$D_{a_i} - D_{a_p} = -0.0001 \text{ m}^3/\text{s}^3 \tag{5.58}$$

matches remarkably well the integral (5.55):

$$g \cdot \int_f \frac{\Delta F}{\Delta t} df = -0.00011 \text{ m}^3/\text{s}^3. \tag{5.59}$$

Although this is a pleasing agreement, it should be remembered that both approaches yield only an approximate estimate of the dissipation.

As have been mentioned above, the spectral difference in Figure 5.32 is a lower-bound estimate of dissipation due to the breaking, because some energy must have already been lost before the spectra were measured. The difference $D_{a_i} - D_{a_p}$ of the total dissipation rates of kinetic energy is also likely to be a lower-bound estimate of the loss of energy from the wave field due to breaking. As have also been already mentioned, some of the energy is expended on work against buoyancy forces whilst entraining bubbles into the water, rather than on generating the turbulence. The fraction of the wave energy dissipated, which is expended on entraining the air can be up to 30% to 50% of the total [Melville *et al.*, 1992] and this defines the limits of accuracy of the segmenting method. For the laboratory measurements of Melville *et al.* [1992], some of the breaking was of a plunging type. In contrast, most of the Lake George breaking was of the spilling type, which spends less energy on entrainment. Therefore, we would expect that in our case the fraction of energy expended this way is at the lower bound of 30% and perhaps even less than that. Nevertheless, the above comparison shows that the proposed method of estimation of wave-breaking dissipation by considering the difference between the *incipient-* and *post-breaking* spectra provides a reasonable magnitude of the total dissipation.

Another interesting observation can be made on the basis of Figure 5.40. Here, one can see that the orbital velocities of the dominant waves did not change between the breaking and non-breaking segments. This implies that the energy, which is obviously gone from the power spectra, must have been the potential energy, rather than kinetic, at least for the dominant waves. What is important here is that the dominant orbital velocities are the same between the segments, and therefore the bottom friction is the same for the breaking and non-breaking wave trains which is essential for the estimates made.

The least known feature of the spectral dissipation function is its directional behaviour, which is the main topic of this Section 5.4, but needed such extended segmenting-method introduction. As mentioned above, the waves are directional, as are all the source functions in (2.56). Therefore, some directional shape, usually isotropic, must be assumed for the dissipation term. There is, however, little, if any, experimental validation of this directional shape.

The segmenting method can be used to obtain *incipient-breaking* and *post-breaking* directional spectra, similar to that used to obtain *incipient-breaking* and *post-breaking* omni-directional spectra in Figure 5.32 above. The Maximum Likelihood Method (MLM) developed originally by Capon [1969] (see also Babanin & Soloviev [1987, 1998b], Young [1994], Young *et al.* [1996]) was used to analyse the wave-array data and the wave directional distributions in this respect.

It was noticed that the main wave propagation direction θ_{max} changes from segment to segment (in Figure 5.41 it is shown for the spectral-peak frequency f_p). This scatter around the mean main direction appeared random, not connected to whether the segment consisted of breaking or of non-breaking waves. Therefore, the non-normalised directional spectra $\phi(f_p, \theta)$ were obtained for each of the segments and turned to have the same main direction ($\theta_{max} = 0$ in Figure 5.42). The connection between the non-normalised directional spectra $\phi(f, \theta)$ and normalised directional distributions of $K(f, \theta)$ in (5.29)-(5.30) is

$$\phi(f, \theta) = A(f)K(f, \theta) \tag{5.60}$$

[see Babanin & Soloviev, 1987, 1998b, for details]. Since MLM does not produce dimensional values for the spectral densities, however, the vertical scale in Figure 5.42 is arbitrary.

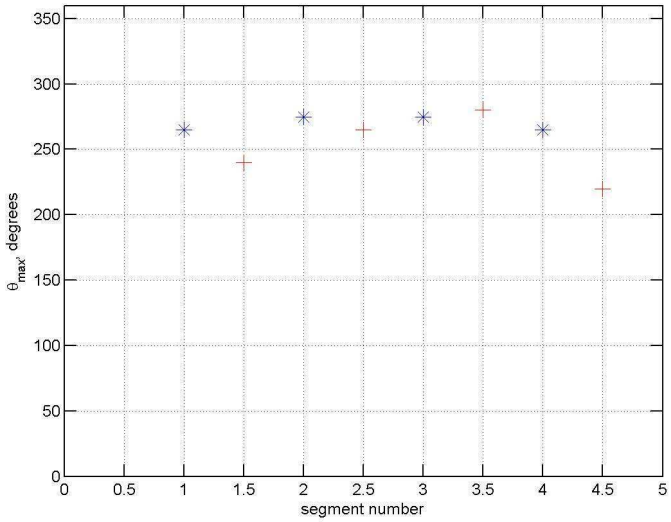

Fig. 5.41. Main direction of subsequent breaking-wave (*) and broken-wave (+) segments.

In Figure 5.42, the solid line designates the mean *incipient-breaking* directional spectrum $\phi_i(f_p, \theta)$ at the spectral peak, and the dotted line – the mean *post-breaking* directional spectrum $\phi_p(f_p, \theta)$. Clearly, the major energy loss occurs at angles oblique to the main propagation direction.

Figure 5.43 shows the ratio of $\phi_i(f_p, \theta)$ and $\phi_p(f_p, \theta)$ spectra. Qualitatively, this ratio reflects the directional behaviour of the dissipation at the spectral peak. Contrary to existing assumptions, the energy loss in the main propagation direction is a minimum, with the loss increasing away from this main direction. Since the dissipation has to start decreasing again at larger angles, certainly in the half-plane opposite to the wave-propagation half-plane, this result implies that the dissipation function $S_{ds}(f, \theta)$ in (2.56), (2.24), (5.39) has to be bimodal in the directional space. Unlike the wind-input function $S_{in}(\theta)$ which is unimodal and has a distinct maximum in the main wind direction, $S_{ds}(\theta)$ may have maxima at angles oblique to the wind-input maximum angle.

The impact of the dominant breaking on the directional dissipation at $2f_p$ is similar, though less pronounced (Figures 5.44, 5.45). There is a noticeable loss of energy in the primary wind/ wave direction, and the oblique peaks are pushed further away. The former can be explained by the influence of the induced breaking. That is, the dominant waves, whose directional distribution is quite narrow, enforce the short-wave breaking in the wind-predominant direction primarily. The trend of the oblique peaks requires further confirmations, understanding and explanations, as does the very directional bimodality of the f_p waves.

Thus, a very long elaboration of this Section 5.4, initially intended for the directional properties of the breaking probability of spectral waves, was needed to demonstrate indications that the directional dissipation rates at oblique angles are higher than the dissipation in the main

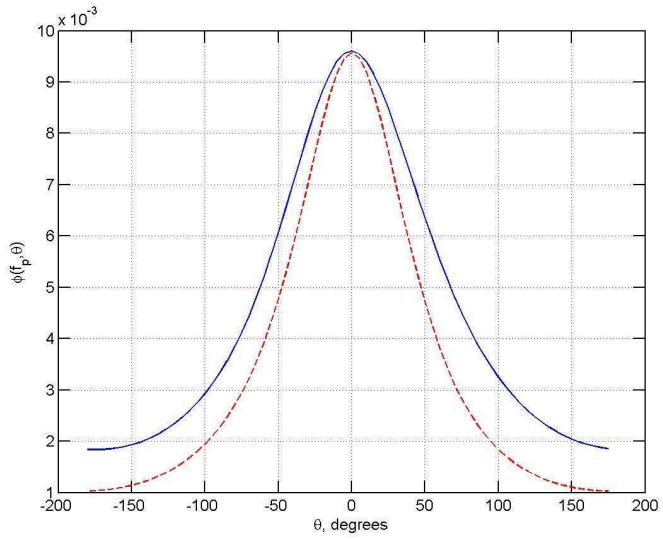

Fig. 5.42. Non-normalised *incipient-breaking* $\phi_i(f_p, \theta)$ (solid line) and *post-breaking* $\phi_p(f_p, \theta)$ (dashed line) directional spectrum (5.60) at peak frequency f_p. Units of the *MLM* directional distributions are arbitrary.

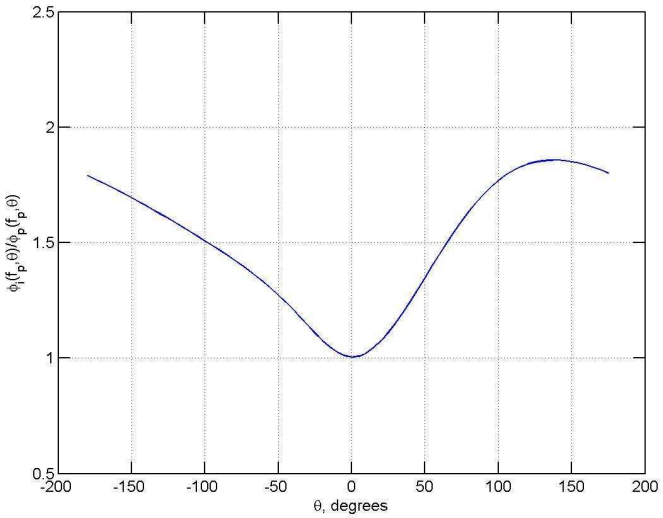

Fig. 5.43. Ratio of *incipient-breaking* $\phi_i(f_p, \theta)$ and *post-breaking* $\phi_p(f_p, \theta)$ directional spectra of Figure 5.42 at peak frequency f_p.

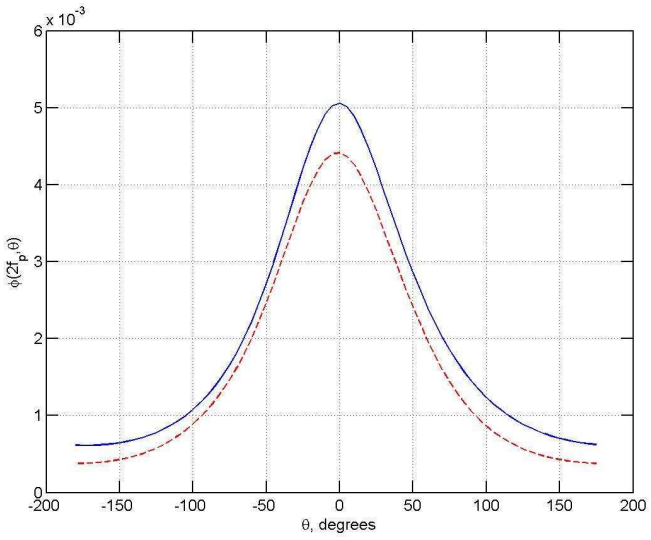

Fig. 5.44. Same as in In Figure 5.42, but for $\phi_i(2f_p, \theta)$ (solid line) and $\phi_p(2f_p, \theta)$ (dashed line) directional spectrum at double peak frequency $2f_p$.

wave-propagation direction. In fact, this conclusion does not necessarily immediately translates into directional properties of the breaking occurrence. As was discussed at a number of occasions above, including this Section, the dissipation consists of contributions of both the breaking probability and breaking severity.

In order to obtain the angular distributions of the breaking occurrence directly, it would be necessary to combine one of the methods able to detect individual wave-breaking events, e.g. one of the acoustic techniques described in Section 3.5, with a method suitable for detecting a direction of propagation of these individual waves, for example, the Wavelet Directional Method (WDM) of Donelan *et al.* [1996] or some of the remote-sensing techniques of Section 3.6. This is, however, a very demanding experimental exercise as it would require very long observations in order to obtain a reliable statistics. Even if the directional plane is subdivided into reasonably broad bins, i.e. $\pm 10^\circ$ or even $\pm 20^\circ$, there will be required many hours of continuous stationary wave-breaking records, particularly given the fact that the overall directionally-integrated rates are typically only of the order of a few percent [e.g. Babanin *et al.*, 2001].

There are two more issues as far as the wave breaking and directional properties of wave fields are concerned. The first one relates to the modulational instability in the three-dimensional wave fields, and the second one to the linear directional focusing.

Indeed, it is a known experimental and theoretical fact that the modulational-instability mechanism experiences limitations in broadband, and particularly in three-dimensional fields [e.g. Brown & Jensen, 2001, Onorato *et al.*, 2002, 2009a,b, Waseda *et al.*, 2009a,b]. Since field waves are spectral and directional, this issue has to be considered seriously when talking about wave-breaking problems with respect to the real oceanic waves.

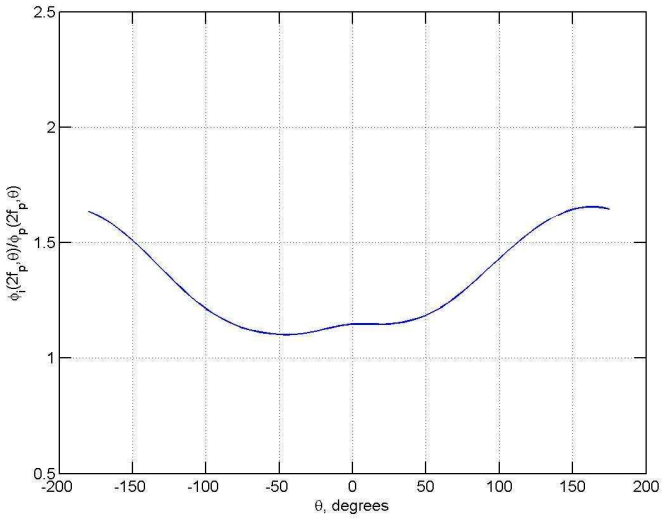

Fig. 5.45. Same as in In Figure 5.43, but for ratio of $\phi_i(2f_p, \theta)$ and $\phi_p(2f_p, \theta)$ directional spectra of Figure 5.44 at double peak frequency $2f_p$.

Brown & Jensen [2001] studied the focusing of unidirectional waves and found that the Benjamin-Feir instability is impaired in focusing (i.e. spectral) wave trains. Such study needs to be extended into spectra typical of field waves. There is a reasonable expectation, however, that the modulational mechanism may work for reasonably steep waves with a narrow spectrum [e.g. Waseda *et al.*, 2009a]. For unidirectional spectral waves, Alber [1978] derived a requirement which can be expressed as

$$M_I > 1 \tag{5.61}$$

(see (5.1) for the definition of M_I), and this condition can be satisfied for spectra of young wind waves [e.g. Onorato *et al.*, 2001].

There is no analogue of M_I and condition (5.61) available for three-dimensional characteristics of the modulational-instability mechanism. In Onorato *et al.* [2002], directional effects were investigated and quantitative criterion β was obtained in terms of width of directional spectrum $D(\theta)$ where θ is angle:

$$D(\theta) = \cos^2\left(\frac{\pi}{2\beta}\theta\right) \tag{5.62}$$

– i.e. if the directional width is greater than $\beta = 15$, then the modulational instability appears to be suppressed. There was a typing error in Onorato *et al.* [2002], and value of β has to be actually multiplied by $\pi/180$, that is the criterion is

$$\beta \approx 0.26 \tag{5.63}$$

(Onorato, 2007, personal communication). Since the Onorato *et al.* [2002] model is weakly non-linear rather than fully non-linear, the criterion should only be regarded as an approximation, but we will use it as a reference point here.

To compare width of the (5.63)-spectrum with observations, integral value A (5.31) was estimated:

$$A^{-1} = \int_{-\beta}^{\beta} D(\theta) d\theta \tag{5.64}$$

which was used in the field study of Babanin & Soloviev [1987, 1998b] to measure directional distributions (the higher is A, the narrower is the spectrum). For $\beta = 0.26$,

$$A = 3.8 \tag{5.65}$$

which is well above the experimentally-observed values of typical directional spectra of wind-generated waves. It should be mentioned that this theoretical estimate is in excellent agreement with the laboratory measurement of Waseda *et al.* [2009a] who concluded that the critical directional spread for a typical JONSWAP spectrum (2.7) is

$$A \approx 4. \tag{5.66}$$

Modulational instability, however, may still be found applicable, at least for the dominant waves if they are steep enough. It is not unreasonable to expect a directional condition analogous to (5.61) being relevant. Parameter A (5.64) can be used for this purpose as it has the proper physical meaning of the inverse relative width of the directional spectrum whose peak is normalised to be 1.

At the spectral peak, a relative steepness (as the wave spectrum develops) is defined by $\sqrt{\gamma}$ where γ is the peak enhancement of the JONSWAP spectrum (2.7). That is, for the peak, we can suggest a directional analogue of M_I as

$$M_{Id} = A\sqrt{\gamma}. \tag{5.67}$$

Now, it is informative to look at how this Index evolves over the wave development. From (Eq.19) of Babanin & Soloviev [1998b], at the spectral peak

$$A = 1.12 \left(\frac{U_{10}}{c_p} \right)^{-0.50} + \frac{1}{2\pi}, \tag{5.68}$$

and from (Eq.44) of Babanin & Soloviev [1998a]

$$\gamma = \frac{7.6}{2\pi} \frac{U_{10}}{c_p}, \tag{5.69}$$

that is

$$\sqrt{\gamma} = 1.10 \left(\frac{U_{10}}{c_p} \right)^{0.50}. \tag{5.70}$$

Therefore,

$$M_{Id} = 1.23 + \frac{1.1}{2\pi} \left(\frac{U_{10}}{c_p} \right)^{0.50} \tag{5.71}$$

is a weak function of the wind forcing, and its value at the spectral peak varies from 1.40 to 1.79 for $\frac{U_{10}}{c_p}$ in the range from 0.89 to 10 where $\frac{U_{10}}{c_p} = 0.89$ signifies the limit of full development [Pierson & Moskowitz, 1964].

Now, if the M_{Id} assumption is valid and the critical value for this Index is in the range of $M_{Id} = 1.4 - 1.8$, the 'focusing' effect of directionality can be overcome by a stronger nonlinearity if waves grow steeper. It is worth noting here that the directional spectra broaden towards frequencies above the peak [e.g. Babanin & Soloviev, 1998b]. This means that, even if applicable at the peak, the directional modulational instability may not be working at higher frequencies and some other causes of breaking and dissipation will have to be found in that spectral band. In this regard, two-phase behaviour of the breaking has indeed been observed in field experiments of Babanin & Young [2005], Manasseh *et al.* [2006], Babanin *et al.* [2007c] (see Section 5.3.2 for a detailed discussion) - i.e. the direct dependence of breaking on spectral density at the peak and an induced breaking/dissipation at higher frequencies.

In any case, the issue of modulational instability in real spectral directional fields cannot be solved now, but with caution we will try to apply our results to the field data. Another problem, of the technical kind, still prevents direct comparisons of breaking rates obtained by means of (5.9) and field observations. Relationship (5.9) predicts the probability of incipient breaking, whereas in the field, at best, we can detect quantities which result from the breaking process, that is we count waves already breaking. Common measures of this type include the acoustic signature of breaking waves, void fraction or surface whitecap coverage as discussed in Section 3. However, a breaking wave emits sound and forms whitecaps over a substantial part of its period whereas the incipient breaking is an instantaneous state, and therefore the probability of encountering such sound or whitecaps is significantly higher than the probability of breaking onset [e.g. Liu & Babanin, 2004].

Qualitative comparisons of the laboratory and field breaking-probability dependences were done in Babanin *et al.* [2007a] and featured well. Here, the Babanin *et al.* [2007a] dependence, already shown in Figure 5.17 is reproduced in the top panel of Figure 5.46 for comparisons with the bottom panel which is the reproduced Figure 2.3. In this bottom panel, we plot frequency (inverse period) of individual dominant waves (from frequency range of $f = f_p \pm 0.3 f_p$) versus steepness of these individual waves. This is done for a Black Sea record with $f_p = 0.25$ Hz (Rec. 244 of Table 5.1) used by Babanin *et al.* [2001] to obtain field breaking rates in the same frequency band.

If there was no shrinking of the wavelength prior to breaking, as described in Section 5.1.1, at each steepness the distribution of the frequencies around $f_p = 0.25$ Hz would be approximately even. It is so for waves of $\epsilon <\approx 0.12$. For steeper waves, and some of these detected deep-water wind-generated three-dimensional waves have an enormous by field standards steepness up to $\epsilon = 0.27$, the distribution is clearly biased towards higher frequencies. Waves with $\epsilon > 0.17$ are all shorter than those of the peak frequency $f_p = 0.25$ Hz, and the higher is the individual steepness, the higher is the individual frequency. Since on average the highest waves are observed at the peak frequency, and the peak is very sharp, the only plausible explanation for this observation is that these abnormally steep, but rare waves are those in transition toward or just after the incipient breaking. As deep-water waves below the peak do not break, and if the near-breakers shorten, distribution of the incipient breakers has to be characterised by higher-than-peak frequencies at abnormally high steepnesses, as it is. The dispersive focusing

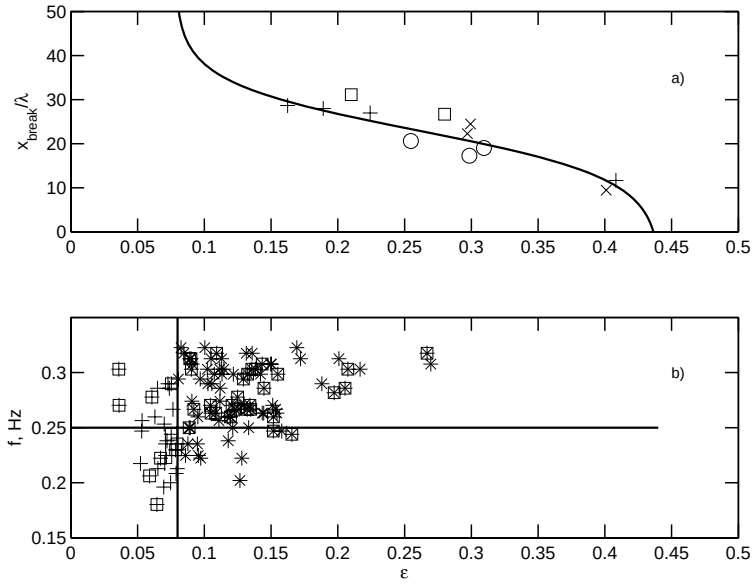

Fig. 5.46. a) As in Figure 5.17 (the filled-circle wind-forced data points are omitted). b) Black Sea. As in Figure 2.3.

or directional focusing, or other linear and quasi-linear processes cannot be attributed with the shortening the wavelength prior the breaking. Thus, the very existence of such abnormally high and shrunk waves indicates that the modulational instability mechanism is most likely still active in these directional field conditions.

Finally, while discussing what implications for the wave-breaking process in general and wave-breaking probability in particular may be brought about by the fact that the wave fields are directional, the directional focusing has to be mentioned [Fochesato *et al.*, 2007]. This is a truly three-dimensional phenomenon which signifies linear superposition of waves/wave-packets of approximately the same carrier frequency converging at an angle with respect to each other.

If the carrier waves are steep enough, the superposition can lead to a very high crest (i.e. double the height of the waves involved in the superposition, in which case non-linear effects may start playing role [e.g. Brown & Jensen, 2001]), reaching the steepness limit (2.46) and ultimately a breaking. Depending on the angle and the length of the converging crests, the breaking can have different severities and spatial/temporal extents.

How frequent is such breaking? In order to achieve the limit (2.46), there has to be a superposition of either multiple wave crests, which should be quite a rare event, or, for example, superposition of only two crests with half-the-limit steepness of $Hk/2 = \epsilon_{limiting} = 0.22$, which crests are quite rare events to begin with (see Figure 5.46 above). Therefore, the breaking due to directional focusing and other types of focusing on that matter could not be expected as a frequent occurrence in the realistic wave fields.

Indirectly, this conjecture is supported by the Wavelet Directional Method of Donelan *et al.*

[1996]. Main assumption of WDM is that at any given time there is only one wavelet of a particular frequency present at the measurement point. If not, the WDM reading fails at that particular instant. Level of the noise in the directional spectra produced by WDM would be an indicator of how often wavelets coming from different directions superpose. The answer is – not that often. Noise in the WDM-estimated field directional spectra is remarkably low [i.e. Donelan *et al.*, 1996], and so it is in laboratory directional spectra [Waseda *et al.*, 2009a], when the directional input was actually known.

On the other hand, the other possible cause of the wave breaking, the modulational instability is also likely to be impaired or even suppressed in such fields as discussed above. Therefore, the physics of the wave-breaking onset in a directional wave field is still a problem in need of further serious investigations.

5.5 Wind-forcing effects

If the wind forcing is superimposed, it can play multiple roles in affecting the wave-breaking probability. Wind action is important on longer scales in altering breaking statistics because of enhancing the wave steepness. At moderate winds, doubling the wind speed leads to achieving the limiting steepness and breaking four times as fast. At stronger wind forcing, this effect slows down (Section 4.1.1). Instantaneously, wind capacity to affect the breaking onset is marginal unless the wind forcing is very strong. See Section 4.1 and above subsections of this Section 5 for more discussion on this topic.

These conclusions were obtained by analysis of quasi-monochromatic wave trains. The field waves are spectral and directional, and this fact adds an additional level of complexity to the topic of wind forcing.

In the spectral environments, waves of different scales are present at the same time and what is a low wind forcing for some components, can be an inevitably strong or even very strong forcing for others. Phase speed $c(f)$ of waves across the spectrum depends on their frequency (2.15), and therefore so is the wind forcing $U/c(f)$.

If doubling the wind forcing causes the waves breaking four times faster, then doubling the wave frequency according to (2.18) hypothetically should have the same effect in terms of the wind forcing U/c. For example, if the wind speed is $U_{10} = 7.8$ m/s, then at frequency $f_1 = 0.2$ Hz there will be $U_{10}/c(f_1) = 1$, whereas at frequency $f_2 = 2f_1 = 0.4$ Hz it will be $U_{10}/c(f_2) = 2$. Therefore, at some small scales (low phase speeds, high relative winds) in the spectrum, the waves theoretically should be breaking very often.

The general pattern in real waves fields, however, is much more complicated, and that is due to a number of reasons. If the frequencies f_1 and f_2 above represent respective spectral peaks in the respective spectra (see Figure 5.29 for a typical view of the wave power spectrum), then the $U_{10}/c(f)$ wind forcing is applied to dominant waves in both cases and the values of the forcing, as far as the flux of momentum/energy is concerned, are unambiguous. If, on the contrary, the first frequency is the spectral peak $f_1 = f_p$ and $f_2 = 2f_p$ is the frequency of waves in the same spectrum, then the translation of $U_{10}/c(f)$ into the wind forcing as such is not that straightforward (that is into the mean-over-wave-period momentum flux which equals the mean stress, i.e. the force over the unit of area).

Indeed, as it has been shown in a number of air-sea interaction studies [e.g. Donelan *et al.*, 2006, Babanin *et al.*, 2007b, Kudryavtsev & Makin, 2007], at strong wind forcing and in presence

of steep dominant waves, particularly if those are breaking, air-flow separation in the lee of these waves can occur. In this case, if the shorter waves riding the dominant ones are under the separated air bubble they experience much lower wind stresses compared to what would be expected from the respective values of $U_{10}/c(f)$ based on their phase speed $c(f)$.

At very strong wind forcing such relative reduction of the wind stress/input is applicable to the dominant waves themselves. The separated-over-the-crest-of-a-dominant-wave air flow does not reattach to the surface until close to the crest of the next wave. As a result, the wind effectively skips the wave troughs and 'does not know' how high/deep the waves are. Consequently, the wave-induced pressure oscillations in the lower boundary layer are weakened, and so is the wind input/stress [Donelan *et al.*, 2006].

Absolute values of the stress always increase as the $U_{10}/c(f)$ goes up, but relative values of the wind forcing can go down, depending on a combination of wind-speed and wave-steepness magnitudes, on whether the waves with corresponding frequency f are the spectral-peak or spectrum-tail waves. The wave breaking occurrence/probability will respond accordingly. Figure 4.2 in earlier Section 4.1.1 illustrates this effect: the first wind-speed doubling led to the breaking happened four times faster, whereas subsequent doubling the wind only reduced the distance-to-breaking three times.

Another complication of the general pattern in the spectral wave fields is dictated by the physics depicted in Radiative Transfer Equations (2.56). There exists a competition between source terms responsible for the wave evolution in RTE. As the wind grows, some of the excessive energy/momentum flux provided to short waves by the wind will be transferred to lower frequencies (faster waves in the spectrum) through non-linear interactions and will not contribute into the growth of wave height/steepness of these short waves.

One way or another, however, but at some stage of the growing wind forcing neither the air-flow separation nor the non-linear interactions seem to be able to digest the amount of energy input by the wind, and wave breaking (dissipation) across the spectrum suddenly goes up. This was demonstrated by Babanin *et al.* [2007c] and this effect can be seen in the earlier Figure 5.27 of Section 5.3.2 above.

In the top panel of this Figure, peculiarity of the wave-breaking-probability behaviour at strong winds is demonstrated. According to (5.9), (5.20), (5.36), the breaking probability and the dissipation function are expected to be determined by the wave spectrum, at least near the spectral peak. As concluded above, the wind influence on wave breaking and energy attenuation is indirect: the wind changes the wave spectrum first, and this change brings about alterations of the breaking as a consequence. In Figure 5.27 (top) the breaking distributions merge together for moderate winds and are clearly enhanced for the two stronger-wind cases across the entire spectral band. Therefore, we could expect that if the wave spectra solely define the breaking/dissipation, the spectra for the last two cases should also be enhanced as a result of the stronger wind forcing.

This is, however, not the case. Figure 5.47 shows the full spectra in log-log scale in the left panel, and in the right panel these spectra are plotted in expanded linear scale in the frequency range of $f = 0.8f_p - 3f_p$. The wave spectra do merge as expected for the moderate winds, but at strong winds of $U_{10} > 14$ m/s a further increase of the wind speed and the wind input does not cause noticeable changes of the wave spectrum either, except at the peak. The excessive wind input, or at least a significant part of it, appears to be dissipated locally through the enhanced breaking.

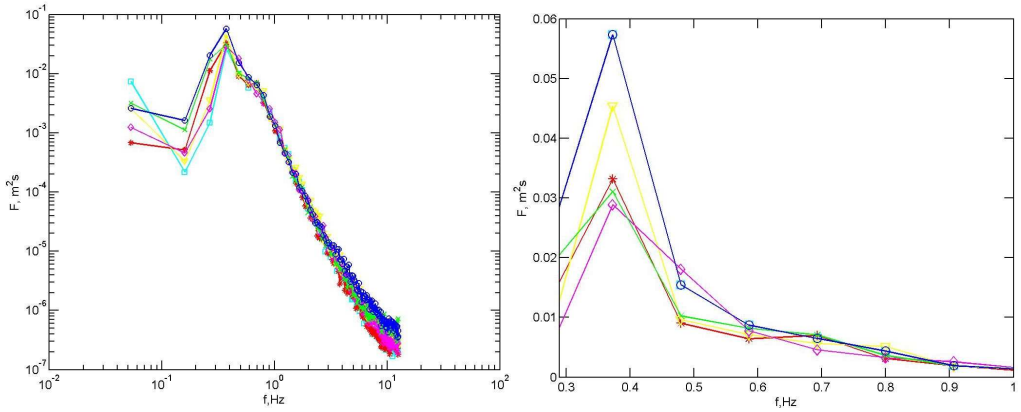

Fig. 5.47. Wave spectra for the records shown in Figure 5.27. (left) Full spectra in log-log scale. (right) Spectra in $f = 0.8f_p - 3f_p$ range in linear scale.

Alternatively, the excessive input could have been handled by the non-linear interactions (S_{in} term in (2.56)) and converted into the growth of the spectral peak. To add an uncertainty, however, we must point out that in the scenarios studied here the peak waves were strongly forced, with $U_{10}/c_p = 2.5$ and 6.5 respectively (records 6 and 5 of Table 5.2) , and thus extensively received the energy for their growth directly from the wind.

Therefore, we should conclude that wind influence on the wave breaking in spectral environments accepts additional roles compared to its effects in case of wind-forced uniform or modulated wave trains. The latter are obviously applicable to the trains of dominant waves and inherent breaking of shorter waves, but important new features of the wind-breaking connection are revealed at the smaller scales in the spectrum.

At light-to-moderate winds, the spectrum responds to the growing wind forcing U_{10}/c_p by increasing the level of its saturation interval α (2.7) up to the certain magnitude only:

$$\alpha = \begin{cases} 8.03 \cdot 10^{-2} \tilde{f}_p^{1.24} & \text{for } \tilde{f}_p \le 0.23, \\ 13.2 \cdot 10^{-3} & \text{for } \tilde{f}_p > 0.23 \end{cases} \tag{5.72}$$

[Babanin & Soloviev, 1998a]. Here,

$$\tilde{f} = \frac{fU_{10}}{g} = \frac{1}{2\pi}\frac{U_{10}}{c_p} \tag{5.73}$$

is dimensionless frequency. While the level α is growing and when the spectral densities overcome the threshold value of (5.32), the waves across the spectrum start to break and the rate of breaking should be increasing in response to the growing level and the induced-breaking effects (see Section 5.3.2, Figure 5.29 and associated discussions).

Once the equilibrium limit of α identified in (5.72) is reached, however, the level of the spectrum tail stops growing. As seen in Figure 5.27, the wave-breaking rates across the spectrum in such conditions remain approximately constant also, that is until the wind speed achieves its own limit. In the Lake George scenarion shown, when the wind speed exceeds this limit of

$$U_{10_{limit}} \approx 14 \text{ m/s}, \tag{5.74}$$

it appears that the further growth of the wind forcing results in abrupt changes of the breaking probability across the spectrum's equilibrium interval.

It should be reminded, however, that connections of the spectral density and the breaking probabilities above are indicative, but by far from being unambiguous. As it was discussed in detail in Section 5.3.2, the breaking rates at scales small relative to the peak are affected by the induced breaking and their dependence on the local spectral density is smeared. Rather, they should depend on the integral of the spectrum over the longer scales (by analogy with the dissipation function (5.36)).

These scales include the spectral peak. If so, Figure 5.47 provides a reasonable explanation of the observed wind effect in terms of the induced breaking. The two spectra which exhibit higher breaking rates of short waves are the ones which correspond to much higher dominant waves. For these two spectra the peak enhancement above the others is very noticeable. This is particularly apparent in the linear scale (right), that is the peak spectral density of the 15 m/s wind (crosses) is 1.5 times higher than the rest of the group, and for the 20 m/s (circles) it is twice as high. If so, modulation of the short waves by the larger dominant waves should be stronger and cause more frequent breaking in the corresponding spectral range.

Therefore, the observed response of the breaking rates across the spectrum to the higher wind speeds, under the virtually unchanged local spectral density, can in fact be a result induced by larger dominant waves rather than by the wind directly. Cause of the high dominant waves, however, still rests with the wind, which in this case managed to pump up the spectral peak while the equilibrium level stayed unchanged. One way or another, the wind forcing is of course the major player in the dynamics of the fields of wind-generated waves, and its multiple roles in the wave-breaking behaviour are still in need of further understanding and quantifying (see also discussion of wind effects on the breaking severity in Section 6).

To conclude this Section 5, and to some extent related results of Section 4, we would like to say that the topic of breaking probability has enjoyed a close attention of the ocean-wave community over the past two decades or so, and at the time of writing is still going through a stage of active progress. Not only some important physical features such as breaking threshold, cumulative effect, limiting breaking steepness were formulated and understood, they have been quantified too. It is instructive to notice that, while the breaking onset due to linear focusing was scrutinised much earlier than the details of onset because of modulational instability, the focusing-breaking probability is yet to be parameterised in terms of the background wave-field conditions. Many other behaviours and characteristics of the breaking probability are still to be identified, appreciated and described. These are first of all related to the breaking occurrence in spectral, and particularly in directional environments.

6 Wave breaking severity

At many occasions above in this paper, it was mentioned and emphasised that the knowledge of the breaking severity is as important as is understanding the physics driving the breaking occurrence. While the latter, however, received a lot of attention from the wave-research community lately, our information on the breaking strength, its variability, environmental dependences and physics remains limited and fragmental.

If the breaking strength is defined as energy loss in a single breaking event (Section 2.7), then the breaking severity coefficient s can be identified in a number of ways, that is through the measurements of the individual breaking wave (2.23), of the group where the breaking occurred (2.31), of spectra of the respective groups before and after the breaking (2.37), of short waves modulated by the longer wave only (2.41). Magnitude of such coefficient varies greatly, from $s = 10\%$ [Rapp & Melville, 1990, or even less as seen in Figure 6.3] up to 99% based on the Black Sea estimates (2.30).

Such range of change of course cannot be disregarded or substituted with some mean value in applications which involve the breaking severity. One of typical applications is wave-energy dissipation function S_{ds} employed in wave forecast models (2.21), (2.56). As defined in (2.21), it can in principle be directly determined as a product of the breaking probability and breaking severity, but since more or less definite parameterisations of the latter are not available a set of inventive indirect methods have been elaborated to estimate the dissipation function [see e.g. The WISE Group, 2007, for a review].

In other applications, such as, for example, engineering aspects of the wave-breaking impact, the breaking-strength magnitude needs to be known explicitly rather than as an element of the overall energy dissipation. More than that, statistical values such as those involved in obtaining the averaged dissipation term may not be helpful in this regard, as extreme or individual events may be sought after. Therefore, quantifying and parameterising the breaking severity is an important outstanding task of the wave-breaking studies.

Section 6 is shorter than other Sections in this paper for obvious reasons. There are not many experimental dependences and no theoretical approaches to discuss. In the two subsections, indicative laboratory (Section 6.1) and field (Section 6.2) results will be outlined in addition to those already mentioned in the definition Section 2.7.

6.1 Loss of energy in initially monochromatic train of steep waves

Features of the severity of breaking resulted from linear frequency focusing have been investigated in a number of laboratory studies, and the reader is referred to the comprehensive paper by Rapp & Melville [1990] and to other studies on this topic discussed in Section 2.7, for details. With respect to the breaking strength Rapp & Melville [1990] concluded that "The loss of excess momentum flux and energy flux was measured and found to range from 10% for a single spilling event to as much as 25% for plunging breakers".

Severity of the wave breaking which occurs due to the modulational instability varies in a much greater range, and appears to be a gradually changing property rather than a characteristic with approximately set values. Some respective results obtained in the course of the laboratory experiment described in Section 5.1 will be discussed here.

In Figure 6.1, an example of spectral distribution of the breaking severity due to a single

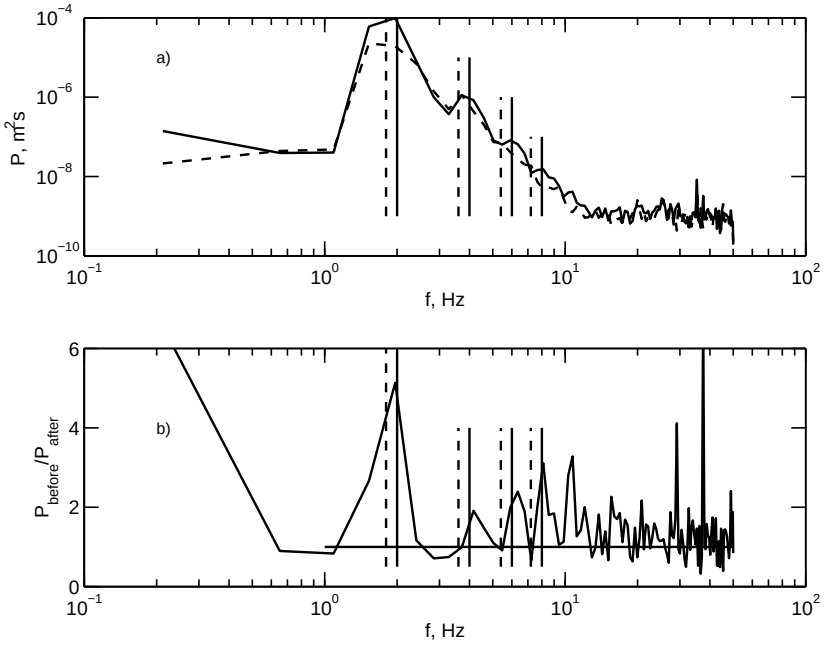

Fig. 6.1. a) Spectra P of the time series of $IMF = 1.8$ Hz, $IMS = 0.30, U/c = 0$. Solid line corresponds to the pre-breaking spectrum measured at the second probe (see solid-line time series in Figure 6.2). Dashed line is post-breaking spectrum measured at the third probe (dashed time series in Figure 6.2). Multiples of IMF are shown with dashed vertical lines. Multiples of the incipient-breaker 2 Hz frequency are shown with solid vertical lines. b) Ratio of the pre-breaking and post-breaking spectra. Solid horizontal line signifies ratio of 1, vertical lines have the same meaning as in the top panel.

event is demonstrated. Spectra of the time series of Figure 6.2 are plotted in Figure 6.1a and their ratio in Figure 6.1b. In the top panel, solid line signifies the pre-breaking spectrum and dashed line the after-breaking spectrum.

Spectral distribution of this breaking-severity event was discussed in Section 2.7 above. In short, we will mention that while it is the main wave which is breaking, the energy is lost from all the harmonics too. The peak is reduced by a factor of 5, and the other harmonics almost completely disappeared. Across the entire frequency range, the average ratio of the two spectra is 1.8 which translates into the overall spectral severity $s_{spectral} = 45\%$ (2.37).

In Figure 6.2, wave series before and after the breaking are compared in physical space. In this Figure, the solid line shows the waves of $IMF = 1.8$ Hz, $IMS = 0.30$, $U/c = 0$ at the second probe (10.53 m from the wavemaker), as in Figure 5.2, and dashed line – on the third probe (11.59 m from the paddle). Breaking of the three incipient breakers seen at probe 2 happened between the two probes. The wave which is seen following the incipient breaker on the second probe also broke between the two probes. This consistent double-breaking, with small time delay, is again in agreement with the field observations [e.g. Donelan *et al.*, 1972]. These

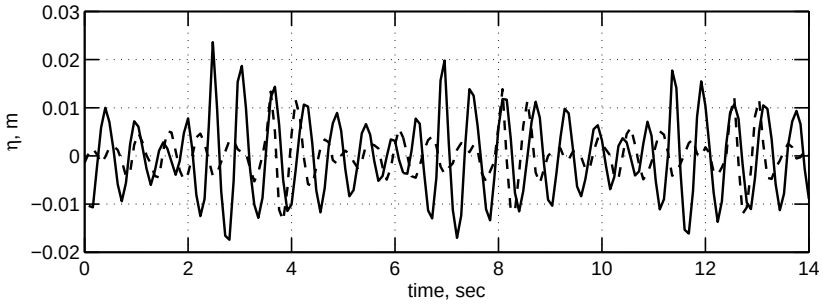

Fig. 6.2. The influence of breaking on the time series. A segment of the surface elevation time series with $IMF = 1.8$ Hz, $IMS = 0.30$, $U/c = 0$. Solid line - surface elevations at the second probe prior to breaking. Dashed line - same waves 1.2 s later at the third probe. The waves propagate from right to left.

breaking processes happened within a period of 1.2 s, the time required by the 1.8 Hz waves to travel the distance between the probes at their phase speed. Therefore, the records made by the third probe are time-shifted by 1.2 s in an attempt to superimpose what should have been the same waves, if the breaking did not take place. Note that the group velocity is different to the phase speed and the individual waves are travelling through the wave envelope seen in the Figure. Therefore, in absence of the breaking, the match of the two shifted time series do not necessarily have to be exact, depending on the phase of individual waves with respect to the envelope (see also Section 2.7 for corresponding discussion of this Figure).

With that in mind, we still see that the two waves which broke practically disappeared, as well as the entire modulation. The only waves which can still be tracked are the second and the third ones after the incipient breaker at probe 2. Overall severity of 45%, integrated over the spectrum above, is quite significant.

The number of waves in the segment has also changed. Between the three incipient breakers at probe 2, one can count 17 waves, and at probe 3 this number is closer to 16, i.e. frequency downshifting has occurred [see also Tulin & Waseda, 1999]. In fact, the two broken waves effectively merged into a single small wave.

When the wind forcing is superimposed over the mechanically generated waves, its overall effect on the wave breaking is very significant. The wind marginally influences the breaking probability, but its influence on the breaking strength is most essential.

With the tank length of about 15 m and wavelengths of the order of $\lambda \approx 0.5 - 0.7$ m, the fetch is short and the wind capacity to change the steepness of mechanical waves is limited, even at strong forcing. Therefore, one would expect only a weak dependence of the distance-to-breaking on the wind speed, which is what is seen in Figure 5.17. The wind, however, does alter this distance. In the experiment, gradual reduction of the Initial Monochromatic Steepness caused the waves breaking further and further from the wavemaker, all the way to the beach at the opposite end of the tank. If then the wind was switched on and its speed gradually increased, the breaking-onset point was brought somewhat back.

The breaking point, however, would not come too far from the beach, certainly not even to

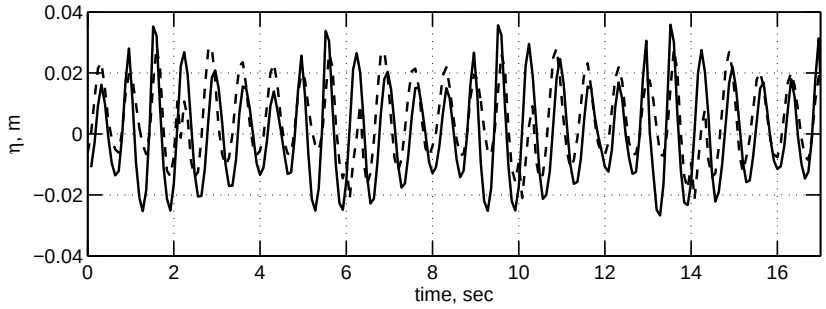

Fig. 6.3. As in Figure 6.2, with wind forcing. A segment of the time series with $IMF = 1.5$ Hz, $IMS = 0.30$, $U/c = 3.9$. Solid line - surface elevations at the second probe prior to breaking. Dashed line - same waves 1.04s later at the third probe. The waves propagate from right to left.

the middle of the tank, and this is not due to the lack of the wind power. The ASIST facility is capable of producing hurricane-strong winds. The reason was the breaking severity. As the wind forcing was increasing and the distance to the breaking decreasing, so was diminishing the breaking strength. In the end, already between the probes 2 and 3 which were 10.53 m and 11.59 m from the wavemaker, the breaking became a mere toppling of the very crest and effectively disappeared when the wind speed was increased further.

This effect is demonstrated in Figure 6.3 which is analogous to Figure 6.2 except the wind forcing is now superimposed and $IMF = 1.5$ is different. The Initial Monochromatic frequency had to be reduced in order to make the waves breaking between the same probes 2 and 3. As it was just mentioned, in presence of the wind forcing it would take fewer wavelengths to the breaking point and therefore longer waves had to be used.

Again, the wave time series are compared immediately before and after breaking. The solid line shows the waves of $IMF = 1.5$ Hz, $IMS = 0.30$, $U/c = 3.9$ at the second probe and the dashed line at the third probe. Breaking of the four incipient breakers seen at probe 2 occurred between the two probes. The breaking was very gentle when visually observed, and there was no double-breaking. With $IMF = 1.5$ Hz, the time necessary to travel the distance between the two probes is estimates as 1.04 s and therefore the record made on the third probe is shifted back correspondingly.

As it was analysed in Section 2.7, due to the difference of the phase speed and group velocity each of the solid-lined waves would approximately move one position ahead within the envelope, and the highest wave should become the second highest (in front of it) in the dash-lined group. Because of this, height of the highest wave would be significantly reduced even without breaking.

Breaking, even though gentle, however, happened and comparison of the breaking impacts in Figures 6.2 and 6.3 is quite instructive. In Figure 6.2, the incipient breaker and the wave following it practically disappeared, as well as the entire modulation. In Figure 6.3, they all are present and each wave in the modulation can be tracked at the third probe. The energy loss was minimal and could not have been quantified within the confidence limits of the respective spectra.

In contrast to Figure 6.2, after the breaking in Figure 6.3 the number of the waves did not change and no downshifting is visible. As seen in the Figure, the breaking resulted in some truncation of the crest of the highest wave in the group, and in smoothing the modulation.

The latter, we believe, is a most essential observation. The fact that the wind influence smears the modulation has already been noticed (i.e. Figure 5.2, Section 5.1.3). It was also seen that the wind impact on the wave breaking as such, at the wave-breaking time scale, is always small or even negligible (Sections 4.1.3, 5.1.3). Therefore, it appears that the wind does affects the severity in most essential way, but most likely it does this indirectly.

As seen in Figure 5.2, forcing of the non-linear mechanically-generated waves by the wind in the course of their evolution does not prevent the modulational instability, neither does it change the number of waves in the modulation. It, however, affects the depth of the modulation R (5.3). It is therefore this depth which probably brings about the variation of the breaking severity, since other modulational properties of the wave train appear to be the same. Thus, the wind action alters the modulation depth on a longer time scale, and the hydrodynamics related to the modulation itself controls the breaking strength at the short scale of the duration of the breaking process.

If so, the breaking severity, like the other wave-breaking features, depends mostly on hydrodynamics rather than on air-sea interactions. In order to investigate this dependence in pure hydrodynamic conditions, wind action may be removed. Physically, the wind seems an unnecessary complication, and the same effect should be possible to achieve by varying the modulation depth through superpositions of different non-linear wave trains and their perturbations. If the modulational depth, however, will ultimately appear to be responsible for the breaking severity in field conditions too, it is a property difficult to employ in spectral applications as there is no obvious way of how information on such characteristic can be obtained from a wave spectrum.

6.2 Dependence of the breaking severity on wave field spectral properties

As with the breaking probability discussed above, spectral and directional distribution of the breaking severity bears the principal uncertainty of how this property, which is not a continuous sequence of instantaneous values, can be converted into the Fourier space. If the number of individual breaking events is counted and energy loss in each of them is measured, then the average value of severity at frequency f in direction θ will depend on the frequency bin $f \pm \Delta f$ and directional bin of $\theta \pm \Delta\theta$ (see Sections 2.5 and 5.4 for more discussion).

With this uncertainty in mind, we can discuss the spectral distribution of the breaking severity in the same way as we did with the breaking probability in Section 5.3.2. In order to obtain a distribution similar to that for the probability in Figure 5.27, we need the count and the strength-measure of individual breaking events in the spectral and directional bins. The bubble-detection technique described in Section 3.5 can provide both.

This techniques employs sound emitted by individual bubbles when these bubbles are created in the course of the breaking. As seen in Figure 3.8, detected bubbles can be identified with a period (frequency f) of the overlying wave. Information on the breaking severity is carried by the bubble size R, if detected simultaneously. This is illustrated in Figure 3.11 for breaking waves in a uniform train. Similar calibration in a spectral environment is yet to be conducted.

In Figure 6.4, the three subplots demonstrate a dependence of the severity-related parameters on wave frequency for the 6 wave records of Table 5.2 depicted previously in Figure 5.27. The

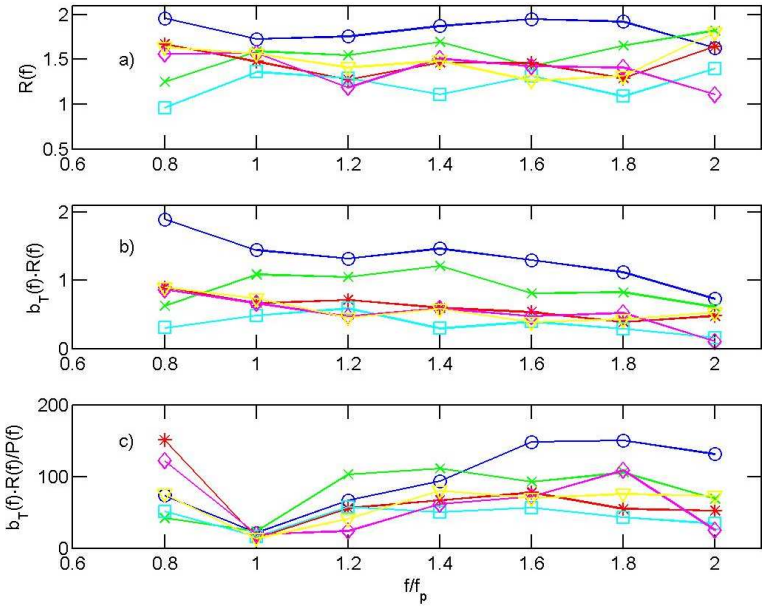

Fig. 6.4. Breaking severity analyses versus wave frequency f normalised by the peak frequency f_p. a) Breaking severity assumed as bubble radius $R(f)$; b) Product of breaking severity $R(f)$ and breaking probability $b_T(f)$; c) Product of breaking severity $R(f)$ and breaking probability $b_T(f)$ normalised by the spectral density $P(f)$. Squares: 12.8 m/s; *: 12.9 m/s; ∇: 13.2 m/s; diamonds: 13.7 m/s; $\times$: 15.0 m/s; circles: 19.8 m/s. The records are from Table 5.2.

mean-bubble-size distribution with wave frequency $R(f)$ is shown in the top panel. Since the bubble size does not depend on how many waves broke and it is quite uniform across the frequency range for each of the records, this means that the severity across the frequency, at least up to the relative frequency of $2f_p$ shown in the Figure, is approximately constant. Since the waves away from the peak, and certainly at the double peak frequency are significantly smaller, this observation implies that the relative strength of the breaking, i.e. severity coefficient s (2.23) goes up at higher-frequencies/smaller-scales.

Since the larger bubbles correspond to more severe breakers, the product of the mean bubble size $R(f)$ and the breaking rate $b_T(f)$ can be treated as a surrogate dissipation rate (2.20) at frequency f. It should be noticed that dependence of R on the wave energy loss is not linear, even in such a refined uniform-wave case as shown in the calibration Figure 3.11. Therefore, the surrogate dissipation must only be interpreted qualitatively, and not even in terms of proportionality.

The distribution of $b_T(f)R(f)$ is shown in Figure 6.4b, and $b_T(f)R(f)$ normalised by the spectral density $P(f)$ in Figure 6.4c. These distributions exhibit features similar to those of $b_T(f)$ in Figure 5.27, including the cumulative effect due to induced breaking at smaller scales.

Further observations can be made in Figure 6.4a with respect to the wind effect on the spectral-breaking strength. The mean bubble size $R(f)$ shows that the largest bubbles were produced by breakers at the highest wind speeds and the smallest bubbles were produced under

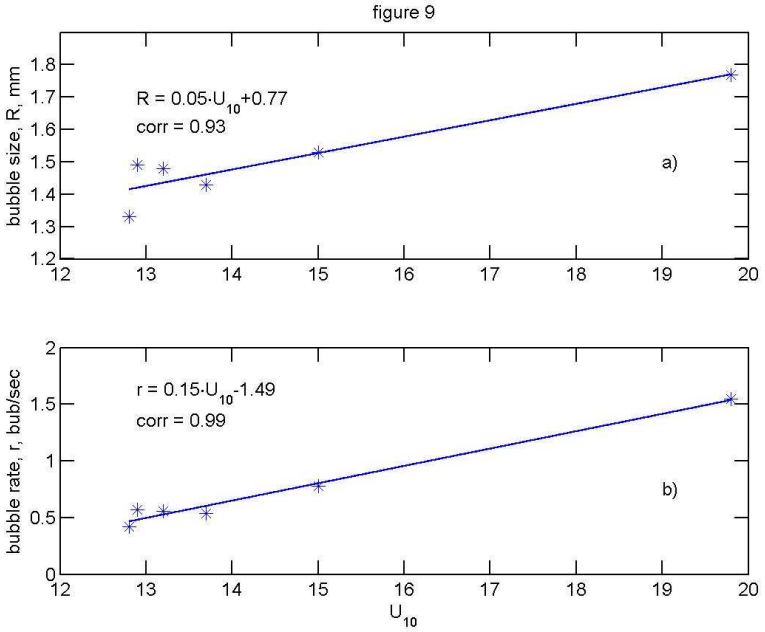

Fig. 6.5. Trends with wind speed U_{10}. a) Mean bubble radius R; b) Count rate. Combined datasets of Figure 6.4 are used.

the lightest winds. This is also illustrated in Figure 6.5, based on the bubble-detection technique both for the breaking severity and the bubble-generation rates. The increase in average bubble size with wind speed is now clear (Figure 6.5a). An increase in bubble-production rate with wind speed can be seen in Figure 6.5b. There is an apparent ordering of the wind speeds with respect to both the bubble rate and the mean radius, with quite high correlation. In summary, higher wind speeds in this Lake George observation generate breaking events more frequently, and the bubbles at higher wind speeds are larger.

Thus, the connection with the wind is opposite to that observed in the laboratory case (Section 6.1) where increased wind forcing associated with a decreased severity. These details expand and reinforce the conclusion already made in Section 6.1 that, although the correlations between the wind and the breaking strength can be well-traced in a particular circumstance, generally speaking the wind influences are indirect. These influences must be coming through the wave dynamics which is imparted by the wind on scales greater than the wave-breaking-event duration. Such dynamics can differ in the two-dimensional modulated wave trains and fully-spectral directional oceanic environments, even if the both are subject to a same wind forcing. Similar conclusion has also been made with respect to the breaking probability (Section 5.3.1 and Figure 5.19).

To conclude the breaking-severity Section 6, we will summarise what is unknown rather than definite knowledge, because the former certainly overweighs. What does the severity depend on? Will it be, for example constant, even if on average, in different wave fields with the same

background steepness, for instance? Does the breaking strength changes across the spectrum, i.e. is the relative energy loss different for the dominant waves and the shorter waves away from the peak? For the latter waves, does their severity depend on whether they break due to inherent reasons or their breaking is induced by larger waves? Is the severity dependent on the wind? How the wave directionality impacts the breaking strength, if it does? Also, for example, how much of the energy loss is spent on work against the buoyancy forces while entraining the bubbles into the water, and what fraction is passed on to the water turbulence? These and other questions should be answered and parameterised for the practical applications, and this topic represents a very interesting physics too.

7 Conclusions. What else do we need to know about the wave breaking?

In the Conclusions, it is sensible to revisit the Abstract which is a very brief summary of both significance of the topic of the paper and of its outcomes. That is, when the problem was introduced, it was stated that the wave breaking represents one of the most interesting and most challenging problems for both fluid mechanics and physical oceanography. It is an intermittent random process, very fast by comparison with other processes in the wave system. Distribution of the wave breaking on the water surface is not continuous, but its role in maintaining the energy balance within the continuous wind-wave field is critical.

The challenges thus outlined made the understanding of such wave breaking and even an ability to describe its onset very difficult, and as a result the knowledge of the physics of the breaking, and even practical parameterisations of the phenomenon have been hindered for decades. Recently, knowledge of the breaking phenomenon has significantly advanced, and this review paper was an attempt to summarise the facts into a consistent, even if still incomplete, picture of the phenomenon.

In this Conclusion Section, we will not be using references which are very detailed in the Sections above. A wide spectrum of achievements in the wave-breaking studies have been attended through the six Sections, and it can be broadened much further if breaking-related topics are incorporated into the discussion. Some of them were mentioned in passing or even in some detail, some of them were not, but it is quite often that their investigations are treated equivalent to the wave-breaking research as such, and the separation of the wave-breaking studies and wave-breaking-related studies adopted in this paper is quite superficial.

The separation had to be done, however, to stay within some reasonable limit for the paper volume which otherwise could be inflated indefinitely. For example, review of the whitecapping dissipation, whose research routinely stands for a synonym to wave-breaking studies, was not conducted here, even though we looked in detail on the breaking probability and breaking severity. These two features combined basically define the dissipation. As it happens, however, the dissipation research it is not a straightforward amalgamation of the two topics, but rather took on its own direction of investigations. A variety of innovative analytical, statistical, probabilistic, numerical, experimental and observational approaches have been developed to deal specifically with the whitecapping dissipation. Effectively, it is a research area in its own right which constitutes a large volume of knowledge, and has to be reviewed separately, particularly given its great applied importance with respect to the wave-forecast modelling.

In this regard, non-breaking dissipation of wave energy has to be clearly outlined and defined too, and studied in conjunction with the breaking dissipation. Such dissipation is often forgotten about, but not all the wave-energy dissipation comes through the breaking, and this fact has to be realised and clearly stated. This will help confusions in forecasting, for example, the swell propagation. While small, by comparison, in presence of breaking, it is only inessential as far as the wave attenuation is concerned. There is an emerging argument that role of non-breaking wave-induced turbulence in the upper ocean may be more essential than that of the breaking-produced turbulence. Non-breaking loss of the wave momentum/energy, passed back to the atmosphere, is another potentially significant physical element on the atmosphere-ocean interface, particularly in case of large-scale applications including climate modelling.

Non-dissipative impacts of the wave-breaking are also many and deserve a special attention and revision. Among others, they include breaking-caused spectral peak downshift, role of the

wave breaking in maintaining the level of the spectrum tail, wind-input enhancement due to wave breaking. The first of the three features mentioned, the downshift, for example, is most universally attributed to the weak non-linear interactions, and this is how it is treated in spectral wave models with very few exceptions. In the meantime, there is a compelling experimental evidence supported to an extent by a theoretical argument that the breaking does move the spectral peak to lower frequencies/wavenumbers. And under appropriate conditions, the rate of this peak-frequency change is much faster compared to the downshifiting brought about by the weak non-linear resonance.

The third of the three items mentioned in the paragraph above, the breaking-caused wind-input enhancement, is further linked to a wider topic of the role of the wave breaking in the small-scale air-sea interactions in general. These interactions affect the physics of the atmospheric bottom-boundary layer. It has been shown, for example, that the wave-breaking characteristics alter the sea-drag dependences in this layer. While such dependences bear a profound importance in the large-scale air-sea interaction modelling, because the sea-drag coefficient is often the parameter which solely defines the momentum flux between the atmosphere and the ocean in such models, the influences of the breaking on the variations of this coefficient have received a very poor attention so far.

Another contribution of the breaking to the air-sea interactions is the generation of spray which makes the air close to the interface a two-phase fluid. Such fluid has a different density since the water droplets are much heavier compared to the surrounding air, and as a result the spray absorbs some momentum of the existing air flow. In general, the suspended droplets may alter the behaviour of the very bottom of the boundary layer, where the interactions as such occur, in a significant way. These effects can potentially modify the air-sea interactions beyond recognition, if the amount of suspended water matter is essential, as it is under extreme wind-forcing/wave-breaking conditions such as bora winds or hurricanes. This has been shown in an escalating number of papers published on the topic over the past 5 years or so.

More byproducts of the wave-breaking studies can be found in the adjacent field of the upper-ocean mixing. Such mixing, at seasonal scale, for example, regulates the dynamic balance between the air and the water bodies, and ultimately negotiates the weather and climate conditions. In this regard, the breaking is responsible for a large proportion of the transfer of the momentum from the wind to the ocean, for generation of turbulence, for injecting the bubbles and thus facilitating the heat and gas exchange across the interface.

Other set of applications the wave-breaking research deals with relate to the breaking in finite water depths. These are depth-limited wave development, i.e. forecast of waves in finite-depth environments, shallow-water breaking (we mention it here separately from the finite-depth conditions due to apparent reasons), wave-bottom interactions, including sediment transport, among many others. While the ultimate criteria for the wave breaking, i.e. conditions (steepness) of the water surface when it loses stability and starts collapsing, should be the same in deep and finite waters, physics of the processes leading to the breaking onset and of the outcomes of the breaking event can be very different. In many regards, the wave breaking in finite and shallow depths is another research field rather than an extension of the deep-water topic into a new environment.

Among many more wave-breaking research areas, we can mention wave breaking in presence of currents, remote sensing applications of the wave breaking, engineering tasks. The latter attend to a set of problems, whose solutions have to be different to those research products

sought after in this paper and whose significance covers needs of marine transport, navigation, ship design, coastal and offshore industries, maritime safety issues, pollution mitigation, naval exercises, fishery, recreational activities at sea, and many others.

Returning to the summary of the content of the present paper, we will very briefly outline the most interesting from our point of view, even if subjective, elements in the chapters above. In Section 3, a large number of techniques for wave-breaking detection and measurements were described. We started from early and traditional ways of observations of the breaking, such as visual means, and went on discussing modern contact and remote-sensing methods applied both in the laboratory and in the field. The Section also includes subsections of some analytical and statistical approaches developed and applied to detect wave breaking and quantify its rates and properties.

Contact measurements are direct and obviously most accurate, and they serve as calibration means for the remote-sensing techniques and theoretical approaches to begin with. It should be emphasised that measuring the surface elevations (wave height) in very steep and non-linear waves, such as those at the breaking onset or in the process of breaking, is not always sufficient to estimate the respective wave energies. Relationships between the potential and kinetic energies in strongly non-linear waves are not known, and therefore measurements of the wave-motion velocity field are necessary to obtain the kinetic and thus the total energy. The good news, however, is that the surface-wave non-linearities appear to decay rapidly away from the surface. Therefore, at least in the deep water, we would expect the deviations from linear wave orbits being essential only very close to the interface, perhaps even within the crest-trough volume.

The contact measurements are apparently more difficult, and often impossible in the field, given the powerful and destructive nature of the breaking events to be measured. Many elaborative remote-sensing methods have been developed to help this problem. The infrared techniques based on disruption of the surface skin layer, for example, have been shown not only to detect the breaking occurrences, but also to indicate the breaking severity.

Most promising in this regard, in our view, are the passive acoustic methods. In particular, the bubble-detection method allows to identify the wave which is breaking and producing bubbles, and therefore to obtain distribution of breaking occurrences and of rates of such occurrences along the spectral frequency and wavenumber scales. Size of the produced bubbles can also be estimated which has a connection with the wave-energy loss, and thus information on the breaking severity is also available within this method. So, the technique has a demonstrated potential to measure all the elements of the spectral distribution of the wave-energy dissipation, and to do that by using a hydrophone. The hydrophones are simple and cheap sensors, and can be deployed below the surface and thus avoid the violent power of the wave breaking as such. Their energy consumption is small and they can be operated on batteries for long-term observations. Information on the time of bubble appearance and on its size is basically just two numbers, and therefore memory requirements for such devices are very modest too.

Analytical methods also described in Section 3 allow to point out presence of breaking events in wave records where the breaking was not registered by any experimental means. Since there are large quantities of wave records available, such methods can be very helpful to enhance their value in case some information on breaking occurrence and breaking statistics is necessary, even if approximate, but was not recorded directly.

Also in absence of direct counting and measuring the wave breaking, a set of statistical approaches outlined interprets the probability functions in order to infer information on the dissipa-

tion due to wave breaking. If compared with other theoretical methods intended for this purpose, this method has the least limiting underlying assumptions. Basically, all that is needed are the valid maximal and minimal experimentally-confirmed values of wave steepness of individual waves achieved in the course of breaking events.

Section 4 is dedicated to numerical simulations of the evolution of non-linear waves leading to the breaking onset, and the imminent breaking stage itself, by means of analytical approaches. The fully non-linear Chalikov-Sheinin model was used, which was also coupled with a model for the atmospheric boundary layer and allowed investigations of the wind influences on the breaking onset. Many new and interesting findings of this Section were further verified, investigated and researched into the stages beyond the breaking onset in experimental Sections 5 and 6.

Breaking-probability issues, both for quasi-monochromatic modulated wave trains and for spectral environments were reviewed in Section 5. For the wave trains, these included evolution of non-linear waves to breaking, direct measurements of a great variety of properties of an imminent breaker, laboratory investigation of the wind influence. The wave-breaking probability is parameterised as distance to the breaking dependent on Initially Monochromatic Steepness of the non-linear trains.

Extending the findings achieved for quasi-two-dimensional modulated monochromatic wave trains into description of the breaking in spectral and directional wave fields is far from straightforward. Some analogies are applicable to the dominant waves in the spectrum which correspond to the narrowbanded spectral peak and therefore exhibit the characteristic features of modulated wave groups. For these waves, parameterisation in terms of background mean wave steepness is possible, in a way similar to that above based on the IMS.

The analogies clearly do not work at smaller scales away from the spectral peak. Particularly challenging is understanding the directional distribution of the breaking probability. Wind-forcing effects on the spectral distribution of the breaking are also discussed.

If results of Sections 4 and 5 are combined, the most important conclusions are the breaking threshold in terms of the background statistical wave steepness, which concept is applicable both to the wave trains and wave fields, the limiting value of individual wave steepness, which identifies a breaking onset for this wave, and the induced-breaking effect for short waves modulated by longer ones. Directional behaviour of the breaking probability is not trivial and very intriguing, but is also very unclear at the present stage. Wind-forcing impacts, both for the breaking probability in wave trains and in the fields, are marginal and even negligible unless the winds are very strong.

The threshold behaviour means that the breaking in wave train/field does not happen at all unless the mean steepness is above some certain level. Once it is above this level, then the breaking rates/probabilities are determined by the magnitude of excess of the mean background steepness over the level. In case of continuous-spectrum environment, there is a threshold value for the spectral density at each spectral scale, which bears the same meaning for breaking of waves of this scale.

Significance of the threshold aspect of wave breaking, which is a certain observational and experimental feature, should not be underestimated. At present, for example, none of the operational wave-forecast models account for the threshold behaviour in their dissipation functions. This means that the models implicitly employ the physics which is not adequate at some circumstances and will predict an active whitecapping dissipation in environments where the waves do not actually break (for example, for swell).

It should be emphasised that wave trains/fields falling below the breaking threshold, i.e. such conditions where the breaking does not happen, do not, however, represent some different kind of non-linear behaviour compared to those waves above the threshold. All the non-linear features of the below-threshold wave fields should be the same, just of a lesser magnitude of course, with the allowance for the smaller steepness/non-linearity. What is different is that individual waves in the course of such impaired non-linear evolution do not reach a limiting steepness beyond which the water surface collapses.

This limiting steepness of $Hk/2 \approx 0.44$, which follows both from the fully non-linear numerical simulations of the breaking onset and from the experiments, is remarkably close to the well known 150-year old Stokes limit. The waves at the breaking onset, however, as they are simulated and observed do not look like the stationary pointy Stokes waves and rather exhibit the characteristic features of the crest instabilities and other transient dynamic properties. In this regard, it is not obvious whether the agreement is coincidental or based on fundamental limitations for the water surface in the gravity field.

The breaking threshold and the limiting steepness should be equally important to all the breaking waves, but it appears that in the spectral fields these arguments become of secondary importance for waves relatively short with respect to dominant waves. Amount of short waves breaking due to inherent reasons, i.e. due to the same reasons as the long waves, is small compared to their induced breaking. The latter can be triggered by the dominant breaking, or caused by modulation of the short waves with the carrying longer waves which modifies the steepness of short waves, or both.

In any case, the experimental evidence shows that the induced breaking essentially changes breaking rates of shorter waves, and at some spectral scales, say at frequencies greater than $2-4f_p$, the induced breaking completely dominates over the inherent breaking, to such an extent that the breaking probabilities at those frequencies should be disconnected from the local spectral density and be determined by the integral of the spectrum over frequencies below, including first of all the spectral peak. In passing, we will mention that this frequency should also identify the transition from the ω^{-4} to ω^{-5} behaviour at the spectral equilibrium interval, as the latter associates with the purely breaking-defined spectrum tail.

The induced breaking brings about the so-called cumulative effect, that is at each higher frequency the breaking is determined by all the waves with frequencies below. Like with the breaking-threshold feature mentioned above, the cumulative effect is a definite observational physical property which is missing in the present dissipation functions. That is, all the operational models and absolute majority of the research spectral wave models currently treat whitecapping dissipation at smaller scales in unrealistic way.

The last chapter before the Conclusions, Section 6 discusses wave-breaking severity. This short Section is dedicated to a topic whose knowledge at the present stage is scarce and quite limited. The loss of energy in the modulated wave trains and behaviour of the breaking strength in spectral environments are briefly discussed.

The breaking severity appears to vary in a very broad range, virtually between 0% and 100% energy loss in an individual breaking event. Most important finding in this regard is the role of the wind. While this role has always been mentioned as marginal as far as the breaking onset and breaking probability are concerned, it emerges of primary significance for the breaking strength.

As shown in laboratory experiments with modulated wave trains, the larger wind forcing increases the breaking probability, but decreases the breaking severity, to a point of practically

cancelling the breaking as such. It appears, however, that the wind achieves this effect not directly, but rather by means of gradually affecting the depth of the wave-group modulations in the course of wave-train evolution. As a result, the modulation depth of wind-forced trains is much smaller compared to those unforced, and this appears to lead to the different energetics of the breaking once it happens. If so, this will be a difficult property to account for in spectral models where information on the wave-group properties, yet alone on the depth of the modulation is basically lost.

Overall, in Section 6 more questions for future studies of the breaking severity are posted, than the answers given. Effectively, Section 6 starts the discussion which is the sub-title of the current Section 7: "What else do we need to know about the wave breaking?"

Apart from the breaking strength, which is the subject of great importance but poor knowledge, we would briefly outline two other most significant outstanding topics of wave-breaking research. The first one is the relative role of the wave focusing and the modulational instability in the breaking of realistic waves observed in field conditions. The second topic is directional properties of wave-breaking characteristics and phenomena.

Indeed, as have been discussed throughout the paper, it appears that in order to break all a wave needs is to reach some limiting steepness. It should not really matter what process leads them to this steepness. In this regard, the modulational instability, for example, is not the cause of the breaking, it is the cause of the modulation of the wave height within non-linear wave trains. In the course of such modulation, the waves may or may not reach the limiting steepness. In the first case they will not be breaking, whereas in the second case they will, although the instability physics is the same in both cases (up to the point of the breaking onset of course).

Broadly, the two physical mechanisms have been held responsible for the waves breaking, i.e. reaching the no-return steepness. The first mechanism, wave focusing can be further subdivided into frequency focusing, amplitude focusing and directional focusing.

The frequency focusing and amplitude focusing both exploit variation of the phase speeds of waves: either because of different frequencies or due to different amplitudes respectively. The frequency dispersion is quite large if the frequencies differ significantly and seems like a good candidate to often provide superpositions of various waves in the field with a continuous wave spectrum. The problem, however, is the fact that changes of the spectrum (i.e. wave height) are much more rapid than changes of the phase speed, as a function of frequency. That is, the waves with close frequencies/heights propagate with close speeds and are not likely to superpose, and the waves which are likely to superpose have so different wave heights that addition of the smaller ones to the primary wave does not alter the height of the latter appreciably. In a wave field with typical primary steepness of $ak = 0.1$, superposition of very many such waves at a single point would be needed in order to reach the limiting steepness of $ak = 0.44$ which becomes an event with a quite low probability.

The frequency dispersion has been one of the standard techniques of making waves break in laboratory, and correspondingly features of the breaking achieved this way have been investigated well. Some of these features are similar to those of the different type of breaking, some are not, as will be discussed below. What is surprising, however, is the apparent lack, if not absence, of studies which would provide a parameterisation or even a reasonable conclusion on how frequent breaking due to the frequency focusing is in a wave field with a typical background wave steepness and typical wave spectrum.

The amplitude dispersion intuitively seems a less likely event compared to the frequency

focusing because differences in wave phase speeds due to the amplitude variation are only of the second order of magnitude. This type of focusing, however, can bring together waves of the same frequency and therefore of close wave heights, and thus can make the breaking of primary wave more probable. Again, parameterisation of the breaking rates due to this type of focusing, or in combination with the other types is not available.

The directional focusing does not rely on the dispersion, but on the contrary on waves propagating with close phase speeds, at an oblique angle with respect to each other. Like with the amplitude focusing above, the advantage of directional focusing is the fact that waves of a similar frequency/height are brought together, and therefore fewer waves are required to reach the steepness limit, but the disadvantage is that steepness of the waves in the converging trains, if the trains are two, have to be close to half of the limiting steepness which is too high for typical wave fields. This, again, makes such type of focusing a rare event, particularly as the directional superposition of even two wavelets with close frequency is seldom in its own right as was discussed in Section 5.

As a result, none of the focusing mechanisms lends itself as an obvious likely candidate to provide reasonably high breaking rates observed in oceanic wave fields. Quantitative comparisons of the focusing-breaking probability with the probability due to modulational instability are impossible because of lack of respective experimental or theoretical dependences.

Parameterisations of the wave breaking brought about by the instability of quasi-two-dimensional wave trains are available and the corresponding breaking rates are quite reasonable from the point of view of those observed in the field, but another problem emerges with respect to applicability of such dependences to three-dimensional wave fields. What is against such direct extrapolation is the known experimental and theoretical results on limitations which the modulational mechanism has in broadband, and particularly in directional fields.

In this regard, it is worth to briefly revisit a number of features of non-linear wave behaviour leading to the modulational-instability breaking, which were revealed both in the two-dimensional simulations/measurements and in field observations as mentioned throughout the paper. Such is the double-breaking found in the laboratory experiments and observed in the field (also possible in case of frequency focusing). Such are the upshifting of spectral energy, the oscillations of the skewness/asymmetry. The dissipation cumulative effect is a certain feature of the wave-instability breaking, which is similar to the breaking due to amplitude focusing but is opposite to the frequency-focusing dissipation outcomes. The fact that doubling the wind input brings about modulational wave breaking four times as fast is consistent with field experiments on wind input. Although all these evidences are indirect, the very quantity of them indicates some quality.

How the modulational instability is possible in three-dimensional wave fields if it is impaired or even suppressed if the directionality becomes significant? A feasible answer is that wave groups remain a coherent quasi-two-dimensional structure at the scale of a few dozens of periods of dominant waves. If so, in the wave fields with the typical background steepness $ak \geq 0.1$ that would be a sufficient time to allow for a breaking wave to develop.

Evidences for such coherent wave groups are many among remote-sensing studies of surface ocean waves. Also, as it was discussed in the paper above, the Wavelet Directional Method which is based on the assumption that wave fields consist of such two-dimensional wavelets, rather than from a superposition of continuous trains of Fourier components intersecting at different angles, provides an indirect support to the existence of the coherent wavelets because it is able to

reproduce the directional properties of wave fields with a very low noise level.

In any case, now that these problems have been formulated it should not take too long to solve them. All the instrumentation means, measurement techniques and theoretical understanding are available, and it only requires attention and an effort of the wave-breaking research community.

The directional behaviours related to the breaking have also been listed above among the three most significant outstanding problems of the wave-breaking studies. Understandably, a lot of respective research was conducted in two dimensions, in theoretical, numerical and laboratory approaches, but as we can see the directional properties are most essential.

In this regard, the word 'directional' artificially unifies quite different and even unrelated physics. For example, investigation of the breaking due to directional focusing is one issue, whereas the impact of wave directionality on the modulational instability is a completely different topic. Yet another set of problems is associated with directional distributions of the breaking probability, breaking severity, whitecapping dissipation. All these problems are due to an additional level of difficulty and complexity when studying a three-dimensional as opposed to two-dimensional phenomenon, whether these are theoretical or experimental investigations. This additional level, however, is needed to be attended as the directionality obviously provides a principal impact on the physics of the wave breaking rather than a mere set of corrections to the existing knowledge.

Overall, in spite of the difficulties and gaps in understanding, we would like to conclude on an optimistic note. The wave-breaking research and knowledge is much better structured today compared to even ten years ago. The physical picture of wave breaking is still not complete, but a consistent image of this interesting and challenging phenomenon is emerging.

Acknowledgment

My main acknowledgment goes to the Editor-in-Chief of *Acta Physica Slovaca* Vladimir Buzek. It was his suggestion which made me to start this review paper and it was his support and encouragement which made me to finish. I am most grateful to all my colleagues on many years of collaborative wave-breaking research; materials of our joint papers form a significant part of this review. I am also thankful to colleagues from the wave-research community, particularly from The WISE Group, endless discussions with whom helped me to shape my current views on the wave breaking phenomenon.

References

ABE, T., ONO, T. & KISHINO, N. 1963 A fundamental study on the prevention of the salty damages due to the foaming of sea water (preliminary report). *J. Oceanogr. Soc. Japan* **18**, 185–192

AGNON, Y., BABANIN, A. V., CHALIKOV, D. & YOUNG, I. R. 2005 Fine scale inhomogeneity of wind-wave energy input, skewness and asymmetry. *Geophys. Res. Lett.* **32**, L12603, doi:10.1029/2005GL022701, 4p

AGRAWAL, Y. C., TERRAY, E. A., DONELAN, M. A., HWANG, P. A., WILLIAMS III, A. J., KAHMA, K. K. & KITAIGORODSKII, S. A. 1992 Enhanced dissipation of kinetic energy beneath surface waves. *Nature* **359**, 219–220

ALBER, I.E. 1978 The effects of randomness on the stability of two-dimensional wavetrains. *Proc. R. Soc. Lond.* **A363**, 525–546

ALPERS, W., ROSS, D. B. & RUFENACH, C. L. 1981 On the detactability of ocean surface wave by real and synthetic aperture radar. *J. Geophys. Res.* **86**, 6481–6498

ARDHUIN, F., CHAPRON, B. & COLLARD, F. 2009 Observation of swell dissipation across oceans. *Geophys. Res. Lett.* **36**, L06607, doi:10.1029/2008GL037030, 4p

ARSENYEV, S. A., DOBROKLONSKY, S. V., MAMEDOV, R. M. & SHELKOVNIKOV, N. K. 1975 Direct measurements of some characteristics of fine-scale turbulence from a stationary platform in the open sea. *Izvestiya, Atmospheric and Oceanic Physics* **11**, 530–533

BABANIN, A. V. & SOLOVIEV, Y. P. 1987 Parametirization of width of directional energy distributions of wind-generated waves at limited fetches. *Izvestiya, Atmospheric and Oceanic Physics* **23**, 645–651

BABANIN, A. V. 1988 Connection of parameters of wind surface current with the wind in the North-West part of the Black Sea. *Morskoi Gidrofizicheskii Zhurnal* **4**, 55–58 (in Russian, English abstract)

BABANIN, A. V., VERKEEV, P. P., KRIVINSKII, B. B. & PROSHCHENKO, V. G. 1993 Measurements of wind waves by means of a buoy accelerometer wave gauge. *Phys. Oceanogr.* **4**, 387–393

BABANIN, A. V. 1995 Field and laboratory observations of wind wave breaking. In *The Second Int. Conf. on the Mediterranian Coastal Environment, Tarragona, Spain, October 24-27, 1995* **3**, E. Ozhan, Ed., Autoritat Potuaria de Tarragona, Spain, 1919–1928

BABANIN, A. V. & POLNIKOV, V. G. 1995 On the non-Gaussian nature of wind waves. *Phys. Oceanogr.* **6**, 241–245

BABANIN, A. V. & SOLOVIEV, Y. P. 1998a Field investigation of transformation of the wind wave frequency spectrum with fetch and the stage of development. *J. Phys. Oceanogr.* **28**, 563–576

BABANIN, A. V. & SOLOVIEV, Y. P. 1998b Variability of directional spectra of wind-generated waves, studied by means of wave staff arrays. *Marine & Freshwater Res.* **49**, 89–101

BABANIN, A. V., YOUNG, I. R. & BANNER, M. L. 2001 Breaking probabilities for dominant surface waves on water of finite constant depth. *J. Geophys. Res.* **C106**, 11659–11676

BABANIN, A. V. & YOUNG, I. R. 2005 Two-phase behaviour of the spectral dissipation of wind waves. In *Proc. Ocean Waves Measurement and Analysis, Fifth Intern. Symposium WAVES2005, 3-7 July, 2005, Madrid, Spain*, Eds. B. Edge and J.C. Santas, paper no.51, 11p

BABANIN, A. V., YOUNG, I. R. & MIRFENDERESK, H. 2005 Field and laboratory measurements of wave-bottom interaction. In *Proc. 17th Australasian Coastal and Ocean Engineering Conf. and 10th Australasian Port and Harbour Conference, 20-23 September 2005, Adelaide, South Australia*, Eds. M.Townsend and D.Walker, The Institution of Engineers, Canberra, Australia, 293–298

BABANIN, A. V. 2006 On a wave-induced turbulence and a wave-mixed upper ocean layer. *Geophys. Res. Lett.* **33**, L20605, doi:10.1029/2006GL027308

BABANIN, A. V., CHALIKOV, D., YOUNG, I. R. & SAVELYEV, I. 2007a Predicting the breaking onset of surface water waves. *Geophys. Res. Lett.* **34**, L07605, doi:10.1029/2006GL029135, 6p

BABANIN, A. V., BANNER, M. L., YOUNG, I. R. & DONELAN, M. A. 2007b Wave follower measurements of the wind input spectral function. Part 3. Parameterization of the wind input enhancement due to wave breaking. *J. Phys. Oceanogr.* **37**, 2764-2775

BABANIN, A. V., YOUNG, I. R., MANASSEH, R. & SCHULTZ, E. 2007c Spectral dissipation term for wave forecast models, experimental study. In *Proc. 10th Intern. Workshop on Wave Hindcasting and Forecasting and Coastal Hazards, Oahu, Hawaii, November, 11-16, 2007*, WMO/IOC Joint Technical Commission for Oceanography and Marine Meteorology (JCOMM), 19p

BABANIN, A. V., TSAGARELI, K. N., YOUNG, I. R. & WALKER, D. 2007d Implementation of new experimental input/dissipation terms for modeling spectral evolution of wind waves. In *Proc. 10th Intern. Workshop on Wave Hindcasting and Forecasting and Coastal Hazards, Oahu, Hawaii, November, 11-16, 2007*, WMO/IOC Joint Technical Commission for Oceanography and Marine Meteorology (JCOMM), 12p

BABANIN, A. V. & MAKIN, V. K. 2008 Effects of wind trend and gustiness on the sea drag: Lake George study. *J. Geophys. Res.* **C113**, C02015, doi:10.1029/2007JC004233, 18p

BABANIN, A. V. & VAN DER WESHUYSEN, A. J. 2008 Physics of "saturation-based" dissipation functions proposed for wave forecast models. *J. Phys. Oceanogr.* **38**, 1831-1841

BABANIN, A. V. & HAUS, B. K. 2009 On the existence of water turbulence induced by nonbreaking surface waves. *J. Phys. Oceanogr.*, in press

BABANIN, A. V., CHALIKOV, D., YOUNG, I. R. & SAVELYEV, I. 2009a Numerical and laboratory investigation of breaking of steep two-dimensional waves in deep water. *J. Fluid Mech.*, submitted

BABANIN, A. V., CHALIKOV, D. & YOUNG, I. R. 2009b Breaking of two-dimensional waves in deep water. In *Int. Conf. in Ocean Eng., ICOE 2009 IIT Madras, Chennai, India, 1-5 Feb. 2009*, V. A. Anantha Subramanian, S. Nallayarasu, S. A. Sannasiraj, Eds., 386–395

BADULIN, S. I., PUSHKAREV, A. N., RESIO, D. & ZAKHAROV, V. E. 2005 Self-similarity of wind-driven seas. *Nonlin. Processes Geophys.* **12**, 891–945

BANNER, M. L., JONES, I. S. F. & TRINDER, J. C. 1989 Wavenumber spectra of short gravity waves. *J. Fluid Mech.* **198**, 321–344

BANNER, M. L. & TIAN, X. 1998 On the determination of the onset of breaking for modulating surface gravity waves. *J. Fluid Mech.* **367**, 107–137

BANNER, M. L., BABANIN, A. V. & YOUNG, I. R. 2000 Breaking probability for dominant waves on the sea surface. *J. Phys. Oceanogr.* **30**, 3145–3160

BANNER, M. L. & SONG, J. 2002 On the determining the onset and strength of breaking for deep water waves. Part 2: Influence of wind forcing and surface shear. *J. Phys. Oceanogr.* **32**, 2559–2570

BANNER, M. L., GEMMRICH, J. R. & FARMER, D. M. 2002 Multi-scale measurements of ocean wave breaking probability. *J. Phys. Oceanogr.* **32**, 3364–3375

BANNER, M. L. & PEIRSON, W. L. 2007 Wave breaking onset and strength for two-dimensional and deep-water wave groups. *J. Fluid Mech.* **585**, 93–115

BASS, S. J. & HEY, A. E. 1997 Ambient noise in the natural surf zone: wave-breaking frequencies. *IEEE J. Oceanic Eng.* **22**, 411–424

BELBEROV, Z. K., ZHURBAS, V. M., ZASLAVSKIY, M. M. & LOBISHEVA, L. G. 1983 Integral characteristics of frequency spectra of wind-generated waves. In *Interaction of Atmosphere, Hydrosphere and Lytosphere in Sea Coastal Zone*, Sofia, Bolgarian Academy of Sciences Press, 143–154

BENJAMIN, T. B. & FEIR, J. E. 1967 The disintegration of wave trains in deep water. Part 1. Theory. *J. Fluid Mech.* **27**, 417–430

BISTER, M. & EMANUEL, K. 1998 Dissipative heating and hurricane intensity. *Meteorol. Atmos. Phys.* **65**, 223–240

BLANCHARD, D. C. & WOODCOCK, A. H. 1957 Bubble formation and modification in the sea and its meteorological significance. *Tellus* **9**, 145–158

BLANCHARD, D. C. 1963 The electrification of the atmosphere by particles from bubbles in the sea. *Progr. Oceanogr.* **1**, 71–202

BONDUR, V. G. & SHARKOV, E. A. 1982 Statistical properties of whitecaps on a rough sea. *Oceanology* **22**, 274–279

BOYD, J. W. R. & VARLEY, J. 2001 The uses of passive measurement of acoustic emissions from chemical engineering processes. *Chem. Eng. Sci.* **56**, 1749–1767

BROWN, M. G. & JENSEN, A. 2001 Experiments in focusing unidirectional water waves. *J. Geophys. Res.* **C106**, 16917–16928

CALABRESEA, M., BUCCINOA, M. & PASANISI, F. 2008 Wave breaking macrofeatures on a submerged rubble mound breakwater. *J. Hydro-Environ. Res.* **1**, 216–225

CAPON, J. 1969 High-resolution frequency-wavenumber spectrum analysis. *Proc. IEEE* **57**, 1408–1418

CARDONE, V. J. 1969 Specification of the wind distribution in the marine boundary layer for wave forecasting. *Tech. Rept. GSL-69-1* New York University, 131p

CAREY, W. M. & BRADLEY, M. P. 1985 Low-frequency ocean surface noise sources. *J. Acoust. Soc. Am.* **78**, S1–S2

CARTMILL, J. W. & SU, M. Y. 1993 Bubble size distribution under saltwater and freshwater breaking waves. *Dyn. Atmos. Oceans* **20**, 25–31

CAULLIEZ, G. 2002 Self-similarity of near-breaking short gravity wind waves. *Phys. Fluids* **14**, 2917–2920

CHALIKOV, D. & SHEININ, D. 1998 Direct modeling of one-dimensional nonlinear potential waves. In *Nonlinear Ocean Waves*, Ed. Perrie W., Advances in Fluid Mechanics **17**, 207–258

CHALIKOV, D 2005 Statistical properties of nonlinear one-dimensional wave fields. *Nonlin. Processes Geophys.* **12**, 1–19

CHALIKOV, D. & SHEININ, D. 2005 Modeling extreme waves based on equations of potential flow with a free surface. *J. Comp. Phys.* **210**, 247–273

CHALIKOV, D 2007 Simulation of Benjamin-Feir instability and its consequences. *Phys. Fluids.* **19**, 016602, DOI:10.1063/1.2432303

CHALIKOV, D 2009 Transformaion of harmonic waves. *Dokladi Akademii Nauk Rossii*, submitted (in Russian)

CHAUDRY, A. H. & MOORE, R. K. 1984 Tower-based backscatter measurements of the sea. *IEEE J. Ocean. Eng.* **9**, 309–316

CHEN, L., MANASSEH, R., NIKOLOVKSA, A. & NORWOOD, A. 2003 Noise generation by an underwater gas jet. In *Proc. 8th Western Pacific Acoustics Conf.*, Melbourne, Australia, 7–9 April, WC21, 1–4

CHITRE M. A., POTTER, J. R. & ONG., S. H. 2006 Optimal and near-optimal signal detection in snapping shrimp dominated ambient noise. *IEEE J. Oceanic Eng.* **31**, 497–503

COMMANDER, K. W. & PROSPERETTI, A. 1989 Linear pressure waves in bubbly liquids: comparison between theory and experiments. *J. Acoust. Soc. Am.* **85**, 732–746

CRAIG, W. & SULEM, C. 1993 Numerical simulation of gravity waves. *J. Comp. Phys.* **108**, 73–83

CRAIK, A.D.D., AND LEIBOVICH, S. 1976 A rational model for Langmuir circulations. *J. Fluid Mech.*, **73**, 401–426

CRAPPER, G. D. 1957 An exact solution for progressive capillary waves of arbitrary amplitude. *J. Fluid Mech.* **96**, 417–445

CUMMINS, W. 1962 The impulse-response function and ship motion. *Schiffstechnik Forshugsh. Schiffbau Schiffsmaschineubau* **9**, 101–109

DAVIS, M. & ZARNIK, E. 1964 Testing ship models in transient waves. In *Proc. Fifth Symp. on Naval Hysrodynamics*, Washington, D.C., Office of Naval Research, 509–540

DEMCHENKO, P. F. 1993 Integral model of atmospheric planetary boundary layer with non-stationary equations for turbulent kinetic energy and its dissipation rate. *Izvestiya Akademii Nauk SSSR. Fizika Atmosferi i Okeana* **21**, 315–320 (in Russian, English abstract)

DIDENKULOV, I. N. 1992 The influence of wave-breaking bubbles on low-frequency underwater ambient noise formation. In *Breaking waves. IUTAM Symposium, Sydney, Australia, 1991*, M.L. Banner, R.H.J Grimshaw, Eds., Springer-Verlag, Berlin, Heidelberg, 181–186

DILLON, T. M., RICHMAN, J. C., HANSEN, C. G. & PEARSON, M. D. 1981 Near-surface turbulence measurements in a lake. *Nature* **290**, 390–392

DING, L. & FARMER, D. M. 1994 Observations of breaking surface wave statistics. *J. Phys. Oceanogr.* **24**, 1368–1387

DOERING, J. C. & DONELAN, M. A. 1997 Acoustic measurements of the velocity field beneath shoaling and breaking waves. *Coastal Eng.* **32**, 321–330

DOLD, J. W. & PEREGRINE, D. H. 1986 Water-wave modulation. In *Proc. 20th Int. Conf. Coastal Eng.*, Taipei, ASCE, 163-175

DOLD, J. W. 1992 An efficient surface-integral algorithm applied to unsteady gravity waves. *J. Comp. Phys.* **103**, 90–115

DONELAN, M. A., LONGUET-HIGGINS, M. S. & TURNER, J. S. 1972 Periodicity in whitecaps. *Nature* **239**, 449–451

DONELAN, M. A. 1978 Whitecaps and momentum transfer. In *Turbulent fluxes through the sea surface, wave dynamics and prediction*, Favre, NATO Conf. Series, K. Hasselmann, Ed., NY: Plenum Press, 74–94

DONELAN, M. A., HAMILTON, J. & HUI, W. H. 1985 Directional spectra of wind-generated waves. *Philos. Trans. R. Soc. Lond.* **A315**, 509–562

DONELAN, M. A. & PIERSON, W. J. 1987 Radar scattering and equilibrium ranges in wind-generated waves - with application to scatterometry. *J. Geophys. Res.* **C92**, 4971–5029

DONELAN, M. A., DRENNAN, W. M. & MAGNUSSON, A. K. 1996 Nonstationary analysis of the directional properties of propagating waves. *J. Phys. Oceanogr.* **26**, 1901–1914

DONELAN, M. A. 1998 Air-water exchange processes. In *Physical Processes in Lakes and Oceans. Coastal and Estuarine Studies* **54**, J. Imberger, Ed., 19–36

DONELAN, M. A. 2001 A nonlinear dissipation function due to wave breaking. In *ECMWF Workshop on Ocean Wave Forecasting, 2-4 July, 2001*, Series ECMWF Proceedings, 87–94

DONELAN, M. A., HAUS, B. K., REUL, N., PLANT, W. J., STIASSNIE, M., GRABER, H. C., BROWN, O. B. & SALTZMAN, E. S. 2004 On the limiting aerodynamic roughness of the ocean in very strong winds. *Geophys. Res. Lett.* **31**, L18306, doi:10.1029/2004GL019460

DONELAN, M. A., BABANIN, A. V., YOUNG, I. R., BANNER, M. L. & MCCORMICK, C. 2005 Wave follower field measurements of the wind input spectral function. Part I. Measurements and calibrations. *J. Atmos. Oceanic Tech.* **22**, 799–813

DONELAN, M. A., BABANIN, A. V., YOUNG, I. R. & BANNER, M. L. 2006 Wave follower field measurements of the wind input spectral function. Part I. Parameterization of the wind input. *J. Phys. Oceanogr.* **36**, 1672–1688

DRAZEN, D., MELVILLE, W. K. & LENAIN, L. 2008 Inertial scaling of dissipation in unsteady breaking waves. *J. Fluid Mech.* **611**, 307–332

DRENNAN, W. M., DONELAN, M. A., TERRAY, E. A. & KATSAROS, K. B. 1996 Oceanic turbulence dissipation measurements in SWADE. *J. Phys. Oceanogr.* **26**, 808–815

DUNCAN, J. H. 1981 An experimental investigation of breaking waves produced by a towed hydrofoil. *Proc. R. Soc. Lond.* **A377**, 331–348

DULOV, V. A., KUDRYAVTSEV, V. N. & BOL'SHAKOV, A. N. 2002 A field study of whitecap coverage and its modulations by energy containing surface waves. *Geophysical Monograph* **127**, 187–192

DYACHENKO, A. I., KUZNETSOV, E. A., SPECTOR, M. D. & ZAKHAROV, V. E. 1996 Analytical description of the free surface dynamics of an ideal fluid (canonical formalism and conformal mapping). *Physics Lett. A* **221**, 73–79

DYACHENKO, A. I. & ZAKHAROV, V. E. 2005 Modulation instability of stokes wave — freak wave. *Pis'ma v ZhETF* **81**, 318–322

DURAISWAMI, R., PRABHUKUMAR, S. & CHAHINE, G. L. 1998 Bubble counting using an inverse scattering method. *J. Acoust. Soc. Am.* **104**, 2699–2717

EBUCHI, N., KAWAMURA, H. & TOBA, Y. 1987 Fine structure of laboratory wind-wave surfaces studied using an optical method. *Boundary-Layer Meteorol.* **39**, 133–151

ESTER, L. & ARNONE, R. 1994 Effect of whitecaps on determination of chlorophyll concentration from satellite data. *Remote Sens. Environ.* **50**, 328–334

FARGE, M. 1992 Wavelet transforms and their applications to turbulence. *Ann. Rev. Fluid Mech.* **24**, 395–457

FARMER, D. M. & VAGLE, S. 1988 On the determination of breaking surface wave distribution. *J. Geophys. Res.* **C93**, 3591–3600

FARMER, D. M., VAGLE, S. & BOOTH, A. D. 1998 A free-flooding acoustic resonator for measurement of bubble size distribution. *J. Atmos. Oceanic Technol.* **15**, 1132–1146

FEIR, J. E. 1967 Discussion: Some results from wave pulse experiments. *Proc. Rpy. S. Lond.* **A299**, 54

FELIZARDO, F. C. & MELVILLE, W. K. 1995 Correlation between ambient noise and the ocean surface wave field. *J. Phys. Oceanogr.* **25**, 513–532

FOCHESATO, C., GRILLI, S. & DIAS, F. 2007 Numerical modeling of extreme rogue waves generated by directional energy focusing. *Wave Motion* **26**, 395–416

GARRATT, J. R. 1977 Review of drag coefficients over oceans and continents. *Mon. Wea. Rev.* **105**, 915–927

GARRETT, W. D. 1967 The influence of surface-active material on the properties of air bubbles at the air/sea interface. *Naval Research Lab. Rept. 6545*, Washington, D.C., 14p

GATHMAN, S. & TRENT, E. M. 1998 Space charge over the open ocean. *J. Atmos. Sci.* **25**, 1075–1079

GEMMRICH, J. R. & FARMER, D. M. 1999 Observations of the scale and occurrence of breaking surface waves. *J. Phys. Oceanogr.* **29**, 2595–2606

GEMMRICH, J. R. & FARMER, D. M. 2004 Near-surface turbulence in the presence of breaking waves. *J. Phys. Oceanogr.* **34**, 1067–1086

GEMMRICH, J. R. 2006 The spectral scale of surface wave breaking. In *Proc. 9th Int. Workshop on Wave Hindcasting and Forecasting, Victoria, B.C., Canada, September 24-29, 2006*, 7p

GEMMRICH, J. R., BANNER, M. L. & GARRETT, C. 2008 Spectrally resolved energy dissipation rate and momentum flux of breaking waves. *J. Phys. Oceanogr.* **38**, 1296–1312

GEMMRICH, J. R. 2009 Strong turbulence in the wave crest region. *J. Phys. Oceanogr.*, submitted

GORDON, H. R. 1997 Atmospheric correction of ocean color imagery in the Earth Observing System Era. *J. Geophys. Res.* **102**, 17081–17106

GUAN, C., HU, W., SUN, J. & LI, R. 2007 The whitecap converage model from breaking dissipation parameterizations of wind waves. *J. Geophys. Res.* **C112**, doe:10.1029/2006JC003714, 9p

HAINES, M. A. & JOHNSON, B. D. 1995 Injected bubble populations in seawater and fresh water measured by a photographic method. *J. Geophys. Res.* **100**, 7057–7068

HARA, T. & JOHNSON, S. E. 2002 Wind forcing in the equilibrium range of wind-wave spectra. *J. Fluid Mech.* **470**, 223–245

HASSELMANN, K. 1960 Grundgleichungen der Seegangsvoraussage (in German). *Schiffstechnik* **7**, 191–195

HASSELMANN, K. 1962 On the non-linear energy transfer in a gravity-wave spectrum. Part I. General theory. *J. Fluid Mech.* **12**, 481–500

HASSELMANN, K., BARNETT, T.P., BOUWS, E., CARLSON, H., CARTWRIGHT, D.E., ENKE, K., EWING, J.A., GIENAPP, H., HASSELMANN, D.E., KRUSEMAN, P., MEERBURG, A., MULLER, P., OLBERS, D.J., RICHTER, K., SELL W. & WALDEN, H. 1973 Measurements of wind-wave growth and swell decay during the Joint North Sea Wave Project (JONSWAP). *Dtsch. Hydrogh. Z. Suppl.* **A8**(12), 1–95

HASSELMANN, K. 1974 On the spectral dissipation of ocean wave due to white capping. *Boundary-Layer Meteorol.* **6**, 107–127

HASSELMANN, K., JANSSEN, P. A. E. M. & KOMEN, G. J. 1994 Wave-wave interaction. In *Dynamics and Modelling of Ocean Waves*, G.J. Komen, L. Cavaleri, M. Donelan, K. Hasselmann, S. Hasselmann, P.A.E.M. Janssen, Cambridge University Press, 113–143

HOLTHUIJSEN, L. H. & HERBERS, T. H. C. 1986 Statistics of breaking waves observed as whitecaps in the open sea. *J. Phys. Oceanogr.* **16**, 290–297

HOLTHUIJSEN, L. H. 2007 *Waves in Oceanic and Coastal Waters*, Cambridge University Press, 387p

HOUMB, O. G. & OVERVIK, T. 1976 Parameterization of wave spectra and long term joint distribution of wave height and period. In *Proc. Symp. Behavior of Offshore Structures* **1**, 144–169

HUA, F. & YUAN, Y. 1992 Theoretical study of breaking wave spectrum and its application. In *Breaking waves. IUTAM Symposium, Sydney, Australia, 1991*, M.L. Banner, R.H.J. Grimshaw, Eds., Springer-Verlag, Berlin, Heidelberg, 177–282

HUANG, N. E., LONG, S. R. & BLIVEN, L. F. 1983 A non-Gaussian statistical model for surface elevation of nonlinear random wave fields. *J. Geophys. Res.* **C88**, 7597–7606

HUANG, N. E., LONG, S. R., BLIVEN, L. F. & TUNG, C. C. 1984 The non-Gaussian joint probability density function of slope and elevation for a non-linear gravity wave field. *J. Geophys. Res.* **C89**, 1961-1972

HUANG, N. E. 1986 An estimate of the influence of breaking waves on the dynamics of the upper ocean. In *Wave Dynamics and Radio Probing of the Sea Surface*, O.M. Phillips, K. Hasselmann, Eds., New York: Plenum, 295–313

HUANG, N. E., SHEN, Z., LONG, S. R., WU, M. C., SHIN, H. H., ZHENG, Q., YEN, N.-C., TUNG, C.C. & LIU, H. H. 1998 The empirical mode decomposition and the Hilbert spectrum for nonlinear and non-stationary time series analysis. *Proc. R. Soc. Lond.* **A454**, 903–995

HWANG, P. A., XU, D. & WU, J. 1989 Breaking of wind-generated waves: breaking and characteristics. *J. Fluid Mech.* **202**, 177–200

HWANG, P. A. & WANG, D. W. 2004 An empirical investigation of source term balance of small scale surface waves. *Geophys. Res. Lett.* **31**, L15301, doi:10.1029/2004GL020080

HWANG, P. A. 2007 Spectral signature of wave breaking in surface wave components of intermediate-length scale. *J. Mar. Sys.* **66**, 28–37

JANSSEN, P. A. E. M. 1994 Wave growth by wind. In *Dynamics and Modelling of Ocean Waves*, G.J. Komen, L. Cavaleri, M. Donelan, K. Hasselmann, S. Hasselmann, P.A.E.M. Janssen, Cambridge University Press, 71–112

JANSSEN, P. A. E. M. 2003 Nonlinear four-wave interaction and freak waves. *J. Phys. Oceanogr.* **33**, 863-884

JESSUP, A. T., KELLER, W. C. & MELVILLE, W. K. 1990 Measurements of sea spikes in microwave backscatter at moderate incidence. *J. Geophys. Res.* **95**, 9679–9688

JESSUP, A. T., ZAPPA, C. J. & YEH, H. 1997a Defining and quantifying microscale wave breaking with infrared imagery. *J. Geophys. Res.* **C102**, 23145–23153

JESSUP, A. T., ZAPPA, C. J., LOEWEN, & HESANY, V. 1997b Infrared remote sensing of breaking waves. *Nature* **385**, 52–55

JESSUP, A. T. & PHADNIS, K. 2005 Measurement of the geometric and kinematic properties of microscale breaking waves from infrared imagery using a PIV algorithm. *Measur. Sci. Tech.* **16**, 1961–1969

JONES, I. S. F. 1985 Turbulence below wind waves. In *The Ocean Surface - Wave Breaking, Turbulent Mixing and Radio Probing*, Y. Toba, H. Mitsuyasu, Eds., Reidel, 437–442

KATSAROS, K. B. 1980 The aqueous thermal boundary layer. *Boundary Layer Meteorol.* **18**, 107–127

KATSAROS, K. B. & ATAKTURK, S. S. 1992 Dependence of wave-breaking statistics on wind stress and wave development. In *Breaking waves. IUTAM Symposium, Sydney, Australia, 1991*, M.L. Banner, R.H.J. Grimshaw, Eds., Springer-Verlag, Berlin, Heidelberg, 119–132

KENNEDY R. M. & SNYDER, R. L. 1983 On the formation of whitecaps by a threshold mechanism. Part I: Monte-Carlo experiments. *J. Phys. Oceanogr.* **13**, 1493–1504

KERMAN, B. R. 1988 *Sea surface sound: Natural mechanisms of surface generated noise in the ocean.* Kluwer Academic, 639p

KERMAN, B. R. 1992 *Natural physical sources of underwater sound: Sea Surface sound.* Kluwer Academic, 749p

KELLER, W. C., PLANT, W. J. & VALENZUELA, G. R. 1986 Observations of breaking ocean waves with coherent microwave radar. In *Radio Probing of the Ocean Surface*, O.M Phillips, K. Hasselmann, Eds., New York: Plenum, 285–293

KJELDSEN, S. P. & MYRHAUG, D. 1980 Wave-wave interactions, current-wave interactions and resulting extreme waves and breaking waves. In *Proc. 17th Coastal Eng. Conf.*, 2277–2303

KNUDSEN, V., ALFORD, R. S. & EMLING, J. W. 1948 Underwater ambient noise. *J. Marine Res.* **7**, 410–429

KOMEN, G. I., CAVALERI, L., DONELAN, M., HASSELMANN, K., HASSELMANN, S. & JANSSEN, P. A. E. M. 1994 *Dynamics and Modelling of Ocean Waves.* Cambridge University Press, UK, 554p

KRAAN, C., OOST, W. A. & JANSSEN, P. A. E. M. 1996 Wave energy dissipation by whitecaps. *J. Atmos. Ocean. Technol.* **13**, 262–267

KUDRYAVTSEV, V. N., MAKIN, V. K. & MEIRINK, J. F. 2001 Simplified model of the air flow above the waves. *Boundary-Layer Meteorol.* **98**, 155–171

KUDRYAVTSEV, V. N. & MAKIN, V. K. 2002 Coupled dynamics of short wind waves and the air flow over long surface waves. *J. Geophys. Res.* **C107**, doi:10.1029/2001JC001251, 13p

KUDRYAVTSEV, V. N. & MAKIN, V. K. 2007 Aerodynamic roughness of the sea surface at high winds. *Boundary-Layer Meteorol.* **125**, 289–303

KWOH, D. S. & LAKE, B. M. 1984 A deterministic, coherent, and dual-polarized laboratory study of microwave backscattering from water waves, Part I: Short gravity waves without wind. *IEEE J. Ocean. Eng.* **9**, 291–308

LAKE B. M. & YUEN H. C. 1978 A new model for nonlinear wind waves. Part 1. Physical model and experimental evidence. *J. Fluid Mech.* **88**, 33–66

LAMMARRE, E. & MELVILLE, W. K. 1992 Void-fraction measurements and sound-speed fields in bubble flumes generated by breaking waves. *J. Acoust. Soc. Am.* **95**, 1317–1328

LAMONTH-SMITH, T., WASEDA, T. & RHEEM, C.-K. 2007 Measurements of the Doppler spectra of breaking waves. *IET Radar Sonar Navig.* **1**, 149–157

LANDAU, L. D. & LIFSHITZ, E. M. 1987 *Fluid Mechanics*, Butterworth-Heinemann, 539p

LANGMUIR, I. 1938 Surface motion of water induced by the wind. *Science* **87**, 119–123

LARGE, W. G. & POND, S. 1981 Open ocean momentum flux measurements in moderate to strong winds. *J. Phys. Oceanogr.* **11**, 324–336

LAVRENOV, I. V. 2003 *Wind-Waves in Oceans: Dynamics and Numerical Simulations.* Springer, 377p

LEIGHTON, T. G. 1994 *The Acoustic Bubble*. Academic Press, London, 613p

LEIKIN, I. A., DONELAN, M. A., MELLEN, R. H. & MCLAUGHLIN, D. J. 1995 Asymmetry of wind generated waves studied in a laboratory tank. *Nonlin. Processes Geophys.* **2**, 280–289

LEWIS, B. L. & OLIN, I. D. 1980 Experimental study and theoretical model of high-resolution radar backscatter from the sea. *Radio Sci.* **15**, 815–828

LIGHTHILL, M. J. 1965 Contrubutions to the theory of waves in non-linear dispersive systems. *J. Inst. Math. Appl.* **1**, 269–306

LIU, P. C. 1993 Estimating breaking statistics from wind-wave time series data. *Ann. Geophys.* **11**, 970–972

LIU, P. C. 2000 Wavelet transform and new perspective on coastal and ocean engineering data analysis. In *Advances in Coastal and Ocean Engineering* **6**, P. L. F. Liu, Ed., World Scientific, 57–101

LIU, P. C., SCHWAB, D. J. & MCLAUGHLIN, R. E. 2002 Has wind-wave modeling reached its limit? *Ocean Eng.* **29**, 81–98

LIU, P. C. & BABANIN, A. V. 2004 Using wavelet spectrum analysis to resolve breaking events in the wind wave time series. *Ann. Geophys.* **22**, 3335–3345

LIU, P. C., CHEN, H. S., DOONG, D.-J., KAO, C. C. & HSU, Y.-J. G. 2007 Monstrous ocean waves during typhoon Krosa. *Ann. Geophys.* **26**, 1327–1329

LONG, M. W. 1974 On a two-scatterer theory of sea echo. *IEEE Trans. Antennas Propag.* **AP-22**, 667–672

LONGUET-HIGGINS, M. S., CARTWRIGHT, D. E. & SMITH, N. D. 1963 Observations of the directional spectrum of sea waves using the motions of the floating buoy. In *Proc. Conf. on Ocean Spectra*, Prentice-Hall, Englewood Cliffs, NJ, 111–136

LONGUET-HIGGINS, M. S. 1969 On wave breaking and the equilibrium spectrum of wind-generated waves. *Proc. Rpy. Soc.* **A310**, 151–159

LONGUET-HIGGINS, M. S. 1974 Breaking waves in deep or shallow water. In *Proc. 10th Conf. Naval Hydrodynamics*, M.I.T., 597–605

LONGUET-HIGGINS, M. S. & TURNER, J. S. 1974 An "entrainment plume" model of a spilling breaker. *J. Fluid Mech.* **63**, 1–20

LONGUET-HIGGINS, M. S. 1975a Integral properties of periodic waves of finite amplitude. *Proc. R. Soc. Lond.* **A342**, 157–174

LONGUET-HIGGINS, M. S. 1975b On the joint distribution of the periods and amplitudes of sea waves. *J. Geophys. Res.* **C80**, 2688–2694

LONGUET-HIGGINS, M. S. & COKELET, E. D. 1976 The deformation of steep surface waves on water. I. A numerical method of computation. *Proc. R. Soc. Lond.* **A350**, 1–26

LONGUET-HIGGINS, M. S. & FOX, M. G. H. 1977 Theory of the almost highest wave: The inner solution. *J. Fluid Mech.* **80**, 721–741

LONGUET-HIGGINS, M. S. & COKELET, E. D. 1978 The deformation of steep surface waves on water. II. Growth of normal-mode instabilities. *Proc. R. Soc. Lond.* **A364**, 1–28

LONGUET-HIGGINS, M. S. 1983 On the joint distribution of wave periods and amplitudes in a random wave field. *Proc. R. Soc. Lond.* **A389**, 241–258

LONGUET-HIGGINS, M. S. & SMITH, N. D. 1983 Measurement of breaking waves by a surface jump meter. *J. Geophys. Res.* **88**, 9823–9831

LONGUET-HIGGINS, M. S. 1984 Statistical properties of wave groups in a random sea state. *Phil. Trans. R. Soc. Lond.* **312A**, 219–250

LONGUET-HIGGINS, M. S. 1985 Accelerations in steep gravity waves. *J. Phys. Oceanogr.* **15**, 1570–1579

LONGUET-HIGGINS, M. S. 1989 Monopole emission of sound by asymmetric bubble oscillations. Part 1. Normal modes. *J. Fluid Mech.* **201**, 525–541

LONGUET-HIGGINS, M. S. & DOMMERMUTH, D. G. 1997 Crest instabilities of gravity waves. Part 3. Nonlinear development and breaking. *J. Fluid Mech.* **336**, 51–68

LONGUET-HIGGINS, M. S. & TANAKA, M. 1997 On the crest instabilities of steep surface waves. *J. Fluid Mech.* **336**, 33–50

LOWEN, M. R. & MELVILLE, W. K. 1991a Microwave backscatter and acoustic radiation from breaking waves. *J. Fluid Mech.* **224**, 601–623

LOWEN, M. R. & MELVILLE, W. K. 1991b A model of the sound generated by breaking waves. *J. Acoust. Soc. Am.* **90**, 2075–2080

LOWEN, M. R. & SIDDIQUI, M. H. K. 2006 Detecting microscale breaking waves. *Meas. Sci. Technol.* **17**, 771–780

LU, N. Q., PROSPERETTI, A. & YOON, S. W. 1990 Underwater noise emissions from bubble clouds. *IEEE J. Oceanic Eng.* **15**, 275–281

LYZENDA, D. R., MAFFETT, A. L. & SHUCHMAN, R. A. 1983 The contribution of wedge scattering to the radar cross section of the ocean surface. *IEEE Trans. Geosci. Remote Sens.* **GE-21**, 502–505

MEZA, E., ZHANG, J. & SEYMOUR, R. J. 2000 Free-wave energy dissipation in experimental breaking waves. *J. Phys. Oceanogr.* **30**, 2404–2418

MANASSEH, R. 1997 Acoustic sizing of bubbles at moderate to high bubbling rates. In *Experimental Heat Transfer, Fluid Mechanics and Thermodynamics*, M. Giot, F. Mayinger, G. P. Celata, Eds., Edizoni ETS, 943–947

MANASSEH, R., YOSHIDA, S. & RUDMAN, M. 1998 Bubble formation processes and bubble acoustic signals. In *Proc. Third Int. Conf. Multiphase Flow*, Lyon, France, 8-12 June, 1

MANASSEH, R., LAFONTAINE, R. F., DAVY, J., SHEPHERD, I. C. & ZHU, Y. 2001 Passive acoustic bubble sizing in sparged systems. *Exp. Fluids* **30**, 672–682

MANASSEH, R., NIKOLOVSKA, A., OOI, A. & YOSHIDA, S. 2004 Anisotropy in the sound field generated by a bubble chain. *J. Sound Vibration* **278**, 807–823

MANASSEH, R., BABANIN, A. V., FORBES, C., RICKARDS, K., BOBEVSKI, I. & OOI, A. 2006 Passive acoustic determination of wave-breaking events and their severity across the spectrum. *J. Atmos. Ocean. Technol.* **23**, 599–618

MANASSEH, R., RIBOUX, G. & RISSO, F. 2008 Sound generation on bubble coalescence following detachment. *Int. J. Multiphase Flows* **34**, 938–949

MEDWIN, H. 1989 Bubble sources of the Knudsen sea noise spectra. *J. Acoust. Soc. Am.* **86**, 1124–1130

MEDWIN, H. & DANIEL, A. C. 1990 Acoustic measurements of bubble production by spilling breakers. *J. Acoust. Soc. Am.* **88**, 408–412

MELVILLE, W. K. 1982 Instability and breaking of deep-water waves. *J. Fluid Mech.* **115**, 165–185

MELVILLE, W. K., LOEWEN, M., FELIZARDO, F., JESSUP, A. & BUCKINGHAM, M. 1988 Acoustic and microwave signatures of breaking waves. *Nature* **336**, 54–56

MELVILLE, W. K., LOEWEN, M. R. & LAMARRE, E. 1992 Sound production and air entrainment by breaking waves: a review of recent laboratory experiments. In *Breaking waves. IUTAM Symposium, Sydney, Australia, 1991*, M.L. Banner, R.H.J Grimshaw, Eds., Springer-Verlag, Berlin, Heidelberg, 139–146

MELVILLE, W. K. 1994 Energy dissipation by breaking waves. *J. Phys. Oceanogr.* **24**, 2041–2049

MELVILLE, W. K., SHEAR, R. & VERON, F. 1998 Laboratory measurements of the generation and evolution of Langmuir circulations. *J. Fluid Mech.* **364**, 31–58

MELVILLE, W. K. & MATUSOV, P. 2002 Distribution of breaking waves at the ocean surface. *Nature* **417**, 58–63

MELVILLE, W. K., VERON, F. & WHITE, J. 2002 The velocity field under breaking waves: coherent structures and turbulence. *J. Fluid Mech.* **454**, 202–233

MEYER, Y. 1989 Wavelets and operators. In *Analysis at Urbana I. London Math. Soc. Lecture Notes*, **137**, Cambridge University Press, 256–365

MEZA, E., ZHANG, J. & SEYMOUR, R. J. 2000 Free-wave energy dissipation in experimental breaking waves. *J. Phys. Oceanogr.* **30**, 2404–2418

MINNAERT, M. 1933 On musical air bubbles and the sound of running water. *Phil. Mag.* **16**, 235–248

MIRONOV, A. S. & DULOV, V. A. 2008 Detection of wave breaking using sea surface video records. *Meas. Sci. Technol.* **19**, doi:1018/0957-0233/19/1/015405, 10p

MIYAKE, Y. & ABE, T. 1948 A study on the foaming of the water. Part 1. *J. Mar. Res.* **7**, 67–73

MONAHAN, E. C. 1969 Fresh water whitecaps. *J. Atmos. Sci.* **26**, 1026–1029

MONAHAN, E. C. & ZIETLOW, C. R. 1969 Laboratory comparisons of fresh-water and salt-water whitecaps. *J. Geophys. Res.* **74**, 6961–6966

MONAHAN, E. C. 1971 Oceanic whitecaps. *J. Phys. Oceanogr.* **1**, 139–144

MONAHAN, E. C., O'MUIRCHEARTAIGH, I. G. & FITZGERALD, M. P. 1981 Determination of surface wind speed from remotely measured whitecap coverage: a feasibility assessment. *SP-167*, Eur. Space Agenacy, Paris 103–109

MONAHAN, E. C., ED. 1986 *Oceanic Whitecaps and Their Role in Air-Sea Exchange Processes.* D. Riedel, Norwell, Mass., 214p

MONAHAN, E. C. & O'MUIRCHEARTAIGH, I. G. 1986 Whitecaps and passive remote sensing of the ocean surface. *Int. J. Remote Sens.* **7**, 627–642

MONAHAN, E. C. & LU, M. 1990 Acoustically relevant bubble assemblages and their dependence on meteorological parameters. *IEEE J. Oceanic Eng.* **15**, 340–349

MONAHAN, E. C. 1993 Occurrence and evolution of acoustically relevant subsurface bubble plumes and their associated, remotely monitorable surface whitecaps. In *Natural Physical Sources of Underwater Sound*, B.R. Kerman, Ed., Kluwer Acad., Norwell, Mass., 503–517

MOORE, K. D., VOSS, K. J. & GORDON, H. 1997 Spectral reflectance of whitecaps: Their contribution to water leaving radiance. *J. Geophys. Res.* **105**, 6493–6499

MORI, N. & YASUDA, T. 1994 Orthonormal wavelet analysis for deep-water breaking waves. In *Proc. of the 24th Intern. Conf. on Coastal Eng.* **31**, Koba, Japan, 412–426

MUNK, W. H. 1947 A critical wind speed for air-sea boundary processes. *J. Marine Res.* **6**, 203–218

NATH, J. H. & RAMSEY, F. L. 1976 Probability distributions of breaking wave heights emphasizing the utilization of the JONSWAP spectrum. *J. Phys. Oceanogr.* **6**, 316–323

NEPF, H. M., WU, C. H. & CHAN, E. S. 1998 A comparison of two- and three-dimensional wave breaking. *J. Phys. Oceanogr.* **28**, 1496–1510

OAKEY, N. S. & ELLIOTT, J. A. 1982 Dissipation within surface mixed layer. *J. Phys. Oceanogr.* **12**, 171–185

OCHI, M. K. & TSAI, C.-H. 1983 Prediction of occurrence of breaking waves in deep water. *J. Phys. Oceanogr.* **13**, 2008–2019

OH, S.-H., MIZUTANI, N. & SUH, K.-D. 2008 Laboratory observation of coherent structures beneath microscale and large-scale breaking waves under wind action. *Experimental Thermal and Fluid Scie.* **32**, 1232–1247

OKAMURA, M. 1986 Maximum wave steepness and instabilities of finite-amplitude standing gravity waves. *Fluid Dynamics Res.* **1**, 201–214

ONORATO, M., OSBORNE, A. R., SERIO, M. & BERTONE, S. 2001 Freak wave in random oceanic sea states. *Phys. Rev. Lett.* **86**, 5831–5834

ONORATO, M., OSBORNE, A. R. & SERIO, M. 2002 Extreme wave events in directional, random oceanic sea states. *Phys. Fluids* **14**, 25–28

ONORATO, M., CAVALERI, L., FOUQUES, S., GRAMSTAD, O., JANSSEN, P. A. E. M., MONBALIU, J., OSBORNE, A. R., PAKOZDI, C., SERIO, M., STANSBERG, C. T., TOFFOLI, A., & TRULSEN, K. 2009a Statistical properties of mechanically generated surface gravity waves: a laboratory experiment in a three-dimensional wave basin. *J. Fluid Mech.* **637**, 235–257

ONORATO, M., WASEDA, T., TOFFOLI, A., CAVALERI, L., GRAMSTAD, O., JANSSEN, P. A. E. M., KINOSHITA, T., MONBALIU, J., MORI, N., OSBORNE, A. R., SERIO, M., STANSBERG, C. T., TAMURA, H. & TRULSEN, K. 2009b On the statistical properties of directional ocean waves: the role of the modulational instability in the formation of extreme events. *Phys. Rev. Lett.* **102**, doi:10.1103/PhysRevLett.102.114502, 4p

PAPADIMITRAKIS, Y. A. & HUANG, N. E. 1988 An estimate of wave breaking probability for deep water waves. In *Sea Surface Sound*, B. R. Kerman, Ed., 71–83

PENNEY, W. G. & PRICE, A. T. 1952 Finite periodic stationary gravity waves in a perfect liquid. *Phil. Trans. R. Soc. Lond.* **A244**, 254

PHELPS, A. D., RAMBLE, D. G. & LEIGHTON, T. G. 1996 The use of a combination frequency technique to measure the surf zone bubble population. *J. Acoust. Soc. Am.* **101**, 1981–1989

PHILLIPS, O. M. 1957 On the generation waves by turbulent wind. *J. Fluid Mech.* **2**, 417–445

PHILLIPS, O. M. 1958 The equilibrium range in the spectrum of wind generated waves. *J. Fluid Mech.* **4**, 426–434

PHILLIPS, O. M. 1984 On the response of short ocean wave components at a fixed number to ocean current variations. *J. Phys. Oceanogr.* **14**, 1425–1433

PHILLIPS, O. M. 1985 Spectral and statistical properties of the equilibrium range of wind-generated gravity waves. *J. Fluid Mech.* **156**, 505–531

PHILLIPS, O. M., POSNER, F. L. & HANSEN, J. P. 2001 High resolution radar measurements of the speed distribution of breaking events in wind-generated ocean waves: surface impulse and wave energy dissipation rates. *J. Phys. Oceanogr.* **31**, 450–460

PHILLIPS, W.R.C. 2003 Langmuir circulation. In *Wind Over Waves II: Forecasting and Fundamentals of Applications,* Eds S.G. Sajjadi, J.C.R. Hunt, Eds., Horwood Publishing, Chichester, UK, 157–167

PHILLIPS, W.R.C. 2005 On the spacing of Langmuir circulation in strong shear. *J. Fluid Mech.* **525**, 215–236

PIERSON, W. J., JR. & MOSKOWITZ, L. 1964 A proposed spectral form for fully developed wind seas based on the similaruty theory of S. A. Kitaigordskii. *J. Geophys. Res.* **69**, 5181–5190

PIERSON, W. J., DONELAN, M. A. & HUI, W. H. 1992 Linear and nonlinear propagation of water wave groups. *J. Geophys. Res.* **C97**, 5607–5621

PIGEON, V. W. 1968 Doppler dependence of radar sea return. *J. Geophys. Res.* **73**, 1333–1341

POWEL, M. D., VICKERY, P. J. & REINHOLD, T. A 2003 Reduced drag coefficient for high wind speeds in tropical cyclones. *Nature* **422**, 279–283

PROSPERETTI, A. 1985 Bubble-related ambient noise in the ocean. *J. Acoust. Soc. Am.* **78**, S2

PROSPERETTI, A. 1988 Bubble-related ambient noise in the ocean. *J. Acoust. Soc. Am.* **84**, 1042–1054

RAMBERG, S. E. & GRIFFIN, O. M. 1987 Laboratory study of steep and breaking deep water waves. *J. Waterway, Port, Coastal, Ocean Eng.* **113**, 493–507

RAPP, R. J. & MELVILLE, W. K. 1990 Laboratory measurements of deep-water breaking waves. *Phil. Trans. R. Soc. Lond.* **A311**, 735–800

RAYLEIGH, LORD 1917 On the pressure developed in a liquid during the collapse of a spherical cavity. *Philos. Mag.* **34**, 94–98

RICE, S. O. 1954 Mathematical analysis of random noise. In *Noise and Stochastic Processes*, N. Wax, Ed., Dover, New York, 133–294

ROBINSON, I. S., WELLS, N. C. & CHARNOCK, H. 1984 The sea surface thermal boundary layer and its relevance to the measurement of sea surface temperature by airborne and space-borne radiometers. *Int. J. Remote Sens.* **5**, 19–45

SCHULZ, E. W. 2009 The Riding Wave Removal Technique: recent developments. *J. Atmos. Ocean. Technol.* **26**, 135–144

SHARKOV, E. A. 2007 *Breaking Ocean Waves. Geometry, Structure and Remote Sensing.* Springer, 278p

SHEMER, L., KIT, E. & JIAO, H.-Y. 2002 An experimental and numerical study of the spatial evolution of unidirectional nonlinear water-wave groups. *Phys. Fluids* **14**, 3380–3390

SHEMER, L., GOULITSKI, K. & KIT, E. 2007 Evolution of wide-spectrum unidirectional wave groups in a tank: an experimental and numerical study. *Europ. J. Mech. B/Fluids* **26**, 193–219

SHEMER, L. & DORFMAN, B. 2008 Spatial vs. temporal evolution of nonlinear wave groups - experiments and modeling based on the Dysthe equation. In *Proc. 27th Int. Conf. on Offshore Mechanics and Artic Eng. OMAE2008, June 15-20, 2008, Estoril, Portugal*, 10p

SKAFEL, M. G. & DONELAN, M. A. 1997 Laboratory measurements of stress modulation by wave groups. *Geophysica* **33**, 9–14

SMITH, J. 1992 Observed growth of Langmuir circulation. *J. Geophys. Res.* **97**, 5651–5664

SMITH, J. 1998 Evolution of Langmuir circulation in a storm. *J. Geophys. Res.* **103**, 12649–12668

SMITH, M. J., POULTER E. M. & MCGREGOR, J. A. 1996 Doppler radar measurements of wave groups and breaking waves. *J. Geophys. Res.* **C101**, 14269–14282

SNYDER, R. L. & KENNEDY R. M. 1983 On the formation of whitecaps by a threshold mechanism. Part I: Basic formalism. *J. Phys. Oceanogr.* **13**, 1482–1492

SNYDER, R. L., SMITH, L. & KENNEDY R. M. 1983 On the formation of whitecaps by a threshold mechanism. Part I: Field experiment and comparison with theory. *J. Phys. Oceanogr.* **13**, 1505–1518

SOLOVIEV, A. V., VERSHINSKY N. V. & BEZVERCHNII, V. A. 1988 Small-scale turbulence measurements in the thin surface layer of the ocean. *Deep-Sea Res.* **35**, 1859–1874

SOLOVIEV, A. V. & LUKAS, R. 2003 Observation of wave-enhanced turbulence in the near-surface layer of the ocean during TOGA COARE. *Deep-Sea Res. I* **50**, 371–395

SONG, J. & BANNER, M. L. 2002 On the determining the onset and strength of breaking for deep water waves. Part 1: Unforced irrotational wave groups. *J. Phys. Oceanogr.* **32**, 2541–2558

SONG, J. & BANNER, M. L. 2004 Influence of mean water depth and a subsurface sand bar on the onset and strenght of wave breaking. *J. Phys. Oceanogr.* **34**, 950–960

STANSELL, P. & MACFARLANE, C. 2002 Experimental investigation of wave breaking criteria based on wave phase speeds. *J. Phys. Oceanogr.* **32**, 1269–1283

STEVENS, C. L., POULTER E. M., SMITH, M. J. & MCGREGOR, J. A. 1999 Nonlinear features in wave-resolving microwave radar observations of ocean waves. *J. Geophys. Res.* **C101**, 14269–14282

STOKES, G. G. 1880 Considerations relative to the greatest height of oscillatory irrotational waves which can be propagated without change of form. In *On the Theory of Oscillatory Waves*, Cambridge University Press, London, England, 225-229

STOLTE, S. 1992 Wave breaking characteristics deduced from wave staff measurements. *Forschungsanstalt der Bundeswehr fur Wasserschall- und Geophysik*, Report FB 1992-4, 21p

STOLTE, S. 1994 Short-wave measurements by a fixed tower-based and a drifting buoy system. *IEEE J. Oceanic Eng.* **19**, 10-22

STRAMSKA, M. & PETELSKI, T. 2003 Observations of oceanic whitecaps in the north polar waters of the Atlantic. *J. Geophys. Res.* **C108**, doi:10.1029/2002JC001321, 10p

SU, M. Y. & CARTMILL, J. 1992 Breaking wave statistics during 'SWADE'. In *Breaking waves. IUTAM Symposium, Sydney, Australia, 1991*, M.L. Banner, R.H.J. Grimshaw, Eds., Springer-Verlag, Berlin, Heidelberg, 161–164

SCHWARTZ, L. W. & FENTON, J. D. 1982 Strongly nonlinear waves. *Ann. Rev. Fluid Mech.* **14**, 39–60

TAYFUN, M. A. 1981 Breaking limited wave heights. *J. Waterways, Harbors and Coastal Eng. Div.* **107**, 55–79

TERRAY, E. A., DONELAN, M. A., AGRAWAL, Y. C., DRENNAN, W. M., KAHMA, K. K., WILLIAMS III, A. J., HWANG, P. A. & KITAIGORODSKII, S. A. 1996 Estimates of kinetic energy dissipation under breaking waves. *J. Phys. Oceanogr.* **26**, 792–807

TERRILL, E. J. & MELVILLE, K. W. 2000 A broadband acoustic technique for measuring bubble size distributions: laboratory and shallow water measurements. *J. Atmos. Oceanic Tech.* **17**, 220–239

TERRILL, E. J., MELVILLE, W. K. & STRAMSKI, D. 2001 Bubble entrainment by breaking waves and their influence on optical scattering in the upper ocean. *J. Geophys. Res.* **C106**, 16815–16823

THE WISE GROUP: CAVALERI, L., ALVES, J.-H.G.M., ARDHUIN, F., BABANIN, A., BANNER, M., BELIBASSAKIS, K., BENOIT, M., DONELAN M., GROENEWEG, J., HERBERS, T. H. C, HWANG, P., JANSSEN, P. A. E. M., JANSSEN, T., LAVRENOV, I. V., MAGNE, R., MONBALIU, J., ONORATO, M., POLNIKOV, V., RESIO, D., ROGERS, W. E., SHEREMET, A., MCKEE SMITH, J., TOLMAN, H. L., VAN VLEDDER, G., WOLF, J. & YOUNG, I. 2007 Wave modelling – The state of the art. *Progr. Oceanogr.* **75**, 603–674

THORPE, S. A. & HUMPRIES, P. N. 1980 Bubbles and breaking waves. *Nature* **283**, 463–465

THORPE, S. A. 1992 Bubble clouds and the dynamics of the upper ocean. *Q. J. R. Meteorol. Soc.* **118**, 1–22

THORPE, S. A. 2004 Langmuir circulation. *Annu. Rev. Fluid Mech.* **36**, 55–79

TKALICH, P. & CHAN, E. S. 2002 Breaking wind waves as a source of ambient noise. *J. Acoust. Soc. Am.* **112**, 456–463

TSAGARELI, K. N. 2009 Numerical investigation of wind input and spectral dissipation in evolution of wind waves. *PhD Thesis*, The University of Adelaide, South Australia, 219p

TOBA, Y. & CHAEN, M. 1973 Quantitative expression of the breaking of wind waves on the sea surface. *Rec. Oceanogr. Works Jpn.* **12**, 1–11

TULIN, M. P., & WASEDA, T. 1999 Laboratory observations of wave group evolution, including breaking effects. *J. Fluid Mech.* **378**, 197–232

TULIN, M. P., & LANDRINI, M. 2001 Breaking waves in the ocean and around ships. In *Proc. Twenty-Third Symp. of Naval Hydrodynamics*, 713–745

VAN DORN, W. G., & PAZAN, S. E. 1975 Laboratory investigation of wave breaking. *AOEL rep. no. 71*, Scripps Inst. of Oceanog., Ref. No. 75–21

VAZQUEZ, A., SANCHEZ, R. M., SALINAS-RODRIQUEZ, E., SORIA, A. & MANASSEH, R. 2005 Experimental comparison between acoustic and pressure signals from a bubbling flow. *Exper. Thermal and Fluid Sci.* **30**, 49–57

VAZQUEZ, A., MANASSEH, R. & SANCHEZ R. M. 2008 A look at three measurement techniques for bubble size determination. *Chem. Eng. Sci.* **63**, 5860–5869

VERON, F., & MELVILLE, W. K. 1999 Pulse-to-pulse coherent Doppler measurements of waves and turbulence. *J. Atmos. Oceanic Tech.* **16**, 1580–1596

WALPOLE, R. E., & MEYERS, R. H. 1978 *Probability and Statistics for Scientists and Engineers*, Macmillan, New York, 580p

WASEDA, T., & TULIN, M.P. 1999 Experimental study of the stability of deep-water wave trains including breaking effects. *J. Fluid Mech.* **401**, 55–84

WASEDA, T., KINOSHITA, T. & TAMURA, H. 2009a Evolution of a random directional wave and freak wave occurrence. *J. Phys. Oceanogr.* **39**, 621-639

WASEDA, T., KINOSHITA, T. & TAMURA, H. 2009b Interplay of resonant and quasi-resonant interaction of the directional ocean waves. *J. Phys. Oceanogr.*, in press

WATSON, K. M. & WEST B. J. 1975 A transport-equation description of nonlinear ocean surface wave interactions. *J. Fluid Mech.* **70**, 815–826

WEISSMAN, M. A., ATAKTURK, S. S. & KATSAROS, K. B. 1984 Detection of breaking events in a wind-generated wave field. *J. Phys. Oceanogr.* **14**, 1608–1619

WENZ, G. M. 1962 Acoustic ambient noise in the ocean: spectra and sources. *J. Acoust. Soc. Am.* **34**, 1936–1956

WEST, B. J., BRUECKNER, K. A. & JANDA R. S. 1987 A new numerical method for surface hydrodynamics. *J. Geophys. Res.* **C92**, 11803–11824

WETZEL, L. B. 1990 Electromagnetic scattering from the sea at low grazing angles. In *Surface Waves and Fluxes: Current Theory and Remote Sensing*, G.L. Geernaert, W.J. Plant, Eds., Kulwer Acad., Norwell, Mass., **2** 109–171

WILLIAMS, G. F. JR. 1969 Microwave radiometry of the ocean and the possibility of marine wind velocity determination from satellite observations. *J. Geophys. Res.* **74**, 4591–4594

WU, C. H., & NEPF, H. M. 2002 Breaking criteria and energy losses for three-dimensional wave breaking. *J. Geophys. Res.* **C107**, 3177, doi:10.1029/2001JC001077

WU, J. 1969 Wind stress and surface roughness at the air-sea interface. *J. Geophys. Res.* **74**, 444–455

WU, J. 1979 Oceanic whitecaps and sea state. *J. Phys. Oceanogr.* **9**, 1064–1068

WU, J. 1988 Variations of whitecap coverage with wind stress and water temperature. *J. Phys. Oceanogr.* **18**, 1448–1453

WU, J. 2000 Bubbles produced by breaking waves in fresh and salt waters. *J. Phys. Oceanogr.* **30**, 1809–1813

XU, D., HWANG, P. A. & WU, J. 1986 Breaking of wind-generated waves. *J. Phys. Oceanogr.* **16**, 2172–2178

YOUNG, I. R. 1994 On the measurement of directional wave spectra. *Appl. Ocean Res.* **16**, 283–294

YOUNG, I. R. & VERHAGEN, L. A. 1996 The growth of fetch limited waves in water of finite depth. Part 1. Total energy and peak frequency. *Coastal Eng.*. **29**, 101–121

YOUNG, I. R., VERHAGEN, L. A. & KHATRI, S. K. 1996 The growth of fetch limited waves in water of finite depth. Part 3. Directional spectra. *Coastal Eng.* **29**, 47–78

YOUNG, I. R. 1999 *Wind Generated Ocean Waves*, Elsevier, 288p

YOUNG, I. R., BANNER, M. L., DONELAN, M. A., BABANIN, A. V., MELVILLE, W. K., VERON, F. & MCCORMIC, C. 2005 An integrated study of the wind wave source term balance in finite depth water. *J. Atmos. Oceanic Tech.* **22**, 814-828

YOUNG, I. R. & BABANIN, A. V. 2006a Spectral distribution of energy dissipation of wind-generated waves due to dominant wave breaking. *J. Phys. Oceanogr.* **36**, 376–394

YOUNG, I. R. & BABANIN, A. V. 2006b The form of the asymptotic depth-limited wind wave frequency spectrum. *J. Geophys. Res.* **C111**, C06031, doi:10.1029/2005JC003398, 15p

YUAN, Y., TUNG, C. C. & HUANG, N. E. 1986 Statistical characteristics of breaking waves. In *Wave Dynamics and Radio Probing of the Ocean Surface*, O.M. Phillips, K. Hasselmann, Eds., Plenum New York, 265-272

YUAN, Y., ZHANG, S. & HAN, L. 2008 Statistical model on the surface elevation of waves with breaking. *Sci. China* **B51**, 759–768

YUAN, Y., HAN, L., HUA, F., ZHANG, S., QIAO, F., YANG, Y. & XIA, C. 2009 The statistical theory of breaking entrainment depth and surface whitecap coverage of real sea waves. *J. Phys. Oceanogr.* **39**, 143–161

YUEN, H. C. & LAKE, M. 1982 Nonlinear dynamics of deep-water gravity waves. In *Advances in Applied Mechanics* **22**, 67–229

ZAKHAROV, V. E. 1966 The instability of waves in nonlinear dispersive media. *Zhurnal Eksperimental'noi i Teoreticheskoi Fiziki* **51**, 1107-1114 (in Russian)

ZAKHAROV, V. E. 1967 The instability of waves in nonlinear dispersive media. *Sov. Phys.–JETP (Engl. Transl.)* **24**, 744–744

ZAKHAROV, V. E. 1968 Stability of periodic waves of finite amplitude on the surface of deep fluid. *J. Appl. Mech. Tech. Phys.–JETR (Engl. Transl.)* **2**, 190–194

ZASLAVSKII, G. M. & SHARKOV, E. A. 1987 Fractal features in breaking wave areas on sea surface. *Doklady Academii Nauk SSSR (Transactions of USSR Academy of Sciences - English Translation)* **294**, 1362–1366

ZHAO, D., & TOBA, Y. 2001 Dependence of whitecap coverage on wind and wind-wave properties. *J. Oceanogr.* **57**, 603–616

ZIMMERMANN, C.-A., & SEYMOUR, R. 2002 Detection of breaking in a deep water wave record. *J. Waterway, Port, Coastal, Ocean Eng.* **128**, 72–78